INFLUENCE OF ULTRASOUND ON OSTEOBLASTS ATTACHED TO TITANIUM *IN VITRO*.

By

OLGA YEVLASHEVSKAYA

A thesis submitted to the University of Birmingham for the degree of DOCTOR OF PHILOSOPHY

School of Dentistry
College of Medical and Dental Sciences
University of Birmingham
October 2023

Abstract

Despite the growing evidence that ultrasonic stimulation can promote bone healing on titanium (Ti)-based implants, the current understanding of mechanisms of action of therapeutic ultrasound is limited. The present work aimed to produce an experimental system which would allow the delivery of a defined dosage of ultrasound to osteoblasts incubated on Ti surfaces *in vitro* and observe the cells responses.

Initially two osteogenic cell lines, Saos-2 and immortalised human mesenchymal stromal cells (hMSCs) were characterised before subsequent ultrasonic treatment. Osteogenic behaviour was analysed in the presence of supplements, consisting of 283 µM ascorbic acid (Asc), 9.3 mM β-glycerophosphate (β-Gly) and 10^{-8} M dexamethasone (Dex), for 14 days. Saos-2 cells exhibited a reduction of 63% in viable cells compared with the negative controls, which was not observed in the hMSCs although the lactate dehydrogenase (LDH) assay did not reveal any cytotoxic effects of β-Gly. However, 5-Bromo-2'-deoxy-uridine (BrdU) staining showed a distinct antiproliferative influence of β-Gly on only Saos-2 cells. Moreover, in hMSCs treated with Asc, Dex, and β-Gly, the expression of *RUNX2, OCN, BSP*, and *ALP* were upregulated, which was not observed in the absence of β-Gly. The presence of β-Gly led to an upregulation of *RUNX2* and *OCN* expression in Saos-2 cells. It was concluded that β-Gly demonstrated a unique proliferative stimulus in Saos-2 cells, by possibly interacting with osteogenesis of relatively mature osteoblast-like cells.

The difficulties associated with cell detachment and counting in mineralising cultures were also investigated. Cells were detached using incubation with either trypsin alone

or in combination with collagenase type 1. Counting with an haemocytometer and trypan blue staining produced less variable, more robust data, compared with the automated counting based on fluorescence-based images.

Additionally, cell attachment of hMSCs to Ti surfaces was studied for implementation into the *in vitro* ultrasonic device. Ti surfaces with roughness, Ra of ~1 µm were prepared by acid etching and demonstrated optimal cell attachment. Ti strips were then designed to attach to transducers oscillating at 20 and 40 kHz. The strips served as an incubation surface for immortalised hMSCs and resonated according to the ultrasound frequency produced by the transducers. Polydimethylsiloxane wells were created to compartmentalise cells exposed to different excitation doses modes whilst incubated in culture medium. After exposure to continuous ultrasound at either frequency for 5 min an LDH assay showed no difference in cell death relative to controls.

The presented system offers potential for studying defined dosage and delivery regimes of ultrasound to osteoblasts incubated on Ti surfaces, while under controlled temperature conditions. Future studies using this setup will include analysis of gene expression and mineral deposition to define the potential role of ultrasonic therapy in dental and orthopaedic implantology.

Acknowledgements

First and foremost, I would like to extend my heartfelt gratitude to my supervisors, Dr Shelton, Prof Walmsley, and Dr Scheven, for their unwavering support and guidance throughout this project. Their expertise and encouragement played such a big role in shaping the success of my work. A big thank you goes out to the dedicated technicians' team of the School of Dentistry 3rd floor laboratories: Lisa, Helen, Jianguo, and Jonathan. Your assistance and cooperation in the lab were truly appreciated.

I would also like to express my appreciation to the EPSRC Grant no EP/R045291/1 for providing the financial support that made this project possible.

Furthermore, I am deeply grateful to the PGR office of the School of Dentistry for creating such a friendly and welcoming community. I have learnt so much from you and I will truly miss our Thursday socials.

A special thank you goes to my family: my mum, dad, and my little brother Nazar for their unyielding support. Your belief in me and your willingness to listen to my science stories meant the world to me.

Lastly, a special and heartfelt thank you goes out to my fiancé, Richard. Your support, love, and understanding have made these years incredibly special. I am forever indebted to you for being my rock and pillar throughout this journey.

To everyone mentioned above, your contributions have shaped me both personally and professionally, and I am grateful beyond words. This achievement wouldn't have been possible without each and every one of you. Thank you from the bottom of my heart.

Table of contents

List of figures

List of tables

List of abbreviations

ALP alkaline phosphatase

ARS alizarin red S

Asc ascorbic acid

ATP adenosine triphosphate

ATPase adenosine triphosphatase

AUD Australian dollar

BMP bone morphogenetic protein

BrdU 5-Bromo-2'-deoxy-uridine

BSP bone sialoprotein

B2M β-2-microtubulin

cAMP cyclic adenosine monophosphate

cDNA complementary DNA

COL1A1 collagen type 1 alpha 1

COL3A1 collagen type 3 alpha 1

Cp crossing point

cp-Ti commercially pure Titanium

DAPI 4′,6-diamidino-2-phenylindole

DCN decorin

DEPC diethylpyrocarbonate

Dex dexamethasone

DMEM/HamsF-12 Dulbecco's modified eagle's medium/ Ham's nutrient mixture F12

DNA deoxyribonucleic acid

ECM extracellular matrix

EDTA ethylenediaminetetraacetic acid

EDX energy dispersive X-ray

FBS foetal bovine serum

FDA food and drug administration

FRH frequency resonance hypothesis

FTIR Fourier transform infrared spectroscopy

GAPDH glyceraldehyde-3-phosphate dehydrogenase

HA hydroxyapatite

hFOB human foetal osteoblasts

HIFU high intensity focused ultrasound

hMSCs human mesenchymal stromal cells

HPRTI1 hypoxanthine phosphoribosyltransferase 1

HSCs haematopoietic stromal cells

LCN lacunocanalicular network

LDH lactate dehydrogenase

LFU low frequency ultrasound

LIPUS low intensity pulsed ultrasound

LMHFV low-magnitude high-frequency vibration

MAPK mitogen activated protein kinase

MgHA/Coll Magnesium-doped hydroxyapatite/collagen

MKI67 marker of proliferation-67

MMP-1 matrix metalloproteinase 1

MTT 3 (4,5-dimethylthiazol-2-yl)-2,5-diphenyltetrazolium bromide

NF-κB nuclear factor-kappa b

NICE national institute for health and care excellence

NO nitric oxide

OCN osteocalcin

OPG osteoprotegerin

OPN osteopontin

OSX osterix

PBS phosphate buffered saline

PC2 polycystin 2

PCNA proliferating cell nuclear antigen

PDMS polydimethylsiloxane

PGE2 prostaglandin 2

PHEX phosphate regulating endopeptidase homolog X-linked

PMMA polymethyl methacrylate

PTH parathyroid hormone

PTHrP parathyroid hormone–related protein

PVDF polyvinylidene fluoride

PZT lead zirconate titanate

qPCR real-time PCR

RANKL receptor activator of nuclear factor kappa-b ligand

RNA ribonucleic acid

ROS reactive oxygen species

RPM rotations per minute

RT reverse transcription

RUNX2 runt-related transcription factor 2

SEM scanning electron microscopy

SPP1 phosphoprotein-1

SV40 simian virus 40

T2DM type 2 diabetes mellitus

TERT transcriptase protein

TGF-β transforming growth factor β

Ti64 titanium 6-aluminum 4-vanadium alloy

TRPV1 transient receptor potential cation channel subfamily V member 1

TRPV4 transient receptor potential cation channel subfamily V member 4

VEGF vascular endothelial growth factor

VSCC voltage sensitive calcium channels

w/v weight/volume

XTT 3'-{1-[(phenylamino)-carbonyl]-3,4-tetrazolium} bis(4-methoxy-6-nitro) benzenesulfonic acid hydrate 3'-1-(phenylamino)-carbonyl--3

YWHAZ tyrosine 3-monooxygenase

β-Gly β-glycerophosphate

μCT micro-computed tomography

1 Introduction

1.1 General introduction

1.1.1 Ultrasonic therapy in bone healing

Bone healing is the key process in fracture repair and osseointegration of titanium-based bone-replacing implants, taking from several months up to 2 years to complete (Marsell & Einhorn, 2011). To enhance bone healing, both with and without Ti-based implants, non-invasive treatments, such as therapeutic ultrasound, have been explored. However, the effectiveness of ultrasonic therapy for bone healing remains a topic of ongoing debate. The primary challenge lies in the incomplete understanding of underlying mechanisms by which ultrasonic therapy influences bone cells and their functions (Della Rocca, 2009).

1.1.2 *In vitro* approach to studying osteoblast responses to ultrasound

Researchers have focused efforts conducting basic research to gain a clearer understanding of cellular responses to this treatment and to determine the optimal exposure regimes. However, achieving a reliable and a defined experimental setup for ultrasonic treatment of cells on Ti has proven challenging due to the presence of cavitation, temperature elevation and the formation of standing waves within culture wells (Secomski et al., 2017). These variations in experimental conditions can lead to differences in the ultrasound dosage experienced by cells, resulting in a lack of a well-defined exposure regime. Additionally, Ti-surfaces are highly reflective, which has the

potential to impede ultrasound stimulation of cells incubated on such surfaces. The current setups usually involve a monolayer of osteoblasts incubated on a polystyrene culture dish with the ultrasonic transducers either immersed into the culture media, placed under the dish or the entire setup placed in a degassed water tank (Padilla et al., 2014). However, these do not resolve the issues with poorly defined ultrasonic dosages. Furthermore, there is not a standardised experimental design involving titanium surfaces to represent a bone-replacing implant. Similarly, a clear method of differentiating between thermal and non-thermal effects of ultrasound on cells is not commonly addressed.

1.1.3 Osteoblast models for *in vitro* studies

Selecting an appropriate cell model demonstrating osteoblastic behaviour poses an additional challenge in establishing a reliable *in vitro* ultrasonic treatment system. Despite the evident advantages of using primary human or animal cells, the cost, ethical considerations and limited growth potential *in vitro* present challenges. As an alternative, cancer-derived or immortalised cell lines offer a cost-effective solution. However, these cell lines may exhibit altered behaviour in comparison with human osteoblasts (Czekanska et al., 2012). While promoting osteoblastic differentiation in these cell lines using ascorbic acid (Asc), dexamethasone (Dex), and β-glycerophosphate (β-Gly) supplements is commonly employed, conflicting reports exist in the literature regarding the extent to which these factors significantly influence cellular behaviour. Consequently, data interpretation following ultrasound treatment of these cell lines may be misleading. This uncertainty arises from the potential

coexistence of the effects of osteogenic supplementation and the thermal and mechanical mechanisms of ultrasound, making it challenging to differentiate between their individual contributions.

1.1.4 Overview of the present work

The present work aimed to produce a reliable and defined *in vitro* system, which will assist in understanding the mechanisms of ultrasonic therapy for bone healing and osseointegration. The initial section of this chapter will provide an introduction to the fundamental concepts of bone physiology and healing. It will explore the necessity for bone replacement using Ti-based implants and examine how ultrasonic therapy can potentially support this process. Subsequently, the challenges related to *in vitro* ultrasonic treatment of osteoblasts on titanium surfaces will be discussed in detail. Emphasis will be placed on understanding the complexities and limitations associated with this experimental setup. Finally, the effects of osteogenic supplementation of two osteoblast cell lines will be addressed to select an appropriate cell model for subsequent ultrasonic exposure. By covering these aspects comprehensively, this chapter will lay the foundation for subsequent investigations on ultrasonic therapy in combination with Ti-based implants for bone replacement.

1.2 Physiology of bone tissue in health

1.2.1 Bone cells and mineralised matrix

Contrary to the popular misconception that bones are not living tissues, each one of the 206 bones of the human skeleton is dynamic and metabolically active. These are

composite structures containing the mineralised extracellular matrix (ECM) and bone cells. The organic component forming approximately 40% of bone mass is primarily made up of collagen type 1a deposited by osteoblasts, as well as other non-collagenous proteins, including proteoglycans, glycoproteins and small integrin-binding ligands N-linked glycoproteins (Lin et al., 2020). The latter are associated with controlling bone remodelling while collagens provide resistance to tensile strains (Poundarik et al., 2018). The inorganic bone matrix is composed of calcium and phosphate-containing hydroxyapatite (HA) needle-like crystals (Mohamed, 2008). Other inorganic components of HA include but are not limited to the inclusions of carbonate, fluoride, magnesium, and sodium ions. These are involved in cell signalling within bone and dictate some of the physical properties of bone including solubility which is crucial in ion homeostasis (Feng, 2009; Poundarik et al., 2018). In addition to providing compressive strength essential in load bearing, the mineralised matrix of bones is the main calcium ion reservoir of the body (Marsell & Einhorn, 2011; Vannucci et al., 2018). Bone ECM is deposited and maintained by 3 types of bone cells - osteocytes, osteoblasts, and bone-lining cells (**Error! Reference source not found.**) (Mohamed, 2008). Whereas osteoclasts resorb old and damaged bone tissue. Osteocytes, osteoblasts and bone-lining cells derive from the multipotent bone marrow mesenchymal cells, also capable of differentiating into adipocytes, chondrocytes and myoblasts (Aubin, 1998). Whereas osteoclasts originate from the haematopoietic stem cell lineage (Boyle et al., 2003).

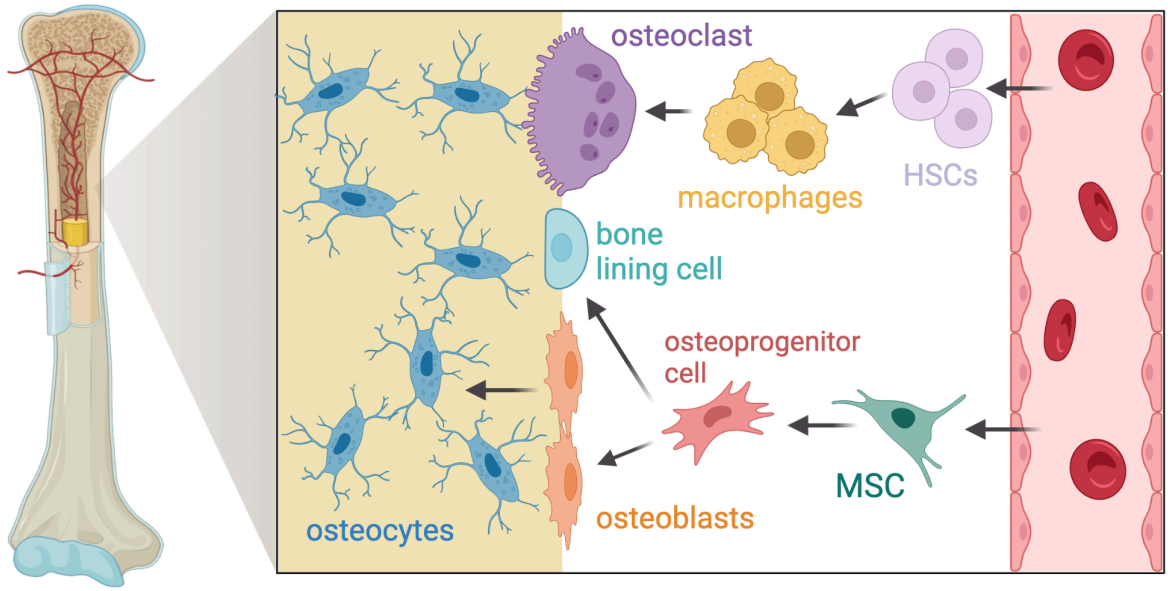

Figure 1.1: Schematic representation of cell types from mesenchymal and haematopoietic lineages involved in bone remodelling. Mesenchymal stem cells (MSCs) differentiate into early osteoprogenitor cells and subsequently mature into osteoblasts or bone lining cells. Osteoblasts further differentiate and transform into osteocytes, the most abundant bone cells. Conversely, haematopoietic stem cells (HSCs) give rise to precursor macrophage-like cells, which fuse to form multinucleated osteoclasts responsible for bone resorption.

1.2.1.1 Osteoblasts

Mineralised matrix forming cells or osteoblasts comprise ~5% of all bone cells and are found on the bone surface. Osteoblastic differentiation of mesenchymal precursor cells is controlled via six signalling pathways including hedgehog (Hh), TGF-β, bone morphogenetic protein and Wnt/beta-catenin signalling (Chen et al., 2012). Initially, mesenchymal stem cells develop into early osteoprogenitor cells following the release of the key transcription factors including runt-related transcription factor 2 (RUNX2) and osterix (OSX) (Ponzetti & Rucci, 2021; Rosenberg et al., 2012). Then, mature osteoprogenitor cells develop into preosteoblasts - which are immature osteoblasts with a limited mitosis capability (Aubin, 1998). Common markers of the early osteoblast stage are alkaline phosphatase (ALP), bone sialoprotein (BSP) and parathyroid

hormone–related protein (PTHrP) (Huang et al., 2007). Early osteoblasts develop to mature osteoblasts characterised by the active synthesis of collagen type 1 and several non-collagenous proteins. The latter are relevant in cell culture and are key controllers of bone nodule formation, a process outlined by 3 stages - cell proliferation, ECM maturation and ECM mineralisation, each characterised by the corresponding signalling protein transcription (Huang et al., 2007). Osteopontin (OPN) production increases during the proliferation stage, whilst ECM maturation is characterised by increased release of BSP. An elevated osteocalcin (OCN) synthesis is typical during the mineralisation phase (Aubin, 2001). While the lifespan of osteoblasts varies between several days to months, following bone nodule formation mature osteoblasts have three potential fate routes. Either reaching terminal differentiation and becoming post-mitotic osteocytes buried in mineralised matrix or becoming quiescent bone lining cells. Alternatively mature osteoblasts undergo apoptosis (Florencio-Silva et al., 2015; Rosenberg et al., 2012).

1.2.1.2 Osteocytes

Osteocytes are the most numerous bone cells and are described as less metabolically active when compared with osteoblasts (Aubin, 1998). These are key regulators of bone remodelling maintaining the balance between bone deposition and resorption (Manolagas, 2000). Buried in the bone matrix, osteocytes are found in lacunae and possess dendritic cell processes residing in canaliculi - a network of channels that create a lacunocanalicular network (LCN) (Casanova et al., 2021) in the mineralised ECM which are crucial in nutrient and oxygen supply to cells (Choi et al., 2022), as well as

in mechanotransduction. The transition of mature osteoblasts into osteocytes is associated with an increase in production of phosphate regulating endopeptidase X-linked, matrix extracellular phosphoglycoprotein, dentin matrix protein 1 and sclerostin (Bonewald, 2011) which are expressed by *PHEX, MEPE, DMP-1* and *SOST* genes respectively. Alternatively, inactive osteoblasts become bone lining cells located on the bone surfaces where bone remodelling does not take place (Aubin, 1998). The role of bone lining cells is debated (Florencio-Silva et al., 2015), however involvement in digesting the non-mineralised bone matrix to facilitate the attachment of osteoclasts has previously been demonstrated (Everts et al., 2002). Furthermore, the report suggested that bone lining cells digested the remaining protein matrix in the resorption pit following osteoclast activity.

1.2.1.3 Osteoclasts

Finally, osteoclasts are multinucleated bone resorbing cells formed as a result of fusion of several mononuclear precursor cells. Osteoclasts degrade bone tissue in the presence of microcracks in the matrix to stimulate normal bone remodelling optimising the load distribution (Jacobs et al., 2010). The key regulator of this is the osteoblast-synthesised receptor activator of nuclear factor-ϰB ligand (RANKL) (Teitelbaum, 2007). RANKL activates RANK receptors on pre-osteoclasts triggering fusion of haemopoietic postmitotic monocytic osteoclast precursor cells. However, when bone resorption is not required, osteoprotegerin is translated by osteoblasts inhibiting RANKL and preventing osteoclastogenesis. Osteoclasts are characterised by the abundance of mitochondria, lysosomes and ribosomes - essential organelles for electrolyte and

degenerative enzymes synthesis (Florencio-Silva et al., 2015). But most interestingly, these cells are capable of polarisation once attached to bone due to the unique cytoskeleton reorganisation of actin filaments into rings and the ruffled cell membrane formation (Teitelbaum, 2007). The described membrane orientation isolates an area of action between the osteoclast and bone. Here, osteoclasts secrete hydrogen ions generated by the action of carbonic anhydrase II via ATPase pumps causing a drop in pH and dissolution of the mineral. This is followed by the matrix metalloproteinase-9 and cathepsin K-mediated breakdown of the collagenous matrix of bones and a subsequent apoptosis of osteoclasts preventing excessive bone resorption (Arana-Chavez & Bradaschia-Correa, 2009). Furthermore, osteoclast action leads to the release of signalling molecules, such as bone morphogenetic proteins and TGF-β recruiting osteoblasts for new bone deposition (Kim et al., 2020).

The bone cells coexist in a continuous balance between bone deposition and resorption, allowing a constant bone remodelling and optimising load distribution. This precise equilibrium is orchestrated by several chemical and mechanical cues which will be described in the next section.

1.2.2 Bone remodelling via mechanosignalling

1.2.2.1 The role of mechanoreceptors

According to (Wolff, 1892) bone remodelling responds to the changes in strain placed on bone to ensure optimum strength and resistance to applied forces. This phenomenon is observed in patients undergoing prolonged bed rest leading to the loss in bone mass of up to 16% in 6 months (Uhthoff & Jaworski, 1978). Similarly, low gravity-induced

bone loss affects space travellers with up to 1.5% bone mass loss per month (Stavnichuk et al., 2020). Furthermore, increased rates of mechanical bone loading generate a higher bone mass as seen in individuals undertaking regular exercise training (Hong & Kim, 2018; Rubin & Lanyon, 1984). While current understanding of molecular pathways involved in increasing bone mass in response to physical activity the latter process is limited, it is thought that a changing mechanical environment is primarily detected and conveyed to osteocytes by mechanoreceptors (Gardinier et al., 2009).

1.2.2.1.1 Focal adhesions

These mechanoreceptors, including integrins, form heterodimeric complexes associated with a group of proteins known as focal adhesions (Figure 1.2A) (Stewart et al., 2020). The former involves talin, paxillin, vinculin, p130Cas and the focal adhesion kinase (FAK) which is bound to the cytoskeleton. When the mineralised extracellular matrix (ECM) experiences a change in mechanical force, integrins transmit signals to the cytoskeleton, leading to activation of various signalling pathways, such as kinase signalling, G protein-mediated signalling, and others (Yavropoulou & Yovos, 2016). These pathways enhance gene transcription of *RUNX2*, osterix (*OSX*), and bone morphogenetic protein 2 (*BMP-2*), thereby promoting osteogenic differentiation.

1.2.2.1.2 Calcium ion channels

Additionally, the influx of calcium ion channels located across the plasma membrane may induce osteogenesis. Piezo1 is a mechanosensitive channel, present in osteocytes, osteoblasts, and osteoclasts. It plays a key role in osteogenesis by allowing influx of cations including Ca^{2+} ions (Xu et al., 2021). Sun et al. (2019) described destructed

osteogenesis in Piezo1-knockout mice leading to a severe loss in bone strength, as demonstrated by a significant decrease in the maximum load-bearing capacity of the femur. Additionally, micro-CT analysis revealed a notable reduction in bone mass and an abnormal trabecular structure.

Another example of mechanically activated calcium channels in osteoblasts is the transient receptor potential cation channel subfamily V member 4 (TRPV4). Within bone tissue, TRPV4 is intricately associated with osteoblastic differentiation through its coupling mechanism with Piezo1 channels (Perin et al., 2023).

The change in membrane potential caused by the Ca^{2+} influx, in turn triggers the opening of voltage sensitive calcium channels (VSCC) (Choi et al., 2022). These allow a further influx of calcium ions, which initiates several pathways, such as NF-ϰB, mitogen activated protein kinases (MAPK), nitric oxide (NO), c-fos, and others (Figure 1.2B) (Knapik et al., 2014).

1.2.2.1.3 Cilia

Primary cilia play a vital role in osteoblast mechanotransduction (Figure 1.2C) as surface membrane protrusions that contain microtubules and possess the ability to sense compression and shear deformation (Ogawa, 2016). When stimulated, polycystin 2 (PC2), an ion channel associated with cilia, transports calcium ions intracellularly, triggering STAT and Wnt signalling pathways that ultimately lead to osteogenic gene transcription (Malone et al., 2007). In addition, primary cilia have been shown to be involved in the synthesis of prostaglandin 2 (PGE2), an important regulator of bone metabolism (Malone et al., 2007).

1.2.2.1.4 Cadherins

Cadherins are membrane-spanning proteins that are intracellularly associated with vinculin and α- and β-catenins, anchoring them to the cytoskeleton (Figure 1.2D). Under shear strain, β-catenin dissociates from the cadherin complex, leading to an increase in its cytoplasmic concentration and upregulation of osteogenic gene expression (Stewart et al., 2020).

1.2.2.1.5 Gap junctions

Osteocytes have the capacity to receive signals about changes in mechanical loading from surface-located osteoblasts through gap junctions (Figure 1.2E). These gap junctions, formed via connexins, consist of two larger subunits termed connexons, which are membrane-spanning proteins allowing cell-to-cell communication in isolation of the extracellular matrix. Gap junctions facilitate the transport of small molecules such as ATP, cAMP, and calcium ions in response to cell deformation or changes in interstitial fluid flow (Yavropoulou & Yovos, 2016). The activity of these channels is enhanced in the presence of PGE2. Donahue (2000) highlighted the increase in the synthesis of gap junctions with the upregulated mechanical loading on bone tissue which suggested that gap junctions play a key role in mechanosignalling processes.

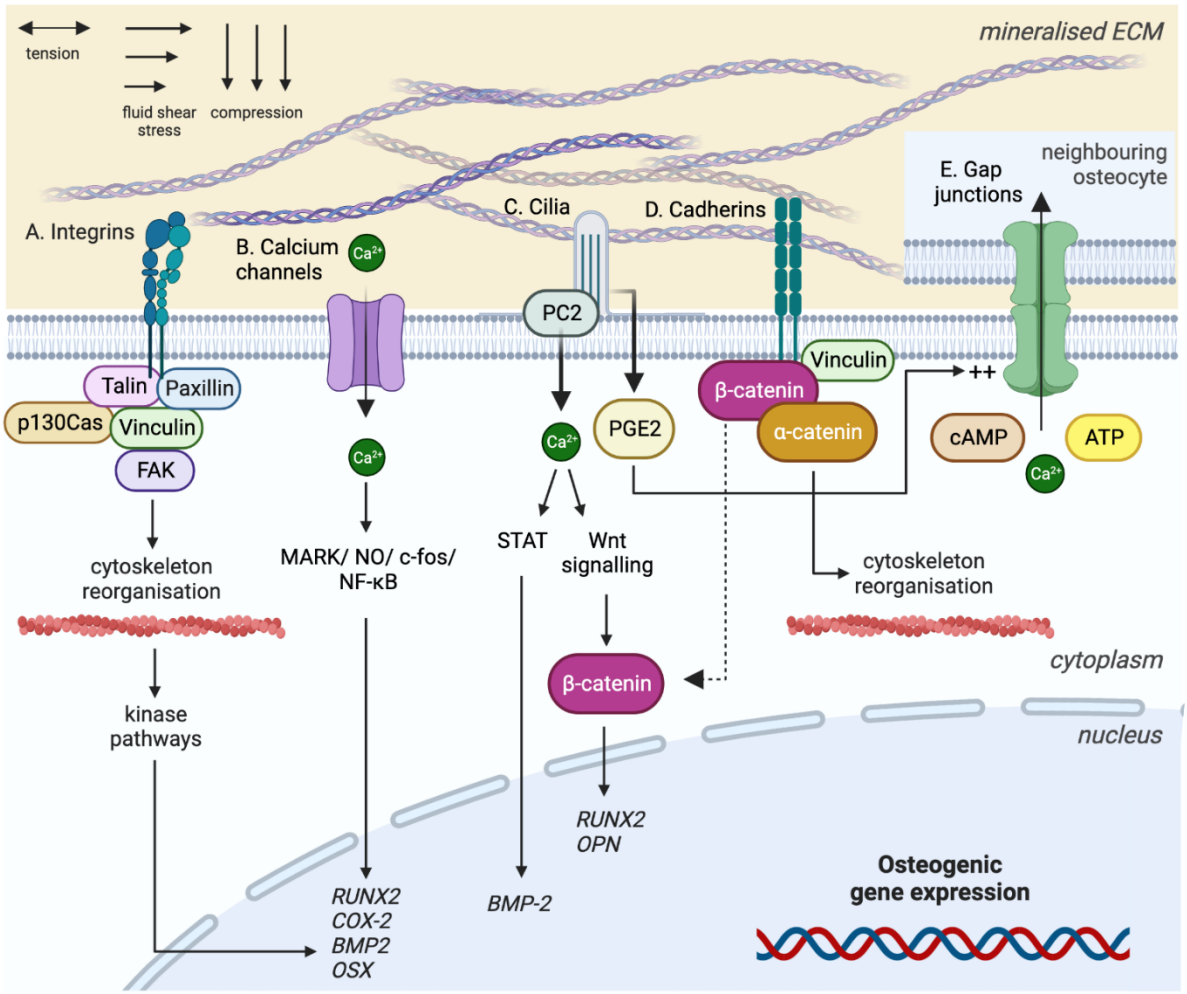

Figure 1.2: Mechanotransduction in osteoblasts involves several pathways: A) Integrins sense mechanical cues from the extracellular matrix (ECM) and transmit the signal via FAK, leading to cytoskeleton reorganization and upregulation of osteogenic behaviour (Stewart et al., 2020). B) Calcium channels allow the influx of calcium ions following mechanical deformation, which induces osteogenesis through the MARK, NO, c-fos, and NF-κB pathways (Xu et al., 2021). C) Deformation of primary cilia also triggers the influx of calcium ions through PC2 channels, upregulating osteogenic gene expression via the STAT and Wnt signalling pathways. Additionally, cilia are associated with increased synthesis of PGE2 (Ogawa, 2016). D) Cadherins are intracellularly anchored with vinculin, α- and β-catenins. When mechanically deformed, cadherins dissociate from the complex, activating Wnt signalling. E) Gap junctions establish communication between osteoblasts and ECM-buried osteocytes, facilitating the passage of small molecules and conveying changes in the mechanical environment of the bone (Yavropoulou & Yovos, 2016).

1.2.2.2 Biophysical signal transduction via mechanoreceptors

Osteocytes develop a network of cell processes, which connect to osteoblasts and osteoclasts in order to communicate changes in mechanical loading of bones. Such mechanisms are essential for detecting a changing functional environment and responding to it accordingly – either resorbing or forming new bone locally to accommodate or resist the mechanical loads (Choi et al., 2022). Several possible mechanisms of how these changes are communicated by the mechanoreceptors in a natural body environment have been proposed (Jacobs et al., 2010). Firstly, the substrate strain is believed to influence bone remodelling via direct deformation of bone cells. It was reported that habitual activity produced bone matrix deformation of ~0.2% (Burr et al., 1996). Meanwhile, osteocytes are attached to mineralised matrix via integrins connecting to the arginine-glycine-aspartic acid region of fibronectin. The latter are mechanoreceptors sensing mechanical forces experienced by the ECM during loading and communicate those intracellularly via focal adhesions (Choi et al., 2022). In turn, focal adhesions transmit signals to the cell nucleus via secondary downstream biomolecular cascades inducing a corresponding change in protein transcription and leading to either osteoblast or osteoclast activation (Turner & Pavalko, 1998). Other communication pathways include cadherins and catenin complexes providing the cell-to-cell adhesion of osteoblasts, mechanosensitive ion channels and others (Alfieri et al., 2019).

Furthermore, mechanotransduction occurs via shear stresses induced in cells by the interstitial fluid flow within the lacunocanalicular network (LCN) (Qin & Hu, 2014). *In vitro* studies using flow-perfusion bioreactors showed that shear stresses stimulated

osteogenic differentiation of rat marrow stromal/stem cells (MSCs). Those were collected from the bone marrow in the presence of osteogenic supplementation, generating more matrix mineralisation compared with cell cultures not subjected to shear stresses (Datta et al., 2006; Sikavitsas et al., 2002). Similarly to the direct substrate deformation mechanism, integrins and focal adhesions are believed to be involved in mechanoreception via interstitial fluid flow (Alfieri et al., 2019). The latter activate several signalling cascades important in bone remodelling. These include but are not limited to the mitogen-activated protein kinases, focal adhesion kinase and G-protein mediated signalling (Turner & Pavalko, 1998). Additionally, bone cells experience pressure fluctuations in interstitial fluid during loading, also known as cyclic hydraulic pressure producing a normal strain (Liu et al., 2010). Gardinier et al. (2009) demonstrated cyclic hydraulic pressure-mediated microtubule reorganisation in MC3T3-E1 osteoblast-like cells and suggested that the response of osteoblasts to cyclic hydraulic loading differed from that to shear stresses, since the latter induced a breakdown of microtubules.

1.2.2.3 Mechanosignalling in bone healing

Mechanosignalling is crucial in bone repair following a fracture, as it is initiated by mechanical deformation of the entire bone (Augat et al., 2021). This phenomenon inspired the development of distraction osteogenesis, a therapeutic method which significantly improved the outcomes of severe fractures and bony deformities (Spiegelberg et al., 2010). Since bone fractures typically result in a period of prolonged rest, the mechanical loading of affected bones is significantly reduced. In contrast,

distraction osteogenesis operates by separating the two fracture fragments by 1 mm daily using an external fixation device, also known as the Ilizarov frame which imposes mechanical strains on a healing bone. This stimulation leads to the formation of a fibrous interzone known as soft callus. Primarily composed of collagen type 1a, the callus subsequently mineralises producing new bone tissue. It is evident that biomechanical conditions are important in both controlling bone turnover in health and in fracture repair.

1.3 Bone healing

Uniquely, bones are capable of regeneration without fibrous scar formation contrasting with the majority of tissues in the human body (Marsell & Einhorn, 2011). The bone healing process involves four major stages: haematoma formation, fibrocartilaginous callus formation, mineralised callus formation and remodelling.

1.3.1 Haematoma formation

Bone fracture is immediately followed by the acute inflammatory phase resulting in formation of a haematoma lasting for ~5-7 days. It forms due to the ruptured blood vessels releasing blood at the fracture site, which then undergoes fibrin-mediated blood clotting (Figure 1.3A). Proinflammatory cytokines recruit numerous white blood cells at the injury site, however their exact role in bone healing is not clear. Some authors describe the involvement of these cells in mesenchymal progenitor cell signalling for subsequent chondrogenic and osteoblastic differentiation which are the main coordinators of soft and hard callus formation (Baht et al., 2018). These are mostly

derived from bone marrow and periosteum (Bahney et al., 2019). Meanwhile, others report the role of macrophages and neutrophils in digestion of tissue debris produced at the fracture site (Bahney et al., 2019). Interestingly, macrophage depletion induced via Fac-induced apoptosis in mice demonstrated poor callus formation and delayed union of bone fractures, further highlighting the importance of immune cells in healing (Raggatt et al., 2014). Additionally, lymphocytes are thought to release vascular endothelial growth factor (VEGF) which promotes angiogenesis at fracture sites (Sheen & Garla, 2019).

1.3.2 Fibrocartilaginous callus formation

In the subsequent phase of bone repair, a soft cartilage callus forms (Figure 1.3B). Firstly, granulation tissue is produced at the haematoma site - a flexible fibrin-rich gel-like structure formed primarily by chondrocytes providing mechanical stability to the non-immobilised fracture. Meanwhile, endothelial cells promote angiogenesis principally via the VEGF pathway to provide a stable blood supply to the tissue while osteoblasts begin to mineralise the callus adjacent to the periosteal layer (Baht et al., 2018). Following formation of the fibrovascular callus after ~11 days post-fracture, chondrocytes undergo a morphological transformation into a terminal hypertrophic state. These are involved in vascularisation and osteogenic differentiation of progenitor cells by synthesising ALP, VEGF, OSX, OPN and others. It is believed that these cells undergo apoptosis during hard callus formation. However, the latest observations indicated the transition of some hypertrophic chondrocytes (HC) into osteoblasts and osteocytes in later stages of bone healing (Yang et al., 2014). This suggests the possible

contribution of chondrocytes to the osteoblast and osteocyte pool at the fracture repair site, which are involved in mineralisation of the soft callus.

1.3.3 Mineralised callus formation

The fibrocartilaginous callus stabilises the fracture allowing formation of a bony callus at approximately 11-28 days after fracture (Figure 1.3C). Then, the callus mineralises via endochondral ossification under the influence of bone morphogenetic proteins (BMPs) synthesised by HC and endothelial cells (Yu et al., 2010). Meanwhile, more osteoprogenitors recruited by the immune cells undergo osteoblast and osteoclast differentiation via the RANKL pathway (Sheen & Garla, 2019). Then, osteoblasts deposit bone mineral, forming immature woven bone tissue, while osteoclasts resorb the mineralised fibrocartilaginous callus. Gradually the latter is fully replaced by bone tissue, allowing greater stability at the fracture site.

1.3.4 Remodelling

The final and longest stage of bone repair is remodelling, lasting for up to 2 years (Figure 1.3D). Immature bone formed earlier undergoes further resorption and bony deposition through the coupled action of osteoblasts and osteoclasts (Baht et al., 2018). Here, mechanotransduction of bone cells plays one of the central roles ensuring optimal bone architecture for the loads it is subjected to. Thus, an increase in mechanical loading is necessary to promote bone remodelling (Ghiasi et al., 2017). This phenomenon gives rise to the use of external physical stimulation to accelerate this long process. Following the bone remodelling stage, a mature lamellar bone forms with

a central medullary space, completely regaining the weight-bearing capacity of the bone (Marsell & Einhorn, 2011).

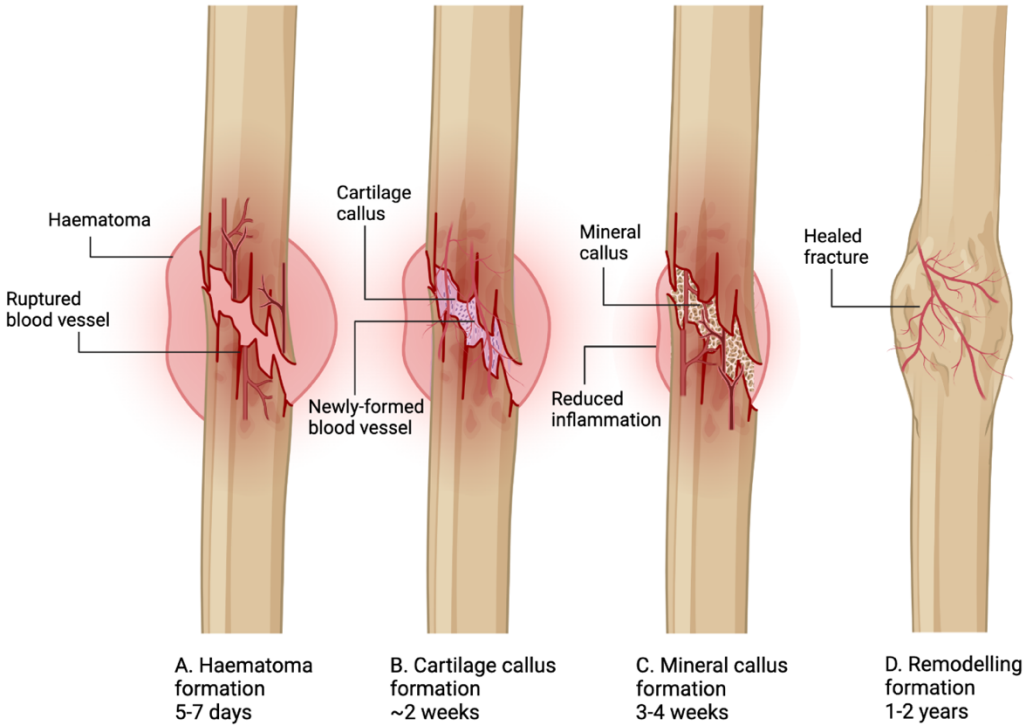

Figure 1.3: Schematic representation of the bone healing process, depicting the stages of (A) inflammation, (B) soft callus formation, (C) hard callus formation, and (D) bone remodelling.

1.3.5 Direct and indirect bone repair

Depending on the degree of fixation of fractures, bone repair can occur via two routes – direct (primary), where osteoblasts are formed by osteogenic differentiation from MSCs or indirect (secondary) healing where a newly formed cartilage is mineralised forming bone tissue. Unlike indirect healing, direct fracture repair does not involve soft callus formation. Moreover, it is characterised by a less pronounced inflammatory phase allowing newly recruited osteoblasts to produce mineralised matrix via intramembranous ossification shortly after the injury (Baht et al., 2018). Most bone fractures heal via indirect healing (Bahney et al., 2019), however direct healing is

possible too given suitable fracture fixation and immobilisation. This can be achieved with a cast, brace, or splint or in the case of highly unstable fractures using internal fixation devices, such as intramedullary nails, screws or wires (Sheen & Garla, 2019).

1.4 Bone substitutes in orthopaedic surgery

1.4.1 The need for bone replacement

Although most skeletal fractures can heal naturally given an appropriate timeframe and suitable immobilisation, it can take from several weeks up to months for a patient to return to normal everyday activities. Moreover, approximately 10% of all injury cases result in delayed healing, malunion or a non-union (Rupp et al., 2018). In these extreme cases of trauma or damage, where the natural healing ability of bones is not capable of repairing the extent of damage, an alternative is necessary to promote bone formation and regaining of function. These cases may occur due to impaired blood supply, infection, cancer, or trauma resulting in significant bone loss (Fernandez de Grado et al., 2018).

1.4.2 Bone grafting

The options for promoting bone formation include bone grafts, delivery of growth factors or synthetic implants. Autografts are the most common choice for bone replacement in dentistry and involve harvesting bone tissue from the same patient receiving the transplant. One of the primary limitations of autografting is the restricted availability of bone volume for transplantation. Consequently, iliac crest is frequently chosen as the donor site due to its sufficient supply of bone tissue (Kumar et al., 2013).

Other options may include tibia, radius and greater trochanter (Myeroff & Archdeacon, 2011). Nevertheless, autografts are considered the best osteogenic bone-substituting material. This is due to the living cells in bone maintaining the tissue and assisting with bone healing. Additionally, these grafts present a lower risk of transmitting infectious diseases or immune rejection. On the other hand, allografts originate from a different human donor but carry infection transmission and immune rejection risks, which are even higher from tissues obtained from animals termed xenografts.

1.4.3 Titanium as a bone and tooth replacing biomaterial

The major limitations of bone grafting catalysed the development of synthetic bone substitutes. These have a long history in medicine with evidence of bone replacement emerging as early as in the 6th century BCE and materials ranging from wood to metal alloys (Hampel et al., 2022). Titanium and its alloys are used to both replace or interact with bone both in orthopaedics and dentistry, respectively (Tapscott & Wottowa, 2020). In both orthopaedic and dental applications, titanium biomaterials facilitate the restoration of missing teeth or bones. However, significant differences exist between the two regarding their applications, material properties, and surgical techniques. Orthopaedic implants include a variety of devices, such as intramedullary nails and femoral stems for hip replacement; femoral, tibial, and patellar components for knee replacement; as well as constituents of shoulder and spine implants. Whereas dental implants are usually inserted into the jawbone to replace missing teeth. A further key distinction is the load-bearing requirement, with dental titanium implants typically subjected to lower forces, compared to their orthopaedic counterparts. Furthermore,

orthopaedic implants, particularly those used in joints are subjected to repetitive loading and significantly higher friction relative to the dental implants. Therefore, the material utilised must exhibit wear-resistant properties. The differences in material requirements between the dental and orthopaedic implants are reflected in the use of various titanium grades and alloys. The most common Ti-based material used in orthopaedics is Ti6Al4V (Ti64) alloy due to its superior strength, whereas dental implants are typically produced from commercially pure titanium (cp-Ti) (Hou et al., 2022).

1.4.3.1 Osseointegration of titanium-based biomaterials

In contrast with other metals used in bone replacement, including stainless steel and cobalt-chromium alloys, Ti-based implants uniquely demonstrate so-called "osseointegration". Branemark (1983) described this as a direct contact between bone and the implant surface, which is usually not observed with other metals where the connection between bone and the implant is mechanical, rather than biological. However, this statement is somewhat inaccurate, since there is a fine layer of proteoglycan between the collagen fibres and the titanium oxide layer (Parithimarkalaignan & Padmanabhan, 2013). Nevertheless, the major advantage of osseointegration is the additional biological stability (secondary stability) of the implant adding to the mechanical stability (primary stability) initially provided by the implant geometry and fixation (Bosshardt et al., 2017). This ensures a long-lasting implantation and a lower risk of both early and late failure (Parithimarkalaignan & Padmanabhan, 2013). While the exact mechanism behind the osseointegration ability

of titanium-based biomaterials remains incompletely understood, it likely stems from a combination of factors. These factors include the material's optimal mechanical properties, its chemical stability in the physiological environment, and a low tendency to elicit an immune response. Failure to satisfy any of these criteria markedly reduces the probability of successful osseointegration of the implant. For example, 316L stainless steel possesses several favourable mechanical properties for bone replacement, such as high modulus of elasticity, strength, and stiffness (Eliaz, 2019). However, it exhibits lower corrosion resistance, when compared with titanium-based implants. The products of corrosion released into the implantation site trigger inflammation, delayed bone healing, poor implant stability and even tissue necrosis (Plecko et al., 2012). These characteristics hinder the successful osseointegration of stainless steel-based implants, whereas the optimal properties of titanium biomaterials discussed further facilitate it.

1.4.3.2 Physical and chemical properties of Ti contributing to osseointegration

Other key material characteristics of titanium alloys include resistance to corrosion due to the oxide layer, which is possibly a contributor to its hypoinflammatory and inert nature. However, it is worth mentioning the disadvantages of titanium biomaterials which limit use in certain applications. For instance, Ti implants are not used in areas of high friction, such as femoral heads due to poor wear resistance to avoid an immune response to wear debris (Hu & Yoon, 2018). In some cases, surface treatment is used to improve Ti material wear, e.g., ion implantation, plasma spraying and chemical coating (de Viteri & Fuentes, 2013). Furthermore, there is a mismatch

in Young's modulus of bone and Ti leading to stress shielding of bones and subsequent implant loosening (Shi et al., 2013). Stress shielding occurs when implants bear a significantly greater load than the equivalent volume of bone tissue, leading to a reduction in strain on the surrounding bone. This phenomenon can upregulate local bone resorption, potentially compromising the fixation of the implant (Huiskes et al., 1992). Although, there appears to be a directly proportional link between the Young's modulus and the strength of implants which is central for the load-bearing bone replacement (Elias et al., 2008). Fortunately, stress shielding may be addressed by using porous titanium structures which generate an improved strain distribution across the implant (Krishna et al., 2007).

1.4.3.3 Surface topography of titanium-based biomaterials

1.4.3.3.1 Macro, micro and nano-scale surface roughness

Another important factor in bone healing around an implant is surface topography of the material. It is classified according to the degree of roughness as macro, micro and nano-scale topographies (Brett et al., 2004). Macro-scale refers to the geometry of implants within the millimetre scale, e.g., length, shapes, or thread geometry on dental implants. Increased macroroughness provides mechanical retention of implants and therefore good primary stability (Lima de Andrade et al., 2017). Furthermore, reports show that macrodesign of implants also positively affects cell adhesion and spreading (Petrini et al., 2021). Whereas, micro and nanotopographies are described as roughness between 1 and 100 µm and $<$ 1 µm respectively (Matos, 2021). Similarly to macrodesign, these were shown to promote osteoblast adhesion and spreading and

uniquely - osteogenic differentiation as well (Martin et al., 1995; Wu et al., 2011). Likewise, many reports, including the one by Cho et al. (2021) demonstrated upregulated gene expression of *ALP, OCN* and collagen type 1a (*COL1A1*) of by osteoblasts on rougher titanium surfaces of surface roughness, Ra = 1.037 µm. The positive effects of microroughness were suggested to arise from increased protein adsorption to the implant surface. Levin et al. (2022) compared the morphology, adherence and proliferation of MG-63 cells on smooth titanium surfaces and tissue culture polystyrene and did not observe any significant differences. However, the proliferation of cells appeared to be significantly slower when titanium surfaces were chemically roughened.

1.4.3.3.2 Protein adhesion to implant surfaces

Protein adhesion is the very first contact between the implants and the living tissues and it is essential for cell attachment via integrins (Hoffman, 1982). Rougher surfaces have a higher surface area, thus more proteins are able to adhere to an implant. Other than surface morphology, the degree of protein adsorption to a material is influenced by surface chemical composition and wettability, with hydrophobic surfaces allowing a greater level of protein attachment. Other external parameters that affect protein adsorption include pH level of the surrounding fluids, temperature and the local ionic concentration (Rabe et al., 2011). The pH of the interstitial fluid dictates the charge characteristics of both proteins and substrates, thereby defining whether a given protein will be attracted or repulsed from a surface. For instance, positively charged protein residues are attracted to the negatively charged titanium surfaces at the

physiological pH of ~7.4 (Barberi & Spriano, 2021). Finally, the properties of proteins themselves influence the rate of absorption to implants as smaller polypeptides diffuse and reach surfaces more rapidly. Conversely, larger proteins establish a greater quantity of bonds with the substrate, resulting in stronger adhesion. Furthermore, minimising electrostatic repulsion of proteins with similar charges allows higher adsorption to the implant surfaces (Barberi & Spriano, 2021). Importantly, as a part of the dynamic interplay between the implants surface and the surrounding tissues, some of the initially attached proteins desorb, while others adsorb irreversibly (Armstrong et al., 2020). Desorption arises from a variety of contributing factors, encompassing alterations in the chemical composition of the surrounding fluids, competitive binding interactions of alternative proteins leading to the displacement of previously adhered ones, and mechanical strains imposed by the interstitial fluid surrounding an implant (Felsovalyi, 2012). Typically, an equilibrium state between proteins adhesion and desorption is reached, where the protein profile on the implant's surface remains relatively stable. Consequently, protein desorption affects the interaction between bone cells and the implant and may affect its short- and long-term success.

1.4.3.3.3 Implant surface modifications

Surface topography of Ti-based implants is routinely modified via chemical, mechanical, and physical methods (Jemat et al., 2015). Acid and alkali etching are common chemical surface modification techniques, inducing topographical and chemical modifications of titanium implant surfaces. This, in turn, affects surface

wettability, inducing protein adsorption. Notably, acid treatment not only enhances surface roughness but also serves to eradicate chemical contaminants, as demonstrated by Liu et al. (2004). On the other hand, mechanical surface modification procedures, such as grid blasting, grinding, and machining have been reported too (Jemat et al., 2015). In contrast to etching techniques, these methods refrain from inducing changes in the chemical composition of the surfaces. Instead, their primary effect lies in the augmentation of surface area, achieved through the controlled removal of material fragments (Hou et al., 2022). Additionally, plasma and thermal spraying may be employed as physical methods of titanium-based implant surface medication (Jemat et al., 2015). Plasma spraying involves the deposition of molten titanium particles onto the surface of the implant. Subsequently, as these particles rapidly cool and solidify, they create a roughen implant surface, enhancing osseointegration with the surrounding bone tissue (Vercaigne et al., 1998). Likewise, thermal spraying encompasses the deposition of particles at elevated temperatures, as documented by Talib and Toff (2004), which provided a detailed exploration of hydroxyapatite spraying. Interestingly, contrary to the report by Gabbi et al. (1992) explaining the osteoconductive properties of the hydroxyapatite-coated implants, Daugaard et al. (2013) did not observe a similar outcome in a canine model. In addition, Ti surfaces may be functionalised via immobilised growth factor adhesion prior to the implantation to assist cell attachment (Wang & Khoon, 2013). In the present study, cp-Ti surfaces were acid-etched to increase roughness, Ra to the commonly used ~1 µm.

1.4.3.4 Clinical challenges associated with Ti-based implants

As with fracture repair, the success of the performance of bone-substituting implants is dependent on bone healing around the implant to establish a stable connection. Ultimately, successful bone healing creates an optimal environment for the osseointegration of titanium-based biomaterials into bone. However, the process of bone healing is slow and often requires prolonged periods of immobilisation. Bone healing and the formation of a stable bone-implant interface necessary for loading a dental implant with a prosthesis may take 4-9 months (Villar et al., 2011). Likewise, full hip or knee replacements require approximately 6 weeks of rest before a patient can return to light activities, e.g., short walks, driving. In contrast, the full rehabilitation process following a total hip replacement takes up to 2 years with some patients receiving a life-long recommendation to avoid certain sport activities (Madara et al., 2019). In addition to the prolonged period required for stable osseointegration to occur even in otherwise healthy individuals, there are many factors which inhibit successful recovery after receiving a bone-replacing prosthesis. For instance, even after a successful placement of a prosthetic tooth crown, subsequent excessive loading may result in implant failure especially in the presence of low bone quantity and quality. It is a particular concern in patients suffering from osteoporosis due to the imbalance in bone remodelling resulting in lower mineral density (Kochar et al., 2022).

1.4.3.5 Causes of osseointegration failure of Ti-based implants

Given the improvements in implant design and fixation techniques over the years, the success rates of Ti-based implants are remarkable (Hu & Yoon, 2018). The primary (early) and secondary (late) failure rates of dental implants are as low as 2% and 5%

of clinical cases respectively (Matos, 2021). Similarly, total hip replacements are reported to have 10 and 15-year survival rates of 85% and 75% respectively (Apostu et al., 2018). Nonetheless, in the unfortunate event of implant failure, the risk of severe complications is significantly high. These are classified into primary and secondary implant failures. The primary failure is often a result of the prosthesis' inability to successfully osseointegrate into the surrounding bone shortly after placement. This can be attributed to factors such as insufficient bone quantity or quality due to prior traumas or radiotherapy-induced bone loss, leading to diminished local bone density. Additionally, improper implant fixation due to surgical technique during the initial placement may contribute to this outcome (Annibali et al., 2008). The secondary failure relates to the challenges in maintaining osseointegration over an extended period (Kang et al., 2019). Comparable to failures in bone healing following an injury, secondary failure most likely arises due to a combination of factors. These include but are not limited to bacterial infections causing peri-implantitis and a consequent failure; inadequate new bone formation around the implant; mechanical overloading of implant and implant fracture (Annibali et al., 2008).

1.5 Medical ultrasound

1.5.1 Introduction of mechanotransduction in bone via non-invasive therapeutic modalities

As evident from the above (4.5.6.1), there is a demand for a non-invasive therapeutic method to improve and accelerate bone healing. Since mechanical loading experienced by bones results in upregulation of bone deposition and vice versa, the majority of

current non-surgical techniques rely on local delivery of energy to the fracture site. A number of *in vitro* studies provided further evidence for this approach. For example, interstitial fluid flow generated by mechanical stress was found to increase the intracellular concentration of cyclic adenosine monophosphate (Reich et al., 1990), one of the key secondary messengers in osteogenic signalling (Ju et al., 2021). Whereas Yourek et al. (2010) demonstrated *in vitro* osteogenic differentiation in human mesenchymal stem cells initiated by the shear force of fluid flow. The notion of mechanotransduction drove researchers to study the application of non-invasive physical modalities to enhance bone deposition. Localised electrical impulses at the fracture site were one of the first investigated forms of energy applied to non-unions with reports dating back as far as 1841 (Nelson et al., 2003). The report described the application of "shocks of electric fluid," which are now understood to be a flow of electric charge. These shocks were applied longitudinally and transversely through the affected bone, leading to a "perceptible" improvement in fracture healing within two weeks. Fukada and Yasuda (1957) reported the piezoelectric properties of bone by observing the generation of electric charges when shear forces were applied. This suggested that mechanical force was transformed into an electrical impulse which in turn, could be responsible for the upregulation in bone remodelling. Indeed, later articles continued to demonstrate an improved fracture healing *in vivo* following treatment with direct current (Aaron & Ciombor, 1993; Friedenberg et al., 1971). Eventually, direct current was given FDA approval in the USA for treatment of non-unions in 1979 (Nelson et al., 2003). Other non-invasive therapeutic modalities

targeting mechanotransduction of bone cells included whole/partial body vibrations. One of the reports described 20 min daily oscillations of the hind limbs of sheep at 30 Hz for 5 days. Whole-body resonance approach was used, while the forelimbs of animals were rested on a stationary structure, surrounded by an active plate to be as control. After conducting dual-energy X-ray absorptiometry, the researchers observed the de novo formation of trabecular bone and an increase in bone mineral density of up to 32% in the treated areas (Rubin et al., 2002). Castillo et al. (2006) described a significant increase in the trabecular mass of mice ulnae following vibrational stimulations between 0-50 Hz. Nevertheless, the clinical efficacy of either electric stimulation or vibrations on bone healing remains disputed (Nelson et al., 2003; Wang et al., 2017).

In the search for an effective and non-invasive accelerated fracture healing treatment, the mechanotransduction potential of ultrasound was also explored. Corradi and Cozzolino (1953) had discussed the use of ultrasound as a source of mechanical vibration to promote bone remodelling. The study described an increased rate of periosteal callus formation following a series of treatments with continuous ultrasound at a frequency of 800 kHz and an intensity of 1.5 W/cm^2. Since then, similarly to other external stimulation methods discussed earlier, many studies have been published demonstrating and challenging the therapeutic effects of ultrasound both *in vivo* and *in vitro*. The present study will explore the evidence provided in these investigations.

1.5.2 Brief history of ultrasonics

1.5.2.1 Discovery and first industrial applications of ultrasound

The use of ultrasound was first reported in the late 18th century by the Italian biologist, Lazaro Spallanzani, who observed echolocation in bats. When blindfolded, the animals were able to orient in space, but this ability ceased when their ears were covered with wax. The researcher deduced that bats primarily depended on their sense of hearing for navigation, utilising sound frequencies that were beyond the range detectable by the human ear (Singh & Goyal, 2007). Nevertheless, there was a lack of substantial scientific advancement in the field of ultrasonics for nearly another century. Later, Pierre and Paul-Jacques Curie (Curie & Curie, 1880), discovered the piezoelectric effect in crystals of quartz, enabling ultrasound generation in a laboratory. However it was not until World War I when ultrasound was first practically applied in submarine echolocation (Kang et al., 2012) that research in the use of ultrasound became more established.

1.5.2.2 First medical applications of ultrasound

1.5.2.2.1 Diagnostic ultrasound

The first documented application of ultrasonics in diagnostics was developed by Dussik (1948). That work, also known as "hyperphonography of the brain" used a through-transmission technique for visualisation of brain tumours, where ultrasound-emitting and receiving devices were placed on either side of the patient's head. The power of the output wave was compared with the received waves and identified ultrasound attenuation. The energy absorbed when ultrasound was passing through the brain tissue was lower than the one passing through the ventricular fluid. The energy was

represented by dark areas on the heat-sensitive paper, with darker patches signifying lower energy absorption and therefore less attenuation. Larger fluid-filled ventricles were perceived as darker patches, which could potentially indicate the presence of a tumour (Campbell, 2013). Another milestone in medical ultrasonics was by Ian Donald's laboratory at the University of Glasgow (Donald et al., 1958) who described the first use of pulsed ultrasound scanning in obstetrics and gynaecology with A-mode scanning at a frequency of 2 MHz, followed by the development of the compound B-mode scanner. The difference between the A- and B-modes lies in the information they provide through sound echoes. A-mode ultrasound operates by analysing the amplitudes of echoes reflected from tissues, with their magnitudes varying based on the tissue's depth. This mode is useful in identifying organ and tumour dimensions, as well as for therapeutic applications on target tissues. On the other hand, B-mode ultrasound, the mode more frequently employed, generates two-dimensional images. Within these images, signal strength is translated into brightness, allowing for a visual representation of tissue structures (Carovac et al., 2011). In 1968, Feigenbaum and Dodge introduced the motion, M-mode scanning, which found its application in cardiology. Here, the echoes are plotted against depth and time on an oscillograph, allowing a real-time evaluation of tissues (Maleki & Esmaeilzadeh, 2012). Furthermore, in the 1970s, the Doppler effect in ultrasound found a significant clinical application in the imaging of vascular structures. This technique utilises the alteration of wave frequency when sound waves are reflected off the moving red blood cells. Depending

on the direction of the cells' movement, this frequency shifts, generating either a color-coded representation or a graph depicting flow velocity over time (Moorthy, 2002).

1.5.2.2.2 Therapeutic ultrasound

Therapeutic ultrasound was introduced into medicine in the late 1930s when several physicians including Reimar Pohlman researched the pain relief effects of ultrasound. Pohlman observed a relief in back pain in patients after a course of ultrasonic treatment at an intensity of 5 W/cm^2. Likewise, in 1932, H. Freundlich, K. Collner, and F. Rogowski suggested that the application of ultrasound to tissues induces a therapeutic response (Bachu et al., 2021). In 1942, (Lynn et al.) proposed utilising focused ultrasound beams to non-invasively achieve a localised effect on the brain. The objective of the treatment was to induce tissue destruction of target brain regions while avoiding skin and skull injury. Despite several attempts to investigate the therapeutic potential of ultrasound in the 1930s and 1940s, the clear medical demand for diagnostic tools likely diverted resources away from therapeutic ultrasound. This, coupled with the significant disruption in scientific communication caused by World War II, may have further marginalised the development of ultrasonic therapy (Fyfe & Bullock, 1985).

The enthusiasm for therapeutic ultrasound for tissue healing finally took off a few years later. Lehmann's *in vitro* and *in vivo* studies on pig tissue in 1950s assessed the importance of heating in ultrasonic therapy. The work proposed that the therapeutic benefits of ultrasound could only be attained in the presence of specific temperature increases of tissues (Cambier et al., 2001). Nevertheless, it was also acknowledged that

the occurrence of cavitation during tissue exposure triggered diverse biological effects, including DNA degradation and perforation of cell membranes (Wells, 1977). Focused ultrasound in ablation of basal ganglia, gave rise to a diverse branch of research into the application of high-intensity pulsed ultrasound (HIFU) in various domains (Fry et al., 1955). The research areas included kidney stone, tumour ablation, as well as glaucoma treatment (Burgess et al., 1986). Whereas, by the 1970s therapeutic ultrasound was applied in physiotherapy and cancer therapy (Miller et al., 2012). In 1988, the first FDA approval was granted for an ultrasound-based therapy for glaucoma. However, this treatment modality was later succeeded by laser therapy (Haut et al., 1990). Later applications involved blood-brain barrier penetration, immune response modulation against tumour cells, and chemotherapy drug delivery.

Nowadays, ultrasound is recognised as one of the key instruments in the field of medical physics. Ultrasonography stands as the primary method for foetal diagnostics in pregnant women, while other applications of medical ultrasound offer promising avenues for research and exploration.

1.5.3 Introduction to acoustics

1.5.3.1 Sound waves

Ultrasound is a mechanical vibration of frequencies above the usual human audible range, i.e., >20 kHz. This form of energy exists as longitudinal waves and the frequency of the wave describes the number of compression-rarefaction cycles undergone per second i.e. the number of times a wave repeats itself per second (Patey & Corcoran, 2021), whilst wavelength is the length of a cycle repeat. The amplitude of a sound

wave is measured in decibels (dB) and refers to its relative strength, also described as loudness (Figure 1.4).

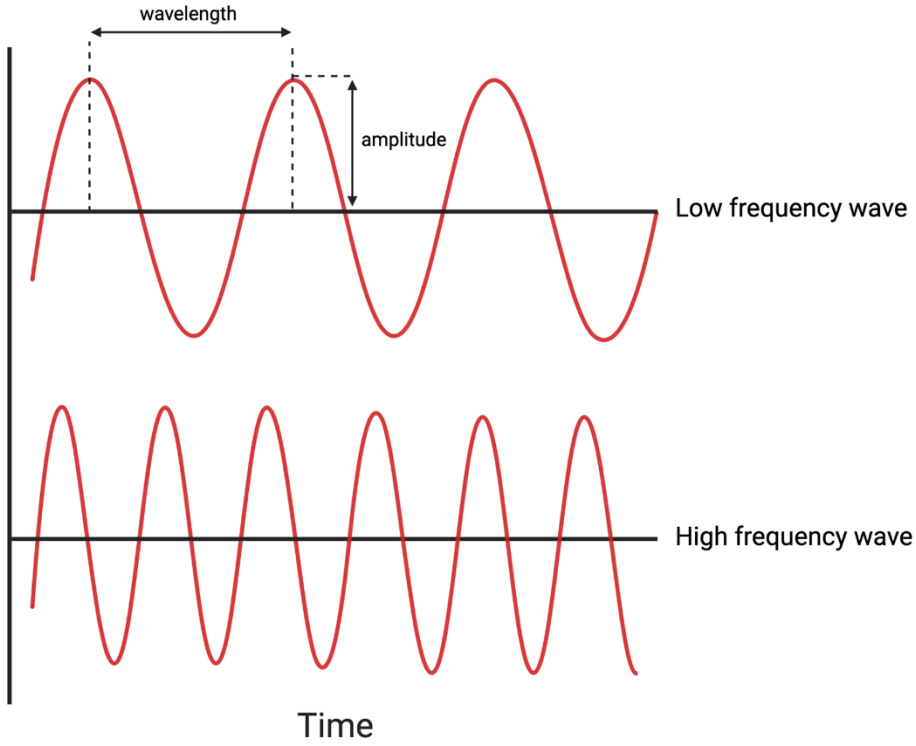

Figure 1.4: Graphical depiction of ultrasound waves, showing wavelength and amplitude. Waves with higher frequency produce a greater number of complete wave cycles per second.

1.5.3.2 Piezoelectric materials

Ultrasound is produced by piezoelectric materials by converting electric charge into a mechanical vibration because of a converse piezoelectric effect. This mechanical deformation happens as a result of the displacement of charged particles, which then exert physical forces on neighbouring atoms and ions (Arnau & Soares, 2008). Ultimately, this process leads to a change in the material's shape or a vibration, which propagates as an ultrasonic wave. Piezoelectric materials are classified into single crystal materials and polycrystals. Quartz stands as a prime example of naturally

occurring single crystal ceramics with piezoelectric attributes. Nonetheless, it is noteworthy that quartz-based transducers often utilise artificially produced quartz due to its diminished inclusion ratio and elevated production yields (Saigusa, 2010). Lead zirconate titanate (PZT) is a polycrystal demonstrating superior piezoelectric performance to quartz and is the most common choice for the ultrasonic transducers used in medicine (Zhou et al., 2014). Namely, PZT demonstrates a greater piezoelectric coupling coefficient, which defines the degree of mechanical energy generated as a result of electric input (Arnau & Soares, 2008). Other polycrystalline options include PZT derivatives PZT-5H and PZT-4, or polyvinylidene fluoride (PVDF).

1.5.3.3 Attenuation of ultrasound

When an object is exposed to a sound wave it oscillates to the frequency of that wave due to the changing pressure areas. As ultrasound encounters boundaries between the transmission media, its waves are absorbed by a material and converted into thermal energy (Hauff et al., 2008). Nevertheless, a portion of the energy will not propagate through the exposed object and instead becomes lost due to wave attenuation. There are three possible attenuation scenarios - reflection, absorption, or scattering (Figure 1.5).

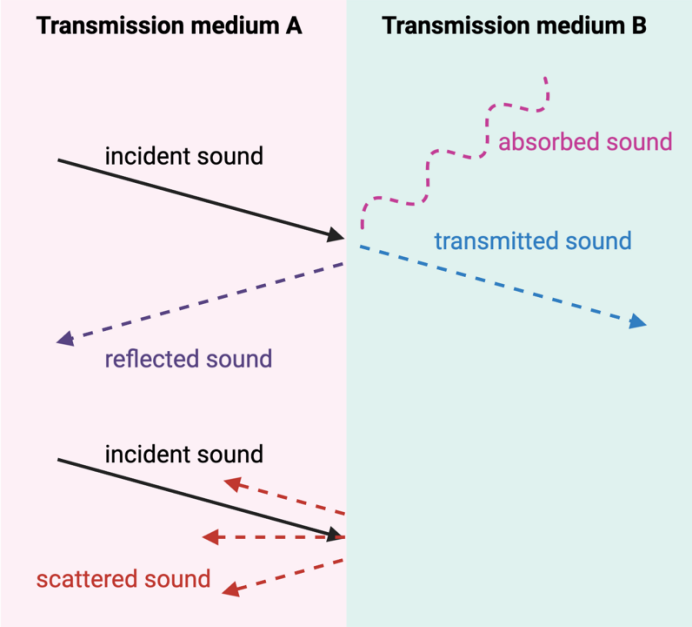

Figure 1.5: Diagram demonstrating the potential behaviour of sound waves encountering different transmission media. When the transmission media have varying acoustic impedances, waves may be absorbed, reflected, or scattered. This contrasts with direct wave transmission, which occurs in media with similar acoustic impedance.

When a wave is reflected, it returns to the source producing an echo and, in some cases, standing waves. The challenges produced by the latter in exposing cells to ultrasound will be explored later in this chapter. Refraction is a similar phenomenon to reflection, however when sound is refracted the change in the incident angle is less prominent relative to the transmission angle. Furthermore, scattering occurs on rough surfaces and heterogeneous transmission media causing sound waves travelling in geometrically unpredictable directions. Wave attenuation occurs due to the difference in acoustic impedance between materials, which is described as resistance of sound energy to pass through a medium defined by its density and elasticity (Patey & Corcoran, 2021). For instance, tissues with higher density such as bones will have a higher acoustic impedance than muscle tissue. Foreseeably, acoustic impedance

mismatch creates difficulties in medical ultrasound applications as waves attenuate and lose energy. Coupling gels are commonly used in epicutaneous ultrasound applications to avoid the boundary between air and skin (Afzal et al., 2022). However, it is significantly harder to address attenuation subcutaneously.

1.5.3.4 Sound propagation in biological tissues

Biological tissues are highly heterogeneous at both cellular and molecular levels, varying in composition, elasticity, and density. These differences introduce additional complexities in sound wave attenuation and propagation speed, which in turn complicate the delivery of a defined and adequate dosage of ultrasound to the target organ. Furthermore, factors such as the depth and thickness of anatomical locations, as well as individual body size variations, affect sound transmission. Predicting wave attenuation and the portion of energy delivered to the target organ poses challenges, especially when encountering bone and metallic surfaces. Bones possess a considerably higher stiffness relative to soft tissues, resulting in increased scattering of ultrasonic waves when they encounter bone tissue. Whereas titanium-based materials are prone to reflecting ultrasound waves. There are several approaches of predicting ultrasonic wave transmission within the body described by Jaros (2019). Numerical methods, such as finite-element method, boundary-element method and finite difference method, involve mathematical modelling of sound transmission, taking into consideration mechanical tissue properties. While flexible and cost-effective, these methods require a high degree of expertise to simulate complex tissue geometry and heterogeneity. These often result in simplifications and assumptions, which in turn introduce uncertainties

in sound transmission models. Alternatively, experimental models may be produced for validating data obtained from numerical models. Such models often include tissue-mimicking materials or animal specimens to simulate sound transmission in a physiologically relevant environment. Thermocouples, hydrophones, or pressure sensors are commonly utilised to quantify the delivery of energy to a target depth within tissues. Despite their utility, experimental models have limitations in replicating the dynamic nature of living tissues.

1.5.4 Current applications of ultrasound in medicine

The diverse range of applications of ultrasound in medicine stems from the correlation between the biological response of living tissues and factors such as ultrasonic wavelength, wave frequency, velocity and intensity. Most of the medical ultrasonic devices discussed in the literature operate within the megahertz frequency range (Sun et al., 2001; Uddin & Qin, 2013). Nevertheless, several studies have revealed that low frequency ultrasound (LFU), below 100 kHz, can also exhibit advantageous biological effects, including elevated nitric oxide and prostaglandins formation (Conner-Kerr et al., 2015; Miller et al., 2012; Reher et al., 2002). These are believed to be involved in the mechanically stimulated bone formation.

1.5.4.1 Destructive ultrasound

Additionally, medical applications of ultrasound vary depending on the intensity. Destructive ultrasound is utilised within the intensity range of 5-300 W/cm^2 (Table 1) in both megahertz and kilohertz frequencies. However, these intensities are harmful for living tissues, hence destructive ultrasound is used in medical procedures where tissue

ablation is required. High intensity focused ultrasound (HIFU) operates at ~1.5 MHz wave frequency and is used in tumour ablation and glaucoma treatment (Kim et al., 2008). Other modes, including the continuous delivery of high intensity ultrasound in the kilohertz frequency range are commonly applied for operative cutting and intracorporeal lithotripsy (Miller et al., 2012). Furthermore, ultrasonic shockwave therapy is used for renal extracorporeal lithotripsy where mineralised kidney stones are separated into small fragments (Manzoor & Saikali, 2023).

1.5.4.2 Diagnostic ultrasound

Diagnostic ultrasound devices utilise much lower intensities of between 0.05 and 0.5 W/cm^2, with a wave frequency of 3-10 MHz (Carovac et al., 2011) (Table 1). In comparison with HIFU, diagnostic ultrasound being non-invasive and free from potential thermal and destructive side effects, makes an excellent imaging method for visualising subcutaneous soft tissues. Furthermore, unlike X-ray imaging and computer tomography, diagnostic ultrasound offers the advantage of eliminating the need for exposing patients to potentially harmful ionising radiation.

1.5.4.3 Therapeutic ultrasound

The need for a therapeutic technique with minimal invasiveness and thermal damage has led to the development of therapeutic ultrasound utilising intensities <3 W/cm^2 (Table 1). Therapeutic ultrasound can be categorised into two modes based on the duty cycle: continuous mode and pulsed mode, each serving distinct purposes in delivering ultrasound therapy. Continuous exposure is maintained without interruption for a duration of approximately 5-20 min per treatment. In contrast, pulsed output is

emitted in brief bursts followed by intervals of no emission. According to Uddin et al. (2021), a traditional, continuous application of therapeutic ultrasound has been shown to facilitate angiogenesis, promote fibroblast and chondrocyte cell proliferation and enhance chondrocyte migration. This mode of ultrasound therapy is commonly employed for chronic wound management, pain management and orthopaedic therapy, as reported by Baker et al. (2001). In contrast to the continuous doses of ultrasound used in HIFU, low-intensity pulsed ultrasound (LIPUS) is often applied with the following parameters: intensity of ~25-250 mW/cm^2, 200-second pulses, pulse ratio of 1:4, pulse frequency of approximately 1 kHz and a treatment duration of up to 20 min per day (Padilla et al., 2014). By employing a pulsed output and limiting ultrasound exposure, the resulting temperature increase is kept to a minimum, ensuring that the biological effects of ultrasound are primarily limited to non-thermal effects. This approach helps to mitigate any potential risks associated with excessive heat generation during the procedure. LIPUS is operated at a 1-3 MHz wave frequency (Rubin et al., 2001) and has been used in physiotherapy, where it aids in promoting ulcer healing, angiogenesis, integration of skin grafts, sonodynamic drug delivery, pain relief and importantly, the acceleration of bone tissue regeneration (Rubin et al., 2001). This wide range of therapeutic applications highlights the diverse benefits of LIPUS in clinical practice (Pomini et al., 2014). The primary objective of the current study was to investigate the impact of therapeutic ultrasound on osteoblasts attached to titanium *in vitro*. The former has the potential to contribute to the understanding of the underlying mechanisms involved in ultrasound therapy on bone tissues.

	Frequency range	Intensity range
Diagnostic ultrasound	3-10 MHz	0.05 and 0.5 W/cm^2
Therapeutic ultrasound	1-3 MHz	<3 W/cm^2
LIPUS	20-200 kHz/0.7–3.0 MHz	25-250 mW/cm^2
HIFU	1-4 MHz	5-300 W/cm^2

Table 1: Approximate ranges of ultrasound frequencies and intensities commonly employed in various medical applications.

1.5.5 Biophysics of medical ultrasound

Ultrasound can cause biological changes via thermal and non-thermal effects (Pomini et al., 2014). Although it is highly likely that during ultrasonic exposure, cells experience both thermal and non-thermal effects simultaneously, it is essential to understand the cell response produced by each individually, particularly when conducting *in vitro* research. Thermal effect involves a local temperature increase whereas, non-thermal or mechanical effects produced by the ultrasonic stimulation involve cavitation and acoustic streaming (Figure 1.6).

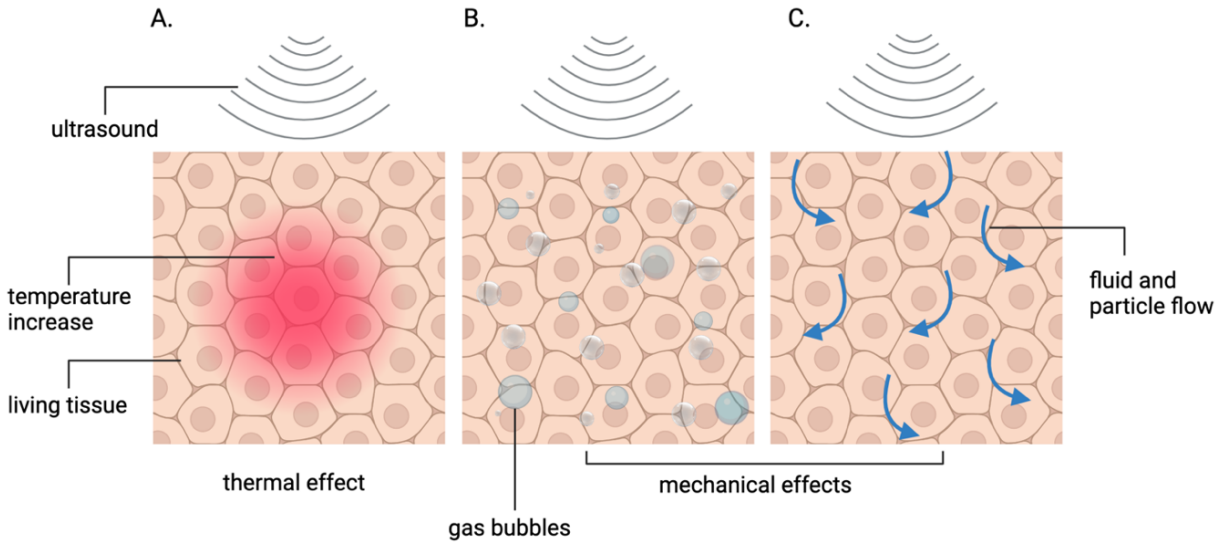

Figure 1.6: Graphical depiction of the thermal and mechanical effects of ultrasound, showing three possible outcomes: (A) a localised temperature increase of a tissue, (B) cavitation resulting from the vibration and potential collapse of gas bubbles, and (C)

acoustic streaming where propagating sound waves generate fluid and particle movement within the tissue.

1.5.5.1 Thermal effect of ultrasound therapy

Thermal effects take place when biological tissues absorb ultrasonic energy which is converted into heat producing a local hyperthermia. The range of temperature increase lies within 1-4°C, however the precise value depends on the duration of the treatment, physical properties of the treated tissue and the treatment regime (Cambier et al., 2001). However, a further temperature increase may have detrimental effects on living tissues, leading to irreversible protein denaturation. This property is exploited in the field of malignant tumour ablation, where HIFU has been successfully employed, as reported by Guzman et al. (2005).

The thermal effect of therapeutic ultrasound has been reported to be beneficial in wound healing and pain relief with the temperature increase (also known as thermotherapy) suggested to cause vasodilation. The latter causes an increased blood flow leading to a delivery of more oxygen, proteins and nutrients (Nadler et al., 2004). Although the molecular mechanisms of the temperature-mediated pain relief are unclear, one hypothesis suggests a direct local action on nerve endings. An example of which, the transient receptor potential cation channel subfamily V member 1 (TRPV1) receptor belongs to the TRP channel family and is responsible for detection of a range of physical and chemical stimuli. The activation of TRPV1 ultimately results in a painful sensation. However, it is reported that its stimulation may provoke the descending antinociceptive pathway eventually allowing analgesia as identified with

ultrasound therapy (Palazzo et al., 2008). TRPV1 is found in various tissues including neuronal, such as the sensory fibres within bones and non-neuronal, such as skin (Jara-Oseguera et al., 2010). Hashish et al. (1986) produced a double-blind controlled study where patients were subjected to ultrasonic therapy following surgical tooth extraction. It was suggested that the anti-inflammatory or healing action must be attributed to the placebo effect due to the significant results in both the test and control groups. Similarly, Nykanen (1995) did not obtain significant evidence of improved shoulder pain relief following LIPUS therapy at 1 MHz, 1 mW/cm^2 for up to 4 weeks. However, Watson (2006) found the thermal increase from the ultrasound stimulated tissue inflammation, i.e. ultrasound presented a pro-inflammatory effect. This agreed with other authors who reported lymphocyte stimulation, angiogenesis and collagen production as a result of ultrasound therapy (Maxwell, 1992; Nussbaum, 1997). Inflammation plays a crucial role in the process of wound healing and ultrasonic stimulation does not exacerbate inflammation but rather optimises it, as indicated by Watson (2006). A further interesting consideration was raised in the report by Baker et al. (2001) arguing that the intensities utilised in therapeutic ultrasound were insufficient to generate a significant thermal effect in tissues beyond the skin or muscle layers. As a result, the author suggested that therapeutic ultrasound may not be effective in the treatment of visceral organs. In contrast, Speed (2001) reported that LIPUS commonly used at 1 MHz was absorbed at depths of 3-5 cm. Alternatively, treatment protocols using long wave ultrasound 45 kHz have been used to achieve a greater depth of penetration that is required in bone healing (Johns, 2002).

Additionally, it is preferable to use a continuous output at higher intensities to achieve a desirable thermal effect, as opposed to LIPUS (Delacour et al., 2019).

1.5.5.2 Cavitation

In addition to its thermal effects, ultrasound also exerts mechanical forces on tissues eliciting a distinct response. Mechanical stimulation of the microenvironment around cells produced by ultrasound causes changes in density and alternating cycles of high and low pressure of the tissue, also known as compression and rarefaction, respectively (Guzman et al., 2005; Huiskes et al., 2000). High rarefaction pressure amplitudes, up to several MPa and decreased wave frequency induce cavitation (Miller et al., 2012). Cavitation, as described by Matos (2021), is a phenomenon characterised by the oscillation of gas-filled cavities in response to the acoustic vibrations produced by the ultrasound waves. These cavities then increase in size and collapse, resulting in shock waves. These are areas of high transient pressures and temperature increase, which have a high potential to damage the surrounding tissues through sonoporation, membrane rupture or temperature-mediated damage (Blackmore et al., 2019; Warnez et al., 2017).

1.5.5.2.1 Stable cavitation

Cavitation can be classified in two distinct types: stable and transient (unstable). Stable cavitation involves the sustained pulsation of gases and requires relatively low ultrasonic intensity of >3 mW/cm^2. These bubbles do not collapse producing a steady microstreaming within the tissue and exerting a gentle mechanical action (Nussbaum, 1997). This could potentially be the key component of the therapeutic nature of

ultrasound. While the mechanism of cavitation on tissue healing is not entirely understood, various effects on cell behaviour have been proposed. Oscillating gas bubbles may exert mechanical forces on the mechanoreceptors of bone cells upregulating remodelling. For example, mechanical stimulation of rat tibia with LIPUS treatment applied for 2 weeks, increased bone density based on computer tomography images (Liu et al., 2018). Furthermore, the study demonstrated a significantly greater bone stiffness in treated bones. Several other *in vivo* investigations found similar effects of ultrasound on bone mechanical properties (Heybeli et al., 2002; Lu et al., 2016; Uddin & Qin, 2015). Webster et al. (1980) reported cavitation-induced increase in collagen synthesis by human embryonic fibroblasts *in vitro*, following a treatment with pulsed ultrasound with a frequency of 3 MHz and intensity of 0.5 W/cm^2 for 5 min. Dinno et al. (1989) found that stable cavitation generated structural changes of plasma membranes of epithelial cells affecting the permeability of calcium ions. These play the role of second messengers in many key cellular processes including cell differentiation and are involved in enzyme activation as a cofactor (Johns, 2002). In addition, the increased permeability of cells has been associated with a local rise in blood pressure contributing to bone healing via oxygen and nutrient delivery (Mundi et al., 2009). Similarly to the elevated temperatures, stable cavitation appears to promote the inflammatory response. LIPUS (1.5 MHz, $30mW/cm^2$, 20 min) was shown to upregulate the production of prostaglandin E_2 (PGE_2) via "mechanical forces" in a mouse osteoblastic cell line, MC3T3-E1 (Kokubu et al., 1999). Secreted by osteoblasts, PGE_2 plays several roles in bone metabolism including mediating bone resorption

during the inflammatory response. Interestingly, PGE_2 is involved in bone deposition at the fracture healing site (Blackwell et al., 2010). In a study conducted by Keller et al. (1993), PGE2 was administered at the osteotomy sites of rabbits, resulting in a dose-dependent enhanced had callus formation. Likewise, the activation of an agonist for the prostaglandin E2 receptor, EP4, induced bone formation in immobilised rat femurs, following bone density measurement. Moreover, Fyfe and Chahl (1984) described an upregulation of the pro-inflammatory histamine release in mast cells of rat's ankle joints following ultrasound therapy at up to 3 MHz, 0.5 W/cm^2. However, the authors did not propose a precise physical mechanism attributable to ultrasound that could account for this observed effect.

1.5.5.2.2 Transient cavitation

On the contrary, transient cavitation involves rapid bubble growth resulting in a violent collapse and involves higher intensities. The collapse is associated with energy release producing a shockwave, which imposes a more pronounced effect on the surrounding biological tissues than stable cavitation (Miller et al., 1996; Xin et al., 2016). Moreover, transient cavitation results in generation of both extracellular and intracellular reactive oxygen species (ROS) (Dyson, 1982). These are a part of the normal cellular metabolism and are formed during the partial reduction of oxygen e.g. in mitochondrial oxidative phosphorylation (Ray et al., 2012). Typically, ROS are counterbalanced by antioxidants, however if an excessive amount of ROS are generated, the state of oxidative stress may occur which results in DNA and RNA damage, peptide denaturation and even cell death (Birben et al., 2012). During bubble

collapse, a sudden energy release produces areas of high pressures of up to several atmospheres, as well as extreme temperatures capable of breaking covalent bonds in water molecules and formation of ROS (Riesz & Kondo, 1992).

1.5.5.2.3 Factors determining the mode of cavitation

Amongst the factors affecting the type of cavitation are the frequency of the ultrasound wave, power, duty cycle and temperature. LIPUS minimises the risk of transient cavitation since gas bubbles can deflate during the "off" periods reducing the pressure in the bubbles (Nussbaum, 1997). Alternatively, a stimulation via transient cavitation can be fatal to cells and is seen in HIFU or cell lysis *in vitro* (Williams & Miller, 1989). Importantly, low frequency of ultrasound increases the likelihood of gas bubble collapse, due to longer waves and greater gaps between compression phases, allowing a larger bubble growth in rarefaction (Coleman & Saunders, 1993). Furthermore, higher acoustic pressures, typically associated with higher intensity ultrasound, create a favourable environment for transient cavitation to occur. Acoustic pressure reflects the degree of compression and rarefaction experienced by the molecules exposed to the sound wave. Therefore, gas bubbles subjected to higher compression undergo a more significant pressure change during rarefaction (Gao et al., 2022). Consequently, they experience more pronounced growth, leading to eventual collapse and the release of energy. The initial size of a gas bubble plays a critical role in determining the acoustic pressure and frequency required to induce bubble growth. This is because initiating bubble growth requires overcoming surface tension forces, which are influenced by the size of the initial bubble (Quarato et al., 2023). However, higher temperatures, often

resulting from the absorption of ultrasound energy by biological tissues, can lead to a reduction in surface tension. This decrease facilitates the growth of cavitation bubbles and increases the likelihood of transient cavitation. Importantly, gas bubble behaviour is also affected the physical properties of biological tissues. Denser and less elastic tissues, such as bone and teeth, exhibit greater resistance to transient cavitation (Church, 2002). This resistance is attributed to the higher forces exerted on gas bubbles within these tissues and their lower tendency to deform elastically under acoustic pressure, in contrast to softer tissues like muscle. As a result, significant bubble growth during rarefaction is limited, reducing the likelihood of bubble collapse. This property is favourable when it comes to the therapeutic application of ultrasound on bone, as it allows for better control over potentially damaging bubble collapse. It is important to recognise that biological tissues with a significant presence of gas particles, such as the lungs or intestine, are particularly susceptible to the detrimental effects of transient cavitation, even at relatively low diagnostic ultrasound intensities (Quarato et al., 2023).

1.5.5.3 Acoustic streaming

Acoustic streaming is an additional non-thermal effect of ultrasound that occurs as a result of sound waves propagating through tissues and generating mechanical pressure and inducing fluid flow. This phenomenon creates a directional movement of fluid particles causing displacement of small molecules and organelles in the ECM and within cells (Conner-Kerr & Oesterle, 2017). Acoustic streaming plays a significant role in various applications of therapeutic ultrasound, such as enhancing drug diffusion,

aiding in the removal of cellular debris, promoting nutrient exchange and facilitating tissue healing (Polat et al., 2011). At higher intensities, such as those involved in HIFU, this leads to the increased flow of extracellular fluid and may result in mechanical tearing of tissues (Johns, 2002). Whereas, in LIPUS acoustic streaming is capable of triggering a response via the cellular signalling pathways, such as Wnt/β-catenin signalling pathway. The latter is fundamental to the bone remodelling process, namely mechanotransduction and may be used for therapeutic purposes to induce bone healing and growth (Miller et al., 2012; Qin & Hu, 2014).

1.5.5.4 Frequency resonance hypothesis

Another non-thermal effect of therapeutic ultrasound on living tissues is termed the frequency resonance hypothesis (FRH). Johns (2002) defined FRH as the direct absorption of ultrasound energy by protein complexes within cells resulting in either a conformational shift or peptide denaturation. This, in turn, produces a change in the cell's signalling pathways. This phenomenon is based on the principle that tissues or structures have unique natural frequencies at which they are most receptive to mechanical stimulation (Fraldi et al., 2015). By applying ultrasound at specific resonant frequencies, therapeutic interventions can be tailored to maximise the desired biological effects. For instance, Blinc et al. (1993) described the acceleration of fibrinolysis of freshly collected human blood where clotting was induced *in vitro* following ultrasonic treatment. The treatment regimen employed in that study used continuous ultrasonic waves in the range of 1-3.4 MHz at an intensity of 0.2-2 W/cm^2 and conducted in a temperature-controlled setting. It was concluded the treatment

upregulated the activity of plasminogen activator (rt-PA), urokinase and streptokinase. These thrombolytic agents play a crucial role in the dissolution of blood clots and are essential for restoring normal blood flow (Ouriel et al., 1995). Similarly, Tachibana and Tachibana (1997) demonstrated enhanced thrombolysis by the urokinase enzyme *in vitro* in the presence of 1.3 MHz continuous ultrasound at 0.3 W/cm^2 for 60 s which suggested activity of the enzyme was altered by ultrasound. However, there are significantly fewer reports available in the literature on FRH employing ultrasound, when compared with cavitation or acoustic streaming and it remains poorly understood. Moreover, it is also important to note that no studies in the English language were found beyond 2002 during the literature search conducted for the present study. Therefore, the frequency resonance hypothesis remains a relatively unexplored notion of ultrasonic therapy.

1.5.6 Ultrasonic cutting in surgery

1.5.6.1 Ultrasonic cutting of soft and hard tissue

Ultrasonic cutting of soft and hard tissue is an increasingly popular alternative to conventional surgical cutting methods. The concept is not new, with the first reports of ultrasonic drilling for tooth cavity preparation described in 1950s (Catuna, 1953). However, the widespread adoption of piezoelectric surgery happened following a report by Vercellotti et al. (2001) detailing an osteotomy protocol using piezoelectric instruments. The benefits of ultrasonic cutting lie in its precision and control during tissue dissection, which effectively minimises trauma to surrounding tissues. Importantly, employing an ultrasonic probe for cutting small blood vessels facilitates

tissue cauterisation and ensures effective haemostasis, thereby reducing risks associated with surgical bleeding control and improving visibility within the operative field (Lucas & Mathieson, 2015). Moreover, compared to conventional cutting methods, ultrasonic cutting requires notably less force from the operator to achieve incisions. However, it is worth noting that ultrasonic cutting entails longer operational times and is limited in its ability to penetrate deeply into tissues (Firoz et al., 2016). The cutting tools typically contain an ultrasonic transducer generating a vibration in the range of 20 to 40 kHz and causing a metallic blade to resonate to its frequency. In turn, the vibration of the sharp blade produces a shearing action on tissues when in contact. When it comes to cutting mineralised tissue, various well-established applications exist, including dental ultrasonic drilling, root planning in periodontology, bone autograft harvesting, and maxillofacial bone cutting utilising systems, such as Piezosurgery® (Parmar et al., 2011).

1.5.6.2 Limitations of ultrasonic surgical cutting

The effects of heat generation during the ultrasonic cutting on cells of the surrounding tissues present a significant concern (Lucas & Mathieson, 2015). Increased temperatures at the cutting sites cause tissue necrosis and damage to the surrounding soft tissues, resulting in impaired post-operative healing. The severity of this damage varies based on the specific temperatures and duration of exposure, with the recognised threshold for bone regeneration typically set at 47°C for 1 min (Eriksson & Albrektsson, 1983). Dolan et al. (2012) exposed murine MSCs, osteoblasts (MC3T3-E1) and osteocytes (MLO-Y4) to the temperatures comparable to those experienced during

surgical cutting. The cells were incubated in culture media at 45°C, 47°C or 60°C for durations of either 30 s or 1 min. After an initial depletion in cell numbers and significant necrosis, 4 days post-treatment at 45°C, MC3T3-E1 and MLO-Y4 cells demonstrated recovery in live cell numbers relative to the controls kept at 37°C. Meanwhile, the recovery of cell numbers exposed to 60°C was not observed until after 14 days. Notably, osteoblastic differentiation of MSCs and mineralisation of MC3T3-E1 cells and MSCs were augmented at 45°C, but not at higher temperatures. These findings were confirmed in numerous *in vivo* studies (Augustin et al., 2008; Eriksson & Albrektsson, 1983; Eriksson et al., 1984; Olson et al., 2011). Similarly, ultrasonic bone cutting generates substantial heat primarily through the absorption of energy from the oscillating blade, frictional forces at the cutting site, and burning of bone debris (Lucas & Mathieson, 2015).

1.5.6.3 Current directions in advancing ultrasonic cutting

Li et al. (2021) highlighted the need for miniaturising ultrasonic surgical devices to facilitate minimally invasive procedures. Presently, a primary constraint on this advancement is the limited volume of piezoelectric material, which restricts the generation of adequate ultrasonic oscillations. Moreover, current research is directed towards improving cutting techniques specifically tailored for cancellous bone, given that the predominant focus of published literature has been on cortical bones (Pourgiv et al., 2024). The spongy nature of the cancellous bone introduces several challenges to the cutting procedure. More debris is generated during cutting in cancellous bone compared to cortical bone, heightening the risk of delayed wound healing and infection

if not adequately irrigated. This debris can also lead to mechanical interference with biomaterials. Furthermore, cancellous bone exhibits higher heat and energy dissipation, increasing the likelihood of microcracks and subsequent distortion of its spongy 3D geometry. Wang et al. (2024) investigated the optimisation of cutting parameters to improve the predictability of crack propagation in ultrasonic cutting. The report highlighted a preference for large amplitude and high-frequency ultrasonic vibrations, while also recommending avoiding transverse cutting to reduce the crack propagation deflection angle.

Thermal osteonecrosis remains a considerable obstacle in surgical cutting, and current strategies to minimise it include employing external irrigation with saline and optimising cutting parameters such as speed, depth, and feed rate. Notably, the influence of the ultrasonic blade design allowing a minimal contact with tissue was also found to reduce the localised heating to some degree (Cardoni et al., 2006). However, despite previous studies demonstrating the effects of elevated temperatures on bone cells *in vitro*, there remains a need to accurately replicate the scenario of an ultrasonically vibrating blade.

1.5.7 Therapeutic ultrasound in bone healing

1.5.7.1 Animal studies

One of the earliest reports on the *in vivo* use of therapeutic ultrasound to improve bone healing was published by Duarte (1983). Using a rabbit model an increased bone volume was found following a 15-min daily treatment of the fibula with low intensity pulsed ultrasound (LIPUS) following osteotomy. This finding was supported by several

reports using animal models. For instance, Pilla et al. (1990) used a daily treatment protocol involving 20-minute intervals of low-intensity pulsed ultrasound (LIPUS) at 30 mW/cm^2 and a frequency of 1.5 MHz administered following fibula osteotomy in rabbits. Similarly, Wang et al. (1994) used 30 mW/cm^2 LIPUS at 0.5-1.5 MHz for 15 min daily following femoral shaft fractures in rats and observed an increased maximum torque of bones and improved healing of fractures when compared with untreated controls. Furthermore, LIPUS application at an intensity of 30 mW/cm^2, with 200 ms pulses and a frequency of 1.5 MHz appeared to induce fracture healing in an ovariectomy-induced osteoporotic rat model (Cheung et al., 2011). Upregulation in the expression of *Col1A1, BMP-2, VEGF,* and *RANKL*, as well as a greater soft callus width and enhanced endochondral ossification were found in the tested group.

References	Study subject	Treatment parameters	Application location	Main outcome in treatment groups
Duarte (1983)	Rabbit	Frequency: 1.65 MHz Intensity: 49.6-57 mW/cm^2 Duty cycle: 0.05% Duration: 15 min daily for up to 15 days	Bilateral osteotomy of fibula and bilateral drilled holes on the cortex of femur	Increased mineralised callus area
Pilla et al. (1990)	Rabbit	Frequency: 1.5 MHz Intensity: 30 mW/cm^2 Duty cycle: 30% Duration: 20 min daily for up to 28 days	Bilateral midshaft fibular osteotomies	Increased initial stiffness and maximum torque of newly formed bone
Wang et al. (1994)	Rat	Frequency: 0.5 and 1.5 MHz Intensity: 30 mW/cm^2	Bilateral closed femoral shaft fractures	Improved fracture gap closure; 22% greater maximum torque

		Duty cycle: 100% and 30% Duration: 15 min daily for up to 21 days		of newly formed bone
Cheung et al. (2011)	Rat	Frequency: 1.5 MHz Intensity: 30 mW/cm^2 Duty cycle: 20% Duration: 15 min daily for up to 21 days	Ovariectomy-induced osteoporotic fracture	Upregulated expression of *COL1A1* and *BMP-2, VEGF, RANKL;* increased mineralised callus area

Table 2: Review of in vivo animal studies, evaluating the effects of therapeutic ultrasound, LIPUS on bone healing.

1.5.7.2 Human trials

Based on the promising animal study results, the application of LIPUS was extended to human patients with severe bone fractures, yielding similarly encouraging outcomes (Table 3). Heckman et al. (1994) appears to be the first author to publish a successful clinical trial on LIPUS treatment of fractures in the English language. The latter study enrolled 67 patients suffering from tibial fractures and described a 25% shorter healing time following treatment with 20 min daily 30 mW/cm^2 LIPUS applied at 1.5 MHz for 20 weeks. Kristiansen et al. (1997) conducted a study involving 60 patients with radial metaphysis fractures and administered ultrasonic treatment for 7 days following the fracture and found accelerated wound healing compared with patients receiving a placebo treatment. Prior to the ultrasonic treatment at an intensity of 30 mW/cm^2, and a frequency of 1.5 MHz, all fractures were reduced to align the bone fragments into their anatomical positions and immobilised with a cast. The placebo treatment

involved an identical device that was not generating ultrasound. Other investigators including Emami et al. (1999) did not observe a therapeutic effect of low intensity ultrasound. The latter trial enrolled 32 individuals with tibial shaft fractures fixed with intramedullary rods. A 20-minute daily application of LIPUS for 75 days did not result in a significant improvement in healing time compared with the control group. Since then, reports on the effectiveness of ultrasound therapy have presented contradictory findings, leading to an ongoing debate regarding its efficacy (Nolte et al., 2001; Rue et al., 2004; Yadav et al., 2008). Poolman et al. (2017) argued that LIPUS did not present a significant benefit in fracture healing based on the literature and therefore should not be used clinically. Several recent literature reviews have underscored the inconclusive nature of evidence presented in clinical trials investigating the use of therapeutic low-intensity ultrasound in fracture management. These reviews have identified limitations such as insufficient details in treatment protocols or ambiguous reporting of results within the included studies (Griffin et al., 2014; Leighton et al., 2017). Additionally, trials demonstrated a significant variability in methodology, which makes direct comparisons between studies challenging. A re-evaluation study conducted by Busse et al. (2016) aimed to assess the functional recovery of patients who underwent intramedullary nail insertion for fractured tibiae. The study followed a randomised, blinded, sham-controlled clinical trial design. The patients in the study received self-administered LIPUS treatment daily, using a coupling gel, at an intensity of 30 mW/cm^2. The primary focus of the study was to evaluate the functional outcomes and recovery of the patients following the LIPUS treatment. No significant difference

was observed in the duration required for patients to resume their normal lifestyle between those who received LIPUS treatment and those who did not. Importantly, factors such as previous treatments, type of fracture, time elapsed since the fracture occurred, and treatment parameters were not accounted for in the analysis. Likewise, Schandelmaier et al. (2017) highlighted the subjective nature of many trials that solely focused on assessing radiographic fracture union without considering the broader treatment outcomes for patients. These outcomes encompass the entire trajectory from the moment of trauma to achieving full weight bearing, which includes factors such as pain relief and the need for re-operation. By neglecting these essential aspects, the trials may not provide a comprehensive evaluation of the overall effectiveness and impact of the treatment on patients' functional recovery and quality of life. Overall, the publication concluded that the treatment outcomes in the test and the control groups did not differ greatly between most studies.

1.5.7.3 Conflicting outcomes of human trials

Despite the number of reports, highlighting the problems associated with studies on the therapeutic effects of ultrasound, more clinical trials with controversial methodologies are being conducted. For example, a study conducted by Mirza et al. (2019) evaluated healing of delayed unions and non-unions following arthrodesis, also referred to as joint fusion. The study specifically examined the efficacy of LIPUS therapy in promoting healing in these cases and reported a 67% success rate. However, the investigation did not report use of control groups and consisted of only 15 participants, making any definite conclusions difficult to establish.

Despite the limited availability of reliable data substantiating the efficacy and safety of LIPUS at that time, the US Food and Drug Administration (FDA) granted approval for its use in fracture treatment in 2000. The equivalent body in the UK - National Institute for Health and Care Excellence (NICE) similarly supported the application of LIPUS to reduce fracture healing time in 2010. However, the NICE-issued statement did highlight the poor reliability of methodologies and the absence of standardisation in LIPUS parameters used in the treatment. These included the high rate of loss of follow-up among patients in many studies, publication bias and variable degree of blinding (Chanen, 2010). Nevertheless, the first and most common commercial LIPUS device to date is produced by Exogen®, although alternative ultrasound delivery systems, such as EBI® OsteoGen and DuoSon are used too. The retrospective study by Pretorius et al. (2022) evaluated the efficacy of the Exogen LIPUS devices in non-unions and delayed unions between 2012 and 2021. The review concluded 82.14% success rates following LIPUS providing that 50% of cases were identified as high risk of bone healing complications. However, it is important to note that while the Exogen system has shown favourable outcomes in fracture healing therapy, the study conducted was small and lacked a comparative design. Consequently, further data is needed to obtain a more robust and comprehensive evaluation of the system's efficacy. Another potential source of variation in results is device calibration. Before deployment in clinical settings, ultrasonic devices usually undergo initial calibration by the manufacturer. However, regular maintenance calibration is necessary throughout the lifetime of these devices to account for any drift or changes in

performance over time. Over the years, several studies highlighted that a high fraction of the ultrasonic therapy devices used clinically do not adhere to the standard. An earlier Canada-based report by Snow (1982) demonstrated that 81% of the tested ultrasound therapy devices exhibited a greater than ±20% variation in power output compared to the indicated output. A subsequent study conducted in the USA revealed that 39% of the devices deviated from the indicated values in at least one setting. (Artho et al., 2002). Likewise, in an Australia-based study, 59% of tested devices were found to generate inaccurate power output above the standard ±20% variation, with the majority of those yielding lower output than required. Additionally, 37% of timers within the tested devices were found to be inaccurate, impacting the duration of treatment (Schabrun et al., 2008). It is evident that inadequate device calibration can significantly impact the therapeutic outcomes of ultrasound treatment, potentially contributing to conflicting outcomes in clinical trials. Moreover, insufficient power output may result in ineffective treatment, while excessive power output beyond the standard may potentially lead to tissue damage.

Despite the undoubted interest in ultrasound therapy for fracture management, supported by positive outcomes observed in several clinical trials, multiple challenges and areas requiring further investigation to optimise its efficacy and clinical application. Further *in vitro* studies may be useful in generating an understanding of the underlying mechanisms and to optimise the application of ultrasound therapy in fracture healing.

References	Sample size	Treatment parameters	Application location	Main outcome in treatment groups
Heckman et al. (1994)	67 patients	Frequency: 1.5 MHz Intensity: 30 mW/cm^2 Duty cycle: 30% Duration: 20 min daily for up to 20 weeks	Open or closed tibial shaft fractures	25% acceleration of fracture healing based on return to load bearing
Kristiansen et al. (1997)	60 patients	Frequency: 1.5 MHz Intensity: 30 mW/cm^2 Duty cycle: 20% Duration: 20 min daily for up to 10 weeks	Dorsally angulated fracture of the distal aspect of the radius	38% acceleration of fracture healing based on radiographic images
Emami et al. (1999)	32 patients	Not reported	Closed tibial shaft fractures	No significant difference in fracture healing based on radiographic images
Rue et al. (2004)	26 patients	Frequency: 1.5 MHz Intensity: 30 mW/cm^2 Duty cycle: 20% Duration: 20 min daily for up to 6.5 weeks	Closed tibial stress fractures	No significant difference in fracture healing based on radiographic images
Yadav et al. (2008)	67 patients	Frequency: 3 MHz Intensity: 1 W/cm^2 Duty cycle: 50% Duration: 10 min daily	Closed tibial stress fractures	36% acceleration of fracture healing based on presence of pain, local tenderness, warmth and a negative fulcrum test
Busse et al. (2016)	501 patients	Frequency: 1.5 MHz	Open or closed tibial fracture	No significant difference in

		Intensity: 30 mW/cm^2 Duty cycle: 20% Duration: 20 min daily for up to 52 weeks		fracture healing based on radiographic images and occurrence of non-unions
Poolman et al. (2017)	26 clinical trials	Varied	Varied	No significant difference in fracture healing
Schandelmaier et al. (2017)	26 clinical trials	Varied	Varied	No significant difference in the rate of return to load bearing, time to return to work, or need for subsequent operations
Pretorius et al. (2022)	28 patients	Frequency: 1.5 MHz Intensity: 30 mW/cm^2 Duty cycle: 20% Duration: 20 min daily for up to 16 weeks	Retrospectively treated range of fracture sites	Improved healing of delayed and non-union fractures based on radiographic images

Table 3: Review of prospective, randomised, double-blinded, placebo-controlled clinical trials investigating the effects of ultrasound therapy, LIPUS on bone healing.

1.5.8 Therapeutic ultrasound in bone healing at the bone-implant interface

1.5.8.1 Osseointegration into titanium implants

Potentially, LIPUS may enhance bone regeneration, and it is conceivable that this therapy may also contribute to an accelerated rate of osseointegration, the process by which orthopaedic or dental implants integrate with surrounding bone tissue. However, in contrast to the extensive number of clinical trials investigating LIPUS therapy for

non-unions and delayed unions, there is a scarcity of evidence regarding the acceleration of osseointegration using LIPUS based on patient models. Several authors have reported the effect of LIPUS on Ti implant integration in animal models using various exposure parameters. As an example, histological examination of femoral-coated implants in dogs following LIPUS stimulation revealed a notable increase of up to 16% in bone ingrowth, compared with the non-exposed side (Tanzer et al., 1996). The following parameters were used: 1.5 MHz wave frequency, 30 mW/cm^2 intensity, 200 s bursts repeated at 1 kHz for 20 min daily up to 4 weeks. Liu et al. (2012) evaluated the osseointegration of titanium dental implants in rabbits. Titanium screws were inserted into the femora and tibiae of the animals. Postoperatively, the screws were exposed to LIPUS using a frequency of 1.5 MHz and an intensity of 40 mW/cm^2 for 10 min, twice a day, for a period of 3 weeks. Bone ingrowth into the implants started earlier and resulted in a higher bone volume compared with the non-treated controls. The implant-bone interface also appeared to be significantly denser based on the computer tomography images in the LIPUS-treated samples. An additional study conducted in rodents using titanium intramedullary nails provided *in vivo* evidence that LIPUS had the potential to enhance osseointegration. The treatment was administered daily for 20 min, utilising a wave frequency of 1.5 MHz. Histological examination showed an increased peri-implant bone volume and implant bone ingrowth in the LIPUS-treated group. Although the difference between the test and the control groups were seen only at the initial stages of implantation of up to 8 weeks (Ruppert et al., 2019). A recent study by Chauvel-Picard et al. (2022) implanted titanium screws

into tibiae of adult mini-pigs followed by 15 min LIPUS treatment at 1 MHz, 300 mW/cm^2 for 10 weeks. The study found a significantly increased trabecular bone volume around the implant on the treated side. An important factor to consider during LIPUS treatment for bone healing around implants is the potential increase in temperature. This temperature increase may arise from the absorption of ultrasonic energy by Ti-based biomaterials, as metals have a higher heat capacity compared with body tissues. Zawiślak et al. (2016) conducted an experiment where a titanium plate was attached to a composite bone model placed in a water bath. Then, the setup was subjected to continuous ultrasound at a frequency of 1 MHz and intensities ranging up to 1.2 W/cm^2 for a duration of 3 min. The highest temperature increase between the Ti plate and the scaffold was 2°C. Therefore, while the increase was not critical, a pulsed output might be preferable to avoid the potential damage to the surrounding bone. Likewise, Kocaoğlu et al. (2011) conducted a study involving the insertion of stainless steel pins into the femora of rats, followed by application of 1 MHz continuous ultrasound at an intensity of 1 W/cm^2 for 5 min for 27 days. The control group did not receive any ultrasonic treatment following the insertion of pins. The application of ultrasound did not result in a substantial temperature increase in the implant and did not induce an osteogenic response.

1.5.8.2 Osseointegration in the presence of underlying health conditions

Ultrasonic therapy was also suggested to be beneficial for achieving osseointegration of Ti implants in patients suffering from osteoporosis and T2DM. Zhou et al. (2016) investigated bone ingrowth of Ti-screws in fully ovariectomised osteoporotic rats. The

animals received Ti tibial implants bilaterally followed by LIPUS treatment at 1 MHz and 40 mW/cm^2 using 200 µs pulsed bursts repeated at 1 kHz for 20 min daily after the surgery for up to 12 weeks. The animals were sacrificed, and tibiae harvested, which showed an increased bone volume and stability around the implants relative to the non-treated bones based on computer tomography and torque tests. Unfortunately, the potential of ultrasonic therapy has not been investigated in models of T2DM that have received Ti-based implants (Liang et al., 2022). Although, Coords et al. (2011) found encouraging conclusions on femoral fracture healing in diabetic rats following LIPUS. The study demonstrated significantly enhanced angiogenesis of the soft callus in the group treated with ultrasound. This suggested the potential beneficial effects of LIPUS in promoting fracture healing in diabetic conditions, highlighting the importance of further investigation in this area to validate and expand upon these initial observations.

However, despite some favourable outcomes, the exact mechanism underlying the osteoblast response to ultrasound on titanium surfaces remains unclear. Comparable with bone fractures, osseointegration of Ti-based implants involves wound healing. Therefore, previous findings on the effects of ultrasonic vibration on mechanotransduction and upregulation of protein synthesis, such as collagen type 1 in bone cells, may potentially be extrapolated to the osseointegration process as well (Palanisamy et al., 2022). Liu et al. (2012) suggested that LIPUS not only mechanically stimulated osteoblasts to synthesise bone mineral, but also increased angiogenesis and secretion of growth factors at the implantation site promoting bone healing. This was

also observed in human periosteal cells *in vitro* expressing greater quantities of *VEGF* following LIPUS treatment (1 MHz, 30 Mw/cm^2 for up to 4 min for 4 days) relative to the non-treated cultures (Leung et al., 2004).

References	Study subject	Treatment parameters	Application location	Main outcome in treatment groups
Tanzer et al. (1996)	Dog	Frequency: 1.5 MHz Intensity: 30 mW/cm^2 Duty cycle: 10% Duration: 20 min daily for up to 4 weeks	Porous transcortical Ti implants bilaterally inserted into femora	18% increase in osseointegration based on histological examination
Kocaoğlu et al. (2011)	Rat	Frequency: 1 MHz Intensity: 1 W/cm^2 Duty cycle: 100% Duration: 5 min daily for up to 4 weeks	Stainless steel intramedullary nail inserted into femur	No effect on callus formation based on radiological images, histological examination, and removal torque testing
Liu et al. (2012)	Rabbit	Frequency: 1.5 MHz Intensity: 40 mW/cm^2 Duty cycle: 20% Duration: 10 min twice a day for up to 3 weeks	Endosseous Ti dental implants inserted into metaphyseal region of femur and tibia	Accelerated osseointegration based on micro-computed tomography (μCT), histological examination, and implant pull-out test
Zhou et al. (2016)	Ovariectomised osteoporotic rat	Frequency: 1.5 MHz Intensity: 40 mW/cm^2	Ti implants bilaterally inserted into the proximal	Accelerated osseointegration based on μCT, histological

		Duty cycle: 20% Duration: 20 min for up to 12 weeks	tibial metaphysis	examination, and removal torque testing
Ruppert et al. (2019)	Rat	Frequency: 1.5 MHz Intensity: 30 mW/cm^2 Duty cycle: 20% Duration: 20 min, 5 times a week for up to 4 weeks	Ti implants bilaterally inserted into femora	Accelerated osseointegration based on μCT and histological examination
Chauvel-Picard et al. (2022)	Mini-pig	Frequency: 1 MHz Intensity: 300 mW/cm^2 Duty cycle: 20% Duration: 15 min daily, 5 times a week for up to 10 weeks	Ti implants bilaterally inserted into tibial crest in the region of tibial metaphysis	Accelerated osseointegration based on bone volume-to-total volume ratio, intersection surface of the volume of interest and trabecular bone thickness around the implant

Table 4: Review of prospective, randomised, double-blinded, placebo-controlled clinical and animal trials investigating the effects of therapeutic ultrasound, LIPUS in bone healing at the bone-implant interface.

1.6 *In vitro* research on therapeutic ultrasound in bone healing

1.6.1 Current evidence

The contrasting information on the effects of ultrasonic therapy on bone healing and the lack of reports investigating its effect on osseointegration with Ti-based implants

generated the need for a more basic scientific approach. Therefore, a number of authors evaluated the effects of ultrasonic stimulation on osteoblast-like cell lines *in vitro*.

1.6.1.1 Reported effects of ultrasound *in vitro*

Doan et al. (1999) compared the effects of continuous stimulation at 45 kHz with using a pulsed output (25% duty cycle) at 1 MHz on the response of human mandibular osteoblasts. Both treatment regimes, namely continuous stimulation at 45 kHz and pulsed output at 1 MHz, upregulated cell proliferation. Additionally, the 45 kHz ultrasound treatment demonstrated a higher synthesis of collagens and non-collagenous proteins whilst production of VEGF and TGF-β was increased to an equal extent at both wave frequencies. This suggested a potential osteogenic and angiogenic effect of ultrasound on osteoblasts. In addition continuous low-intensity ultrasound exposure of bone rudiments in mice found a positive effect on the process of endochondral ossification (Nolte et al., 2001). The study used a multiwell plate system with the ultrasonic transducer placed at the bottom and coupled with a gel. It is unclear whether the controls were placed in the same dish. In addition, Yang et al. (2005) demonstrated an increase in integrin expression and actin cytoskeleton reorganisation in LIPUS-exposed mouse osteoblastic cell line, MC3T3-E1 (1.0 MHz at 125 mW/cm^2 intensity, 10 min/day). The exposure was carried out in a degassed water tank and identified an increased alkaline phosphatase (ALP) activity, upregulated mineralised bone nodule formation, cytoskeleton reorganisation and collagen production in the LIPUS-treated cells. In contrast to these findings, Takayama et al. (2007) did not observe increased proliferation of osteoblast-like rat clonal cells (ROS 17/2.8) subjected to LIPUS

although there was an upregulation in expression of osteogenesis-associated genes including *RUNX2, OSX*, and *BSP*. The cells were subjected to a single exposure of LIPUS at a wave frequency of 1.5 MHz and an intensity of 30 mW/cm^2 for a duration of 20 min, with the transducer immersed into the culture dish. Sawai et al. (2012) used several cell lines including Saos-2, MC3T3-E1 and LM8 human and mouse osteosarcoma cell lines respectively exposed to LIPUS at 1.5 MHz wave frequency and 30 mW/cm^2 intensity for 20 min daily. The study demonstrated an increase in cell migration and VEGF protein synthesis in MC3T3-E1 cell line, both of which are essential for bone formation *in vivo*. A study involving a human odontoblast cell line, MDPC-23 identified that the continuous kHz-range ultrasound enhanced cell proliferation and differentiation following exposure to 25 kHz waves of the intensity of 25 mW/cm^2 (Man et al., 2012). However, the authors did not observe an effect on cell migration in ultrasonically treated cultures, as assessed using a scratch wound healing assay. Similarly, Ghorayeb et al. (2013) reported that treatment with ultrasound at a frequency of 45 kHz and a range of intensities from 10 to 75 mW/cm^2 for 5 min led to an observed increase in the number of MDPC-23 *in vitro*. This effect stood in contrast to the results from odontoblasts exposed to a "sham" treatment, which served as the control. The authors proposed that these findings could signify the potential enhancement of dental tissue repair through the application of LIPUS treatment.

1.6.2 *In vitro* studies involving titanium surfaces

Fewer studies have explored the effect of ultrasound on bone cells actually incubated on the materials used for bone replacement. Carina et al. (2017) exposed hMSCs to

LIPUS at 1.5 MHz and 30 W/cm^2 while incubated on magnesium-doped hydroxyapatite/collagen (MgHA/Coll) scaffolds. As a result of exposure to LIPUS, an induced osteoblast differentiation of hMSCs and upregulated expression of *OPN, OCN* and *VEGF* were observed. Given that continuous ultrasound finds application in physiotherapy for pain relief, tissue healing enhancement, and inflammation management, it becomes necessary to investigate the consequences of continuous ultrasound on osteoblasts cultivated on biomaterial surfaces (Aiyer et al., 2020). However, the majority of the available literature focused on evaluating the effects of LIPUS stimulation alone, rather than continuous stimulation. For example, Hsu et al. (2011) incubated osteoblast-like MG63 cells on Cp-Ti surfaces and used 1 MHz LIPUS at 0.15 W/cm^2 and observed a significant increase in cell numbers. Whereas, An et al. (2018) proposed that LIPUS (1.0 MHz, 100 mW/cm^2, 10% duty cycle for 10 min) enhanced osteoblastic differentiation of bone marrow mesenchymal stem cells also incubated on acid-etched Ti-surfaces. The study reported increased cell proliferation, pseudopodia and mineralised matrix nodule formation which were not observed in the control cultures. In addition, osteogenic gene expression of *OCN, BMP-2, ALP, COL1A1* and *RUNX2* was enhanced in the presence of LIPUS treatment. Nevertheless, there is very little information published regarding the effects of cellular interactions with titanium materials specifically when exposed to ultrasound *in vitro*.

References	Cell/tissue type	Treatment parameters	Application mode	Main outcome in treatment groups
Doan et al. (1999)	Human mandibular osteoblasts	Frequency: 1 MHz Intensity: 0.2-2 W/cm^2 Duty cycle: 25% Duration: 5 min Or Frequency: 45 kHz Intensity: 5-50 mW/cm^2 Duty cycle: 100% Duration: 5 min	6-well plate floating on water in a degassed water tank lined with rubber absorbers	Increased cell proliferation; upregulated production of collagen and angiogenic markers
Nolte et al. (2001)	Murine metatarsal rudiments	Frequency: 1.5 MHz Intensity: 30 mW/cm^2 Duty cycle: 20% Duration: 20 min daily for 6 days	Transducer immersed into culture medium within a 6-well plate	Upregulated endochondral ossification
Yang et al. (2005)	MC3T3-E1 or primary rat osteoblasts from the calvaria	Frequency: 1MHz Intensity: 62.5, 125 or 250 mW/cm^2 Duty cycle: 100% Duration: 10 min daily for 11 days	A well plate floating on water in a degassed water tank	Increased ALP activity, mineralised nodule formation and cytoskeleton reorganisation
Takayama et al. (2007)	ROS 17/2.8	Frequency: 1.5 MHz Intensity: 30 mW/cm^2 Duty cycle: not reported Duration: 20 min	Transducer immersed into culture medium within a well plate	Increased ALPase activity, cell numbers and expression of *RUNX2, OSX, BSP*; upregulated mineralised nodule formation
Hsu et al. (2011)	MG-63 on cp-Ti	Frequency: 1 MHz Intensity: 0.05, 0.15 or 0.30 W/cm^2	Transducer immersed into culture medium	Increased cell migration and mineralised nodule formation

		Duty cycle: 20% or 100% Duration: 3 min	within a 24-well plate	
Sawai et al. (2012)	MC3T3-E1, LM8 and Saos-2	Frequency: 1.5 MHz Intensity: 30 mW/cm^2 Duty cycle: 20% Duration: 20 min	6-well plate floating on water in a degassed water tank	No significant effect on cell proliferation; upregulation of VEGF synthesis and cell migration in MC3T3-E1 only
Man et al. (2012)	MDPC-23	Frequency: 45 kHz Intensity: 25 mW/cm^2 Duty cycle: 100% Duration: 6 doses of 5 min every 48 hours/ 3 doses of 10 min every 48 hours/ 30 min once	Transducer immersed into culture medium within a 6-well plate	Increased cell numbers and mineralised nodule formation; no effect on scratch wound closure; upregulated expression of *COL1A1, DMP-1, OCN*
Ghorayeb et al. (2013)	MDPC-23	Frequency: 45 kHz Intensity: 10, 25 or 75 mW/cm^2 Duty cycle: 100% Duration: 5 min	Transducer immersed into culture medium within a 6-well plate	Upregulated cell proliferation
Carina et al. (2017)	hMSCs on MgHA/Coll scaffold	Frequency: 1.5 MHz Intensity: 30 mW/cm^2 Duty cycle: 20% Duration: 20 min for 5 or 7 days	Transducer positioned at the base of a 6-well plate, coupled with a coupling gel	Increased osteogenic differentiation and cell proliferation
An et al. (2018)	Rat BMSCs on cp-Ti	Frequency: 1 MHz Intensity: 100 mW/cm^2	Not reported	Increased cell proliferation and mineralised

		Duty cycle: 10% Duration: 10 min		nodule formation; upregulated expression of *OPN, OCN, BMP-2, ALP, RUNX2* and *COL1A1*

Table 5: Review of in vitro studies investigating the effects of kHz-range and MHz-range therapeutic ultrasound on osteogenic behaviour on bone and tooth cells.

1.6.2.1 Factors contributing to contrasting outcomes *in vitro*

Overall, research outcomes reporting the effects of ultrasound *in vitro* exhibit a significant degree of variation. This could be attributed, in part, to the introduction of ultrasound into *in vitro* systems, which introduces multiple variables that can affect cell viability and behaviour. Factors such as temperature increase, cavitation, and ultrasound attenuation can complicate the interpretation of results and make it challenging to isolate specific effects of ultrasound on cellular interactions *in vitro*. Furthermore, integration of Ti-based biomaterials into studies involving ultrasound has proven difficult as seen from the low number of publications on the subject. Therefore, current research efforts have shifted towards developing a well-defined *in vitro* model that can deliver a controlled amount of ultrasound energy to cells while mitigating other confounding effects, such as increased temperature.

1.6.2.2 Experimental systems for ultrasonic treatment of cells *in vitro*

1.6.2.2.1 Transducer immersed in a tissue culture dish

Current *in vitro* ultrasound exposure systems used to treat cells vary significantly between publications. A common (Figure 1.7A), as seen with the DuoSon transducers (SRA Developments, UK) (Patel et al., 2015). Despite the simplicity and cost-

effectiveness of the system there are also disadvantages associated with it. Firstly, continuous ultrasonic stimulation causes a temperature increase of culture medium, and the described setup offers no temperature control. Interestingly, Reissis et al. (2013) reported that human mesenchymal stem cells did not exhibit significant changes in metabolism when exposed to a temperature of 48°C. Despite the benefits of a small degree of local heating for pain relief and increased blood flow *in vivo*, the latter report is unlikely to be accurate, since cells *in vitro* are significantly more vulnerable to temperature fluctuations. As demonstrated by multiple research groups (Schulte, 2015), a minor temperature increase will inevitably produce a biological response - a highly unfavourable outcome when investigating solely mechanical effects of ultrasound on cells.

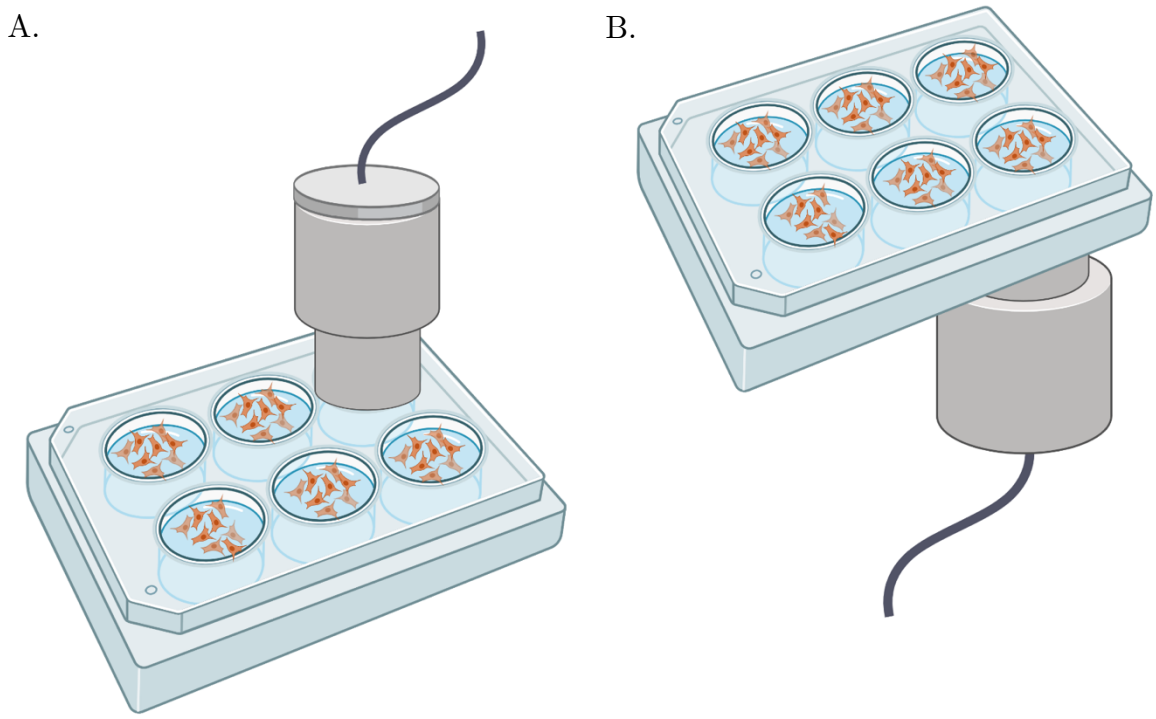

Figure 1.7: Illustration of common approaches to expose cells to ultrasound in vitro. The ultrasonic transducer may be immersed into the culture media (A) or placed below the dish with a coupling gel (B).

1.6.2.2.2 Culture dish placed on top of transducer

Other systems, such as Exogen (Bioventus, USA) offer an *in vitro* ultrasonic treatment setup, where the culture dish is placed on top of the transducer joined with a coupling gel (Figure 1.7B) (Sant'Anna et al., 2005). While such a system offers advantages in terms of a lower risk of cell culture contamination, it is also susceptible to temperature increases (Patel et al., 2015). Furthermore, both systems are frequently employed with multiwell cell culture dishes, which can result in unintended sound wave propagation to neighbouring wells. This unintended exposure to ultrasound may induce biological effects in cells that were potentially considered as negative controls (Leskinen, 2015). A study assessing the impact of 45 kHz ultrasound on murine odontoblast-like cells (MDPC-23) cultured in 6-well plates revealed that the lateral spread of the waves to adjacent wells was directly proportional to the increase in cell numbers and temperature within those wells (Patel et al., 2015). The authors applied continuous ultrasound at intensity levels ranging from 10 to 75 mW/cm^2. Later Gupta et al. (2022) conducted a comparable investigation and reported an increased acoustic pressure experienced by cells sonicated in 6-well plates as opposed to those in Petri dishes. Additionally, the paper suggested that a greater quantity of dead cells was observed in 6-well plates as compared with Petri dishes, possibly attributable to mitochondrial or endoplasmic reticulum rupture. Moreover, placing a transducer above or below a well plate creates a complex acoustic field. It arises from the formation of standing waves, which modify the radiation force (Figure 1.8). These are two identical acoustic waves moving in opposite directions and cancelling each other out when superimposed.

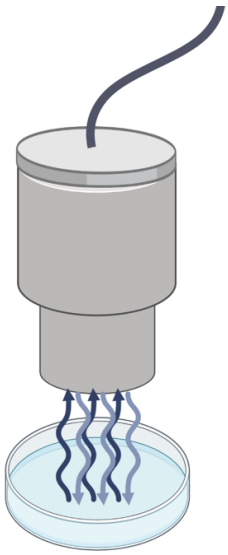

Figure 1.8: Diagram demonstrating formation of standing waves within a cell culture dish. Incident sound waves (dark blue arrows) are reflected from the culture dish surface (light blue arrows). The reflected waves travel in the opposite direction to the incident waves, superimposing upon each other and resulting in a cancellation effect.

One of the causes of this phenomenon is the mismatch in acoustic impedances between materials. For example, culture medium and air, culture medium and the dish surface or culture medium and the transducer. Thus, when sound waves pass through acoustic interfaces, a portion of those is reflected (the latter is proportional to the difference in acoustic impedance between the materials) creating standing waves (Secomski et al., 2017). These produce significant difficulties in defining the dosage of ultrasound energy experienced by cells. Scheven et al. (2009) partially addressed the issue of wave reflection off the culture dish surfaces by placing a silicone-based mat underneath the well plates.

1.6.2.2.3 Culture dish immersed in water tank

Cavitation is another critical factor to consider in *in vitro* ultrasonic treatment systems. Patel et al. (2015) irradiated cells immersed in a container in a glass tank filled with degassed water to avoid cavitation (Figure 1.9).

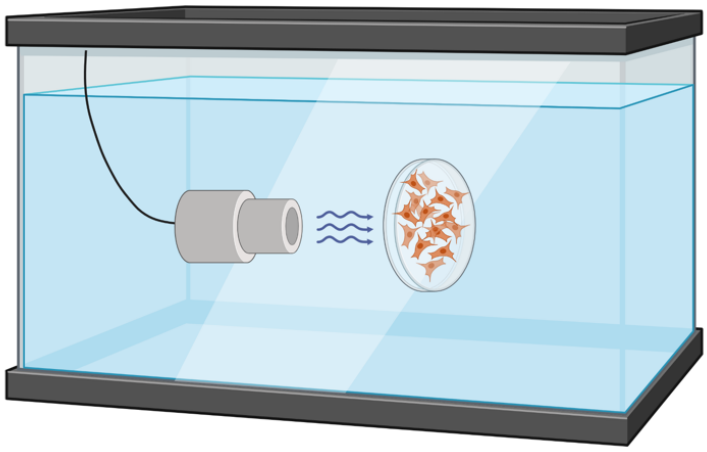

Figure 1.9: Diagram depicting an alternative in vitro ultrasonic treatment setup where the biological sample and transducer are located in a tank filled with degassed water to expose cells within a culture vessel to ultrasound.

In addition, this system offered superior temperature control of the culture media compared with other designs that involved well plates placed above or below the transducer. Water tank systems also enable the reduction of standing wave formation between the tank surfaces and water by incorporating acoustic absorber tiles. Furthermore, by positioning the transducer longitudinally relative to the water tank, the sound reflection due to the water-air boundary may be eliminated (Snehota et al., 2020). However, the challenge of standing wave formation between water, the cell culture dish and culture medium remains.

1.6.2.2.4 Implementing titanium into experimental setup

In addition, the experimental setup for the present study becomes further complicated by the presence of the implant-mimicking titanium surfaces. Traditionally, cells are incubated on these materials *in vitro* to identify the material's toxicity, compatibility for cell adhesion and replication, as well as performance of the osteoblast-specific

behaviour (Kirkpatrick & Mittermayer, 1990). However, since metal surfaces are highly reflective, the delivery of ultrasound to cells on titanium is challenging. The issues associated with standing wave formation, temperature increase and the unknown ultrasound dosage experienced by cells is even more prominent in the presence of titanium. Therefore, the described experimental setups cannot be usefully applied to study the osteogenic behaviour of cells on titanium exposed to ultrasonic treatment. In search of a novel approach for delivering ultrasound to cells on titanium, the present study represents the first description of a device specifically designed to address the limitations discussed.

1.7 Identifying a reliable osteoblast model system for ultrasonic treatment on titanium

1.7.1 Osteoblast-like cell models for *in vitro* studies

When working *in vitro*, researchers are commonly presented with a choice of either working with primary cells derived from human patients and animals or using immortalised cell lines. While it is important to acknowledge the advantages of using animal cell models, such as having an unlimited pool of healthy cells, this chapter will focus exclusively on human-derived cell models. By specifically exploring human cell models, this research aimed to enhance the relevance and applicability of the findings to human biology, thereby laying the foundation for potential future clinical applications.

1.7.1.1 Primary osteoblasts

1.7.1.1.1 Benefits of primary cells as an osteoblast model

Human primary cells are undoubtedly advantageous for retaining biological relevance by representing the true differentiated phenotype and avoiding interspecies variations. Commonly employed human osteoblasts provide a reliable *in vitro* model, primarily owing to their osteogenically differentiated phenotype, a characteristic not typically found in other primary cell types. Primary osteoblasts are often obtained from bone fragments discarded in surgical waste. Subsequently, osteoblasts are extracted from the bone tissue through enzymatic digestion (Gallagher, 2003). These cells are capable of forming mineralised nodules *in vitro* in the presence of osteogenic supplementation. Bellows et al. (1986) observed the formation of bone-like nodules in cultures containing foetal rat calvarial cells. The nodules were covered with osteoblast-resembling cells following 3 days of incubation and subsequently the nodules were mineralised. Alternatively, primary bone marrow cells may be obtained from various locations including bone marrow, adipose tissue, umbilical cord, amniotic fluid and placenta (Ansari et al., 2021). These are capable of differentiating down adipocyte, chondrocyte and osteoblast lineages (Owen, 1988). Similarly to primary osteoblasts, osteogenically-treated hMSCs demonstrate nodule formation *in vitro* (Song & Tuan, 2004). More recently, Mechiche Alami et al. (2016) described the ECM produced by hMSCs consisting of collagen type 1 fibres in association with needle-like crystals, as well as numerous matrix vesicles. Furthermore, *in vitro* isolated hMSCs demonstrated a comparable pattern of osteogenic gene expression, including *RUNX2, ALP*, and *OCN*, with that observed *in vivo* (Pettersson et al., 2017). In addition, primary human cells

allow bypassing of ethical dilemmas related to working on animal models, as well as minimise costs by not having to maintain animals in a laboratory.

1.7.1.1.2 Limitations of primary cells as an osteoblast model

Establishing a human primary bone cell model poses challenges due to the origin of the hMSCs from the bone marrow, which necessitates a painful isolation procedure (Ansari et al., 2021). Moreover, the pool of human primary osteoblasts is limited and usually only obtained during orthopaedic surgical interventions (Czekanska et al., 2012). Primary cells also exhibit a slow rate of replication when acclimating to *in vitro* conditions and are not capable of maintaining the biological phenotype past several passages. These cells usually undergo only a limited number of division cycles before reaching replicative senescence (Hayflick & Moorhead, 1961). This process is driven by the progressive shortening of telomeres after each division, triggering the DNA-damage response and inhibiting further cell cycle progression (Hernandez-Segura et al., 2018). Lastly, primary bone cells are notoriously heterogeneous due to the varying genetic makeup of donors. Even within the same individual, differences in genetic makeup can result from isolating bone cells from different skeletal donor sites (Czekanska et al., 2012). The former is observed by a greater osteogenic potential of the hMSCs isolated from femora in contrast with those originating from the iliac crest (Mechiche Alami et al., 2016). The difference may be associated with the increased mechanical load on femora contributing a greater differentiation potential (Henrich et al., 2016). The age of the donor also affects the cell's behaviour *in vitro*. Martínez et al. (1999) described slower proliferation and decrease in *OCN* expression in osteoblasts *in vitro* derived

from the femoral heads of donors over 50 years old when compared with younger donors.

In summary, primary cells offer a representative osteoblast model, but inherent variability, maintenance and difficulties with availability and cell isolation present significant challenges.

1.7.1.2 Osteoblast-like cell lines

The introduction of cell lines can be attributed to Alexis Carrel and colleagues in 1912, as noted by Jedrzejczak-Silicka (2017). In their study, cells derived from a chicken embryo's heart underwent numerous passages, leading to immortality. The cell line was maintained under aseptic conditions in culture media, with regular washing using an isotonic solution, for a period of 34 years. Initially, the researchers mistakenly believed that all cells were immortal under tissue culture conditions. However, the indefinite proliferation observed in that study may have been a result of a DNA mutation, as suggested by Jiang (2010).

Over the years, cell lines have revolutionised basic cell research, making it more accessible and diverse. There are now over 3,600 cell line options available, representing a wide range of cell types derived from over 150 different species (Kaur & Dufour, 2012). Immortalised cell lines overcome many of the disadvantages of primary cells. Cell lines demonstrate a significantly faster cell growth than primary cells with a generation time as short as 12 hours (Verma et al., 2020), are easily maintained *in vitro* and yield an unlimited number of cells, which reduces time and costs required for the primary cells. Cell typically maintain the cell-specific phenotype for a significantly

higher number of *in vitro* passages compared with primary cells (Wei & Yixin, 2014). However, genetic instability can still occur in cultured osteosarcoma cell lines, although at a significantly later stage (Muff et al., 2015). Hausser and Brenner (2005) described the enhanced proliferation and mineralised matrix deposition with increasing passage number of Saos-2 cells over approximately 100 passages, although interestingly, a lower specific ALP activity was noted in later passages.

1.7.1.2.1 Origins of cell lines

Cell lines originate from diverse sources which can include human and animal tissues, tumour samples, embryos, or specific cell types isolated from different organs or organisms. By definition, when primary cells are subcultured *in vitro* they become a cell line (Bols et al., 2011). However, some of those, also known as finite cell lines, will not have the infinite proliferation capacity. To produce an infinite cell line, cells may be sourced from cancerous tissue or immortalised experimentally. Human osteosarcoma-derived cells present the commonest form of osteoblast-like cell lines used in basic research which include but are not limited to Saos-2, MG-63, U-2 OS, HOS and 143B (Tippett et al., 2023). These cell lines represent distinct stages in osteoblastic differentiation. For instance, U-2 OS and MG-63 cell lines are recognised as a preosteoblast cell line and early-stage osteogenic differentiation respectively (Saldaña et al., 2011). While, HOS, 143B, and Saos-2 cells are commonly associated with the later stages of osteogenic phenotype (Wilkesmann et al., 2020). Similarly to normal osteoblasts, Saos-2 cells are known to express the receptor for parathyroid hormone (PTH). PTH protein is normally involved in calcium ion level regulation and bone

remodelling stimulating bone deposition by osteoblasts (Berdiaki et al., 2010). In addition, Saos-2, MG-63, and U2-OS express receptors for the active form of vitamin D - $1,25(OH)_2D_3$ (Mahonen et al., 1990) and treatment with $1,25(OH)_2D_3$ was correlated with the subsequent upregulation of *OCN* expression. The absence of 1,25(OH)2D3 in osteoblasts contributes to skeletal disorders such as rickets, as it plays a critical role in stimulating both osteoblast and osteoclast differentiation (Kriebitzsch et al., 2009).

1.7.1.2.1.1 De novo cell immortalisation

Aside from obtaining cells from tumour origins, there are various techniques available for de novo cell immortalisation. The former refers to techniques which enable "healthy" somatic cells proliferate indefinitely. Tumour suppressor genes, such as p53, retinoblastoma (Rb) and p16, normally regulate cell growth and prevent uncontrolled cell division. Disruption or inactivation of these genes can lead to the bypassing of normal cellular checkpoints, allowing cells to divide indefinitely and acquire an immortal phenotype. These genes are mutated in the majority of human cancers (Beauséjour et al., 2003). Gene inactivation may be performed via viral transformation, where simian virus 40 (SV40) is commonly used. This results in SV40 large T antigen (LTAg) synthesis, which inhibits action of the p53 protein by binding to it (Ozer et al., 1996).

Alternatively, the proliferative capacity of cells may be enhanced by inducing expression of telomerase reverse transcriptase protein (TERT). TERT is the catalytic subunit of telomerase, an enzyme involved in maintaining the length of telomeres,

which are protective caps at the ends of chromosomes (Steele et al., 2010). The presence of TERT prevents senescence by maintaining the integrity of telomeres and counteracting the senescence caused by the DNA-damage response (Soice & Johnston, 2021). Typically, TERT is actively synthesised by germ cells, haematopoietic and stem cells. However, it is not abundant in most adult somatic cells. The overexpression of the TERT gene in cell lines is achieved via ectopic expression by plasmid or viral transfection. Moreover, inbreeding of genetically modified mice with desired traits results in offspring with the mutated alleles providing a source of immortalised cell lines (Steele et al., 2010). However, this method typically involves additional techniques or modifications beyond inbreeding and is only feasible for animal models.

1.7.1.2.2 Stability of cell-specific phenotype in cells lines

1.7.1.2.2.1 Cell proliferation

Importantly, the discussed manipulations, as well as the cancerous origins of cell lines, often result in a full or partial loss of the tissue-specific phenotype and function, producing a less clinically relevant experimental model. For instance, many cancerous cell lines lack contact inhibition properties enabling uncontrolled proliferation (Pavel et al., 2018). When in contact with other cells, the direction of cellular migration is changed via cytoskeletal reorganisation to allow for cell monolayer formation (Mayor & Carmona-Fontaine, 2010). Conversely, the absence of contact inhibition results in cancer and improper wound healing *in vivo*, as well as a multi-layered cell culture *in vitro*. The former leads to a higher cell density than in primary cultures of the same time point, possibly creating oxygen and serum deficits which may affect cell behaviour. In addition, the proliferation dynamics of cancer-derived cell lines differ

from those of healthy cells. Czekanska et al. (2014) compared the proliferation rates, osteogenic gene activity and mineralised matrix deposition of the latter with the primary human osteoblasts. The authors observed significant differences in cell division in both cell lines relative to the primary cells. MG-63 cells demonstrated a major proliferation increase on the sixth day of incubation with 87% more cells than the normal osteoblasts. Whereas Saos-2 showed a significantly earlier initiation of the exponential phase on day 2.

1.7.1.2.2.2 Formation of mineralised extracellular matrix

Other deviations of cell lines from healthy osteoblasts relate to the deposition of mineralised matrix. There have been reports dating back over 40 years (Bellows et al., 1986; Cho et al., 1992; Tenenbaum & Heersche, 1982) describing the *in vitro* formation of mineralised bone (osteoid) nodules by primary cell monolayers. However, the formation of osteoid by cell lines displays significant differences. A study evaluating mineral formation in the matrix vesicles in human foetal osteoblasts (hFOB) and Saos-2 cells found distinct patterns of apatite formation (Bozycki et al., 2021). In contrast with the apparent ability of Saos-2 to form apatite crystals, hFOBs deposited amorphous calcium phosphate complexes and demonstrated a lower presence of annexins and tissue non-specific ALP in the plasma membrane. These are thought to be involved in apatite formation via assisting calcium ion influx into the matrix vesicles. It is worth noting that bone formation in a 2D culture is not possible *per se*, since osteoblasts require a vascularised 3D construct to deposit bone (Blair et al., 2017), however mineralised ECM may still be observed.

1.7.1.2.2.3 Osteogenic differentiation

Furthermore, in contrast with primary cells, cell lines typically represent a phenotype of only one differentiation stage due to cycle arrest (Czekanska et al., 2012). For instance, human osteosarcoma-derived MG-63 and Saos-2 cell lines are commonly used as osteoblast-like models of the earlier and late stages of differentiation respectively. Pautke et al. (2004) described a significant deviation in osteogenic gene expression of human osteosarcoma cell lines, MG-63, Saos-2, and U-2 OS relative to primary human osteoblasts. Saos-2 cells demonstrated a reduced expression of collagen type 3 (*COL3A1*) and osteoprotegerin (*OPG*), both involved in early osteogenesis (Volk et al., 2014; Yu et al., 2011). Whereas most MG-63 cells failed to express *OC, BSP* and decorin (*DCN*), known to be abundant in mature osteoblasts (Fielding et al., 2019; Komori, 2020; Robey et al., 2020). Furthermore, only half of the U-2 OS cells produced *COL1A1* and none of the cultures were positive for *OCN* and *DCN*. Hence, the origin and the phenotype of cell lines must be considered carefully to represent osteoblasts of a particular stage of osteogenic differentiation.

1.7.1.2.2.4 Intraspecific variation of phenotypes

Other considerations that affect the clinical relevance of results obtained from cell lines include the intraspecific variation among individuals. Since these cells are typically sourced from a single donor, it becomes challenging to extrapolate findings to predict clinical outcomes in patients (Li, 2011). Moreover, Kaur and Dufour (2012) also highlighted that cell lines distributed between laboratories are frequently contaminated with mycoplasma or even other cell lines. In the case of the HeLa cell line, it has often

been observed that these cells completely take over a mixed cell population after several passages.

Cell lines are undoubtedly advantageous compared with primary cell lines in terms of the ease and cost of maintenance, as well as sourcing. However, with the above issues in mind, it is essential to appreciate the limitations of the bone-derived cell lines as osteoblast models *in vitro*. Cell lines may be used in the initial stages of research to provide an indication of cell behaviour on various biomaterials and in the presence of therapeutic agents or external physical stimulation. However, these cell lines should not be used as a substitute for primary cells when seeking a reliable indication of cell responses.

1.7.2 Osteogenic differentiation *in vitro*

The present section was published by Yevlashevskaya et al. (2023).

1.7.2.1 Osteogenic supplementation of culture media

Osteogenic supplementation consisting of ascorbic acid (Asc), dexamethasone (Dex), and β-glycerophosphate (β-Gly) is routinely used to induce osteogenic behaviour in both primary cells and cell lines. Cells are typically incubated until approximately 80% confluency followed by the addition of the osteogenic factors to the culture media. Asc serves as a cofactor for proline hydroxylation involved in collagen synthesis. The former is required for mineral matrix deposition (Rodan et al., 1987). Dex induces osteogenic differentiation by upregulating the transcription of *RUNX2* (Vater et al., 2011). While β-Gly supplies a source of organic phosphate for extracellular matrix mineralisation (Langenbach & Handschel, 2013).

1.7.2.2 Conflicting reports on effects of osteogenic supplements on osteoblasts

Although the present osteogenic cocktail has been long used in tissue culture, there are conflicting outcomes in the literature. The reported cell responses differ depending on the origin and maturity of the osteoblast model, as well as concentrations of the osteogenic supplements. For instance, relatively immature osteoblasts, MG-63 demonstrated signs of osteogenic behaviour at up to 250 µM Asc with the upregulation of *RUNX2* and secreted phosphoprotein-1 (*SPP1*) both associated with early osteogenesis (Valenti et al., 2014). However, higher concentrations of Asc downregulated expression of bone-specific genes, whereas 750 µM Asc induced apoptosis. Conversely, a study involving a more fully differentiated Saos-2 cell line reported induced matrix mineralisation accompanied by apoptosis when exposed to 283 µM Asc and 7.5 mM β-Gly (Cmoch et al., 2014) which indicated a possible involvement of β-Gly in apoptosis, however this was not addressed in the report. Similarly, Orimo and Shimada (2006) outlined the potential link to apoptosis in reduced cell numbers of Saos-2 incubated in the presence of 10 mM β-Gly. However, several authors (Cmoch et al., 2014; McQuillan et al., 1995) observed enhanced ECM mineralisation by Saos-2 cells at a similar β-Gly concentration with no significant indication of cell death. Furthermore, the importance of supplementation with Dex in phenotypically mature osteoblast models, such as Saos-2 has been debated. For example, Prideaux et al. (2014) omitted the use of Dex in Saos-2 cultures and still observed ECM mineralisation and osteogenic gene expression typical of osteoblasts. Notably, the signs of phenotypic progression into those of osteocytes including the development of dendritic cell processes was also reported. The effects of Dex on less

committed osteoblasts also have been reported to vary. Human alveolar bone cells were shown to demonstrate increased osteogenic potency in terms of the ALP activity and ECM mineralisation in the presence of Dex (Tabassum, 2022). The same report described a decreased cell proliferation in agreement with Coelho and Fernandes (2000), which reported significantly higher cell numbers in hMSCs exposed to 10^{-8} M Dex. In contrast with Sordi et al. (2021) showing a decrease in cell proliferation in 10 mM Dex-supplemented human exfoliated deciduous teeth cells. One likely cause of the contrasting reports could be the genetic heterogeneity of the osteosarcoma tumours used as the source for osteoblastic cell lines (Mohseny et al., 2011). However, the exact reason for this difference is not yet fully understood.

1.7.2.3 Saos-2 cell lines and hMSCs as osteoblast models *in vitro*

The diverse effects of the components within osteogenic media on osteoblastic cell lines are concerning due to the potential difficulty in comparing experimental results between publications. Furthermore, this raises concerns regarding the translation of these findings to *in vivo* outcomes. Thus, to generate comparable data representing osteoblast behaviour, it is necessary to test the key aspects, such as proliferation, cell death and osteogenic gene expression in the presence of Asc, Dex and β-Gly for a particular osteosarcoma cell line. The present work compared the former in Saos-2 cells and a non-carcinogenic osteogenic cell model to provide a detailed characterisation of cell behaviour prior to the exposure to ultrasound.

1.7.2.3.1 Saos-2

The previously mentioned Saos-2 cell line was originally derived from an 11-year old Caucasian female patient suffering from primary osteosarcoma (Fogh & Trempe, 1975). It demonstrates a mature osteoblastic phenotype according to the presence of Vitamin D - 1,25$(OH)_2D_3$ receptors, high *COL1A1, OCN, OPN* and *ALP* expression, as well as the mineralised ECM deposition (Rodan et al., 1987). Energy-dispersive x-ray analysis of the mineralised matrix produced by Saos-2 cells, revealed a %-weight ratio of Ca:P similar to that of the human bone (Prideaux et al., 2014). The study also demonstrated the osteogenic behaviour of the Saos-2 cell line within a 3D collagen-based matrix. This was evidenced by the observed increase in expression of osteogenic markers such as *PHEX* and *MEPE* after 35 days of incubation. Importantly, the cancer-associated genetic alterations produce a significant variation to the typical osteoblastic phenotype. For instance, Saos-2 cells demonstrate a reduced generation time and the absence of contact inhibition (Pautke et al., 2004). Interestingly, Saos-2 cells exhibit a slower proliferation rate compared to another osteosarcoma cell line, MG-63. This suggests a potentially closer resemblance of Saos-2 cells to primary osteoblasts (Dvorakova et al., 2023). Saos-2 cells are known to have several genetic alterations, including mutations in the p53 tumour suppressor gene, involved in cell cycle regulation and accountable for the disrupted proliferation pattern (Michalakis et al., 2021).

1.7.2.3.2 hMSCs

To represent more physiologically relevant and non-cancerous osteoblasts, an immortalised human bone marrow cell line (hMSC) was selected. The hMSCs were immortalised via serial passaging combined with the viral transfection of SV40 large T

antigen (Applied Biological Materials Inc). Similarly to other cell lines, the hMSC line demonstrates a shorter doubling time. However, unlike cancer-derived cells, these cells possess contact inhibition properties and have the potential to differentiate into adipogenic, chondrogenic, and osteogenic phenotypes. This property is typical of stem and stromal cells (Robert et al., 2020), providing a model system with greater physiological relevance while still allowing the convenience of working with an immortal cell line.

This assessment will demonstrate the relevance of the Saos-2 as an osteoblast-like model for ultrasound exposure on titanium surfaces.

1.7.3 Osteogenic differentiation on Ti-based biomaterials *in vitro*

1.7.3.1 The role of scaffold materials in osteoblastic behaviour

The materials commonly used in the manufacture of tissue culture dishes include polystyrene, glass, polyethylene and others (Dwivedi et al., 2020). Hence, most *in vitro* studies describe observations obtained using these materials. However, in an *in vivo* environment, cells in a tissue interact with neighbouring cells as well as the ECM. Depending on the tissue type, cells demonstrate a variety of spatial orientations within the ECM. Some cell types, like osteocytes and chondrocytes, are completely encapsulated within ECM, while others, such as endothelial cells, reside on the ECM surface (Adams & Watt, 1993). This intricate cellular-ECM interaction is crucial for maintaining tissue structure and function *in vivo*. In bones, the ECM plays one of the central roles in cell differentiation of osteoblasts (Alcorta-Sevillano et al., 2020). Unlike in any other tissue type, the mineralised ECM of bones presents a unique architecture

displaying specific cell binding sites on proteins including collagens, fibronectins, and laminins. These allow a specific anchorage of the cell cytoskeleton to ECM via integrin interactions affecting cell growth and development (Cooke et al., 2008). Hence, a further critical consideration when characterising an osteoblast model is its interaction with the scaffold material. In an attempt to mimic the complex ECM-osteoblasts interactions, researchers developed novel surface coating techniques. For instance, Cooke et al. (2008) described surfaces with the immobilised proteins typical for the bone ECM to assist osteoblast attachment. Alternatively, 3D culture systems may be employed. These utilise a variety of materials including fibrous collagen matrix, hydroxyapatite-based scaffolds, alginate-based materials, and more (Nasello et al., 2020).

1.7.3.2 Attachment of osteoblasts to titanium surfaces

As biomaterials play an increasingly integral role in tissue replacement applications, it becomes critical to understand the attachment of cells to implant surfaces. Therefore, one of the challenges in the current research is to enhance cell attachment to titanium surfaces, which are utilised in manufacturing the *in vitro* ultrasonic treatment device. Surface topography influences the behaviour of osteoblasts and consequently impacts the osseointegration of implants. Rougher surfaces, in particular, promote a stronger bond between the bone and the implant, enhancing osseointegration. Section 1.4.3.3.1 provides an in-depth evaluation of how the macro-, micro-, and nanotopography of materials impact cell behaviour.

1.8 Aims and objectives

The present investigation represents an innovative approach to developing a novel ultrasound treatment device design specifically tailored for implant-mimicking titanium surfaces. This study aims to comprehensively explore various aspects of research, including the selection of appropriate cell models, osteogenic differentiation protocols, and *in vitro* techniques. This project aims to bridge existing gaps in the literature by proposing a novel experimental design for ultrasonically stimulating osteoblasts attached to titanium surfaces. The hypothesis of this research work proposes that ultrasound in the kHz range stimulates osteogenic behaviour in osteoblasts cultured on implant-mimicking titanium surfaces. To prove the latter, the study aims to achieve the following objectives:

1) Establish a reliable *in vitro* osteoblast model suitable for subsequent ultrasonic exposure and define the effects of osteogenic supplementation on the osteoblast-characteristic behaviour of cells.
2) Generate a Ti-implant model for cell incubation *in vitro*.
3) Design an ultrasound Ti cell culture system and overcome challenges of wave reflection, standing waves and overheating in the presence of Ti materials.

2 Materials and methods

2.1 Cell counting in osteogenically supplemented cultures

To obtain accurate cell numbers and effectively characterise osteoblast models for studying ultrasonic exposure on titanium surfaces, this study compared two cell detachment methods and two counting methods. By comparing the results obtained from different detachment methods and counting techniques, we aimed to determine the most reliable and accurate approach for characterising osteoblast models in the context of ultrasonic exposure on titanium surfaces.

2.1.1 Cell culture

Saos-2 cells were maintained in Dulbecco's Modified Eagle's Medium/ Ham's Nutrient Mixture F12 (DMEM/HamsF-12) (Sigma, UK) supplemented with 1% w/v (weight/volume) penicillin/streptomycin (Sigma, UK), 1% w/v L-glutamine (Sigma, UK) and 10% w/v foetal bovine serum (FBS) (Sigma, UK). Cells were incubated at 37°C in an atmosphere of 5% CO_2 (Heracell™ 150i, Thermo Scientific™, UK). Saos-2 cells were seeded onto a 6-well plate (Nunc, Denmark) at a density of 8.4 x 10^3 cells cm^{-2} and expanded for 7 days in osteogenic medium containing 283 µM Asc (Sigma, UK), 9.3 mM β-Gly (Sigma, UK) and 10^{-8} M Dex (Sigma, UK). The culture media was replaced every 2 days.

2.1.2 Manual cell counts using trypsin

In the present study, cell counting using a haemocytometer, also commonly referred to as manual cell number estimation, was employed. Following a 7-day incubation of cells

in osteogenic medium containing Asc, Dex and β-Gly, the medium was removed and discarded from the wells. Then, the cell layers were washed with PBS to minimise trypsin inactivation by any remaining media. Cells were detached from the polystyrene surfaces with pre-warmed 0.25% w/v trypsin in 1mM ethylenediaminetetraacetic acid (EDTA) for 10 min at 37°C, 5% CO_2 followed by trypsin inactivation with equal volume of culture media. The resulting cell suspension was transferred into a 15 ml Falcon tube and centrifuged (Universal 320 R, Hettich, Germany) at 180 x g for 3 min to obtain a cell pellet. The supernatant was removed and discarded, and the cell pellet resuspended in 1 ml culture medium. 20 µl of the resulting suspension was transferred into a clean Eppendorf containing an equal volume of 0.4% w/v trypan blue (Gibco, UK). The mixture was vortexed and then incubated for ~3 min at room temperature to allow stain incorporation into cells, after which 7 µl of the mixture was transferred into each chamber of a Neubauer haemocytometer. Uniformly dark blue cells were considered dead, whereas live cells only showed a blue border due to the intact plasma membranes. Cell numbers were obtained by counting non-stained, live cells in each of the four peripheral quadrants of the haemocytometer and calculating the mean value. Trypan blue-stained cells were considered dead, whereas non-stained cells were assumed to be live.

2.1.3 Manual cell counts using trypsin and collagenase type 1

A cell counting technique identical to that described above was used with the exception of cells being detached from the polystyrene surfaces with 0.05% w/v trypsin in 1mM EDTA and 0.8% w/v collagenase type 1 (Gibco, UK) for 10 min at 37°C in 5% CO_2.

2.1.4 Automated cell counting using DNA staining

The DNA of cells was stained with a fluorescence dye and quantified as follows: culture media was aspirated, and cell layers washed with PBS. Then, cells were fixed with 10% w/v formalin for 10 min at room temperature and permeabilised with 0.1% w/v Triton^{TM} X-100 (Sigma, UK) solution for 10 min, followed by fixing in 1% w/v bovine serum albumin (Sigma, UK) for 1 hour. Sytox green (ThermoFisher, UK) in 1:500 dilution was used to stain DNA for 10 min at room temperature followed by visualisation with confocal microscopy (LSM 700, Zeiss, Germany). Images were taken at four random points in the area of 1.2 mm^2 in each well. The stained cell nuclei were counted using Image segmentation algorithm in ImageJ and Fiji (StarDist plugin) as described by Labno, 2014 and the number of cell nuclei was used to indicate cell numbers.

2.2 Effects of osteogenic stimulation on Saos-2 and hMSCs

2.2.1 Cell culture and osteogenic differentiation

Human osteosarcoma cell line, Saos-2 derived from the 11-year-old, female patient was obtained from the laboratory stores, whereas the immortalised human mesenchymal stromal cell (hMSCs) and purchased from ABM (T0520, Abm, Canada). Saos-2 cells were maintained in DMEM/HamsF-12 culture medium supplemented with 1% w/v penicillin/streptomycin (Sigma, UK), 1% w/v L-glutamine (Sigma, UK) and 10% w/v FBS (Sigma, UK). hMSCs were grown in DMEM (low glucose, pyruvate) (Gibco, UK) with 0.5% w/v penicillin/streptomycin and 10% w/v FBS (Gibco, UK). Both cell lines were incubated at 37°C in an atmosphere of 5% CO_2. Cells were seeded onto a 6-well

plate at a density of 8.4 x 10^3 cells cm^{-2} and expanded for 72 hours until confluence which was considered day 0 of the experiment. Induction of osteogenic differentiation was initiated on day 0 using 283 µM Asc, 9.3 mM β-Gly and 10^{-8} M Dex. The following combinations of osteogenic supplements were established: control (no osteogenic supplementation); Asc Dex β-Gly; Asc Dex; Asc β-Gly; Dex β-Gly; Asc; Dex and β-Gly. Cells were incubated in the different supplemented culture media for up to 14 days with a change of media every 3 days. Cell growth in terms of numbers was examined every 2 days until day 14 of incubation. First, cell monolayers were detached from the polystyrene surface using 0.25% w/v trypsin in 1mM EDTA (Sigma, UK) and 0.8% w/v collagenase type 1 for 10 min at 37°C, centrifuged (Centrifuge 5415 D, Eppendorf, UK) at 180 x g for 3 min and resuspended in 1 ml 10% w/f FBS in DMEM/HamsF-12. Viable cell counts were performed using trypan blue staining and a haemocytometer as described later in this section.

2.2.2 Alizarin red S staining

To examine mineral deposition in cell cultures Alizarin red S staining (ARS) was performed on day 14 of incubation in osteogenic media as described by Gregory et al., 2004. The culture media was removed from the wells and cells were washed with 500 µl phosphate buffered saline (PBS) three times. PBS was pipetted on the walls of the wells rather than on the cell layers directly to avoid cell detachment. Cells were fixed with 10% w/v formalin for 15 min at room temperature followed by washing with PBS three times for 5 min each to remove excess formalin. Alizarin red S stain was adjusted to pH 4.2 with dropwise addition of 1% w/v ammonium hydroxide solution and a pH

meter (Accumet AB150, Thermo Fisher Scientific, UK). The deposited mineral was stained with 40 mM ARS for 20 min at room temperature on an automated shaker (SK-O180-S, DLAB Scientific, China) to ensure equal distribution of the stain across wells. Then, the excess stain was removed, and cell layers washed with PBS three times for 5 min each. This was followed by phase contrast microscopy to visualise the stained mineral. Stain quantification was performed by extracting the stain with 200 µl 10% w/v acetic acid for 10 min at room temperature followed by removing the stained extracellular matrix and cells using a cell scraper. The resulting mixtures were transferred into clean Eppendorf tubes. The Eppendorf tubes were thoroughly vortexed (SciQuip vortex mixer, SciQuip, UK) and incubated first in a water bath (SBB Aqua 26 Plus, Appleton woods, UK) at 85°C for 10 min, then in crushed ice for 5 min. Cell debris were separated from the stained supernatant by centrifuging (Universal 320 R, Hettich, Germany) at 13200 x g for 15 min. Subsequently, 150 µl of the stained supernatant was transferred into a clean Eppendorf tube and neutralised with 45 µl 0.1% w/v ammonium hydroxide. at was followed by 45 µl of the resulting solution being transferred to a clear 96-well plate and the optical density of the samples was quantified with a plate reader (ELX 800, BioTek, USA) at 405 nm and compared against a standard curve of serial dilutions. The 2-fold serial dilutions were prepared using 2 mM to 7.8 µM ARS (all adjusted to pH 4.2 which was the standard approach in earlier experiments).

2.2.3 LDH assay

The lactate dehydrogenase (LDH) cytotoxicity assay was performed to examine cell death in cultures by quantifying the release of LDH. The LDH-Glo™ kit was used (Promega, UK) as per the manufacturer's instructions. Briefly, LDH storage buffer contained 200 mM Tris-HCl (pH 7.3), 10% w/v glycerol and 1% w/v BSA and was used for dilution and storage the culture media samples stored at 4°C. A 2 µl aliquot of culture media was collected on day 7 of incubation in osteogenic media and diluted in 50 µl of the LDH storage buffer. 25 µl of this solution was transferred into an opaque walled, transparent base 96 well plate and mixed with an equal volume of LDH detection reagent. The LDH detection reagent contained 95.5% w/v LDH detection enzyme mix and 0.5% w/v reductase substrate and was prepared immediately before use. Luminescence was recorded using a plate reader (Tecan Spark, Switzerland) after 60 min incubation at room temperature. Two negative controls were used in this experiment: a no cells control to assess the background luminescence of the culture media and a no treatment control to assess cell death in cultures without the osteogenic supplementation. A positive control containing LDH was prepared by permeabilising the no treatment control cells with 10% w/v Triton-x100 for 10 min immediately before collecting the culture media samples. The results were expressed as a percentage relative to the control group without osteogenic treatment.

2.2.4 Assessment of gene expression using qPCR

2.2.4.1 RNA extraction

Cells were incubated in osteogenic culture media as described previously up to 14 days in T25 flasks (Sigma, UK). Total RNA was isolated every 2 days up to day 14 of

osteogenic treatment using the RNeasy Mini kit (Qiagen, UK). The samples were washed with PBS and incubated in 1 ml of the RLT lysis buffer at room temperature until the cell monolayer was dissociated. The lysate was transferred into a RNase-free Eppendorf tubes and thoroughly mixed using vortex. Then, 1 ml 70% w/v molecular grade ethanol was transferred to the lysed cells and vortexed again. 700 µl of the mixture was pipetted into the RNeasy spin column and centrifuged (Centrifuge 5415 D, Eppendorf, UK) at 12000 x g for 30 s. The procedure was repeated with the remaining mixture of cell lysate and ethanol. Then, 350 µl of the RW1 wash buffer was placed in each Eppendorf tube to remove any non-specifically bound organic molecules and centrifuged at 12000 x g for 30 s. Genomic DNA was digested using the On-Column DNase kit (Sigma, UK) by adding the DNase solution directly to the membranes of the spin columns and incubating for 15 min at room temperature. The samples were washed with RW1 again as described before. Any salts remaining on the spin column membranes due to the buffers used earlier were removed with two successive RPE wash buffer washes – first, 500 µl of the RPE was placed on the membrane and centrifuged at 12000 x g for 30 s followed by another 500 µl of the RPE placed on the membrane and centrifuged at 12000 x g for 2 min (Qiagen, UK). The spin columns were placed in a clean set of collection tubes and centrifuged at 13200 x g for 1 min to dry. RNA was collected by adding 30 µl of RNase-free water to the samples and centrifuging at 12000 x g for 1 min before storing the RNA samples at -80°C until later use. The quality of the resulting RNA was established using spectrophotometry (Genova Nano, Jenway™, UK). Purity was assessed at the

absorbance ratio of 260 nm/280 nm with the ratio ~2.0 considered 'pure', whereas RNA concentration was recorded at 260 nm wavelength.

2.2.4.2 cDNA synthesis

Complementary DNA (cDNA) was produced from the collected RNA via reverse transcription (RT) using the Tetro cDNA synthesis kit (Bioline, UK). The RT master mix contained 1 µl of the 10 mM dNTP mix, 4 µl of the RT buffer, 1 µl of the RNase inhibitor and 1 µl of reverse transcriptase (200 U/ µl). The reaction contained 8 µl of the master mix, 2 µg of RNA sample and diethylpyrocarbonate (DEPC) - treated water with the final reaction volume of 20 µl. The mix was transferred to the thermocycler (Veriti, 96 well thermal cycler, Applied Biosystems, USA) and incubated at 45°C for 1 hour to allow RT followed by 85°C for 5 min to terminate the reaction. The resulting cDNA samples were aliquoted in multiple RNase-free Eppendorf tubes to avoid repeated freeze-thaw cycles and stored at -20°C.

2.2.4.3 qPCR

Real-time PCR (qPCR) was performed using LightCycler® 480 SYBR Green I Master and 480 LightCycler® system (Roche Diagnostics). The expression of the following osteogenic markers was analysed: runt-related transcription factor 2 (*RUNX2*); osteocalcin (*OCN*); bone sialoprotein (*BSP*); alkaline phosphatase (*ALP*) and phosphate regulating endopeptidase homolog X-linked (*PHEX*). The expression of a marker of proliferation (*MKI67*) and proliferating cell nuclear antigen (*PCNA*) were used to estimate cell proliferation. The primer sequences (Table 6) were designed using Ensembl (https://www.ensembl.org) and primer 3 (https://primer3.ut.ee/). The

qPCR reaction mix was prepared by combining 1 µl of forward primer, 1 µl of reverse primer, 100 µl of syber master mix and 100 µl of RNase-free water. Initially, primers were resuspended in RNase-free water to achieve 100 µM concentration as per the manufacturer's instructions (Sigma, UK). Primer efficiency was assessed prior to examining gene expression of the samples by producing a 10-fold serial dilution of target cDNA from 100% to 0.1% in RNase-free water. A standard curve of log cDNA concentrations against crossing points (Cp) values was produced. The target DNA molecule increase factor of 2 ± 0.2 was considered efficient. Furthermore, qPCR melting curves were assessed for each primer to ensure specific amplification (Figure 7.1). After confirming the efficiency of primers, 9 µl of the qPCR reaction mix and 1 µl of cDNA were transferred to each well of the 96-well plate (Roche, UK) in duplicates to account for inaccuracies caused by pipetting. The plates were sealed with the film provided in the kit and centrifuged (Centrifuge 5415 D, Eppendorf, UK) at 12000 x g for 3 min (Universal 320 R, Hettich, Germany). The plate was placed in the LightCycler® 480 (Roche, UK) and preincubated at 50°C for 2 min followed by 95 °C for 10 min. Then, the samples were subjected for 45 cycles consisting of the following settings: 95°C for 20 seconds for DNA denaturation, then 60°C for 20 s to allow primer annealing, followed by 72°C for 30 s for DNA extension.

2.2.4.4 qPCR analysis

Gene expression analysis was performed in the LightCycler 480 software using the second derivative maximum method. The latter involves an algorithm which identifies crossing points (Cp) – the number of PCR cycles after which the exponential phase of

the target sequence amplification begins. Cp is marked by the increase in fluorescence of the products above the one of background. The gene expression values were normalised to the expression of the house-keeping gene tyrosine 3-monooxygenase (*YWHAZ*). The choice of the reference gene was determined based on the expression stability of glyceraldehyde-3-phosphate dehydrogenase (*GAPDH), YWHAZ,* beta-2-microtubulin *(B2M)* and hypoxanthine phosphoribosyltransferase 1 (*HPRTI1)*, as evaluated by the BestKeeper software. The method involves calculating the mean value of Cp of all reference genes within a sample. This mean value is then compared to the Cp value of each individual reference gene using Pearson correlation coefficients. Subsequently, a stability rank of housekeeping genes is generated. The reference gene exhibiting the highest stability index is deemed optimal (Pfaffl et al., 2004). ΔCp values are determined by comparing the Cp values obtained from the reference genes with those of the target genes, while accounting for the primer-specific amplification efficiencies as described previously.

2.2.5 Examination of cell proliferation rate

Cell proliferation was examined on day 4 of incubation with osteogenic culture media to avoid examining confluent cell layers where proliferation may have been influenced by contact inhibition. BrdU (5-Bromo-2'-deoxy-uridine) uptake was examined to visualise replicating cells as per the manufacturer's instructions (Abcam, UK). Prior to the experiment the BrdU-exposure time was optimised on Saos-2 cells to allow enough time for cells to proliferate. Various incubation durations were assessed, including 2, 4, 6, and 8 hours. Minimal to no fluorescence was observed after 2 and 4

hours of incubation. Ultimately, a 6-hour incubation period with BrdU was chosen as it yielded an adequate fluorescence signal while allowing the experiment to be completed within the same day. Importantly, optimisation was not conducted on the hMSCs cells, representing a limitation of this assay, given their longer doubling time compared to Saos-2 cells. Following optimisation, culture media and cells were exposed to the BrdU labelling solution for 6 hours at 37°C, 5% CO_2. Then, cells were rinsed three times with the washing buffer provided in the kit at room temperature to remove any non-incorporated BrdU stain. Samples were fixed with ethanol fixative (50 mM glycine, 70% w/v ethanol) for 20 min at -20°C and washed three times with the washing buffer again. Then, samples were incubated with anti-BrdU antibody for 30 min at 37°C and washed again, followed by the incubation with anti-mouse-Ig-fluorescein antibody for 30 min at 37°C. A mounting media containing DAPI was applied for 10 min at room temperature to prevent sample dehydration and stain all cell nuclei. BrdU and DAPI incorporation was examined using fluorescence microscopy (Eclipse TE300, Nikon, Japan). The following negative controls were established to prevent non-specific staining: 1) no BrdU 2) no anti-BrdU antibody 3) no secondary antibody. The proliferation rate in the presence of β-Gly was compared to the one in the absence of β-Gly, which served as a positive control. Images were captures using digital camera (D5100, Nikon, Japan). Brightness and contrast were enhanced equally in all images using Image J brightness and contrast tool without obscuring or eliminating any details. BrdU stained and non-stained nuclei were counted manually.

Gene	Function	Primer Sequence
Tyrosine 3-monooxygenase, *YWHAZ*	Involved in enzyme binding activity, commonly used as a house-keeping gene for gene expression normalisation in qPCR	F-ACTTTTGGTACATTGCTTCAA R-CCGCCAGGACAAACCAGTAT
Osteocalcin, *OCN*	Associated with bone remodelling and matrix mineralisation in osteoblast	F-GGCAGCGAGGTAGTGAAGAG R-CTGGAGAGGAGCAGAACTGG
Alkaline phosphatase, *ALP*	Involved in mineralisation, seen at earlier stages of osteoblastic differentiation	F-TGCTCTGCGCAGGATTG R-GGAGACACCCATCCCATCTC
Runt-related transcription factor 2, *RUNX2*	Induces osteoblastic differentiation in mesenchymal stem cells	F-CGCCTCACAAACAACCACAG R-TCACTGTGCTGAAGAGGCTG
Phosphate regulating endopeptidase homolog X-linked, *PHEX*	Osteocyte-associated gene involved in bone mineralisation control	F-ACTTTGCACTGCACTGGACT R-TCCATCAGAAGGGCCGTAGA
Marker of proliferation Ki-67, *MKI67*	Highly expressed in replicating cells, downregulated in cells at G0	F-GCCCGGGGACGTAGCCTGTA R-ACCGTCGACCCCGCTCCTTT
Proliferating cell nuclear antigen, *PCNA*	Involved in DNA replication by acting as a cofactor for DNA polymerase-delta	F-CCACGTCTCTTTGGTGCAG R-CCGGCGCATTTTAGTATTTTGG

Table 6: Forward and reverse primers were designed to assess the expression of osteogenic differentiation markers and cell proliferation markers with qPCR.

2.3 Optimisation of titanium surface roughness to increase cell attachment

2.3.1 Ti surface preparation

To identify the surface roughness of ultrasonic Ti devices allowing the highest cell attachment level an *in vitro* study was carried out. Commercially pure grade 2 titanium was selected for this study due to its widespread use in the manufacturing of dental implants (Sidambe, 2014). Ti discs of 15 mm diameter and 1 mm thickness were purchased from TML, UK to fit into a standard 24-well plate. Surface roughness was standardised by initially polishing the disc surfaces using an automatic polishing machine (Phoenix beta polisher, Buehler, USA) with abrasive paper of a grit size 320, 800 and 1200 consecutively at 200 rotations per minute (RPM) for 7 min each. Then, a composite surface with a series of diamond suspensions (Struers A/S, Denmark) of a grain size 9, 3 and 1 µm consequently were used for fine grinding of the Ti surfaces at 200 RPM for 7 min each. During the polishing procedure, the discs were fixed to plastic cuvettes using double-sided adhesive tape for easier handling. The operator manually positioned the cuvettes, ensuring that the Ti discs were in contact with the rotating polishing machine, effectively polishing the surfaces of the discs. Significantly, this technique resulted in variability in the degree of polishing due to the varying pressure applied by the operator to the cuvettes attached to the Ti discs. Hence, polishing was omitted in later experiments involving Ti paddles. Following polishing, the discs were acid-etched by immersion into 39% w/v hydrochloric acid for 1 hour at 25°C, 40°C or 60°C. This was followed by chemical cleaning with a sonicator (VITA, In-Ceram, Vitasonic, Germany) by fully immersing discs first in acetone, then in deionised water

for 10 min each. Surface roughness was measured by contact profilometry (Form TalySurf Series 2, TaylorHobson, USA). Scanning electron microscopy, SEM combined with energy dispersive X-ray spectroscopy, EDX (EVO MA10, ZEISS, Germany) were used to observe the surface and study the elemental composition of the disks following acid etching. Ti discs were sterilised by autoclaving at 121°C for 40 min ready for tissue culture experiments. Furthermore, surface roughness and chemical composition were assessed as described previously to ensure no significant changes produced by autoclaving.

2.3.2 Tissue culture

Sterile Ti discs were transferred in a 24-well plate (Nunc, Denmark) using sterile forceps and 0.5 ml DMEM/HamsF-12 (Sigma, UK) supplemented with 1% w/v penicillin/streptomycin, 1% w/v L-glutamine and 10% w/v FBS was added to each well. Saos-2 cells were seeded directly on the Ti surface at cell density of 8.4 x 10^3 cells/cm^2 before incubation at 37°C in 5% CO_2 for 24 hours. To assess cell attachment, viable cells on the Ti surface were counted. Each disk was transferred to an empty well and rinsed with PBS 3 times. Then, cells were detached from the Ti surface by incubation in 0.5 ml 0.05% w/v trypsin in 1mM EDTA (Sigma, UK) and 0.8% w/v collagenase type 1 (Gibco, UK) for 10 min at 37°C. The action of detachment enzymes was inhibited with 0.5 ml of 10% w/v FBS in DMEM/HamsF-12. The cell suspensions were places in Eppendorf tubes and centrifuged (Centrifuge 5415 D, Eppendorf, UK) at 180 x g for 5 min. Cell pellets were resuspended in 1 ml 10% w/v FBS in DMEM/HamsF-12. Viable cells were counted using the trypan blue exclusion assay as

described earlier. The optimum Ti surface roughness for the following experiments was chosen based on the highest average number of attached cells.

2.4 Ultrasonic exposure of cells *in vitro* on titanium surfaces

2.4.1 Ultrasound generation

The ultrasound generation system (Figure 2.1) was composed of the ultrasonic driver (PDUS210, PiezoDrive, Australia), ultrasonic transformer (TX210-600 and TX210-400, PiezoDrive, Australia), custom-made 20/40 kHz sonotrodes and Ti paddles. The system was controlled with the PiezoDrive software. The model system was based on the image-based ultrasonic shaking test developed for high-strain material testing by Seghir and Pierron (2018). Originally, the test was designed to characterise the viscoelastic properties of materials and involved a high-power ultrasonic transducer producing heterogeneous deformation of the sample. In the test, an infrared camera was used to observe the temperature profile proportional to that of the sample deformations. Similarly, in the present investigation the Ti paddles were connected to the transducer producing a standing wave along the paddle when generating ultrasound (Ballard et al., 2022). As the standing wave reflected from the distal end of the paddle back to the proximal end, wave intersection points were generated, also known as nodes. Antinodes were points where the standing wave did not cross the original sound wave. Unlike the traditional systems where cells are exposed to an acoustic field, the Ti paddles oscillating at 20 or 40 kHz produce two forms of deformation - maximum strain with zero displacement in the centre of the paddles (node) and a maximum displacement level with a lower strain level at the ends

(antinodes) (Ballard et al., 2022). Consequently, cells incubated on the paddle surfaces resonated to the oscillations along the Ti paddles. The mechanical stresses, which cells were exposed to varied depending on the location on the paddle as described previously. The degree of vibration of the paddles was varied by changing the current amplitude.

$$E = V \times I \times t$$

(E – electrical energy, V – voltage, I – current, t – time)

This was based on the principles of piezoelectricity, where a greater electrical energy delivery resulted in a higher deformation of the piezoelectric material within the transducer producing a vibration. In turn, electrical energy was directly proportional to the power output:

$$P = \frac{E}{t}$$

(P – power, E – electrical energy, t – time)

A detailed characterisation report of the Ti paddles is provided within the Appendix chapter (Figure 7.2, Figure 7.3). There, Dr Aleksander Marek used ultra high-speed imaging and infra-red imaging to track the displacement amplitude and temperature profile of the Ti paddle during the ultrasonic vibration, respectively. A high contrast, speckle pattern was applied by spray painting to the Ti paddles for digital image correlation. The latter was used to track and image the movement of the paddles when vibrating.

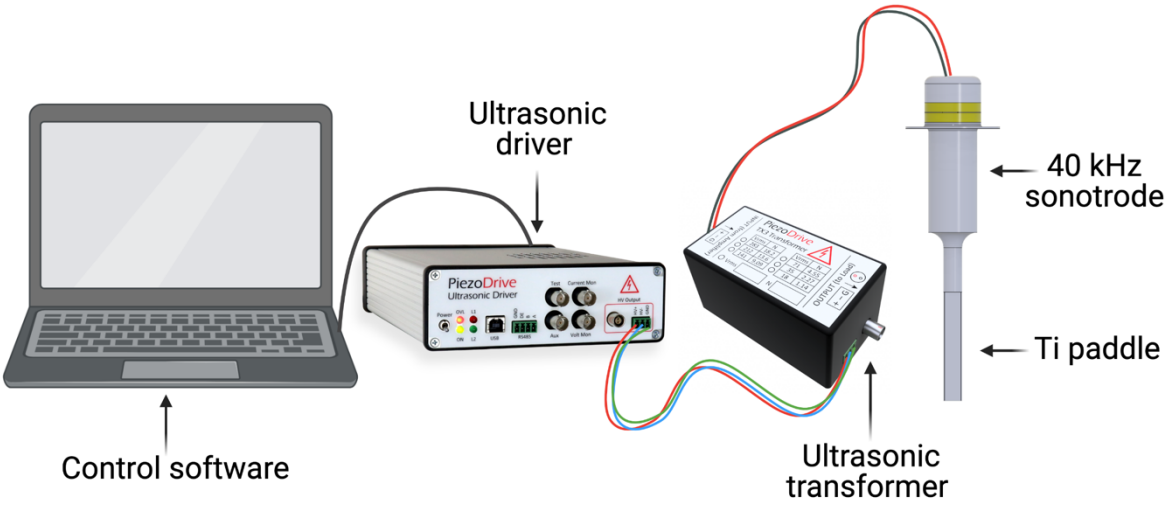

Figure 2.1: Diagram depicting an ultrasound generation system assembled for in vitro ultrasonic exposure of cells on titanium surfaces.

2.4.2 Titanium substrate

Commercially pure grade 2 Ti strips (paddles) acted as substrates for cell incubation and were produced via machining by colleagues at the University of Glasgow, UK (Figure 2.2). The strips were designed to attach to sonotrodes oscillating either at 20 or 40 kHz via a screw-on mechanism. During the ultrasonic exposure the strips resonated generating variable strain modes along the strip stimulating the attached cells which will be discussed later. To promote cell attachment the Ti surfaces were roughened to Ra ~0.9 µm by polishing followed by acid etching in 39% w/v hydrochloric acid at 40°C as per the previously described protocol.

Figure 2.2: Models of titanium paddles manufactured to act as cell incubation substrates and designed to attach to transducer (sonotrodes) for oscillation at 20 (A) and 40 kHz (B). 20 and 40 kHz strips are 118 and 57.5 mm respectively excluding the screw.

2.4.3 Preparation of the well boundary for Ti strips

Polydimethylsiloxane (PDMS) wells were made on the Ti paddles to isolate the surfaces for cell growth. Each well had an area of 216.3 and 108.2 mm^2 on 20 and 40 kHz strips, respectively. PDMS is a non-toxic material which sets into a gel and forms a waterproof, stable boundary with Ti. The PDMS wells were manufactured using the SYLGARD 184 silicone elastomer kit (Dow Corning, USA). The silicone prepolymer and a curing agent were mixed at a ratio 10:1 respectively for ~5 min followed by degassing in a vacuum chamber until the visible air bubbles escaped. A polypropylene mould was designed in Autodesk fusion 360 software and 3D printed using printer (M200 Plus, Zortax, Poland) and polypropylene fibres (BASF SE, USA) (Figure 2.3). A pre-set PDMS mixture was poured in the polypropylene mould, incubated at 50°C for 1 hour and allowed to cure at room temperature for 48 hours. The remaining PDMS mixture was stored at -80°C and reused for manufacturing wells at a later time. After setting, the PDMS wells were removed from the polypropylene moulds and secured on the Ti paddle by placing small amounts of pre-set PDMS on the periphery of the

paddle and attaching the well on it (Figure 2.4). The PDMS seal was allowed to set by following the same procedure as described in well preparation.

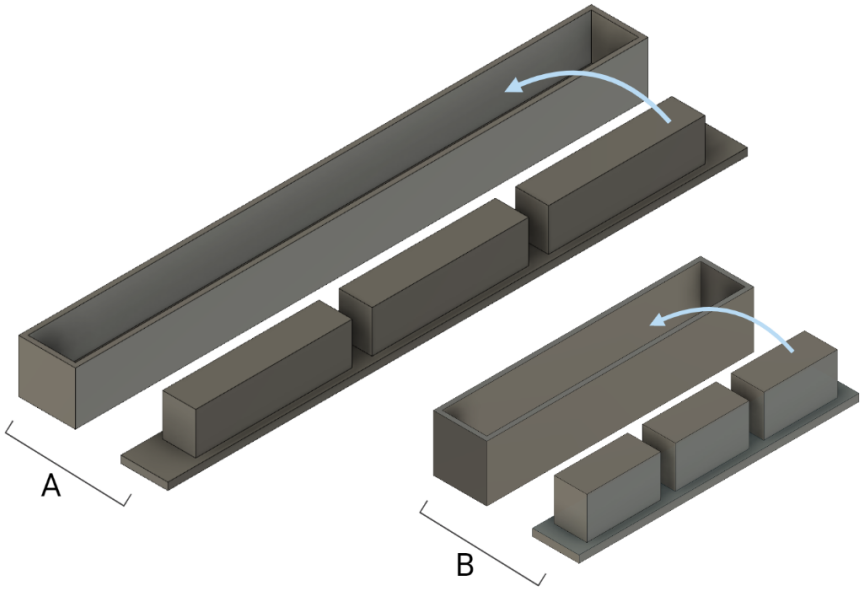

Figure 2.3: Models of polypropylene moulds 3D-printed to manufacture PDMS wells for cell compartmentalisation on 20 and 40 kHz titanium strips (A and B respectively). The moulds were composed of 2 components with the inner part inserted into the outer part as shown by arrows.

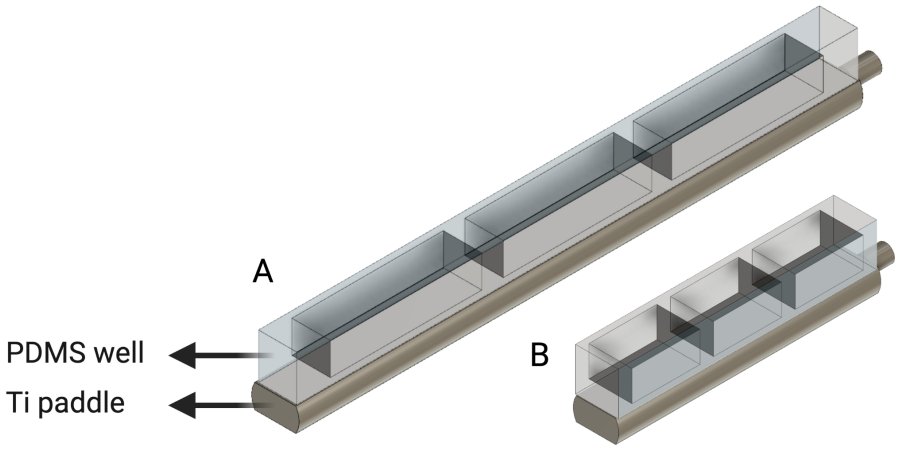

Figure 2.4: Models of PDMS boundaries attached to 20 (A) and 40 kHz (B) titanium paddles to create wells for cell incubation.

2.4.4 Temperature changes of culture media during ultrasound exposure

To assess whether ultrasound produced by the transducers (sonotrodes) caused temperature increase of the Ti strips, temperature readings of the culture media within the wells on the Ti strips were taken during 7 min of continuous ultrasonic stimulation. The effect of increase of current from 0.05 to 0.15 A was explored to identify an optimum setting for cell stimulation. Type K thermocouple probes of 1.5 mm in diameter (pico, UK) were immersed in culture media in each of the 3 PDMS wells on the Ti strips. The setup was placed in the tissue culture incubator and was allowed to reach ~37°C (Figure 2.5). The ultrasonic excitation parameters used in this analysis are summarised in Table 7. Thermocouples were connected to a data logger (TC-08, pico, UK) which recorded culture media temperature every second of the exposure.

Parameter of ultrasonic exposure	Magnitude, units
Wave frequency	20 kHz/ 40 kHz
Voltage	1 V peak-peak
Maximum load power	210 W
Current	0.05 - 0.15 A
Duration	7 min
Exposure mode	Continuous

Table 7: Ultrasonic exposure parameters.

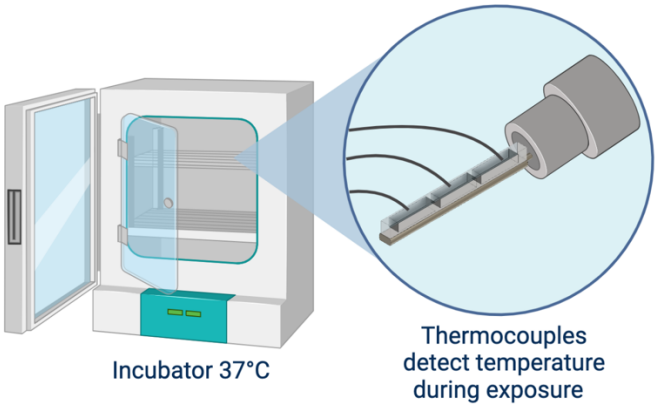

Figure 2.5: Illustration of thermocouples submerged in culture media within PDMS wells on Ti paddles of ultrasonic transducers. The setup was placed in a tissue culture incubator at 37°C.

2.4.5 Tissue culture

To unsure sterile conditions during cell incubation cell culture chambers were designed to fit the Ti strips (Figure 2.6) by using Autodesk fusion 360 software. Polypropylene (BASF SE, USA) was used as a material to 3D print the chambers due to its non-toxic properties, suitability to be sterilised using high temperatures and affordability. The chambers and the Ti strips were sterilised by autoclaving at 121°C for 40 min.

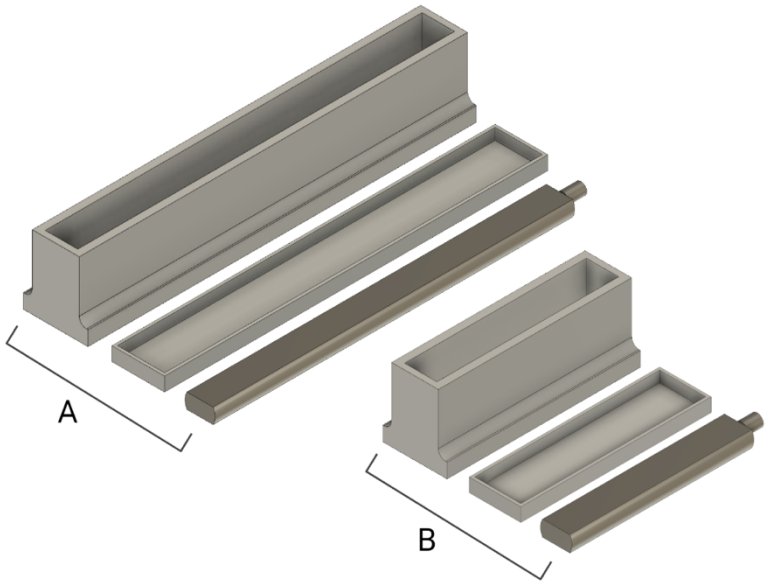

Figure 2.6: 3D printed polypropylene chambers for tissue culture experiments on titanium strips included an incubation container and a lid. The chambers were designed in two sizes to fit 20 and 40 kHz titanium strips (A and B respectively).

Then, the strips were placed inside the chambers with 10 and 5 ml of DMEM/HamsF-12 supplemented with 1% w/v penicillin/streptomycin, 1% w/v L-glutamine and 10% w/v FBS added to each well on the 20 and 40 kHz paddle respectively. hMSCs were seeded directly on the Ti surface at cell density of 8.4 x 10^3 cells/cm^2 which was termed day 0 of the experiment. Cells were allowed to attach to the strips following the 24-hours incubation at 37°C in 5% CO_2. Subsequently, the strips were removed from the chambers using sterile forceps (autoclaved as described previously) and attached to the sonotrodes inside the tissue culture incubator for ultrasound stimulation. The parameters of ultrasonic exposure are summarised in Table 7. An identical procedure with the ultrasonic transducer turned off was performed to establish a negative control.

2.4.6 LDH assay and cell count following ultrasonic exposure

To assess cell viability following ultrasonic stimulation an LDH assay was carried out as described before. The culture media aliquots were collected immediately prior and after the exposure to ultrasound, as well as 24 hours after the exposure to assess cell death over time. Additionally, a trypan blue viability assay was performed immediately after and then also 24 hours after the ultrasonic exposure to confirm the findings of the LDH assay and compare the cell number increase between the ultrasonically stimulated cultures and controls. Cells were detached from the titanium surfaces with trypsin and collagenase type 1 and counted using haemocytometer as described above.

2.5 Statistical analysis

All experiments were set up with three technical replicates (i.e., 3 paddles) and undertaken independently 3 times, n=3. The data was presented as the median of 3 biological replicates as well as the minimum, maximum, lower quartile, and upper quartile values. Differences in parametric data were compared using Brown-Forthyse and Welch ANOVA tests and $P < 0.05$ was considered statistically significant. Statistical analysis was carried out using GraphPad Prism, Version 9.5.0 (GraphPad Software, San Diego, California US).

2.6 Illustration design

The scientific illustrations used in the present thesis were created by the author using Biorender.com.

3 Results

3.1 Cell counting in osteogenically supplemented cultures

Due to difficulties in obtaining reliable cell numbers in mineralising cultures presented by incomplete resuspending of cell pellets the below cell counting techniques were tested. The method with the most consistent and accurate results was chosen for the subsequent experiments.

3.1.1 Cell detachment from incubation surfaces

Following osteogenic supplementation containing Asc, Dex and β-Gly, cell detachment from polystyrene surfaces of cell culture dishes using trypsin alone revealed significantly lower viable cell numbers than with trypsin and collagenase type 1 (Figure 3.1). However, when cells were incubated on Ti surfaces under identical conditions the enzymatic detachment method appeared to be less effective. SEM of osteogenically-supplemented cells cultured on Ti surfaces showed cells remaining on the Ti discs indicating incomplete cell detachment following enzymatic treatment (Figure 3.2). Although fewer cells were observed on the Ti surfaces incubated in trypsin and collagenase type 1 compared with trypsin only.

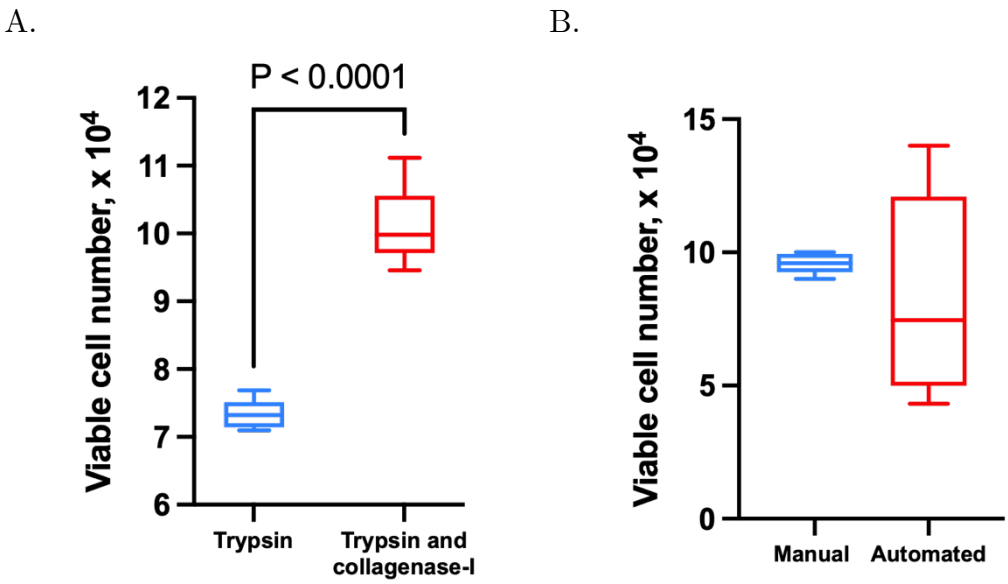

Figure 3.1: Box-and-whisker plots demonstrating mean viable Saos-2 cell numbers obtained by using different cell detachment and counting techniques. Cell detachment from titanium surfaces improved when trypsin was used in combination with collagenase type 1 (A). Manual cell counting with an haemocytometer provided more consistent data in comparison with the automated cell counting involving DNA staining (B). n=3.

A. Cell detachment with trypsin

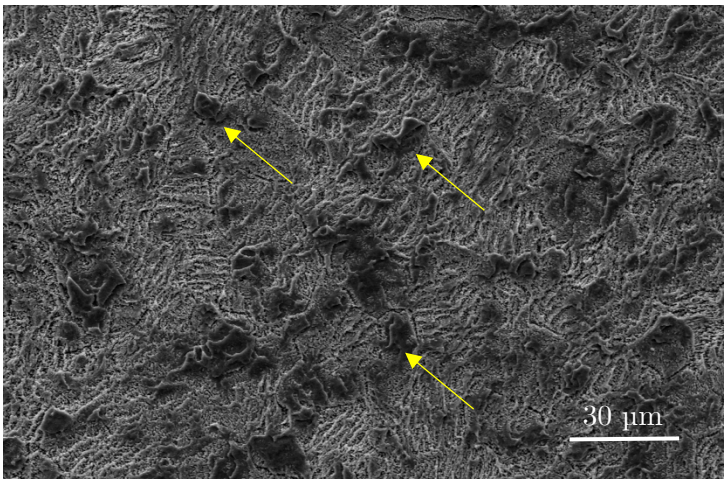

B. Cell detachment with trypsin and collagenase type 1

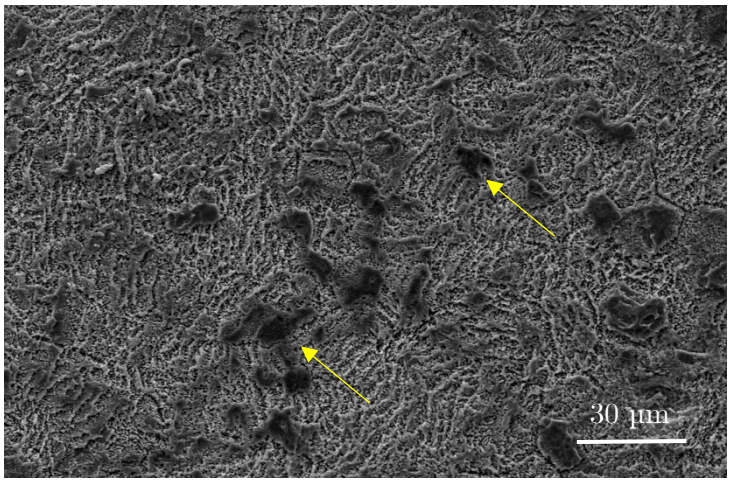

Figure 3.2: SEM micrographs of enzymatically treated Saos-2 cells on Ti surfaces. (A) Complete cell detachment was not achieved after 10 min of treatment with trypsin. (B) Treatment with trypsin and collagenase type 1 resulted in fewer cells remaining on the surfaces when compared with trypsin alone. Yellow arrows indicate several cells attached to the titanium surfaces.

3.1.2 Comparison of cell counting techniques

Manual counting with a haemocytometer and trypan blue staining produced less variable data when compared with the automated cell counting using DNA fluorescence staining and image-segmentation software (Figure 3.1B). Figure 3.3 shows stained nuclei of Saos-2 cells after 7 days of incubation in osteogenic media containing

Asc, Dex and β-Gly from the same tissue culture dish well. Cell density was not identical across the wells. The highest cell density was observed in the centre (Figure 3.3A), consistent with the cell seeding in the well centre, whereas fewer cells were seen at the periphery (Figure 3.3B). Therefore, capturing 4 pictures in random positions across the well did not guarantee a reliable representation of cell numbers. Furthermore, multiple cell layers presented difficulties for automated cell counting as cells at the base of the wells were superimposed on cells in the more superficial layers. Figure 3.4 demonstrates the difficulty with cell recognition by Fiji and ImageJ in these cultures. The areas of high cell densities on the original images (A) were either not well segmented into individual cells (C) or cells were not recognised at all (B), making the method inaccurate and unreliable.

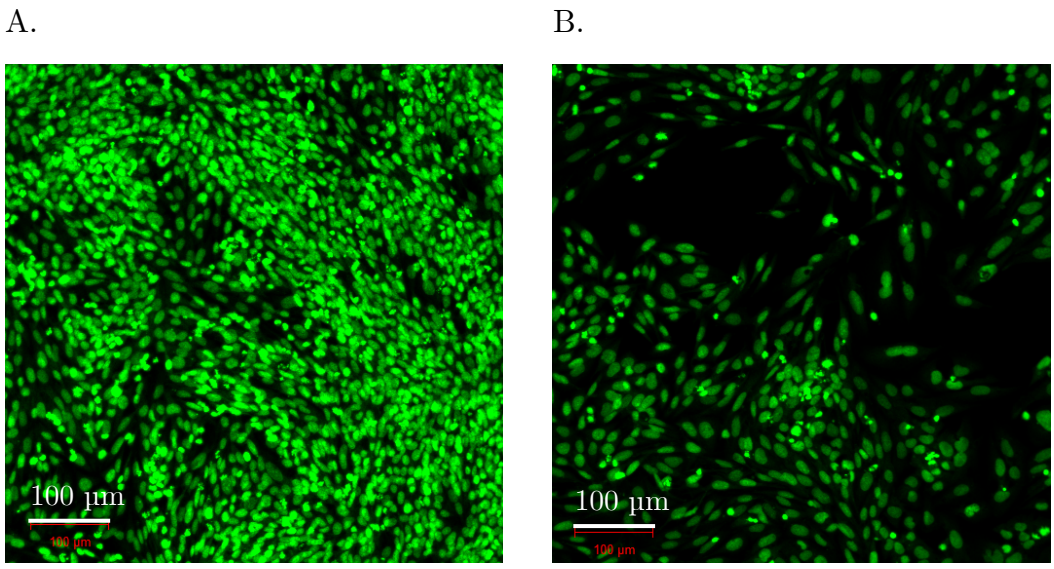

Figure 3.3: Confocal micrographs showing fluorescence staining of DNA in Saos-2 cells after 7 days of incubation in osteogenic media containing Asc, Dex and β-Gly. The central part of the well (A) had a higher cell density compared with the periphery (B) producing difficulties with comparing images sourced from different wells. Multiple cell layers created areas of high signal density inadequate for manual or automated counting.

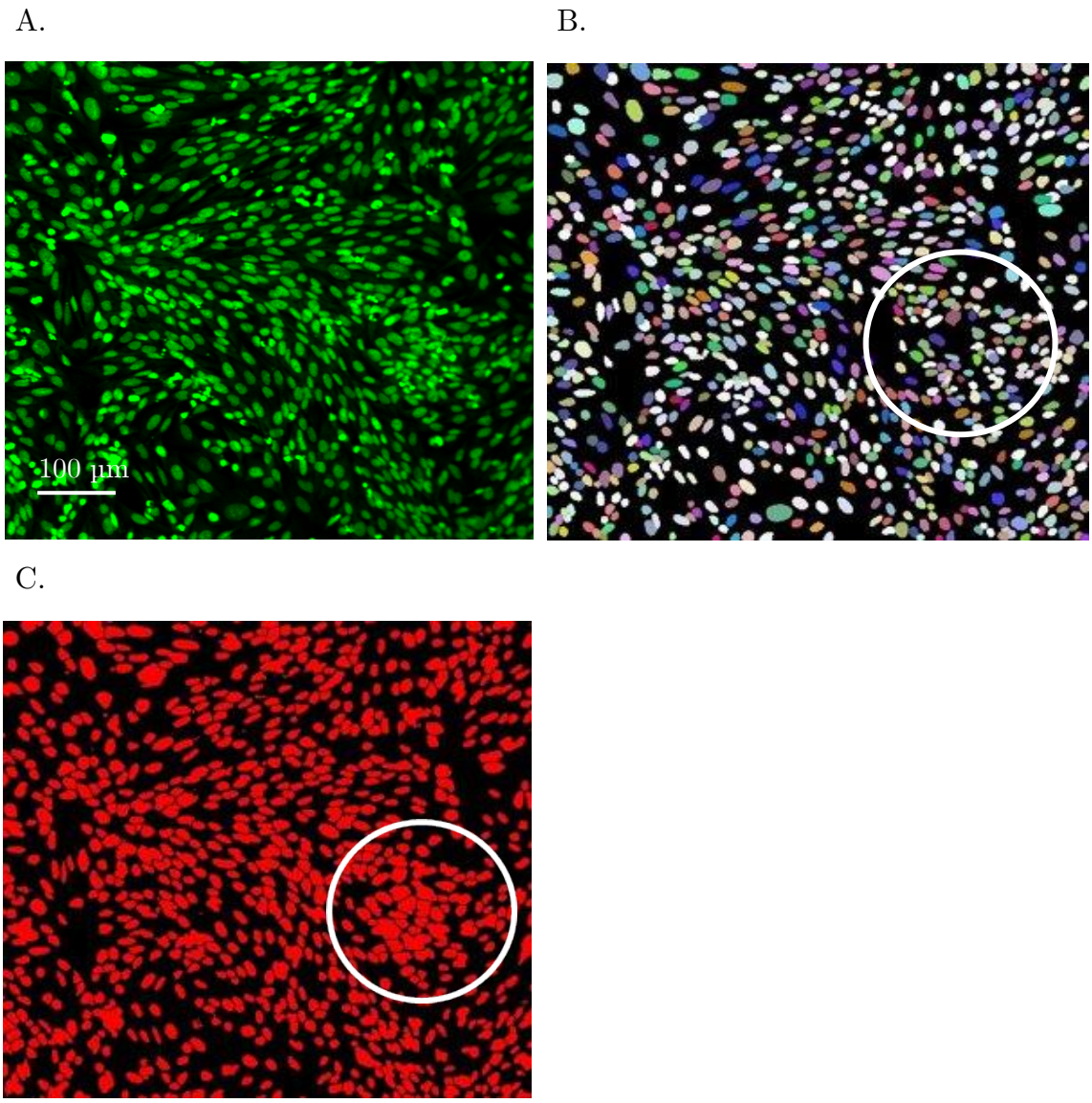

Figure 3.4: Confocal micrograph of osteogenically supplemented (Asc, Dex and β-Gly) Saos-2 cells (A) with sytox green-stained DNA. The cell numbers were obtained using image-analysis software, either (B) Fiji (StarDist) or (C) ImageJ. The areas of high cell density (indicated with white circles) appear to be not recognised, B or poorly segmented, C.

3.2 Effects of osteogenic stimulation on Saos-2 and hMSCs

3.2.1 Cell numbers

The effect of different combinations of osteogenic supplements on cell growth was studied by quantifying viable cell numbers over the course of 14 days. Saos-2 cultures exposed to β-Gly demonstrated a significantly lower number of viable cells compared

with Dex and/or Asc supplemented cultures as well as controls after day 4 of incubation (Figure 3.5) and at all subsequent time points examined. In contrast, the number of viable hMSCs was not statistically significantly affected at any time points examined by any of the osteogenic supplements in comparison with controls (Figure 3.6).

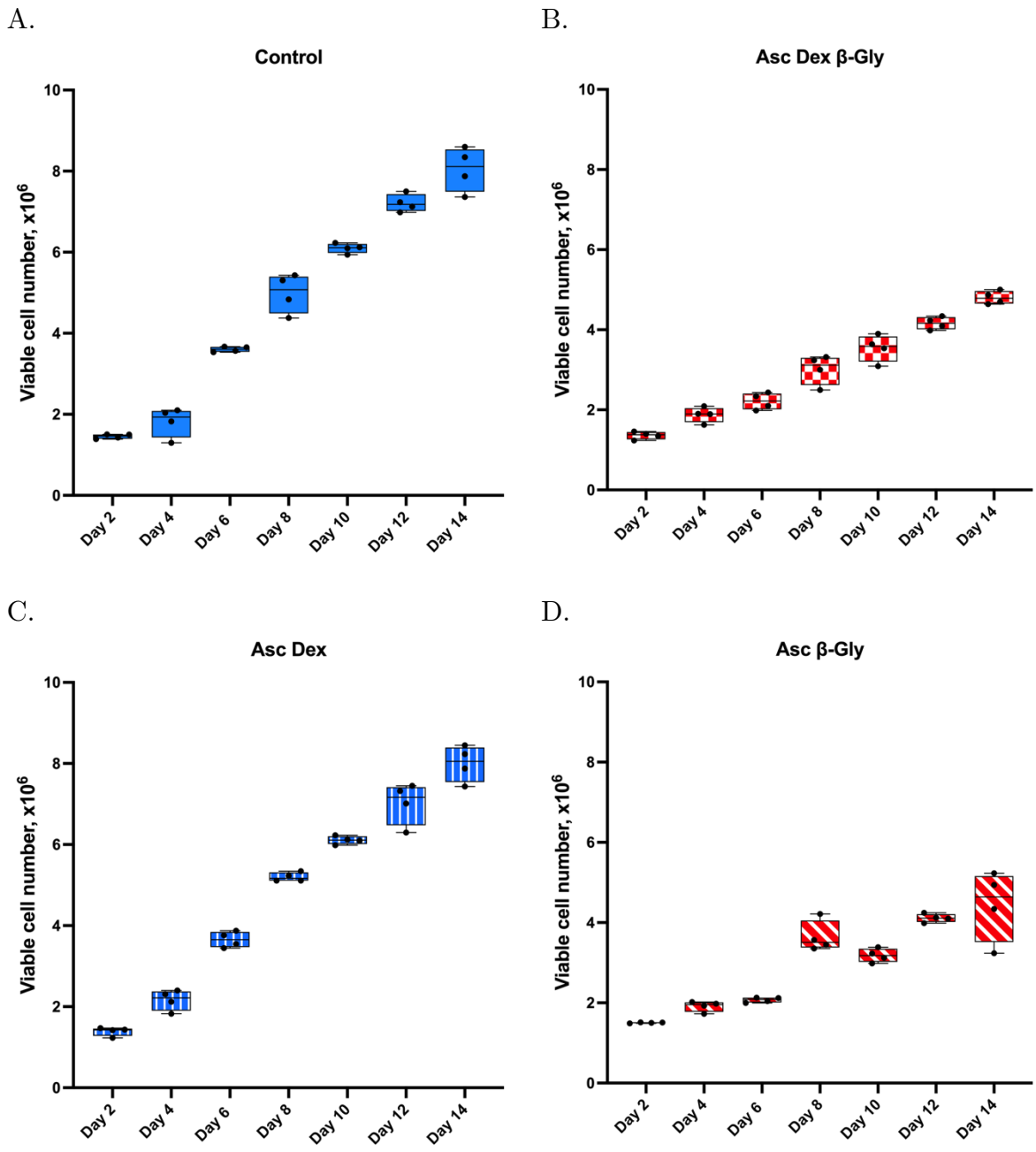

E.

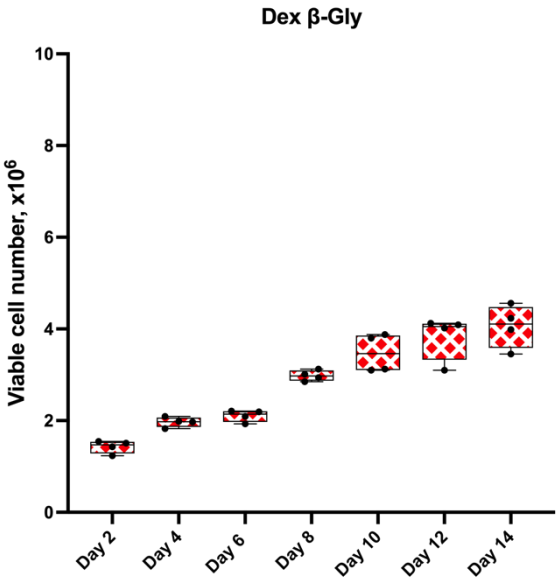
Dex β-Gly
Viable cell number, x10^6
0
2
4
6
8
10
Day 2
Day 4
Day 6
Day 8
Day 10
Day 12
Day 14

F.

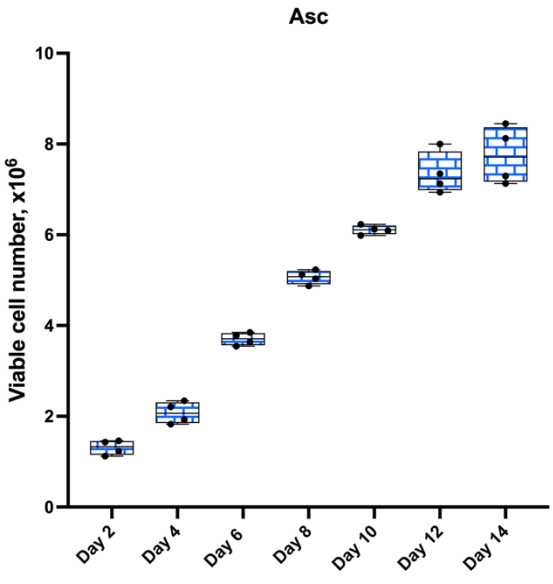
Asc
Viable cell number, x10^6
0
2
4
6
8
10
Day 2
Day 4
Day 6
Day 8
Day 10
Day 12
Day 14

G.

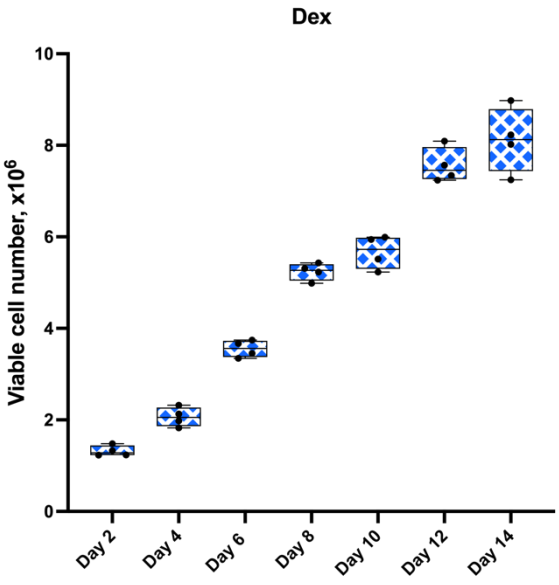
Dex
Viable cell number, x10^6
0
2
4
6
8
10
Day 2
Day 4
Day 6
Day 8
Day 10
Day 12
Day 14

H.

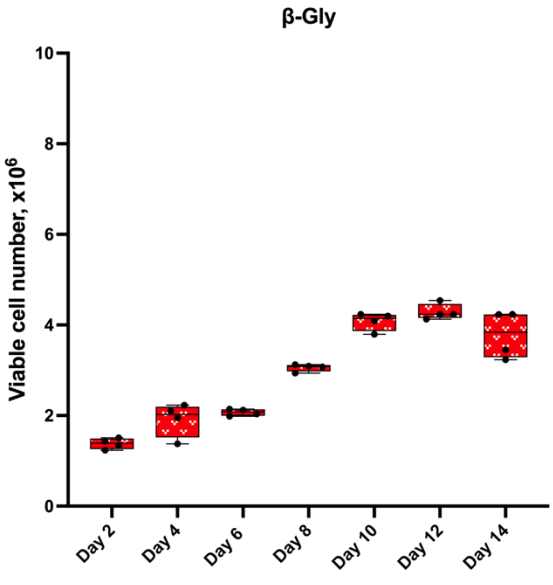
β-Gly
Viable cell number, x10^6
0
2
4
6
8
10
Day 2
Day 4
Day 6
Day 8
Day 10
Day 12
Day 14

I.

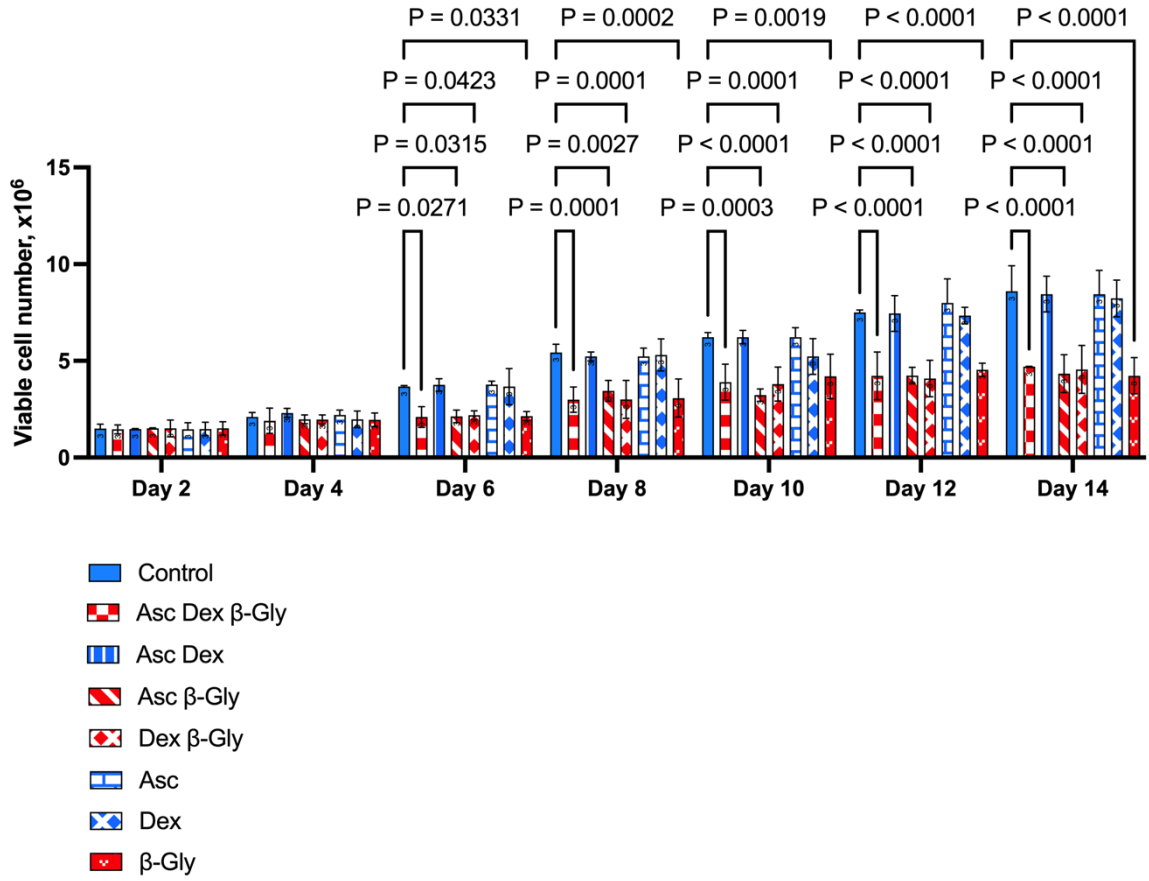

Figure 3.5: Box-and-whisker plots showing median, minimum, and maximum values and upper and lower quartiles of viable Saos-2 cell numbers after incubation with different combinations of osteogenic supplements for 14 days (A-H). Numbers of Saos-2 cells were reduced in the presence of β-Gly after 4 days of supplementation (B,D,E,H) relative to the control of the corresponding day (A). Asc and/or Dex did not affect Saos-2 numbers compared with the control (C,F,G). Bar chart (I) demonstrates the statistical analysis of differences in viable cell numbers at each time point. Significantly lower cell numbers were observed in β-Gly-containing cultures after 4 days of incubation. Red bars represent cultures with β-Gly and blue bars do not. n=3.

A.

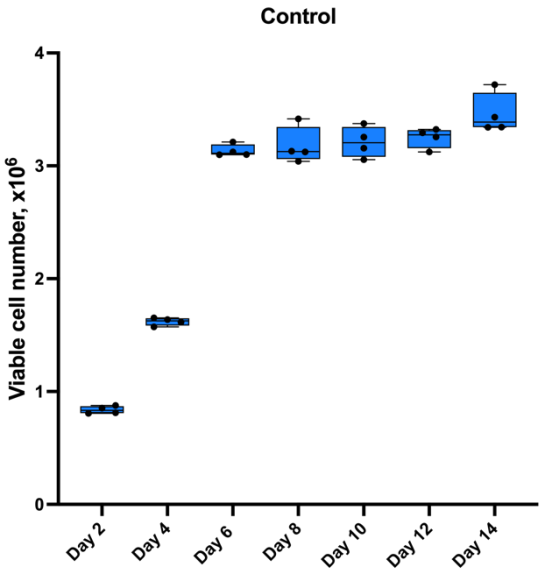
Control
Viable cell number, x10^6
0
1
2
3
4
Day 2
Day 4
Day 6
Day 8
Day 10
Day 12
Day 14

B.

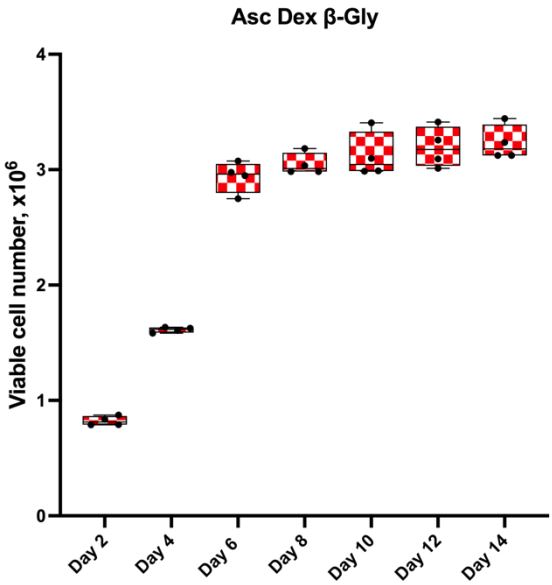
Asc Dex β-Gly
Viable cell number, x10^6
0
1
2
3
4
Day 2
Day 4
Day 6
Day 8
Day 10
Day 12
Day 14

C.

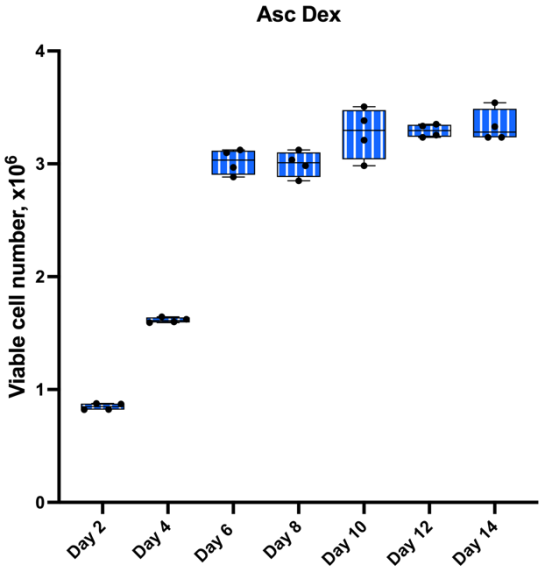
Asc Dex
Viable cell number, x10^6
0
1
2
3
4
Day 2
Day 4
Day 6
Day 8
Day 10
Day 12
Day 14

D.

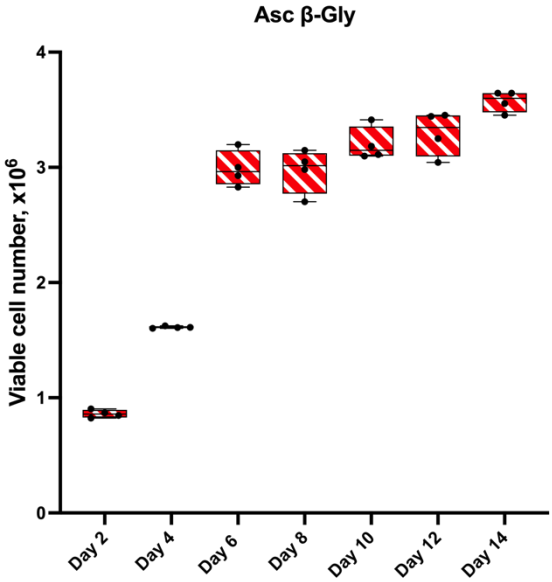
Asc β-Gly
Viable cell number, x10^6
0
1
2
3
4
Day 2
Day 4
Day 6
Day 8
Day 10
Day 12
Day 14

E.

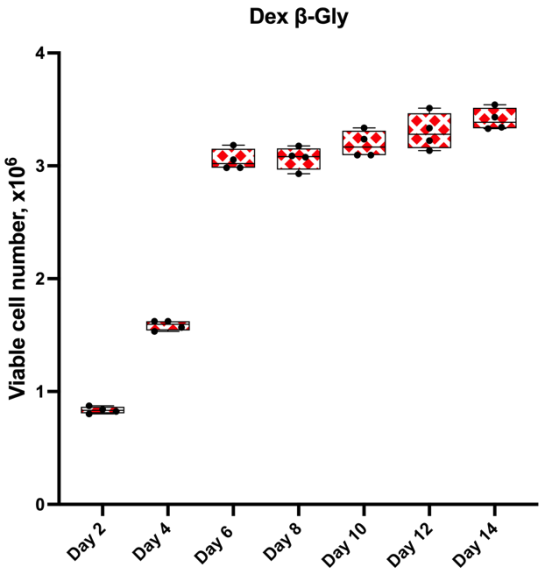
Dex β-Gly
Viable cell number, x10^6
0
1
2
3
4
Day 2
Day 4
Day 6
Day 8
Day 10
Day 12
Day 14

F.

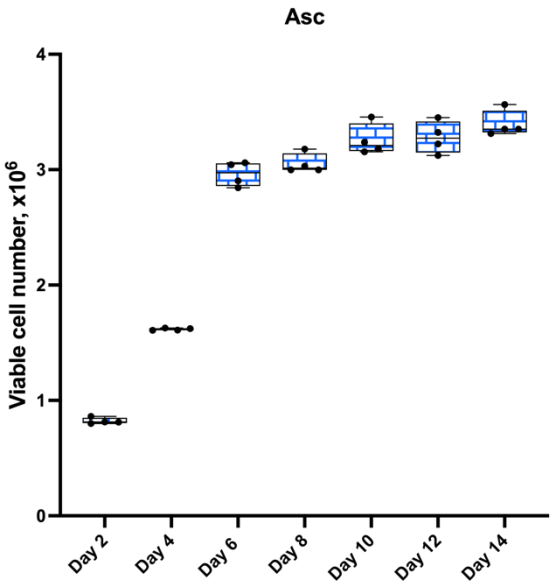
Asc
Viable cell number, x10^6
0
1
2
3
4
Day 2
Day 4
Day 6
Day 8
Day 10
Day 12
Day 14

G.

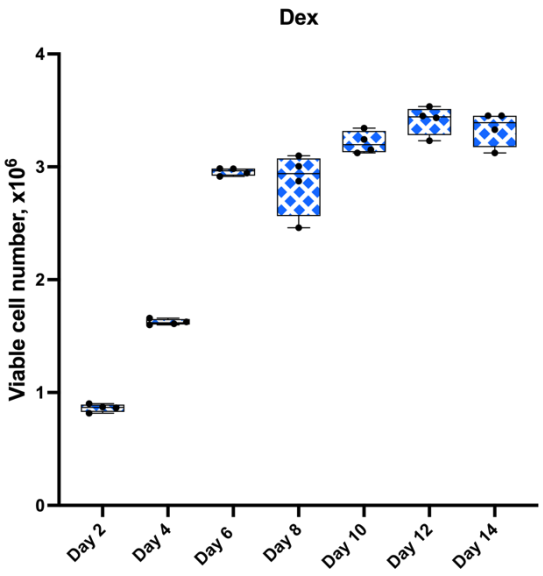
Dex
Viable cell number, x10^6
0
1
2
3
4
Day 2
Day 4
Day 6
Day 8
Day 10
Day 12
Day 14

H.

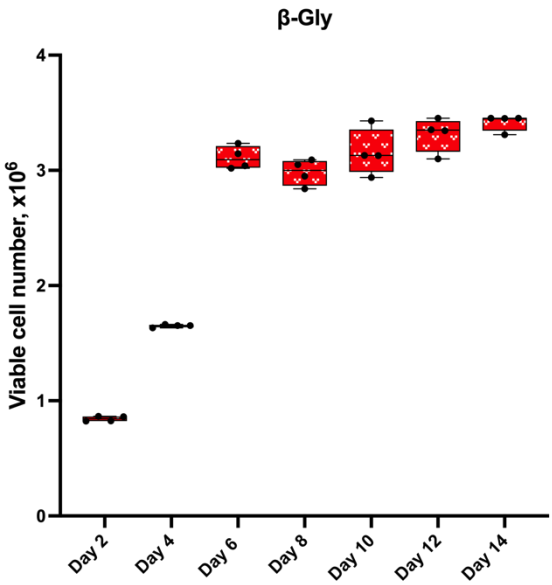
β-Gly
Viable cell number, x10^6
0
1
2
3
4
Day 2
Day 4
Day 6
Day 8
Day 10
Day 12
Day 14

I.

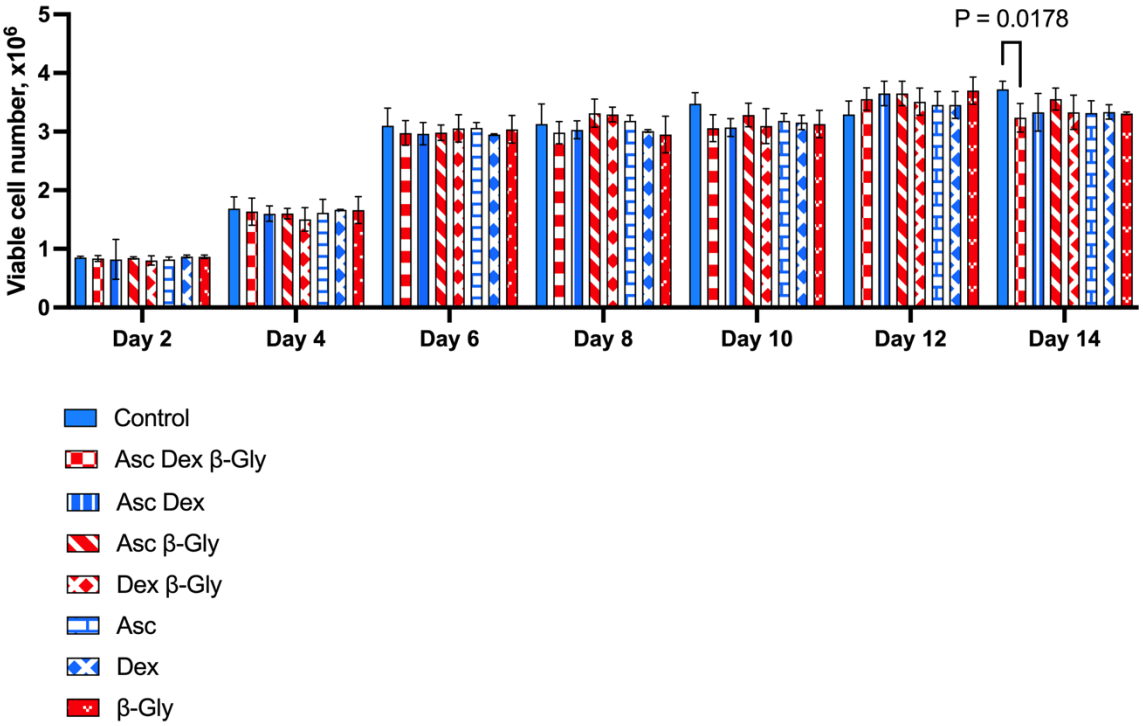

Figure 3.6: Box-and-whisker plots showing median, minimum, and maximum values and upper and lower quartiles of viable hMSCs cell numbers after incubation with different combinations of osteogenic supplements for 14 days (A-H). The trends in cell growth remained the same in all osteogenic media. Statistical analysis is presented in a bar chart (I). In contrast with the Saos-2 cells (Fig. 5), there was no significant change in hMSCs numbers with the addition of β-Gly or Asc and/or Dex compared with controls. Red bars represent cultures with β-Gly, and blue bars do not. n=3.

3.2.2 Proliferation assay

Saos-2 cells incubated in the presence of β-Gly showed significantly fewer (3.1%) BrdU-stained nuclei than cells not exposed to β-Gly (Figure 3.7, Figure 3.9) where 35.6% of all nuclei were stained with BrdU. Hence, the proliferative activity of Saos-2 was decreased in the presence of β-Gly. No statistically significant difference was identified in the number of BrdU-stained nuclei in hMSCs with 23.7% of BrdU stained nuclei in β-Gly exposed cells and 25% of BrdU stained nuclei in negative controls (Figure 3.8, Figure 3.9). Therefore, cell proliferation was not affected by the presence of β-Gly in hMSCs relative to controls. Negative controls with either no BrdU, no anti-BrdU antibody or no secondary antibody did not generate any fluorescence, suggesting specificity of the fluorescence signal.

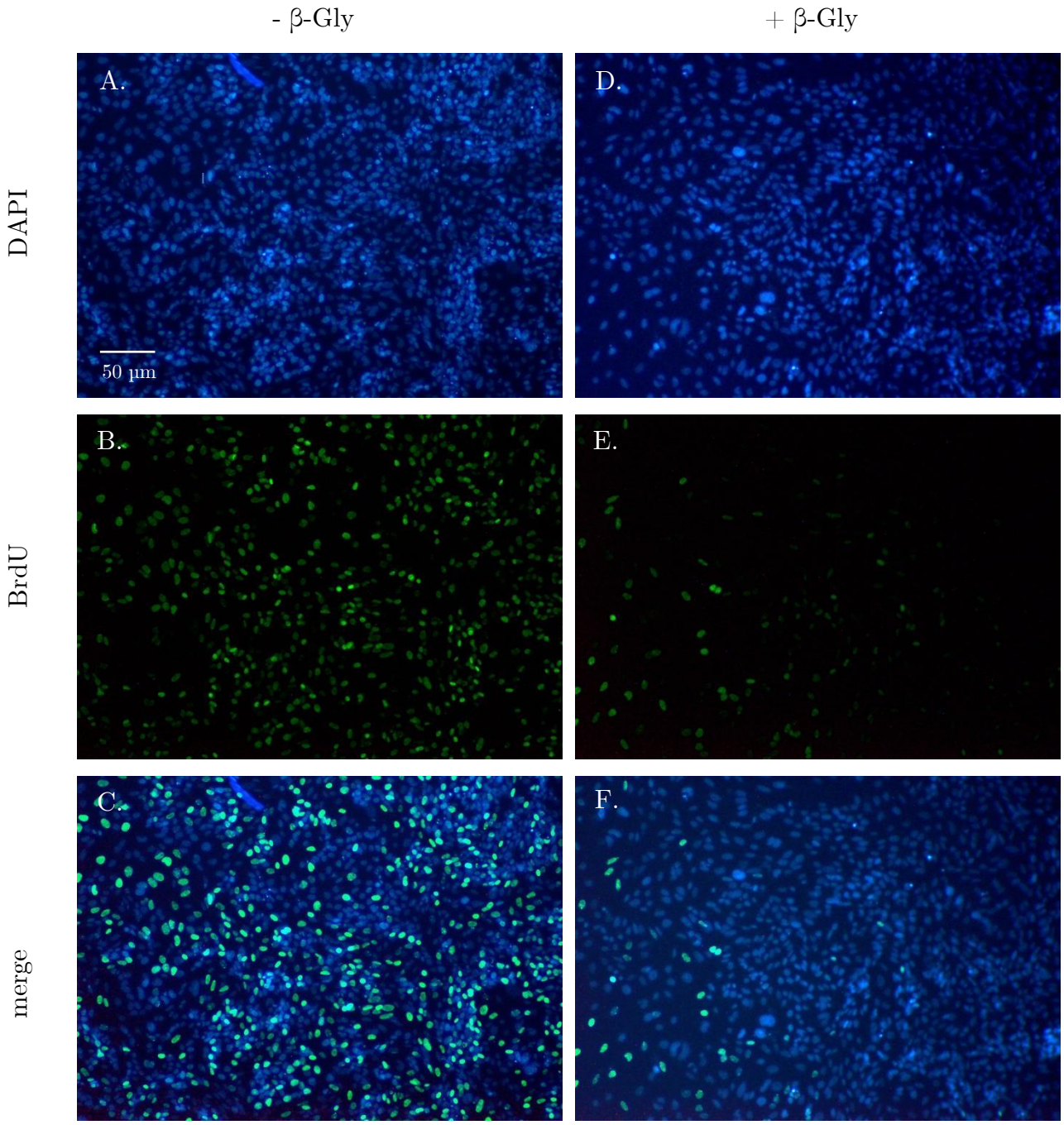

Figure 3.7: Representative confocal fluorescence micrographs of BrdU staining of Saos-2 cells after 4 days supplementation with β-Gly. DAPI staining was used to identify all cell nuclei and images superimposed on BrdU staining to identify the proportion of BrdU positive cells. Saos-2 cells exposed to β-Gly (D-F) demonstrated a lower proportion of BrdU stained nuclei than Saos-2 controls (A-C). n=3.

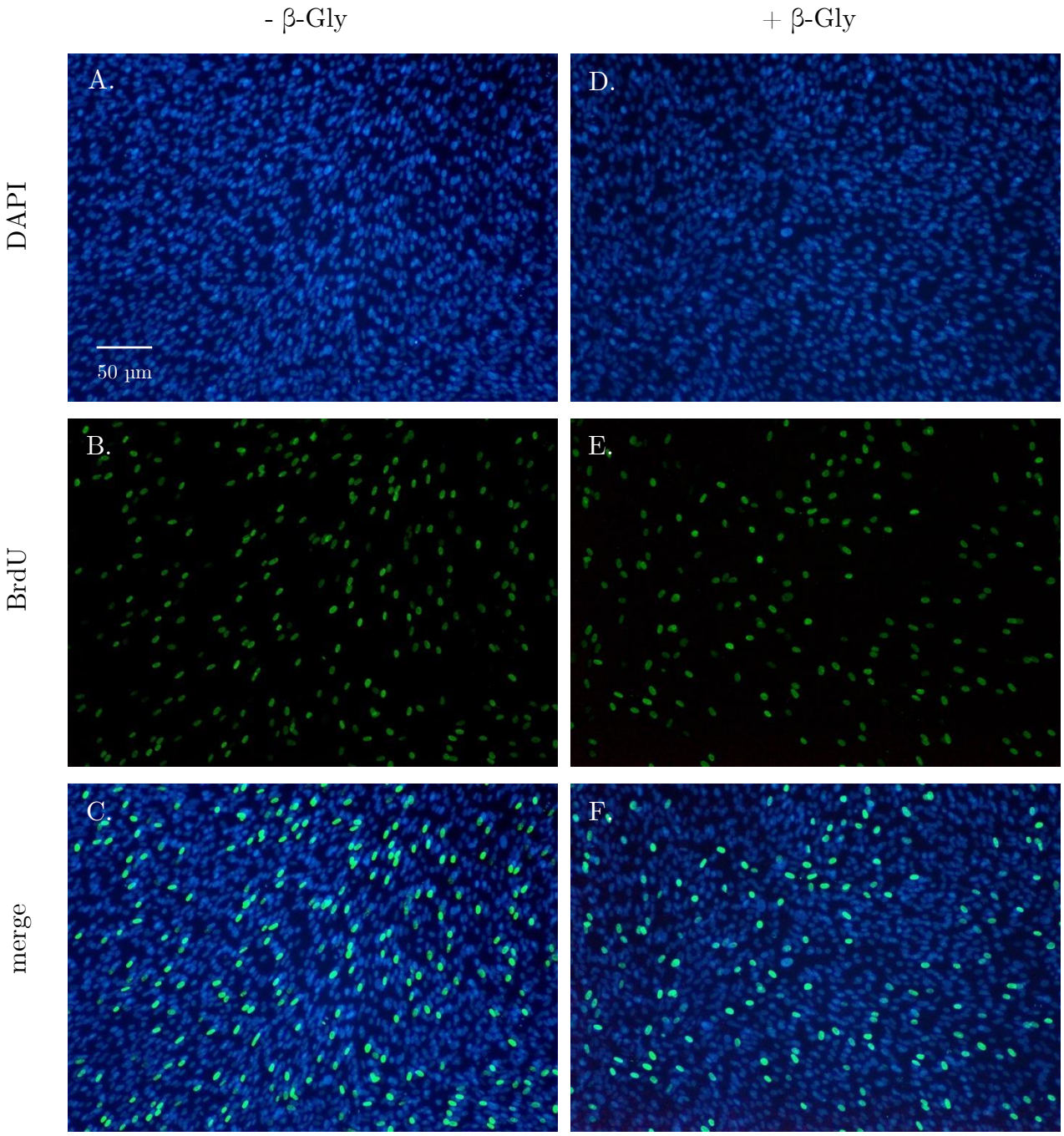

Figure 3.8: Representative confocal fluorescence micrographs of BrdU staining of hMSCs after 4 days supplementation with β-Gly. DAPI staining was used to identify all cell nuclei and images superimposed on BrdU staining to identify the proportion of BrdU positive cells. The proportion of BrdU-labelled hMSCs nuclei did not differ significantly between β-Gly-supplemented (D-F) and non-supplemented (A-C) cultures. n=3.

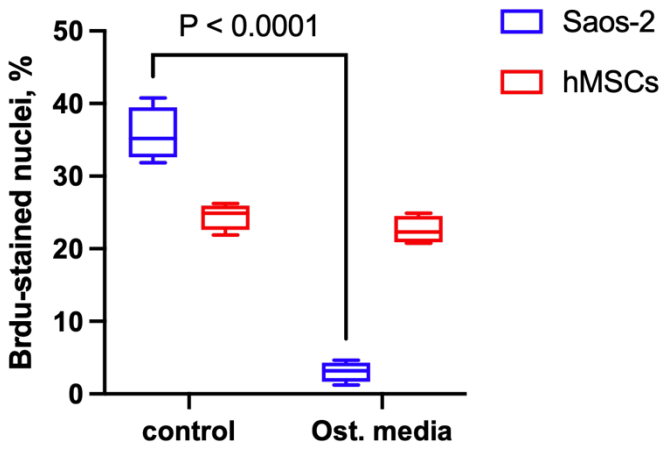

Figure 3.9: Graph showing percentage of BrdU positive cells in Saos-2 and hMSC cultures exposed to plain medium or β-Gly supplemented medium (Ost. media). Saos-2 exposed to β-Gly demonstrated a lower proportion of BrdU stained nuclei than Saos-2 controls, 3.1% and 35.6% respectively. β-Gly-supplemented and non-supplemented hMSCs cultures did not show a significant difference in the proportion of BrdU labelled nuclei – 23.7% and 25% respectively. n=3.

3.2.3 Alizarin red S staining

Alizarin red S (ARS) staining was used to assess mineral matrix deposition in osteogenically-supplemented cultures on day 14 of incubation. ARS showed a 24 and 4-fold increase in mineral matrix production in β-Gly supplemented Saos-2 and hMSC cultures respectively (Figure 3.10). Asc and Dex did not appear to affect mineral deposition in either cell line. However, there was an increased amount of ARS in hMSCs than in Saos-2 cultures in the absence of β-Gly.

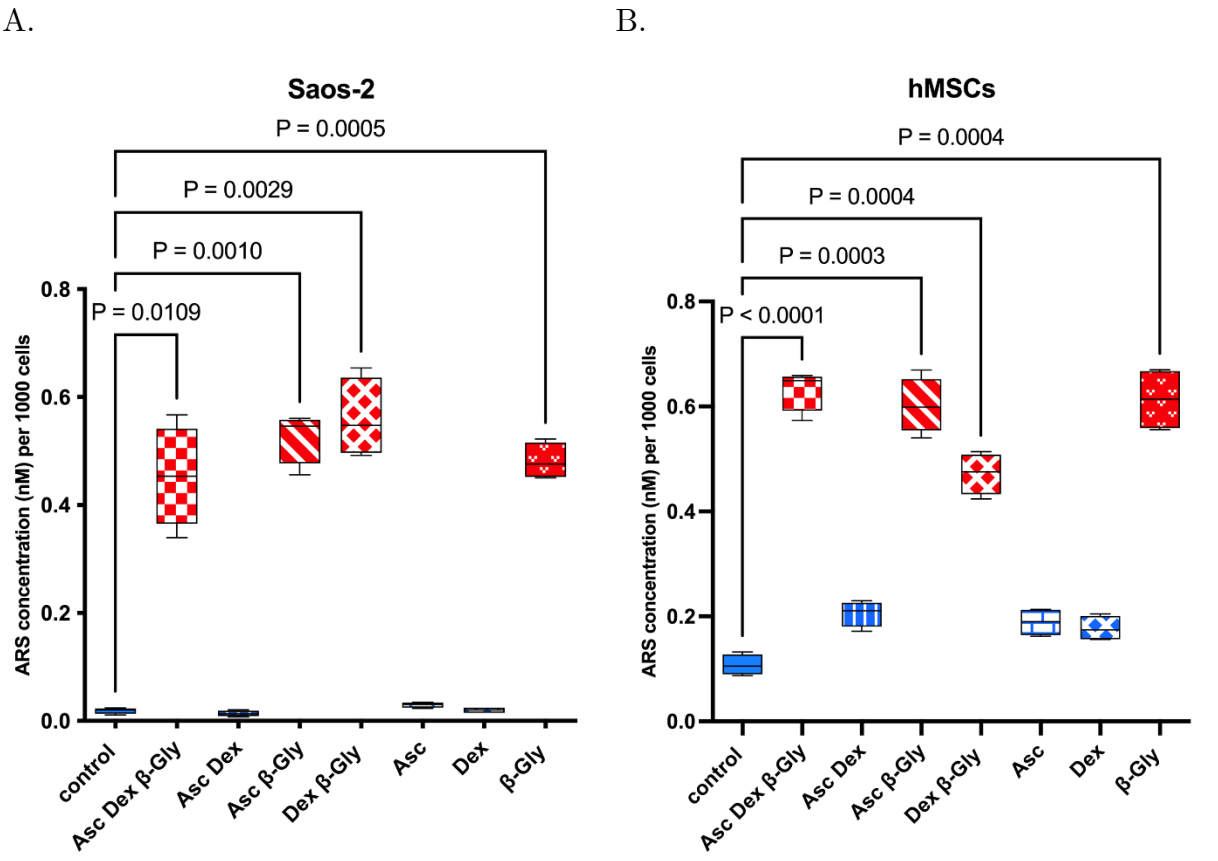

Figure 3.10: Box-and-whisker plots of ARS staining. ARS showed a significant increase in mineralised extracellular matrix synthesis in the presence of β-Gly in both Saos-2 (A) and hMSC (B) cultures. Asc and Dex did not increase mineral matrix production in either cell line. n=3.

3.2.4 Cytotoxicity assay

To evaluate the cause of the reduced Saos-2 cell numbers in cultures containing β-Gly an LDH assay was performed. No significant change in LDH release was observed between the osteogenically treated cells and the controls (Figure 3.11) in either Saos-2 (A) or hMSCs (B).

A. B.

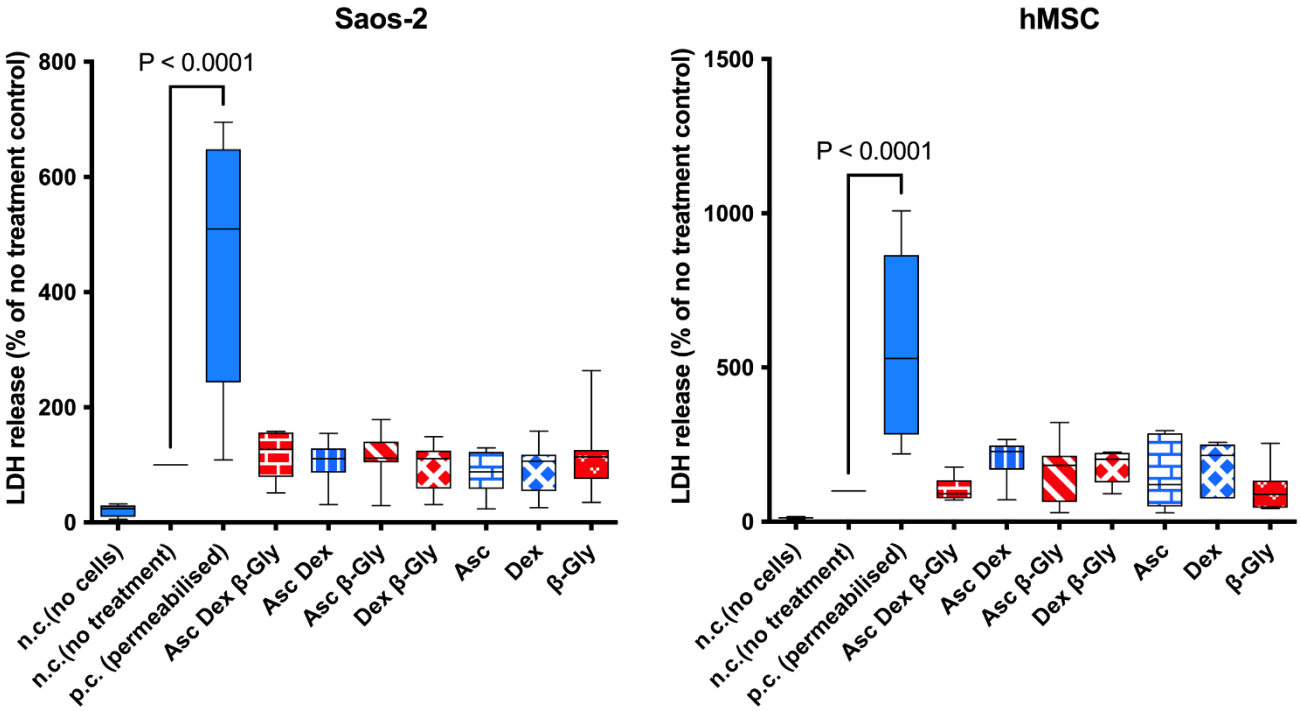

Figure 3.11: Box-and-whisker plots of LDH assay following osteogenic supplementation. The assay demonstrated LDH released from damaged/dead cells. A negligible amount of LDH was detected in the no-cells negative control (n.c.). A 4.5-fold increase in LDH was observed in the positive control (p.c.) containing Triton-permeabilised cells when compared with no treatment controls. No significant change in LDH release was seen between the different osteogenic supplemented cultures in either Saos-2 (A) or hMSCs (B). n=3.

3.2.5 Gene expression analysis

The expression of proliferation markers and osteoblast-associated genes was normalised to the expression of a housekeeper gene, *YWHAZ* and determined every two days of incubation with the different combinations of osteogenic supplements (Figure 3.12, Figure 3.13). Saos-2 cells demonstrated a gradual decrease in *MKI67* (Figure 3.12A) and *PCNA* (Figure 3.12B) expression during the 14 days, however a clear difference between cells exposed to different combinations of Asc, Dex and β-Gly was not identified. hMSCs showed a similar trend for *MKI67* expression (Figure 3.13A) but a more marked decrease in the mRNA synthesis of *PCNA* (Figure 3.13B) after 4 days of osteogenic supplementation than Saos-2 (Figure 3.12B). *RUNX2* expression was significantly upregulated by the presence of osteogenic supplements in Saos-2 cells and increased during the incubation period relative to the negative controls (Figure 3.12D). In contrast, the *RUNX2* activity increased only at day 8 of the experiment and thereafter in osteogenically supplemented hMSCs (Figure 3.13D). *ALP* expression was upregulated in the Dex, Asc, β-Gly supplemented hMSCs (Figure 3.13C) and reached a maximum on day 8 of incubation. Saos-2 showed an upregulation of *OCN* in the presence of β-Gly (Figure 3.12E) at day 8 whilst *PHEX*, an osteocyte-associated gene was significantly upregulated in all Saos-2 cultures containing osteogenic supplements at day 8 of incubation (Figure 3.12F). No significant trend in *PHEX* expression was observed in hMSCs (Figure 3.13F) at any stage of the experiment.

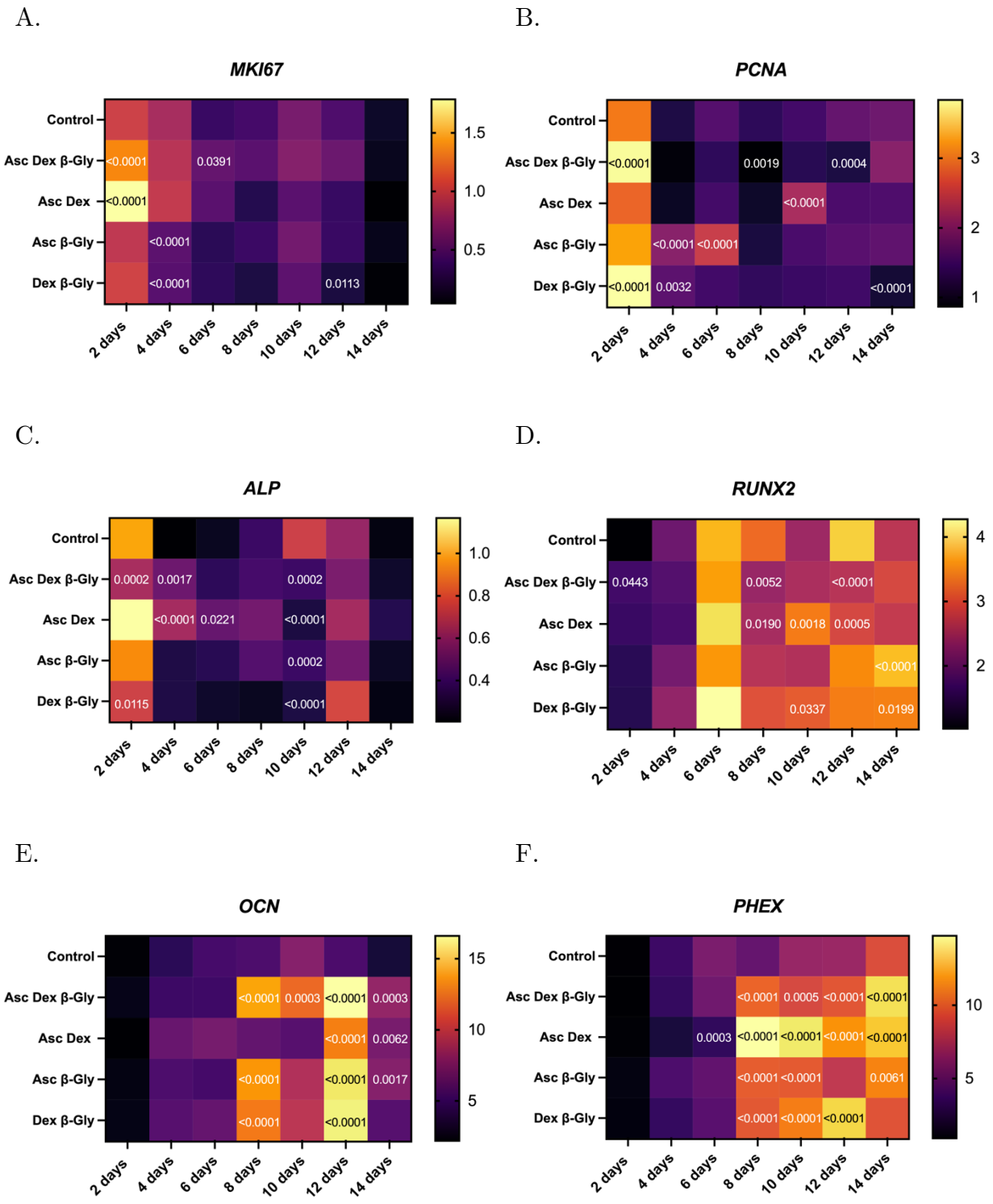

Figure 3.12: Heatmaps of the relative gene expression levels by Saos-2 cells incubated in osteogenic media over 14 days and compared with the expression of YWHAZ. The expression of proliferation markers MKI67 (A) and PCNA (B) decreased over 14 days in all conditions. The activity of ALP decreased (C) followed by significantly upregulated RUNX2 expression (D) as of day 4 in the presence of β-Gly. A later osteoblast marker, OCN and the osteocyte-characteristic marker, PHEX both increased expression levels after 8 days in β-Gly supplemented Saos-2 (E, F). n=3.

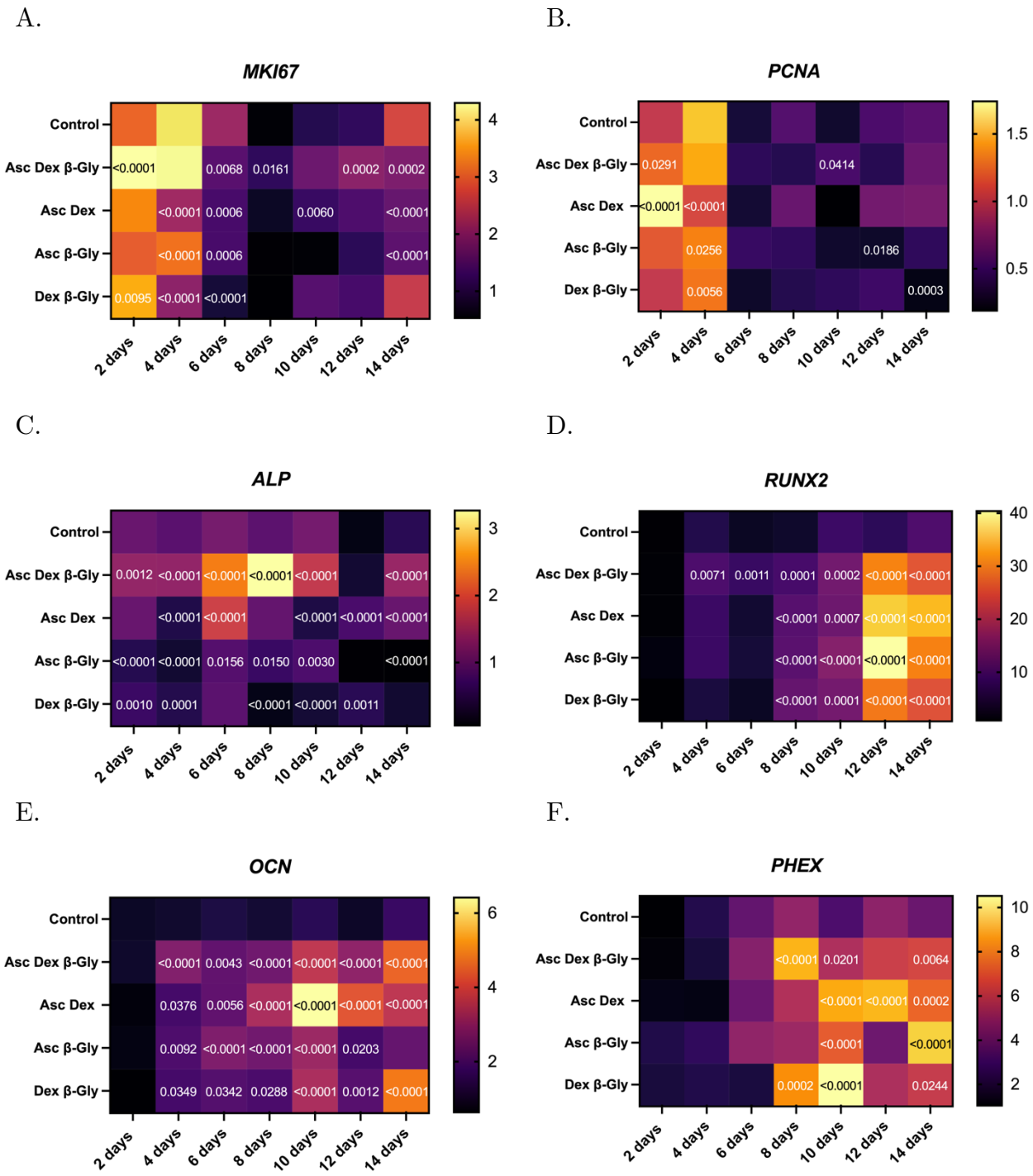

Figure 3.13: Heatmaps for the relative gene expression levels by hMSCs incubated in osteogenic media for 14 days and compared with the expression of YWHAZ. Like the Saos-2, hMSCs showed downregulation in the expression of MKI67 (A) and PCNA (B) in all culture conditions. RUNX2 expression increased only after 8 days of incubation in hMSCs (D). A less obvious increase in the transcription of OCN and PHEX after 8 days in β-Gly supplemented hMSCs (E, F) was seen than in Saos-2. n=3.

3.3 *In vitro* characterisation of titanium substrates for cell growth

3.3.1 Titanium surface preparation

Figure 3.14 demonstrates surface roughness achieved following surface polishing and acid etching. Higher etching temperatures produced a rougher surface relative to the non-treated control as observed using contact profilometry (Figure 3.15). Arithmetic average roughness, Ra was obtained by calculating the average deviation of maximum peak and maximum valley values relative to the mean height of the surface. EDX analysis did not show significant chemical contamination on the control discs surface or discs acid-etched at 25°C. There was a small percentage of carbon (1.19%) and aluminium (1.19%) on the discs treated at 40°C and 60°C respectively (Figure 3.16). Both possibly resulted from contamination from the polystyrene container used to store the discs or tools used to handle the discs. The corrosion-resistant nature of titanium was likely to prevent any significant chemical effect of acid-etching on the discs.

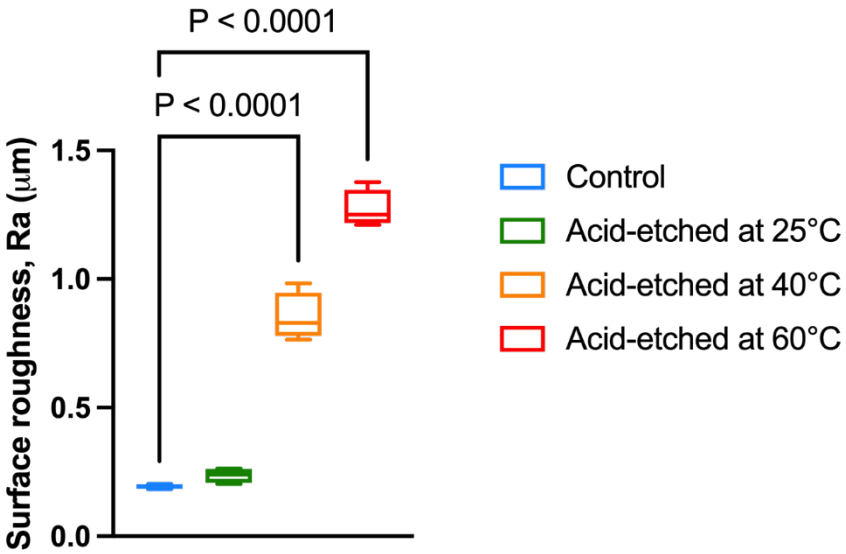

Figure 3.14: Box-and-whisker plots demonstrating surface roughness, Ra of Ti discs. Ra increased with increasing temperature of hydrochloric acid etching. Etching at 25^{o}C did not produce a significant roughening effect, whereas 40^{o}C and 60^{o}C generated a noteworthy increase in surface roughness. n=4.

A. Control

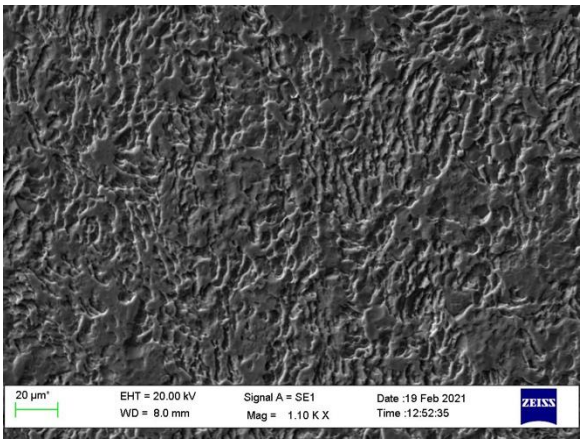

B. Acid-etched at 25°C

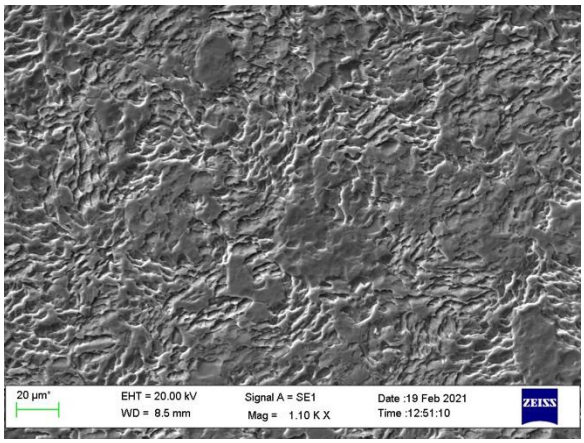

C. Acid-etched at 40°C

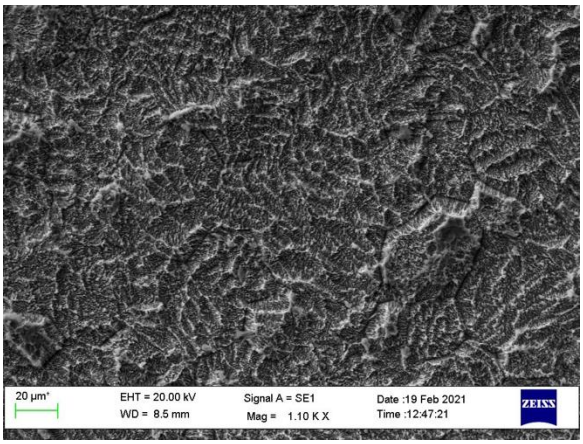

D. Acid-etched at 60°C

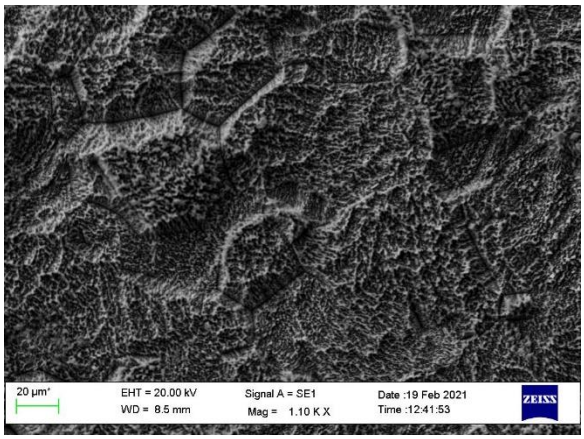

Figure 3.15: SEM micrographs showing surface roughness of Ti discs. The roughness visibly increased with the increased temperature of acid etching.

A. Control

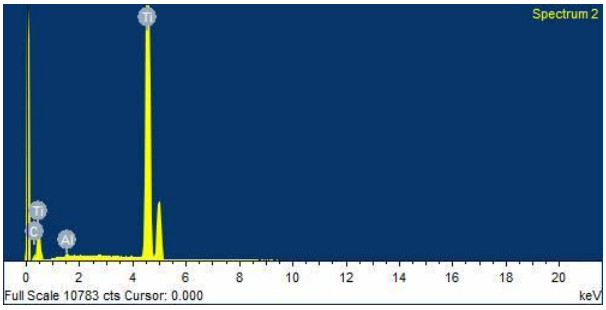

Element	Weight, %	Atomic, %
Ti	100.00	100.00

B. Acid-etched at 25°C

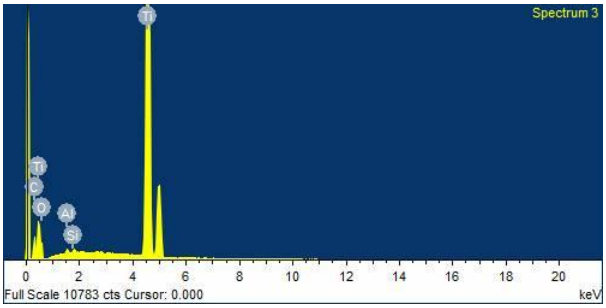

Element	Weight, %	Atomic, %
Ti	100.00	100.00

C. Acid-etched at 40°C

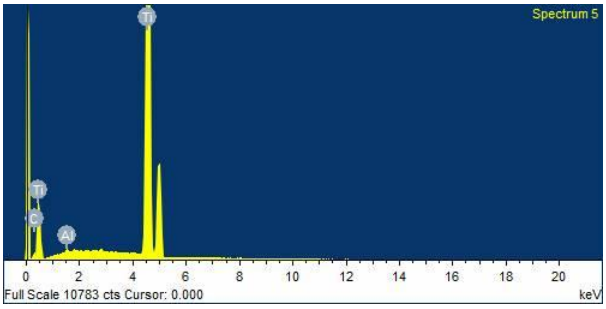

Element	Weight, %	Atomic, %
Ti	98.81	95.41
C	1.19	4.59

D. Acid-etched at 60°C

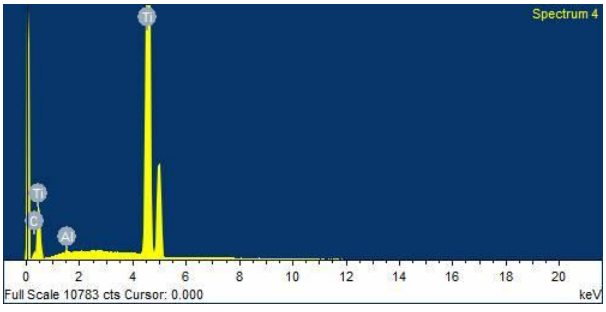

Element	Weight, %	Atomic, %
Ti	98.81	99.66
Al	1.19	0.34

Figure 3.16: Charts representing EDX analysis of chemical composition of the discs following acid etching. There was no significant contamination of the Ti discs following acid etching. n=3.

3.3.2 Tissue culture

Saos-2 cell attachment onto Ti discs was assessed by enzymatically detaching the cells from the discs and subsequently quantifying viable cells using the trypan blue exclusion assay. Cell attachment improved with greater values of surface roughness following 24-hours incubation (Figure 3.17). The highest cell number was observed on discs with surface roughness, Ra ~1 µm (acid-etched at 40°C) with the 2.7, 3,7 and 2-fold increase in the number of cells on the surfaces acid-etched at 20°C, 40°C and 60 °C respectively.

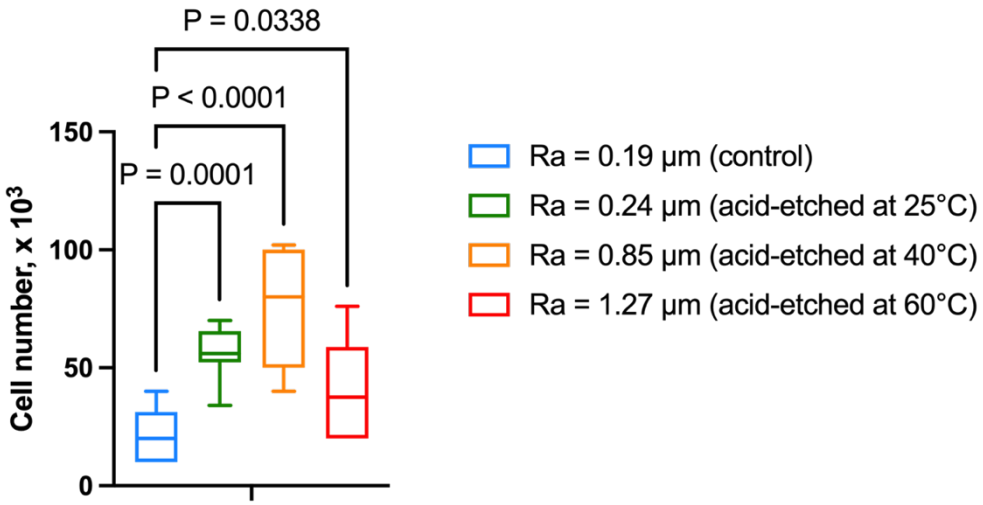

Figure 3.17: Box-and-whiskers plots showing the mean number of viable Saos-2 cells attached to the Ti surfaces per disc. The attachment improved with the increased surface roughness of acid-etched Ti discs. Discs, acid etched at 40^{o}C with roughness, Ra ~ 1µm demonstrated the most significant increase in cell attachment and were used in the subsequent experiments. n=3.

3.4 Ultrasonic exposure of cells *in vitro* on titanium surfaces

3.4.1 Temperature changes of culture media during ultrasound exposure

Following a continuous ultrasound exposure at both 20 and 40 kHz using a range of currents from 0.05 to 0.15 A, the temperature of culture media around Ti paddles increased directly proportionally to the increase in current (Figure 3.18, Figure 3.19). Stimulation at 0.075 A, 0.1 A and 0.15 A showed a significant temperature increase above 37^{o}C at both 20 and 40 kHz, hence these currents could not be used for the subsequent tissue culture experiments due to the likely fatal thermal damage to cells. A current of 0.05 A did not increase the temperature of culture media above the physiological range at either 20 or 40 kHz, therefore it was considered appropriate for application to cells *in vitro*. Distal, middle, and proximal parts of the paddles also demonstrated different temperature increases depending on the current used. The temperature of culture media was highest at the distal end and lowest at the proximal end. However, at 0.05 A the difference in temperatures across the paddle was minimal at both 20 and 40 kHz with the maximum temperature reaching 38.1^{o}C at the proximal end with 20 kHz.

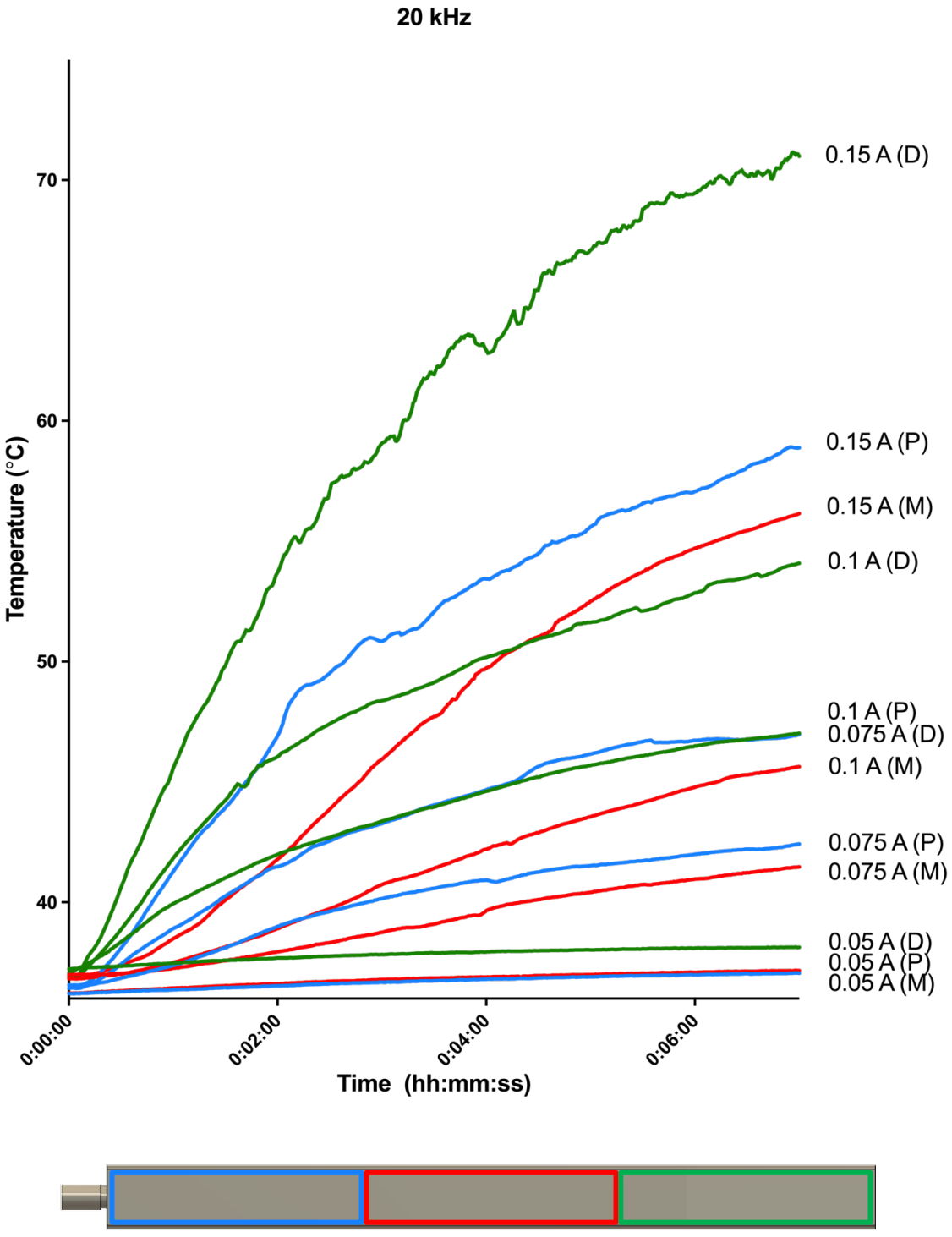

Figure 3.18: Line graph demonstrating temperature changes of culture media across Ti paddles during the exposure to 20 kHz ultrasound. The Ti paddles were exposed to ultrasonic stimulation at different current levels for 7 min while in a 37°C incubator. Current above 0.05 A increased the temperature of the media above 37°C which would be harmful for cell incubation. Distal (D) end of the paddle showed the highest temperature increase across all tested currents relative to the middle (M) and proximal (P) parts. n=3.

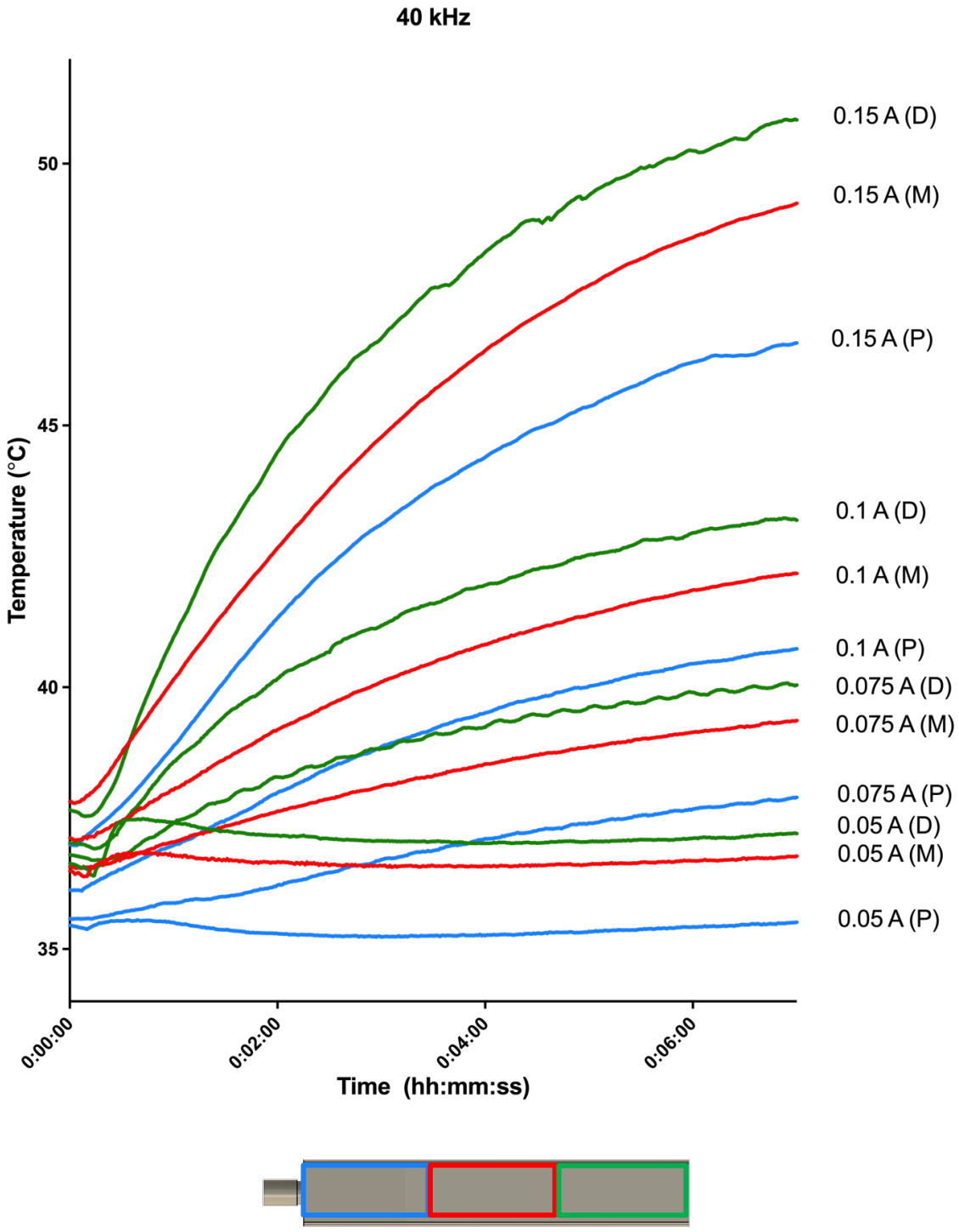

Figure 3.19: Line graph demonstrating temperature changes of culture media across Ti paddles during the exposure to 40 kHz ultrasound under identical conditions to the described in Fig.18. Paddles oscillating at 40 kHz demonstrated a lower temperature increase at all tested currents relative to 20 kHz. Similarly, to 20 kHz, the temperature increase of the media at currents up to and including 0.05 A was within the physiological range with the distal (D) end experiencing the highest increase relative to the middle (M) and proximal (P) parts. n=3.

3.4.2 Cytotoxicity assay and cell count following ultrasonic exposure

After 24 hours following ultrasonic exposure of cells attached to the Ti paddles, cell counts were performed. Due to the differences in temperature across the paddles, cell counts from the proximal, middle, and distal parts of the treated cultures were compared with the corresponding parts of the non-treated controls. The number of live cells on the proximal end of the 20 kHz paddle was significantly lower than the in the control ($P = 0.013$). However, live cell numbers did not differ significantly between exposed and control cultures in either the middle or distal parts using 20 kHz, nor on any section of the 40 kHz paddle (Figure 3.20). Cytotoxicity induced by ultrasound was assessed before, immediately after and 24 hours after the ultrasound exposure. No significant difference in the concentration of LDH released by cells was identified on the proximal, middle, and distal sections of the paddles and the corresponding non-treated controls at any point before or after the exposure. Hence, cytotoxicity was not induced by the ultrasonic excitation at 20 and 40 kHz over 5 min (Figure 3.21).

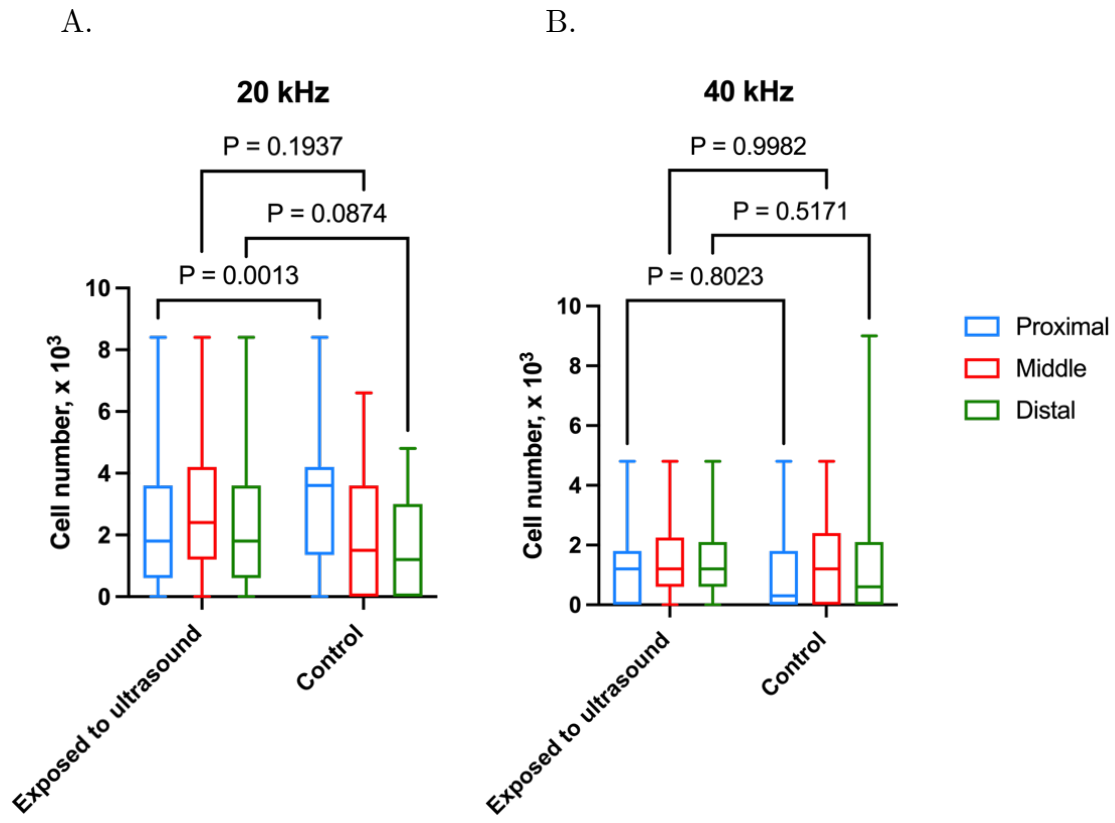

Figure 3.20: Box-and-whisker plots showing viable cell numbers of Saos-2 within proximal, middle and distal wells on the Ti paddle exposed to ultrasound. Cell number on the proximal end of the Ti paddle oscillating at 20 kHz was significantly decreased compared with the control. Cells numbers did not differ significantly on the remaining part of the 20 kHz paddle or on any segment of the 40 kHz paddle. n=3.

A.

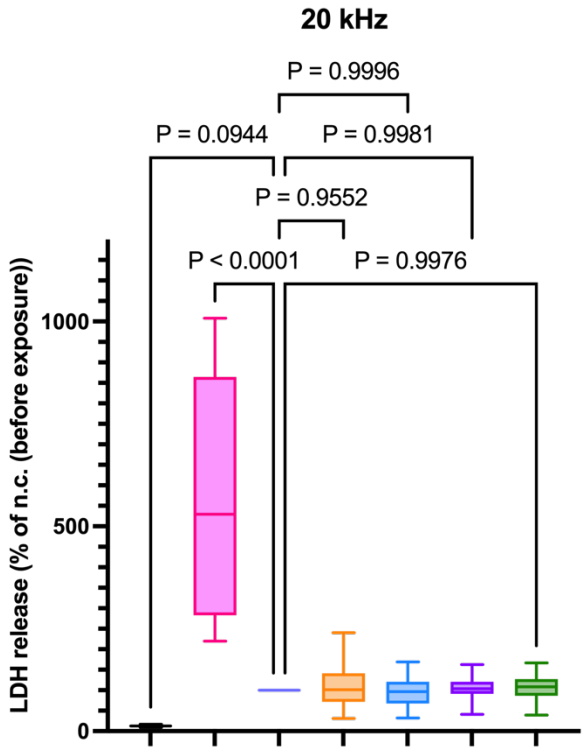
20 kHz
P = 0.9996
P = 0.0944
P = 0.9981
P = 0.9552
P < 0.0001
P = 0.9976
LDH release (% of n.c. (before exposure))
1000
500
0

B.

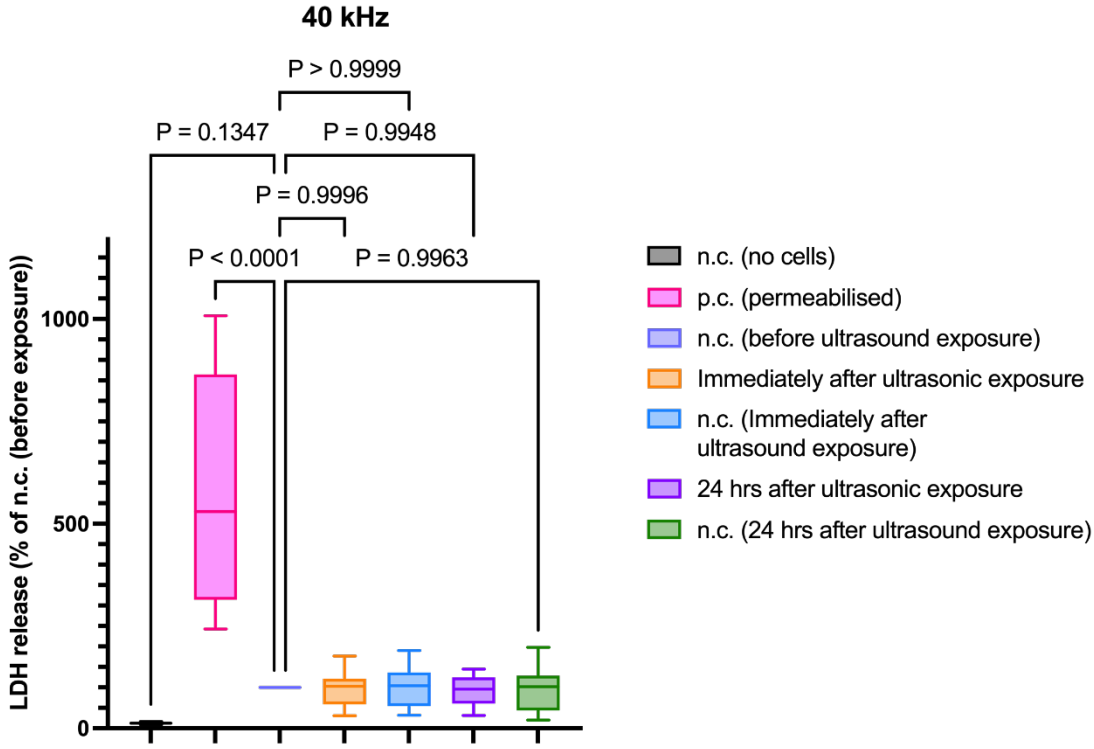
40 kHz
P > 0.9999
P = 0.1347
P = 0.9948
P = 0.9996
P < 0.0001
P = 0.9963
LDH release (% of n.c. (before exposure))
1000
500
0
n.c. (no cells)
p.c. (permeabilised)
n.c. (before ultrasound exposure)
Immediately after ultrasonic exposure
n.c. (Immediately after ultrasound exposure)
24 hrs after ultrasonic exposure
n.c. (24 hrs after ultrasound exposure)

Figure 3.21: Box-and-whisker plot demonstrating the percentage LDH release by ultrasonically stimulated hMSCs. The LDH concertation was not significantly affected by the ultrasonic exposure at 20 (A) or 40 kHz (B). Triton-permeabilised positive controls demonstrated a noticeable increase in LDH release indicating an accurate experimental outcome. The data was compared with the non-treated (n.c. before ultrasound exposure) control which was considered as 100%. n=3.

4 Discussion

4.1 General discussion

A novel experimental design was developed to facilitate the precise exposure of cells to a controlled setting of ultrasound whilst attached to titanium surfaces to mimic implants conditions and geometry. Several specific objectives were defined to ensure a comprehensive investigation. Firstly, two osteogenic cell lines were examined and compared to establish the most suitable bone cell model. This evaluation allowed identification of optimal cell counting techniques and to understand the effects of osteogenic supplementation on cellular behaviour, providing a well-defined osteoblast model for subsequent experiments. Next, the study focused on examining how surface modifications of titanium affected osteoblast attachment, allowing to select an optimum surface treatment for the ultrasonic treatment device. This step was crucial to ensure the validity and reliability of the experimental setup, enabling us to obtain more clinically relevant results. Finally, a cell ultrasonic treatment system was developed that enabled the precise and defined exposure of cells to therapeutic ultrasound whilst adherent to Ti. This innovative system allowed further exploration and study of the effects of ultrasound therapy on osteoblasts in a controlled manner, which may open new avenues for research in the future.

4.2 Cell counting in mineralising cultures

One of the commonest analyses employed in *in vitro* studies involves assessment of cell viability and numbers. With regards to osteoblasts, these may provide a useful indication of the impact of a chemical or physical treatment on cells and cellular response to an implant biomaterial. Understandably, the techniques for obtaining cell numbers must be rapid, reliable, and affordable. A further question in the reliability of cell counts arises when dealing with confluent mineralised matrix forming cultures. In the present study, several cell detachment and counting techniques were tested to identify a method that would yield accurate viable cell numbers in osteogenically supplemented cultures.

4.2.1 Cell dissociation using proteolytic enzymes

4.2.1.1 Trypsin and collagenase type 1 for dissociation of osteoblasts

Typically, proteolytic enzymes such as trypsin, collagenase or Accutase™ are used to cleave the adhesion proteins on cells during a ~10 min incubation (Lai et al., 2022). Trypsin, a serine endopeptidase, which catalyses cleavage between the carboxylic acid group of arginine or lysine and the adjacent amino acids amine end, effectively fragmenting proteins. Alternatively, collagenase type 1, also known as matrix metalloproteinase 1 (MMP-1), is a member of the MMP family, which plays a role in breaking down the extracellular matrix (Cabral-Pacheco et al., 2020). Collagenase type 1 specifically hydrolyses triple-helical collagens, which are the most abundant component of the extracellular matrix, making it a common choice for isolating cells from primary tissues. In the present study, trypsin alone did not achieve complete degradation of the mineralised matrix, as evidenced by the significantly reduced cell

numbers compared with cells detached using a combination of trypsin and collagenase type 1 (Figure 3.1A). Moreover, a high degree of cell clumping, also known as cell agglomerates, was observed when using trypsin, possibly compromising the accuracy of cell numbers too due to the inability to differentiate between individual cells. The presence of cell clumps can also create difficulties in downstream applications, such as cell counting, flow cytometry, or single-cell analysis, potentially resulting in inaccuracy. The primary reason for clump formation in osteogenically supplemented cell cultures is the adherent nature of mineralised matrix. Moreover, excessive pipetting or prolonged enzymatic incubation can cause cell damage, leading to release of DNA, which may contribute to formation of cell clumps (Jager et al., 2016).

Consequently, the combination of trypsin and collagenase type 1 was adopted for cell detachment in all subsequent experiments. However, it is important to note that even with the addition of collagenase type 1, complete cell detachment from the titanium substrate was not achieved which was a limitation of the present study (Figure 3.2). Thus, the presented cell numbers should be considered relative rather than absolute.

4.2.1.2 Strategies to improve enzymatic dissociation of osteoblasts

4.2.1.2.1 Prolonged incubation with proteolytic enzymes

To enhance the dissociation of the mineralised matrix, a potential strategy could involve extending the incubation time with proteolytic enzymes. However, careful consideration must be given to the possible repercussions of this approach. Prolonged incubation could increase the risk of unwanted cleavage of outer cell membrane proteins, potentially leading to apoptosis as a consequence of trypsin-induced proteome

alteration (Lai et al., 2022). This can have detrimental effects on cell viability, leading to inaccuracies in live cell counting, as well as significant alterations in cellular functions. These concerns are particularly relevant when passaging osteoblasts for subsequent cultures, as maintaining cell viability and functionality is essential for reliable and consistent experimental results (Huang et al., 2010).

4.2.1.2.2 Use of cell scrapers

Mechanical scraping of cell layers from well surfaces is an alternative cell isolation/dissociation technique (Heinemann et al., 2021), however it inevitably results in cell damage by potentially tearing cells, raising concerns about the release of DNA from dying cells during the scraping process. This, in turn, may promote cell aggregation and further complicate the dissociation process (Volovitz et al., 2016). Moreover, cell scraping may induce changes in cellular morphology and fails to address the issue of cell clump formation. It is also important to acknowledge that the presence of cell debris produced during mechanical cell dissociation can significantly impact the quality of the resulting cell suspension and the debris may be mistaken for dead cells, when using methods such as trypan blue exclusion assay or fluorescence labelling. The increased number of apparent dead cells may undermine the data reliability. Similarly, mechanical agitation of culture media by pipetting or shaking the culture dish may result in cell damage.

4.2.1.2.3 Other methods of improving cell dissociation

Other possible methods for preparing a single cell suspension may include optimisation of proteolytic enzyme selection. Papain is a less well-known protease used for the

preparation of single-cell suspensions when compared with trypsin or collagenases. It is derived from the skin of papaya fruit and degrades tight junctions between cells, potentially aiding cell dissociation (Stremnitzer et al., 2015). Furthermore, ready-made mixtures of proteolytic enzymes, such as Accutase™ maybe employed. Importantly, human embryonic stem cells were reported to have maintained undifferentiated morphology, gene expression and proliferation patterns following the incubation with Accutase™ (Bajpai et al., 2008). This is contrary to trypsin-detached cells, which failed to proliferate and showed a higher death rate in the same study. In contrast to other enzymes employed for cell detachment, Accutase™ permits extended incubation times of up to 50 minutes without compromising cell viability (Alm et al., 2014). This extended duration can facilitate more effective dissociation of osteoblasts and mineralised ECM.

Additionally, free DNA released as a result of cell damage may be addressed via incubation with DNase-I (Reichard & Asosingh, 2019). DNase-I cleaves phosphodiester bonds of DNA reducing the formation of cell agglomerates.

The enzyme concentration can also be raised to improve the detachment yield, but it's important to note that excessively high concentrations can induce cytotoxicity (Salzig et al., 2013). Finally, it is crucial to select the optimum incubation temperature for a specific enzyme, with most options typically necessitating incubation at 37°C (Salzig et al., 2013). Nevertheless, some enzymes, such as Accutase™ demonstrate optimal activity at room temperature.

4.2.2 Cell counting in mineralising cultures

4.2.2.1 Manual cell counting

Typically, the most commonly used approach involves detaching cells from culture surfaces using proteolytic enzymes, creating a cell suspension, and then counting the cells using a haemocytometer, e.g. Neubauer haemocytometer (Absher, 1973). Reports indicate that 71% of the surveyed researchers perform cell counts using this technique (Ongena et al., 2010). In the present study, manual counting was employed in mineralising osteoblast cultures (Figure 3.1A). While the method allowed an effective discrimination of dead cells and cell clumps accounting for its popularity amongst laboratories, the counts were significantly time-consuming. Furthermore, manually counted cell numbers were less reliable with larger sample sizes due to the increasing operator errors throughout the process (Phelan & Lawler, 1997). The results obtained using this technique were also susceptible to variability among different operators. Nevertheless, manual counting remains the preference of many authors over automated methods, due to the frequent need for equipment calibration and the challenge of effectively distinguishing between cell debris and actual cells. Price considerations also significantly influence the choice of counting method, with manual counting emerging as the most cost-effective option.

Possibly, a strict standardisation of the counting approach in manual counting may prove advantageous in achieving consistent results. Interestingly, Zhang et al. (2020) introduced an enhanced method for manual cell counting with the Neubauer haemocytometer. In contrast to the conventional practice of counting cells only on the two outer lines within each grid square, the authors counted cells on all four lines and

then divided the total by two. This modification yielded a significant reduction in the average counting error when compared to the traditional approach.

4.2.2.2 Fluorescence-based automated cell counting

Automated cell counting has been developed to address the limitations of manual counting methods providing a more consistent and reliable performance. Interestingly, in the present work, the comparison of counting techniques demonstrated a more consistent result of manual counting of Saos-2 cells, when compared with the numbers obtained with automated counting based on fluorescent DNA staining (Figure 3.1B). This was, in part attributed to non-uniform distribution of cells within wells due to varying cell density. Consequently, cell counts varied according to the specific location where the image was captured within the well (Figure 3.3). Therefore, cell counts based on fluorescence images are susceptible to operator variation, due to the inherent challenges in standardising the precise image locations. Importantly, differentiation between live and dead cells was not possible in this case. This is because all cells were permeabilised using Triton^{TM} X-100 prior to staining with Sytox Green, allowing the fluorescent dye to penetrate the membrane of both dead and live cells. Moreover, Saos-2 cells, like many osteosarcoma cell lines (Pautke et al., 2004), lack contact inhibition, leading to the formation of multiple cell layers which can complicate the observation of single cells during counting (Figure 3.4). Thus, fluorescent staining is not applicable in multilayer cell cultures due to the cell layers superimposing each other and blocking the fluorescent signal. Consequently, ImageJ or Fiji-based cell/nuclei segmentation software were unable to distinguish nuclei in highly populated cell areas (Figure 3.4

B&C). Nevertheless, fluorescent labelling may be recommended when using confluent non-mineralising cultures growing in a single layer due to cost and time-effective application of the ImageJ software. Previous reports described a similar difficulty producing a single cell suspension from osteoblast-like cultures. Morelli et al. (2021) described an alternative deep learning algorithm for counting fluorescent stained cells with improved distinction of cell boundaries in areas of high cell density. However, it remains unclear whether this approach could be applied to multiple cell layers.

4.2.2.3 Alternative approaches to cell counting

The automated methods offer several other configurations to obtaining cell numbers *in vitro*. Firstly, a cell suspension may be prepared and visualised with a bright field microscope, similar to manual counting. However, in automated methods, cell numbers are determined using counting software that analyses the micrographs. Software tools such as ImageJ or deep learning algorithms are employed to generate cell counts based on the acquired images (Grishagin, 2015; Morelli et al., 2021). Alternatively, operator-free cell counting can be achieved following the manual enzymatic detachment of cells, employing systems like Vi-CELL BLU (Beckman Coulter, USA) or Countess (Invitrogen, USA) (Cadena-Herrera et al., 2015). However, the former automated methods may have limitations in accurately identifying dead or unhealthy cells. Another technique proposed by Yang et al. (2018) involved a quantitative analysis of fluorescent signals produced by DNA staining in osteogenic cultures. While this technique did not provide absolute cell numbers, it offered a viable alternative to manual or automated image-based cell counting by providing relative cell quantities.

Moreover, it could be used for cell counts on opaque surfaces where light microscopy is not possible. This is in contrast to *in situ* nuclear staining such as using DAPI stain presents difficulties on opaque surfaces, which is commonly the case when testing biomaterials including titanium. Finally, another cell counting method involves flow cytometry, widely regarded as a gold standard of cell characterisation. It enables fast and a highly detailed analysis including cell size, surface protein profile, total DNA as well as absolute cell numbers (McKinnon, 2018). However, flow cytometry is costly and requires a significant level of expertise to operate effectively.

4.2.3 Future work

The present study did not achieve a complete cell detachment off titanium surfaces when using trypsin and collagenase type 1 for cell dissociation. In future research, an alternative approach may include colorimetry-based assays, which may be used in adherent cultures. These assays rely on reduction of tetrazolium compounds by viable cells, producing a light absorbance signal. The signal is detected by a spectrophotometer and is proportional to the viable cell number (Riss et al., 2013). A common example of those compounds is 3'-{1-[(phenylamino)-carbonyl]-3,4-tetrazolium} bis(4-methoxy-6-nitro) benzenesulfonic acid hydrate 3'-1-(phenylamino)-carbonyl--3, (XTT), which is converted into the orange-pigmented formazan by metabolically active cells. The former is soluble in aqueous solutions, enabling estimation of the number of viable cells in mineralising adherent cell cultures incubated on titanium. This method allows to avoid cell dissociation using proteolytic enzymes, potentially increasing the accuracy of cell numbers.

4.3 Characterisation of osteogenic cell lines

The selection of an appropriate bone cell model for *in vitro* investigations is crucial as it plays a pivotal role in determining the potential translation of data to future *in vivo* studies or clinical trials. The present work attempted to identify an osteoblast model system for the subsequent ultrasonic exposure on titanium surfaces.

The present section was published by Yevlashevskaya et al. (2023).

4.3.1 Effect of β-Gly on hMSCs and Saos-2 cell numbers

A further key aspect in understanding the effects of therapeutic ultrasound on bone cells is the minimisation of other factors that could potentially alter cellular behaviour. Initially, it was necessary to select a cell model that would be robust, easy to maintain yet still representative of osteoblasts. Using osteosarcoma cell lines offered a cost-effective and straightforward approach however, the distinct cell origins can lead to diverse osteogenic differentiation gene expression profiles, mineralised matrix deposition and cell proliferation rates. Due to the conflicting literature reports outlined in section 1.7.2.2, this study aimed to analyse and compare the roles of Asc, Dex, and β-Gly in the behaviour of Saos-2 and hMSCs. While Asc, Dex, and β-Gly are frequently utilised to induce osteogenic differentiation *in vitro*, the literature is conflicting regarding the effects of the latter on cells, particularly concerning the origin of the cell model (Fogh & Trempe, 1975; Pautke et al., 2004).

Remarkably, Saos-2 cells exhibited a significant decrease in live cell numbers on exposure to β-Gly after 4 days of supplementation (Figure 3.5), which suggested cell

death or a reduction in proliferation induced by β-Gly. In contrast, such an effect was not observed in the presence of Asc and/or Dex, consistent with previous findings (Valenti et al. (2014) and Cmoch et al. (2014)). These indicated that Asc and/or Dex supplementation had no impact on cell numbers in osteosarcoma cell lines, such as MG63 and Saos-3. This suggested a possible anti-proliferative or toxic effect of β-Gly in these cell lines. Furthermore, hMSCs (Figure 3.6) did not show the same decrease in live cell numbers when exposed to β-Gly, which signified a different response to this substance compared with Saos-2 cells. Typically, β-Gly is hydrolysed by osteoblasts *in vitro* increasing the phosphate concentration of the culture medium and promoting the mineralisation of the ECM (Chung et al., 1992; Tenenbaum & Heersche, 1982). However, inorganic phosphate concentrations of 5-7 mM have been known to induce apoptosis in osteoblasts (Meleti et al., 2000). A potential cause of that phenomenon is the mitochondrial damage resulting from hyperpolarisation of the electrochemical gradient across the inner mitochondrial membrane and subsequent release of excessive reactive oxygen species (Kanatani et al., 2003; Nguyen et al., 2015). However Pisciotta et al. (2012) indicated that the organic phosphates, such as β-Gly, in equivalent amounts did not produce a similar response. Moreover, osteoblasts are believed to be adapted to elevated phosphate concentrations, which has been attributed to the involvement in bone remodelling (Meleti et al., 2000). Lundquist et al. (2007) showed that increasing phosphate concentration *in vitro* above that of blood plasma (˜1.5 mM) led to the upregulated expression of type II Na+ -Pi cotransporters in osteoblasts. These transport proteins were considered to be specific to mineral-producing cells and

allowed phosphate influx for mineral nodule formation while other ubiquitous transporters found in most cell types provide phosphates for metabolic purposes. This highlights the necessity of elevated phosphate concentration for osteogenic differentiation of cells.

4.3.2 The impact of β-Gly on cell cycle of hMSCs and Saos-2 cells

4.3.2.1 The potential β-Gly-mediated cell cycle arrest in Saos-2 cells

In the present study, a concentration of 9.3 mM β-Gly was utilised and found to be noncytotoxic to Saos-2 cells according to the LDH assay (Figure 3.11). In contrast BrdU staining revealed that β-Gly caused a significant decrease in proliferation of Saos-2 cells but not hMSCs (Figure 3.7, Figure 3.8, Figure 3.9). As the cell cycle progresses, it is reported that a decrease in cell proliferation rate and arrest in the G0 phase will occur (Tang et al., 2008). This phenomenon could account for the decrease in cell numbers observed during the later phases of Saos-2 incubation. Mature cell phenotypes, as demonstrated by Saos-2 enter a non-dividing, G_0 state via either terminal differentiation, senescence or quiescence (Kumari & Jat, 2021). During this state cells express low to non-detectable levels of *MKI67* and *PCNA* mRNA (Uxa et al., 2021). *MKI67* gene codes for Ki-67, a protein involved in the formation of the perichromosomal layer necessary for chromosome condensation in mitosis (Sun & Kaufman, 2018). It is expressed in G_1, S, G_2 and M phases of the cell cycle (Bologna-Molina et al., 2013). Whereas *PCNA*, typically transcribed in G_1 and S (Schiller et al., 2003), codes for an accessory protein for DNA polymerase alpha (Bologna-Molina et al., 2013). Hence, the increased activity of *MKI67* and *PCNA* were used as indicators

of cell proliferation in addition to BrdU staining. A significantly lower *MKI67* expression level characteristic of G_0 was observed in the later stages of the experiment in all osteogenic conditions both in the Saos-2 cells and hMSCs (Figure 3.12A, Figure 3.13A). Furthermore, the decrease in *PCNA* expression after 2 and 4 days in all Saos-2 and hMSCs cultures respectively suggested cell cycle arrest in G_0 or exit from G_1 and S. The reduction in transcription of both genes in all osteogenic conditions including those not containing β-Gly was possibly caused by quiescence.

4.3.2.1.1 The potential for quiescence in Saos-2 osteoblasts

Quiescence is a temporary cell cycle arrest which typically arises from nutrient and/or oxygen deprivation or the build-up of toxic metabolites with increased cell numbers in longer term cell cultures (Krampe & Al-Rubeai, 2010). However, a complete cell cycle arrest hMSCs was not observed in the BrdU staining, despite a decrease in the activity of *MKI67* and *PCNA* genes (Figure 3.8G-H). Additionally, quiescence may occur due to contact inhibition of cells when reaching confluence. As Saos-2 cells lack contact inhibition presumably arising from the cells malignant source tissue (Kumar et al., 2018), it was not likely to be the cause of the sharp decrease in expression of *MKI67* and *PCNA* in these cells. On the other hand, the unlimited growth of Saos-2 results in a multi-layered cell culture system which leads to a higher cell density than hMSCs cultures at equivalent time points and possibly created an oxygen and serum deficit. Moreover, previous reports showed that stiffness of mineralised ECM in osteosarcoma was significantly higher than that deposited by healthy osteoblasts due to enhanced deposition of collagen type 1, collagen type 3, fibronectin and other ECM components

(Cui et al., 2020). Indeed, complete detachment of Saos-2 cells from the polystyrene surface was achieved only after a complete 10 min incubation with trypsin and collagenase type 1 when compared with hMSCs, which took ~5 min to detach. Possibly this contrast was observed due to the difference in physical properties of the ECMs of the two cell lines. Combined, the increased cell density and a stiffer ECM of the Saos-2 cells could restrict oxygen diffusion to cells, potentially resulting in hypoxic culture conditions at the base of the dish. Short-term hypoxia triggers quiescence in some cells, which can be reversed if normal oxygen concentration is restored (Muz et al., 2015). Furthermore, Blagosklonny (2013) demonstrated that cells in quiescence could progress into senescence by expression of the cyclin-dependent kinase inhibitor p21 involved in arresting the cell cycle permanently. However, when in hypoxic conditions, quiescence fails to convert into senescence. This would suggest that if Saos-2 cells were deprived of oxygen, proliferation was ceased by quiescence. This also agreed with the decrease in Saos-2 cell numbers with increasing volume of mineralised matrix produced during incubation, however oxygen diffusion analysis is necessary to confirm this hypothesis.

4.3.2.2 Terminal differentiation as a possible cause of decreased cell proliferation

A marked decrease of BrdU-stained nuclei observed only in β-Gly-exposed Saos-2 (Figure 3.7C, F) implied a unique role of β-Gly in the cell cycle arrest of Saos-2. Decreased BrdU uptake showed that fewer Saos-2 cells were in S phase after 4 days of incubation that corresponded with a reduction in proliferation. A possible cause for the latter is cell cycle arrest triggered by terminal differentiation of Saos-2. Terminal differentiation leads to a permanent cell cycle exit in most cell types (L. A. Buttitta &

B. A. Edgar, 2009). Interestingly, while some species, such as reptiles and amphibians, are capable of exiting such arrest during limb regeneration, this ability is not typical of mammalian cells (Laura A. Buttitta & Bruce A. Edgar, 2009; Ogura et al., 2017). Terminally differentiated mammalian osteoblasts become either lining cells, osteocytes or undergo apoptosis (Aubin, 1998). It is necessary to highlight the mature osteoblastic phenotype of Saos-2 relative to the earlier phase of osteogenic differentiation of hMSCs as the latter affects proliferation kinetics in cells. Coelho and Fernandes (2000) reported decreased proliferation of human bone marrow cells in the presence of β-Gly after 42 days and linked it with progression of osteogenic differentiation. Interestingly in the present study, *PHEX*, an osteocyte associated marker was upregulated in osteogenically induced Saos-2 cultures, unlike hMSCs further confirming the phenotypic difference of the two in the presence of β-Gly. However, Saos-2 cells continued to express *PCNA* and *MKI67* as well as synthesising mineralised matrix which are not typical of terminally differentiated cells. Although, it is worth noting that osteocytes are notoriously difficult to maintain *in vitro* (Kalajzic et al., 2013), so terminal differentiation should not be excluded as the cause of the anti-proliferative effect of β-Gly on Saos-2.

4.3.3 The role of β-Gly in osteogenic behaviour of hMSCs and Saos-2 cells

4.3.3.1 Extracellular matrix mineralisation

In contrast to Asc and Dex, the presence of β-Gly allowed ECM mineralisation in both cell lines (Figure 3.10). Remarkably, Saos-2 cells showed a significantly greater mineral deposition than hMSCs, possibly due to a more mature osteoblastic phenotype of Saos-

2. It is worth noting that the presence of mineralised ECM in Saos-2 cultures should be interpreted with caution. Beresford et al. (1993) showed that nodule formation by osteosarcoma cells *in vitro* is only possible in the presence of β-Gly which further adds to doubts regarding physiological relevance of these cells. Specifically, cell lines are known to exhibit dystrophic mineralisation of the ECM in the presence of high concentrations of β-Gly. This is a non-apatitic mineralisation, occurring due to the precipitation of phosphate and calcium ions in culture media (Langenbach & Handschel, 2013; Mechiche Alami et al., 2016). The latter leads to false-positive mineralisation and cannot be distinguished using common mineral staining techniques such as Alizarin red S staining or Von Kossa staining. However, the nature of the mineral deposits may be determined using either energy dispersive X-ray (EDX) analysis or Fourier transform infrared spectroscopy (FTIR) in the future experiments (Bonewald et al, 2003). Additionally, previous reports showed that stiffness of mineralised ECM in osteosarcoma is significantly higher than that deposited by healthy bone cells due to the enhanced deposition of collagen type 1, collagen type 3, fibronectin and other ECM components (Cui et al., 2020).

Nevertheless, based on the literature the mineralised matrix produced within cell culture conditions demonstrates several properties of *in vivo* bone, such as birefringence in the presence of polarised light and a visible border between the mineralised and non-mineralised matrix (Tenenbaum & Heersche, 1982). A study evaluating the quality of the mineralised extracellular matrix deposited by Saos-2 cells found that the collagen phenotype was similar to that of human bone, although a greater degree of lysyl

hydroxylation was observed (Fernandes et al., 2007). The former is a distinctive feature of the bone-specific collagen type 1 presented as a unique amino acid cross-linking. In addition, unlike MG-63 cells the, Saos-2 cell line showed a similar pattern of mineralised matrix deposition and *ALP* expression to human osteoblasts.

4.3.3.2 Osteogenic gene expression

Furthermore, β-Gly appeared to affect osteogenic gene expression in both cell lines. *RUNX2* is an important regulator of osteogenic differentiation (James, 2013) and *ALP* has often been described as an early osteogenic marker (zur Nieden et al., 2003). Although ALP proteins are not unique to bone, the *ALP* expression level may be inadequate for addressing osteoblast differentiation. Saos-2 cells showed no particularly defined patterns of *RUNX2* or *ALP* expression depending on the osteogenic supplements provided and no significant difference was detected between treated and control cells (Figure 3.12C-D). This suggested that Asc, Dex and β-Gly did not affect early osteoblastic differentiation in Saos-2 cells as expected due to the relatively "mature" phenotype. This was in contrast to the hMSCs where an upregulation of *RUNX2* and *ALP* expression was observed in cells subjected to Asc and/or Dex and/or β-Gly promoting early osteoblastic differentiation (Figure 3.13C-D). Expression of *OCN* was increased in Saos-2 in the presence of β-Gly (Figure 3.12E). Increased *OCN* transcription indicated β-Gly interaction with the later stages of osteogenesis, whilst the activity of *OCN* in hMSCs did not appear to be affected exclusively by β-Gly and was upregulated in all supplemented cultures after day 10 (Figure 3.13E). This implied a transition of hMSCs into a later stage of osteogenic differentiation during the course

of the experiment similarly to healthy osteoblasts described in the literature (Aubin, 1998). These findings suggested a potential distinct role of β-Gly in later osteogenic differentiation of Saos-2 cells not detected in hMSCs. Based on this data, it was likely β-Gly affected Saos-2 proliferation via interacting with molecular pathways in late osteogenesis. Given that Saos-2 cells showed a deviation in key cell activities in the presence of β-Gly, these alterations could potentially have influenced outcomes when these cells were exposed to ultrasound. The hMSCs provided a more representative model system for osteoblasts, and as a result, it was used in the subsequent experiments on the ultrasonic exposure system.

4.3.4 Future work

Despite the previously described potency of both Saos-2 and hMSCs to demonstrate osteoblastic phenotypes, the key difference between the two cell lines was the malignant origin of Saos-2. As it was concluded, this factor probably influenced the observed change in Saos-2 proliferation in the presence of β-Gly. However, as the hMSCs did not originate from malignant tissue and displayed a more "normal" cell phenotype compared with Saos-2 cells, the hMSCs must have undergone some alterations to establish the cell line. Therefore, the hMSCs did not represent a fully "healthy" phenotype, so for further investigations, using a primary cell source would be advantageous. This approach could provide an improved representation of healthy osteoblast behaviour in response to the experimental conditions.

4.4 *In vitro* characterisation of titanium substrates for cell growth

To better represent osteoblastic behaviour on Ti-based bone implants, researchers commonly use Cp-Ti surfaces as cell substrates *in vitro*. The adhesion of cells to the material surface is a crucial factor influencing both the long- and short-term success of implant performance. Therefore, this study aimed to modify the titanium surfaces to enhance cell attachment *in vitro* to the Ti-based ultrasonic device.

4.4.1 Optimal surface roughness for cell attachment to titanium

4.4.1.1 Effect of surface topography on the attachment of Saos-2

Surface microroughness was increased using acid etching (Figure 3.14, Figure 3.15). After a 24-hour incubation of Saos-2 cells on titanium discs with various surface roughness (Ra), it was observed that discs with Ra ~1 µm acid-etched at 40°C demonstrated the highest number of cells (Figure 3.17). As a result, the titanium ultrasonic device was roughened to the same extent to ensure consistent and predictable cell behaviour. The existing *in vivo* evidence supports the notion that an implant surface roughness ranging from 1-2 µm allows an optimal balance between the mechanical interlocking between the implant and bone while minimising the risk of peri-implantitis. The former is associated with rougher implants of approximately 10 µm (Le Guéhennec et al., 2007). Moreover, in agreement with previous reports (Cho et al., 2021; Martin et al., 1995; Wu et al., 2011), the increased surface area of the rougher surfaces allows for an improved attachment rate of cells. Similarly, a study by Ramaglia et al. (2011), demonstrated a superior attachment of Saos-2 cells on roughened titanium surfaces. This enhanced attachment was accompanied by a

significant upregulation in the expression of α2 subunit of integrin in cells. The authors further suggested that the α2 subunit binds to collagen type 1 in the ECM, which correlated with greater deposition of mineralised ECM on rougher titanium surfaces.

4.4.1.2 Effect of surface chemistry on the attachment of Saos-2

Interestingly, the present study observed a reduction in cell attachment to surfaces that underwent acid etching at 60°C when compared with those etched at 40°C (Figure 3.17). Remarkably, the difference in Ra values for these surfaces, which measured 0.85 µm and 1.27 µm, respectively was not significant, as far as cell attachment is concerned (Levin et al., 2022). The underlying factors contributing to this phenomenon may involve chemical transformations induced by the higher temperature utilised during the acid etching process. Consequently, these alterations may have led to variations in the surface wettability of titanium, thereby accounting for the differences observed in the quantity of adherent cells. A study examining the surface topography and chemistry of cp-Ti (grade 4) following acid etching with a mixture of HCl and H_2SO_4 at various temperatures and durations demonstrated, that Ti surfaces became more hydrophilic when etched at 60°C and 70°C compared to surfaces treated at lower temperatures (Lin et al., 2014). Moreover, the level of chemical contamination with TiH_2 observed on the surfaces, as determined by X-ray diffraction, was found to correlate with the temperature of the acid etching process. The former is known to impact the mechanical properties of titanium materials, yet the precise role of TiH_2 in cell attachment is unclear. (Lin et al., 2014). Nevertheless, further testing of the

chemical composition of the acid etched Ti discs would be necessary to explain the reduced cell attached to surfaces etched at 60°C.

4.4.2 The importance of surface wettability in cell attachment

As described previously, rougher surfaces allow a greater surface area for protein adsorption, which occurs within the first milliseconds following implantation of the titanium-based material (Barberi & Spriano, 2021). However, this is not the sole mechanism influencing a cells' ability to attach to the material surface. Surface roughness also has a direct impact on surface wettability - the extent of interaction between a surface and a particular fluid, while material is immersed in a different fluid (liquid or gas) (Gulfam & Chen, 2022). The wettability of a surface is influenced by the surface free energy of a solid and the surface tension of a liquid. Metavarayuth et al. (2021) described this phenomenon of surface free energy as the availability of "vacant intermolecular bonding sites" to which proteins can readily attach. Hence, a higher surface energy exhibited by rougher surfaces enhances the probability of adhesive protein adsorption. In turn, this affects cell adhesion, growth, and proliferation (Rosales-Leal et al., 2010). It has been suggested, that cells tend to attach and proliferate more readily on hydrophobic surfaces (low water wettability) when compared with hydrophilic surfaces (high water wettability) (Barberi & Spriano, 2021). This difference may arise because the strong attraction of water molecules to hydrophilic surfaces hinders the availability of bonding sites for protein adsorption (Xu & Siedlecki, 2007). Interestingly, some reports claim that hydrophilic surfaces provide a better environment for cell attachment (Tomšíčková et al., 2013). Wei et al. (2009)

suggested that these variations may stem from the use of different materials and surface topographies in the studies and therefore not directly comparable. Furthermore, the adsorption rate of proteins at an implant surface depends on the charge of a particular protein, its structural stability and pH of the liquid to generate an overall repulsive or attractive effect (Barberi & Spriano, 2021).

Although the present study did not directly assess proliferation rates of Saos-2 cells on titanium, existing reports, including Levin et al. (2022), have indicated that cell attachment and proliferation rates tended to be lower on chemically treated titanium surfaces. Tomšíčková et al. (2013) suggested this trend arose from the alterations in titanium surface chemistry and/or charge caused by acid- and alkali-etching. Interestingly, in the present study the EDX analysis (Figure 3.16) did not demonstrate a significant chemical contamination of titanium discs following acid etching. Performing additional hydrophilicity/hydrophobicity testing would help determine whether the treatment resulted in surface energy changes. Such analysis may be performed by measuring contact angle of water droplets on the acid-etched titanium surfaces.

4.4.3 Relevance of data on osteoblast attachment to titanium

Given the fundamental distinctions in cellular behaviour outlined in section 1.7.1.2 between healthy osteoblasts and osteosarcoma cell lines, it is important to address the significance of the acquired data concerning the attachment of 'normal' osteoblasts to titanium. The existing literature reports similar behaviour of osteosarcoma-derived cell models and primary cell types on titanium surfaces. Saldaña et al. (2011) compared

the cell attachment and gene expression of human osteoblasts to those of Saos-2, MG63 and U-2 OS cells on Ti6Al4V surfaces. While none of the cell lines appeared to perfectly mimic primary osteoblasts, it was concluded that Saos-2 cells were the optimal choice of cell model to present osteoblastic behaviour on metallic surfaces. As expected, an enhanced proliferative rate of the cell lines was described, however, only Saos-2 appeared to express a similar pattern of *OCN* and *ALP* relative to the healthy osteoblasts. Moreover, the findings suggested that all the cell lines showed altered adhesion patterns on titanium relative to human osteoblasts, with the greater adhesion rate seen with primary cells. Likewise, Shapira and Halabi (2009) compared the behaviour of Saos-2 and MG-63 cells on roughened titanium surfaces and observed a significantly higher proliferation rate of MG-63, as well as a greater *ALP* activity in Saos-2 cells. In addition, a study examining the impact of surface energy alterations on primary hFOBs and osteoblastic cell lines, namely MC3T3-E1, MG-63, and Saos-2, revealed consistent patterns in cell morphology changes. Notably, MG-63 cells exhibited a comparable response in terms of cell proliferation and ECM mineralisation to that observed in hFOBs (Lim et al., 2008).

In summary, previous reports examining osteoblast behaviour, including their attachment to titanium surfaces, have consistently shown a parallel trend between Saos-2 cells and human osteoblasts. This suggests the possibility of a similar response to acid-etched titanium surfaces in primary osteoblasts to what was observed in Saos-2 cells in the present study. Nevertheless, further *in vitro* assessments are required to validate this hypothesis.

4.4.4 Future work

Subsequent work could benefit from further testing of the surface free energy of titanium surfaces after acid etching. This additional analysis would enable to test whether the surface modification induced a chemical change in the titanium surfaces, potentially altering the surface free energy, and subsequently, possibly impacting cell attachment. A classic test involves measurements of contact angle between the surface and a liquid. Typically, a series of liquid droplets with varying surface tensions is sequentially placed onto the material of interest, and an image is captured for each droplet. Then, the angle between the surface and the droplet is measured using a computer software e.g., ImageJ. The contact angle of below or above 90° indicates the material's hydrophilicity or hydrophobicity, respectively. Subsequently, cell attachment and proliferation tests could be conducted, employing cell counting and BrdU assays, respectively.

4.5 Novel experimental setup for studying cells on titanium

4.5.1 Significance of the present work

The prolonged rehabilitation times following implantation of bone-replacing materials including knee and hip replacement surgery maintain the interest in ultrasonic therapy of bone tissues. The clinical and *in vivo* studies on therapeutic ultrasound yielded inconclusive findings, necessitating a simplified *in vitro* approach that involves exposing osteoblasts to ultrasound (Snehota et al., 2020). Nevertheless, the former face a significant challenge due to the absence of a standardised and well-defined experimental system. The present study attempted to produce a reliable experimental

system for exposing cells to a defined setting of ultrasound on commercially pure titanium surfaces commonly used in implant manufacturing.

4.5.2 Benefits of the novel Ti-based ultrasonic treatment device

4.5.2.1 Key innovations in the design

The ultrasound-generating device demonstrated in this study (Figure 2.1) presented a significant advancement over traditionally employed systems involving titanium described in section 1.6.2.2 (Patel et al., 2015; Sant'Anna et al., 2005; Snehota et al., 2020). Instead of subjecting osteoblasts to distant ultrasonic irradiation, the cells were incubated directly on the vibrating surfaces of the device. This innovative approach minimised sound wave reflections off the titanium surfaces, thus controlling the strain experienced by osteoblasts - a feature that is challenging in the presence of standing waves resulting from reflections. Additionally, the novel design effectively reduced the risk of culture contamination, a common concern when immersing the transducer in the culture medium and a practice often employed in cell ultrasound treatment. Moreover, the use of PDMS boundaries compartmentalised osteoblasts subjected to varying levels of strain due to the uneven vibration distribution across the titanium paddles. This configuration proved instrumental for subsequent research, particularly in accurately quantifying the required levels of strain for inducing osteogenic behaviour, including extracellular matrix mineralisation. The proposed device also facilitated the treatment of individual titanium paddles at a time. This approach eliminated the inadvertent exposure of cells in neighbouring wells, as could occur in multi-well plate systems (Leskinen, 2015).

Importantly, the ultrasonic device was cost effective and could be replicated in most laboratory facilities. Moreover, titanium paddles could be reused following tissue culture. To ensure a biological and chemically clean titanium surface in subsequent experiments, the paddles should undergo a cleaning process involving ultrasonic cleaning in acetone and distilled water, followed by autoclaving. If required, an alternative clinically relevant material could be employed for the vibrating paddles, thereby expanding the system's range of applications.

4.5.2.2 Defined level of strain experienced by ultrasonically treated osteoblasts

A common difficulty with assessing the reliability of experimental data is the lack of precise reporting or the inability to quantify the exact extent of osteoblast stimulation by ultrasound (ter Haar et al., 2011). This may be attributed to the complexity of the acoustic field within the culture plate generated as a result of multiple factors. These may include acoustic impedance mismatch between materials, sound wave reflections, and differences in transducer setting. The device presented in this study was adapted from the image-based ultrasonic test designed by Seghir and Pierron (2018). The test developed by the authors involved capturing of infrared radiation emitted from the tested surface during ultrasonic vibration, in addition to monitoring sample deformation using an ultra-high-speed camera. The sample displacement was calculated using a mathematical equation based on the sample shift values obtained from the images (Grediac et al., 2016). These were subsequently correlated with the data acquired from the infrared camera, facilitating the estimation of strain distribution across the sample. Importantly, such an experimental configuration

allowed to define the level of strain delivered to the cells by alternating the transducer power and matching it with strain experienced by the cells (Ballard et al., 2022). This was in contrast with the commonly used *in vitro* ultrasound treatment systems where the ultrasonic dosage was not defined (Alassaf et al., 2013; Leskinen & Hynynen, 2012; Patel et al., 2015; Snehota et al., 2020).

Additionally, the present setup allowed to omit the concept of wave intensity as the measure of ultrasonic stimulation *in vitro*, by providing a method of defining strain distribution across the sample. Although, ultrasound intensity is relevant *in vivo*, for instance when describing prenatal scanning due to the insignificant variations in patient sizes. However, it does not provide an accurate measure of strain experienced by cells in tissue culture. This is due to the variety of experimental setups used by authors resulting in differing distances between the transducers and the sonicated surface. The following equation demonstrates that ultrasonic intensity decreases with the increasing distance from the sound source:

$$I \propto \frac{1}{d^2}$$

(I - intensity, d - distance from the source of ultrasound)

The latter is also known as the inverse square law. Hence intensity is not comparable unless identical setup designs are presented (ultrasound physics and instrumentation). Additionally, as ultrasound passes through media of different acoustic impedances (including culture media, culture dish or water, if the tank system is used), wave attenuation alters intensity further (Secomski et al., 2017). Therefore, one should be

cautious when comparing experimental outcomes *in vitro* based on the intensity parameters of the ultrasound exposure.

4.5.3 Operational temperature analysis of the device

Maintaining temperature up to 37°C poses a significant challenge in traditional *in vitro* systems employed for ultrasonic treatment. The absorption of ultrasonic waves by the culture medium induces particle vibrations, consequently elevating the temperature of the medium above the physiological threshold. Although this problem may be partially alleviated by exposing cells to ultrasound while they are immersed in a degassed water tank (Patel et al., 2015), this method is not feasible when dealing with titanium surfaces. The main challenge stems from the formation of standing waves within the tank, which results from the reflective nature of titanium surfaces.

To assess the compatibility of the proposed setup for tissue culture experiments, temperature fluctuation, the heating of titanium paddles during ultrasonic oscillation was investigated via recording the temperature of culture media. Frequencies of 20 or 40 kHz were tested during a 7 min continuous ultrasonic treatment. As expected, the temperature increase was directly proportional to the current used to produce ultrasound on both titanium paddles (Figure 3.18, Figure 3.19). Although this was not tested experimentally in the present study, the reason for the increased heating phenomenon was possibly consistent with Ohmic heating. According to the former, metal ions resisted the flow of electrons within the material leading to the conversion of a portion of electrical energy into heat. Higher current produced a greater resistance and therefore a higher temperature. Using a lower current of 0.05 A at both frequencies

of 20 and 40 kHz maintained the culture media temperature within the physiological range, hence it was used in the subsequent experiments. Furthermore, the increased heating effect at higher electric power could be attributed to the conversion of electrical energy into heat by the piezoelectric component of the transducer (Shi et al., 2021). Electric power, in this context, is directly influenced by the current flowing through the system:

$$P = \frac{V}{I}$$

(P – power, V – potential difference, I – current)

In addition, a possible electric impedance mismatch between the transducer components could decrease the efficiency of power transfer between those (Rathod, 2019). The energy loss typically occurs in the form of heat. Nonetheless, despite the reduction in harmful temperature increase was successful, the level of cell stimulation generated by ultrasound at 0.05 A may have been insufficient to elicit a notable osteogenic impact. While it was rather speculative assumption, a series of experiments evaluating osteogenic behaviour of osteoblasts would be necessary to assess the former. In future experiments, a pulsed ultrasonic treatment mode may be considered at currents above 0.05 A to prevent a temperature increase above the physiological range (Cambier et al., 2001). Additionally, a higher volume of culture medium may be used to allow a better temperature control. It is important to acknowledge that the temperature of the paddles was not directly evaluated. It is plausible that the temperature fluctuations observed in the culture media may not precisely reflect those of the paddles. This difference could potentially pose a greater risk of cell death due

to elevated temperatures of the paddles. An infrared camera may be employed to assess the temperature increase of the paddles when not in contact with culture media or cells.

The temperature increase of culture media varied according to the position on paddles with the highest increase observed at the distal end. A possible explanation for the phenomenon were different levels of strain experienced by the proximal, middle, and distal parts of the paddle. However, Seghir and Pierron (2018) reported a different temperature profile along the polymethyl methacrylate (PMMA) paddle in the original setup resulting from the harmonic motion produced by the ultrasonic oscillation. According to the latter, the maximum strain was in the middle part, whereas the distal and proximal ends experienced minimal strain. This resulted in a temperature increase in the centre of the paddle and no temperature change on the ends. The characterisation report produced by colleagues at the University of Southampton also indicated that the maximum temperature increase occurred in the middle of the Ti paddles at both 20 and 40 kHz (Figure 7.2, Figure 7.3). Importantly, these tests were performed without the PDMS wells attached to the paddles, thereby not accounting for the alteration in strain distribution resulting from the additional mass on the paddles. Moreover, the contrast in strain distribution presented in the literature and the present study may have arisen from the manual fixation of paddles to the transducer. Possibly, the movement generated from the oscillating paddles produced heat resulting in the unexpected temperature profile within the paddles. Alternatively, a spanner should be used to securely tighten the paddles to the transducer. However,

regardless of any heating pattern of the different wells, a heterogeneous strain profile was likely to result in differing cell responses, hence the cells were compartmentalised into 3 separate wells. This was to allow for detection of varying proliferation rates, osteogenic gene expression or levels of mineralised extracellular matrix deposition.

4.5.4 Cytotoxicity testing of the device

With regards to cellular behaviour, the present ultrasonic treatment setup did not appear to be cytotoxic to the immortalised hMSCs at either 20 or 40 kHz following the LDH assay (Figure 3.20). Similarly, Ballard et al. (2023) modified the image-based ultrasonic test to visualise cells under the influence of 20 kHz ultrasound. The study used a PMMA paddle instead of titanium. In agreement with the present results, the Presto Blue assay results indicated that the viability of MG-63 osteosarcoma cells did not appear to be influenced by ultrasonic stimulation, when compared with the non-treated control cultures. Moreover, phase contrast microscopy demonstrated normal cell morphology during the stimulation. Given the similarities in the ultrasonic setup detailed in this study, it was probable that osteoblasts incubated on titanium paddles underwent a comparable level of deformation as outlined by Ballard et al. (2023). Although there are not many other reports on the biological effects of ultrasound within the kilohertz range, a number of previous *in vitro* studies using a traditional multiwell setup had a similar outcome. Reher et al. (2002) used a continuous exposure of 45 kHz ultrasound at the range of intensities between 5 and 50 mW/cm^2. Human mandibular osteoblasts were incubated in a 6-well plate floating in a 37°C water bath and the transducer immersed in the culture medium. A significantly increased cell

proliferation and DNA synthesis was observed in the test samples. More recently, Gupta et al. (2022) exposed an human osteosarcoma cell line, Saos-2 to 45 kHz treatment at 10-75 mW/cm^2 while incubated in single well plates. Cells subjected to a higher intensity treatment of 75 mW/cm^2 showed endoplasmic reticulum and mitochondrial damage as well as an increased cell death. In contrast, lower intensity stimulation did not cause such a damaging effect on cells. However, contrary to some articles reporting cell proliferation changes following ultrasonic treatment (Doan et al., 1999; Man et al., 2012; Patel et al., 2015; Savva et al., 2019), the present study did not identify a significant change in cell numbers after 24 hours (Figure 3.21). A cell proliferation assessment, such as the BrdU assay would be necessary to confirm the latter.

4.5.5 Limitations of the device

4.5.5.1 Paddle-to-transducer interface

It is necessary to highlight the limitations and areas for improvement of the current Ti-based *in vitro* ultrasonic device. The major drawback of the system is associated with difficulties in connecting the paddles to the ultrasonic transducer while maintaining sterile conditions. The latter includes a screw mechanism, where the transducer is rotated around the paddles which are kept stationary manually. Such procedure demonstrates a high risk of damaging the PDMS wells, causing culture media leakage and disturbing the sterility of the experiment. It is recommended to use sterile pliers or a similar tool to support the Ti paddles while rotating the transducer. Additionally, an alternative fixation mechanism may be considered. For instance, the

paddles may be securely attached to the transducer via quick release fasteners, clip and clamps mechanisms or magnetic connections. Furthermore, these may be useful in addressing the variability in paddle-to-transducer fixation, which is observed in manually screwed on paddles, potentially contributing to the elevated temperature observed at the proximal end of the paddles during ultrasonic vibration.

4.5.5.2 Duration of experiment and labour intensity

In the investigation described in section 2.4.5, three technical replicates were completed for each ultrasonic frequency, namely 20 and 40 kHz and a non-treated control. A total of nine Ti paddles was included per investigation, and a single transducer was used with the paddles containing cells treated subsequently. The described method took approximately 2.5 to complete. Therefore, a further consideration should be given to using multiple transducers to enable simultaneous oscillation of several paddles. This approach would effectively reduce the duration of the test. Simultaneous treatment offers the advantage of minimising variables linked to temperature fluctuations from frequent opening and closing of the tissue culture incubator, transducer heating, and potential operator errors arising from prolonged, labour-intensive experiments.

4.5.5.3 PDMS well preparation

While the PDMS wells attached to the Ti paddles provided a non-cytotoxic, waterproof boundary for maintaining cells in a physiologically relevant environment, the preparation procedure had several drawbacks. To secure the PDMS wells on the paddle surface, a small amount of pre-set PDMS was placed on the periphery of the wells, followed by incubation at 50°C for 1 hour and at room temperature for 48 hours to

ensure gelation. However, upon positioning the wells on the paddles, the pre-set PDMS spread beyond the well's perimeter onto the Ti surface. This phenomenon reduced the surface area available for cell attachment, due to the inability of cells to adhere to PDMS (Jastrzebska et al., 2018). Moreover, the spread was uneven, resulting in differences in the quantity of attached cells between wells. The significance of these differences in the accuracy of further investigations, such as qPCR and ARS staining, may be studied by approximating cell numbers 24 hours following seeding, using methods described in 4.2.2.3. A potential approach for future work may involve application of minimal volume of pre-set PDMS with a syringe and needle. An alternative tactic to well adhesion may be the use of medical grade super glues. These are commonly based on cyanoacrylate and find applications in various surgical procedures, such as skin wound closure, haemostasis (bleeding control), and fixation of bone fractures (Habib et al., 2013). Cyanoacrylate surgical glues have lower viscosity than pre-set PDMS, enabling a better application precision and control, as well as a cleaner finish. Additionally, the setting time of these adhesives ranges from a few seconds to minutes, simplifying the preparation procedure (Wellington et al., 2022). However, it is important to reconsider the sterilisation process for the prepared paddles, as most surgical glues are not designed to endure extreme temperatures, such as those encountered during autoclaving. In such cases, it may be necessary to attach pre-autoclaved PDMS wells and Ti paddles in a laminar flow hood using aseptic technique. Furthermore, it will be necessary to test the adhesion strength between PDMS and

titanium, when using cyanoacrylate glues, using a pull-off test on a universal testing machine (UTM) (Webber et al., 2015).

4.5.6 Potential clinical importance of the novel *in vitro* system

The method presented in this thesis for the *in vitro* ultrasonic treatment of cells provided a well-defined and temperature-controlled environment, effectively eliminating the issue of standing wave formation often encountered in alternative experimental configurations. The significance of establishing a reliable *in vitro* setup is evident in its potential to study the possibility of enhancing the postoperative recovery rates for bone-replacement procedures using ultrasonics. The inconclusive outcomes of clinical trials, highlighted in section 1.5.7, demonstrated the inability to reliably identify ultrasonic regimes to enhance bone healing around implants using the existing model systems. Furthermore, specific clinical scenarios with a greater risk of implant failure necessitate additional therapeutic approaches, with ultrasound emerging as a potential option. Likewise, the device may be employed in studying the response of osteoblasts to the simultaneous action of elevated temperature and vibration, as experienced in the ultrasonic cutting of bone (1.5.6).

4.5.6.1 Limitations of therapeutic management of failed bone implants

Bone prosthesis failure is commonly addressed via revision surgery, although these tend to be less successful than the primary implantation and are associated with greater costs (Copuroglu et al., 2013). For example, ~20% of patients undergoing hip replacement procedures are expected to require a secondary revision within 15 years subsequent to their initial surgery (Deere et al., 2022). Furthermore, according to

Bayliss et al. (2017) the average age of patients undergoing primary joint replacement is 69.4 years. Thus, any future revisions with advanced age carry increased risks of poor recovery or even morbidity from the general anaesthesia and failed wound healing (Bentov & Reed, 2014). Additionally, failed implants remain a significant clinical challenge for patients with underlying health conditions, including diabetes, cardiovascular disease, obesity, and bone remodelling disorders.

4.5.6.1.1 Implant failure in osteoporosis

Osteoporosis patients often require bone replacing or supporting implants due to the high frequency of fractures. However, osseointegration of implants is compromised due to decreased proliferation of osteoblasts and excessive bone resorption by osteoclasts, which collectively lead to a reduction in bone deposition (Fini et al., 2000). Keller et al. (2004) described the detrimental effect of osteoporosis-mimicking conditions on osseointegration of implants in rabbits with a potential likelihood of long-term failure. The latter was based on the reduced bone mineral density, as well as irregular patterns of trabecular bone, and thinner cortical bone. Additionally, Fini et al. (2000) showed a decreased bone mineral density in ovariectomised rats causing poor osseointegration of various biomaterials, including titanium. These findings indicate that osteoporosis could significantly elevate the risk of early implant failure by impeding osseointegration. In dentistry, osteoporosis is associated with alveolar ridge resorption and changes to the trabecular component of mandible and maxilla (Gibreel et al., 2022). It is noteworthy that dental implants directly engage with trabecular bone, effectively distributing strains generated during chewing and biting onto it (Misch et

al., 1999). Consequently, the stability of dental implants in patients with compromised bone remodelling requires additional management which include bisphosphonate (BP) therapy currently. These attach to hydroxyapatite surfaces and inhibit osteoclastic bone resorption (de-Freitas et al., 2016). However, the safety and efficacy of BP therapy is debated due its link with osteonecrosis of the jaw. The latter is characterised by non-healing exposed necrotic bone in the maxillofacial region and is thought to be caused by BP toxicity and subsequent infections (Chien et al., 2021). The jawbone has a particularly high remodelling rate possibly to adapt to the constant loads imposed by chewing (Matsuura et al., 2014). Hence, the risk of BP-linked necrosis is higher, especially during active wound healing, e.g., following invasive techniques such as implant placement or tooth extraction (Chien et al., 2021). It is evident that currently there is no reliable solution for improving osseointegration in osteoporotic patients after Ti-based implant placement.

4.5.6.1.2 Implant failure in obesity and diabetes

Obesity is also affiliated with implant failure although the mechanisms by which bone turnover is impaired are not well understood, it is clear that excess fat negatively affects bone mass (Pollock et al., 2011). It is possible, that obesity-induced insulin resistance downregulates osteoblast signalling via mitogen-activated protein kinases (MAPK) and phosphatidylinositol-3 kinase (PI3K/Akt) pathways (Pramojanee et al., 2014). This supported the notion that type 2 diabetes mellitus (T2DM) patients demonstrated reduced mineralised matrix production by osteoblasts as well as a lower bone density and consequently delayed wound healing (Gómez-de Diego et al., 2014).

Moreover, the increased local concentration of pro-inflammatory factors, including tumour necrosis factor-α and interleukin-1β induces osteoclastogenesis for bone resorption (Jiao et al., 2015). The same research reported that diabetic patients underwent an 87% longer bone healing process than healthier candidates. In addition, the occurrence of a non-union was 43% for T2DM patients, whereas only 10-16% of healthy patients showed similar complications (Marin et al., 2018). Similarly, Xiao et al. (2022) demonstrated poor osseointegration of titanium screws into cortical bone in diabetic rats, as well as lower bone quantity and decreased expression of osteoblastic markers, including *BMP-2, OCN, RUNX2,* and *OPN*. The findings suggested a decrease in mineralization at the site of implantation, which raises the potential for early implant failure in diabetic models.

All the above create a case for a post-injury/implantation therapy to accelerate prolonged bone healing. This would achieve a potential improvement in the quality of life of recovering patients, as well as bring a financial benefit by shortening the rehabilitation time.

4.5.6.1.3 Thermal effects in ultrasonic cutting of bone

While ultrasonic cutting offers improved control over excessive tissue heating compared to conventional methods, the issue is not entirely eliminated. In the present study, temperature above 37°C was not desirable when studying purely non-thermal effects of ultrasound on cells *in vitro*. However, the device also allows to study the impact of high temperatures on cells during ultrasonic stimulation by increasing current. Furthermore, some reports demonstrated the therapeutic effects of limited exposure to

mildly elevated temperatures *in vitro* (Dolan et al., 2012). Nørgaard et al. (2006) exposed hMSCs to up to 44°C for 1 hour and observed upregulated *ALP* expression and mineralised matrix deposition when compared with the controls incubated at 37°C. Similarly, hMSCs and MG-63 cells were shown to upregulate mineralised nodule formation and ALP production at 39–41°C for 1 hour. However, increased temperature had an inhibitory effect on cell proliferation (Shui & Scutt, 2009). There is considerable interest in investigating the combined effect of ultrasonic vibration and elevated temperature on cells in bone cutting to define optimal exposure regimens that minimise tissue damage while promoting healing. The constraints in understanding these phenomena are comparable to those encountered when studying the behaviour of osteoblasts on titanium, such as wave attenuation, temperature instability, and contamination risks. Therefore, the novel experimental setup for studying the effects of ultrasound on cells could be employed to mimic the conditions experienced by cells during ultrasonic bone cutting.

4.5.6.1.4 Ultrasonic therapy for bone healing around dental implants

Previous chapters explored the uses and limitations of dental implants used to restore missing teeth, and the need to accelerate bone healing around implants to assist osseointegration. This can be explored *in vitro* using the presented device for ultrasonic vibration of bone cells on Ti surfaces. However, the setup could also have a more direct clinical application in dentistry. There are several approaches to dental implant surgery, including one-step, two-step, and three-step procedures, each with its own advantages and considerations. In the three-step surgery, the dental implants are

initially inserted into the jawbone, followed by the placement of an abutment to connect the implant to the final restoration. Finally, a crown, bridge, or denture is attached to the implant via the abutment (Gupta et al., 2023). The two-step or one-step procedures, involving multiple steps within a single surgical session, may be applicable in certain clinical cases, depending on factors such as the patient's oral health, bone quantity, and the complexity of the case. Often, prior to the placement of the final restoration, several months are allowed for the osseointegration of the implant into the jawbone. This phase, critical to ensuring the implant's stability and longevity, may be compromised by inadequate bone healing, particularly in cases with underlying health conditions such as osteoporosis (4.5.6.1.1, 4.5.6.1.2). However, given that the implant is exposed to the oral cavity at this stage, it becomes possible to induce vibrations directly to the implant itself using a modified version of the ultrasonic shaking device, achieved through direct contact between the two. It may be hypothesised, that bone cells surrounding the dental implant would undergo a similar stimulation to what is observed in the current *in vitro* setup, potentially leading to upregulated osteogenesis. However, prior to drawing such conclusions, additional *in vitro* tests would be necessary to observe the response of osteoblasts ultrasonically vibrated on the Ti paddles.

4.5.6.1.5 Other possible applications

Low-magnitude high-frequency vibration (LMHFV) is also considered a potential therapeutic strategy for bone healing. LMHFV utilises a much lower frequency of motion in the range of 20–90 Hz, when compared to ultrasonic therapy. The effects of

such therapy on bones have been reported extensively both *in vitro* and *in vivo* (Steppe et al., 2020). LMHFV appears to enhance osteoblastic differentiation in hMSCs, based on the increased expression of key osteogenic markers such as *RUNX2, OSX*, *COL1A1, OCN, and ALP*, along with upregulated mineralized matrix deposition (Chen et al., 2016; Lu et al., 2018). Similarly, LMHFV improved bone healing following femur osteotomy in rats, as evidenced by increased bone formation observed at 2-4 weeks post-procedure. Additionally, LMHFV stimulated angiogenesis and promoted callus remodelling following a closed femoral fracture in ovariectomised rats (Cheung et al., 2012; Choy et al., 2020). Importantly for this work, numerous parallels exist between LMHFV and ultrasound therapy, particularly regarding their osteoinductive effects on osteoblasts and the challenges with demonstrating these *in vitro*. The primary constraints are cantered around the complexity of mechanical stimulation and the standardisation of experimental protocols. The presented device may be readily adapted to generate oscillations within the LMHFV range, making it suitable for investigating the effects of low frequency vibrations *in vitro*.

4.5.6.2 Socioeconomic effects of implant failure

It is estimated that patients with complications of total knee and hip replacements undergo an additional 2 years of readmission for clinical management (Ekegren et al., 2018; Judge et al., 2020). These results in significant pain, lifestyle adjustment(s) and an inability to work. As a result, such prolonged healing periods generate a significant economic and emotional impact on patients. Delayed bone healing presents a burden on healthcare systems across the globe. Judge et al. (2020) reported that NHS, England

spent £897 and £1007 million annually for primary care, inpatient and outpatient costs for total hip and knee replacements, respectively. Furthermore, an additional average expenditure of £9,000 is dedicated to the management of postoperative complications, including those resulting from underlying factors like osteoporosis, age, and high BMI score.

There is a clear need for a supplementary minimally invasive therapy to assist bone healing around Ti implants and increase healing rates to improve patient's quality of life. The experimental system described in this thesis could be easily replicated by researchers for testing different exposure regimes of ultrasound treatment of various cell types, while clearly reporting the extent of stimulation received by cells. This setup will facilitate a comprehensive understanding of the mechanisms activated by therapeutic ultrasound, ultimately resolving of the debate concerning its effectiveness in the context of bone healing. Additionally, the device may be used to study other ultrasound applications, such as bone cutting.

4.5.7 Future work

Future work on ultrasonic stimulation of osteoblasts attached to titanium surfaces *in vitro* using the presented device will provide an indication of the possibilities of ultrasonic therapy in osseointegration of titanium implants. Namely, the prospective studies should encompass the exposure of osteoblasts to 20 or 40 kHz ultrasound for ~5 min daily over a duration of 7 to 14 days. Subsequently, this should be followed by assessment of cell proliferation, such as the BrdU assay, an analysis of osteogenic gene expression utilising qPCR, and an evaluation of mineralised matrix deposition, which

can be achieved through techniques like Alizarin red S or Von Kossa staining. In order to enhance the clinical relevance of the data, primary human osteoblasts may be employed as the preferred osteoblast model.

5 Conclusions

The present project aimed to establish a well-characterised experimental setup for investigating the impact of ultrasonic excitation on osteoblasts incubated on titanium surfaces, commonly used in dental and orthopaedic implants.

1) The current study showed that Saos-2 cell line maybe used as a model for osteogenesis *in vitro*, however the anti-proliferative-effect of osteogenic supplementation with β-Gly must be considered when using these cells. It was likely, that β-Gly affected Saos-2 cells through interactions in later stages of osteogenic differentiation.
2) The study also established an optimal cell counting protocol for mineralising cultures, allowing to dissociate cell aggregates and obtain accurate cell numbers. The former involved the combination of trypsin and collagenase type 1, followed by a manual cell count using a haemocytometer.
3) It was demonstrated that the highest degree of cell attachment to titanium surfaces of the ultrasonic device could be achieved via increasing surface roughness, Ra to approximately 1 µm.
4) Finally, a novel titanium-based *in vitro* ultrasonic tool was introduced, generating a defined strain field of ultrasound in a temperature-controlled setting without affecting viability of osteoblasts. Furthermore, the device minimised sound wave reflections off titanium, which was not typical of the traditionally used designs.

In summary, the findings strongly support the suitability of the suggested ultrasonic setup for studying the osteogenic behaviour of osteoblasts under the influence of a defined strain of ultrasound. The described experimental has a potential to effectively minimise any significant deviation in cell activity that could be attributed to the setup itself. Future work evaluating osteogenic gene expression and mineralised matrix deposition will reveal the effects of ultrasonic treatment on osteoblasts attached to titanium surfaces.

6 References

Aaron, R. K., & Ciombor, D. M. K. (1993). Therapeutic effects of electromagnetic fields in the stimulation of connective tissue repair. *Journal of Cellular Biochemistry*, *52*(1), 42-46. https://doi.org/10.1002/jcb.240520107

Absher, M. (1973). Hemocytometer Counting. In P. F. Kruse & M. K. Patterson (Eds.), *Tissue Culture* (pp. 395-397). Academic Press. https://doi.org/https://doi.org/10.1016/B978-0-12-427150-0.50098-X

Adams, J. C., & Watt, F. M. (1993). Regulation of development and differentiation by the extracellular matrix. *Development*, *117*(4), 1183-1198. https://doi.org/10.1242/dev.117.4.1183

Afzal, S., Zahid, M., Rehan, Z. A., Fayzan Shakir, H. M., Javed, H., Aljohani, M. M. H., Mustafa, S. K., Ahmad, M., & Hassan, M. M. (2022). Preparation and Evaluation of Polymer-Based Ultrasound Gel and Its Application in Ultrasonography. *Gels*, *8*(1), 42. https://doi.org/10.3390/gels8010042

Aiyer, R., Noori, S. A., Chang, K. V., Jung, B., Rasheed, A., Bansal, N., Ottestad, E., & Gulati, A. (2020). Therapeutic Ultrasound for Chronic Pain Management in Joints: A Systematic Review. *Pain Medicine*, *21*(1526-4637 (Electronic)), 1437-1448. https://doi.org/10.1093/pm/pnz102

Alassaf, A., Aleid, A., & Frenkel, V. (2013). In vitro methods for evaluating therapeutic ultrasound exposures: present-day models and future innovations. *Journal of Therapeutic Ultrasound*, *1*(2050-5736 (Print)). https://doi.org/10.1186/2050-5736-1-21

Alcorta-Sevillano, N., Macías, I., Infante, A., & Rodríguez, C. I. (2020). Deciphering the Relevance of Bone ECM Signaling. *Cells*, *9*(12), 2630. https://doi.org/10.3390/cells9122630

Alfieri, R., Vassalli, M., & Viti, F. (2019). Flow-induced mechanotransduction in skeletal cells. *Biophysical Reviews*, *11*(5), 729–743. https://doi.org/10.1007/s12551-019-00596-1

Alm, J. J., Qian, H., & Le Blanc, K. (2014). Clinical Grade Production of Mesenchymal Stromal Cells. In C. A. V. Blitterswijk & J. De Boer (Eds.), *Tissue Engineering* (2 ed., pp. 427-469). Academic Press. https://doi.org/https://doi.org/10.1016/B978-0-12-420145-3.00013-4

An, Y., Song, Y., Wang, Z., Wang, J., Wu, G., Zhu, G., & Chen, L. (2018). Effect of low-intensity pulsed ultrasound on the biological behaviors of bone marrow mesenchymal stem cells on titanium with different surface topographies. *American Journal of Translational Research*, *10*(1), 67-76.

Annibali, S., Ripari, M., La Monaca, G., Tonoli, F., & Cristalli, M. P. (2008). Local complications in dental implant surgery: prevention and treatment. *ORAL & implantology*, *1*(1), 21–33.

Ansari, S., Ito, K., & Hofmann, S. (2021). Cell Sources for Human In vitro Bone Models. *Current osteoporosis reports*, *19*(1), 88-100. https://doi.org/10.1007/s11914-020-00648-6

Apostu, D., Lucaciu, O., Berce, C., Lucaciu, D., & Cosma, D. (2018). Current methods of preventing aseptic loosening and improving osseointegration of titanium implants in cementless total hip arthroplasty: a review. *Journal of International Medical Research*, *46*, 2104–2119. https://doi.org/10.1177/0300060517732697

Applied Biological Materials Inc, A. B. M. (2023). *Immortalized Human Bone Marrow Mesenchymal Stem Cells SV40T*. https://www.abmgood.com/immortalized-bone-marrow-mesenchymal-stem-cells-sv40-t0520.html

Arana-Chavez, V. E., & Bradaschia-Correa, V. (2009). Clastic cells: Mineralized tissue resorption in health and disease. *International Journal of Biochemistry and Cell Biology*, *41*(3), 446–450. https://doi.org/10.1016/j.biocel.2008.09.007

Armstrong, M. J., Rodriguez, J. B., III, Dahl, P., Salamon, P., Hess, H., & Katira, P. (2020). Power Law Behavior in Protein Desorption Kinetics Originating from Sequential Binding and Unbinding. *Langmuir*, *36*(45), 13527-13534. https://doi.org/10.1021/acs.langmuir.0c02260

Arnau, A., & Soares, D. (2008). Fundamentals of Piezoelectricity. In A. A. Vives (Ed.), *Piezoelectric Transducers and Applications* (pp. 1-38). Springer Berlin Heidelberg. https://doi.org/10.1007/978-3-540-77508-9_1

Artho, P. A., Thyne, J. G., Warring, B. P., Willis, C. D., Brismée, J.-M., & Latman, N. S. (2002). A Calibration Study of Therapeutic Ultrasound Units. *Physical Therapy*, *82*(3), 257-263. https://doi.org/10.1093/ptj/82.3.257

Aubin, J. E. (1998). Advances in the osteoblast lineage. *Biochemistry and Cell Biology*, *76*(6), 899-910. https://doi.org/10.1139/o99-005

Aubin, J. E. (2001). Regulation of Osteoblast Formation and Function. *Reviews in Endocrine and Metabolic Disorders*, *2*(1), 81–94. https://doi.org/10.1023/A:1010011209064

Augat, P., Hollensteiner, M., & von Rüden, C. (2021). The role of mechanical stimulation in the enhancement of bone healing. *Injury*, *52*, 78–83. https://doi.org/10.1016/j.injury.2020.10.009

Augustin, G., Davila, S., Mihoci, K., Udiljak, T., Vedrina, D. S., & Antabak, A. (2008). Thermal osteonecrosis and bone drilling parameters revisited. *Thermal osteonecrosis and bone drilling parameters revisited*, *128*, 71–77.

Bachu, V. S., Kedda, J., Suk, I., Green, J. J., & Tyler, B. (2021). High-Intensity Focused Ultrasound: A Review of Mechanisms and Clinical Applications. *Annals of biomedical engineering*, *49*(1573-9686 (Electronic)), 1975–1991.

Bahney, C. S., Zondervan, R. L., Allison, P., Theologis, A., Ashley, J. W., Ahn, J., Miclau, T., Marcucio, R. S., & Hankenson, K. D. (2019). Cellular biology of fracture healing. *Journal of Orthopaedic Research*, *37*(1), 35-50. https://doi.org/10.1002/jor.24170

Baht, G. S., Vi, L., & Alman, B. A. (2018). The Role of the Immune Cells in Fracture Healing. *Current osteoporosis reports*, *16*, 138–145. https://doi.org/10.1007/s11914-018-0423-2

Bajpai, R., Lesperance, J., Kim, M., & Terskikh, A. V. (2008). Efficient propagation of single cells Accutase-dissociated human embryonic stem cells. *Molecular reproduction and development*, *75*(5), 818–827. https://doi.org/10.1002/mrd.20809

Baker, K. G., Robertson, V. J., & Duck, F. A. (2001). A review of therapeutic ultrasound: Biophysical effects. *Physical Therapy*, *81*(7), 1351–1358. https://doi.org/10.1093/ptj/81.7.1351

Ballard, M., Aleksander, M., & Fabrice, P. (2023). The image-based ultrasonic cell shaking test. *PLoS ONE*, *18*(9). https://doi.org/10.1101/2023.05.04.539476

Ballard, M., Marek, A., & Pierron, F. (2022). *An ultra-high-speed imaging study of ultrasound mediated mechanotransduction* UltraSurge annual meeting,

Barberi, J., & Spriano, S. (2021). Titanium and protein adsorption: An overview of mechanisms and effects of surface features. *Materials*, *14*(7), 1590. https://doi.org/10.3390/ma14071590

Bayliss, L. E., Culliford, D., Monk, A. P., Glyn-Jones, S., Prieto-Alhambra, D., Judge, A., Cooper, C., Carr, A. J., Arden, N. K., Beard, D. J., & Price, A. J. (2017). The effect of patient age at intervention on risk of implant revision after total replacement of the hip or knee: a population-based cohort study. *Lancet*, *8*(389), 1424-1430. https://doi.org/10.1016/S0140-6736(17)30059-4

Beauséjour, C. M., Krtolica, A., Galimi, F., Narita, M., Lowe, S. W., Yaswen, P., & Campisi, J. (2003). Reversal of human cellular senescence: Roles of the p53 and p16 pathways. *EMBO Journal*, *22*(16), 4212-4222. https://doi.org/10.1093/emboj/cdg417

Bellows, C. G., Aubin, J. E., Heersche, J. N. M., & Antosz, M. E. (1986). Mineralized bone nodules formed in vitro from enzymatically released rat calvaria cell populations. *Calcified Tissue International*, *38*(3), 143-154. https://doi.org/10.1007/BF02556874

Bentov, I., & Reed, M. J. (2014). Anesthesia, Microcirculation, and Wound Repair in Aging. *Survey of Anesthesiology*, *58*(4), 760-772. https://doi.org/10.1097/01.sa.0000450931.09309.5f

Berdiaki, A., Datsis, G. A., Nikitovic, D., Tsatsakis, A., Katonis, P., Karamanos, N. K., & Tzanakakis, G. N. (2010). Parathyroid hormone (PTH) peptides through the regulation of hyaluronan metabolism affect osteosarcoma cell migration. *IUBMB Life*, *62*(5), 377-386. https://doi.org/10.1002/iub.320

Beresford, J. N., Graves, S. E., & Smoothy, C. A. (1993). Formation of mineralized nodules by bone derived cells in vitro: A model of bone formation? *American Journal of Medical Genetics*, *45*(2), 163-178. https://doi.org/10.1002/ajmg.1320450205

Birben, E., Sahiner, U. M., Sackesen, C., Erzurum, S., & Kalayci, O. (2012). Oxidative stress and antioxidant defense. *World Allergy Organization Journal*, *5*(1), 9-19. https://doi.org/10.1097/WOX.0b013e3182439613

Blackmore, J., Shrivastava, S., Sallet, J., Butler, C. R., & Cleveland, R. O. (2019). Ultrasound Neuromodulation: A Review of Results, Mechanisms and Safety. *Ultrasound in Medicine and Biology*, *45*(7), 1509-1536. https://doi.org/10.1016/j.ultrasmedbio.2018.12.015

Blackwell, K. A., Raisz, L. G., & Pilbeam, C. C. (2010). Prostaglandins in bone: Bad cop, good cop? *Trends in Endocrinology and Metabolism*, *21*(5), 294-301. https://doi.org/10.1016/j.tem.2009.12.004

Blagosklonny, M. V. (2013). Hypoxia, MTOR and autophagy: converging on senescence or quiescence. *Autophagy*, *9*(2), 260–262. https://doi.org/10.4161/auto.22783

Blair, H. C., Larrouture, Q. C., Li, Y., Lin, H., Beer-Stoltz, D., Liu, L., Tuan, R. S., Robinson, L. J., Schlesinger, P. H., & Nelson, D. J. (2017). Osteoblast differentiation and bone matrix formation in vivo and in vitro. *Tissue Engineering - Part B: Reviews*, *23*(3), 268–280. https://doi.org/10.1089/ten.teb.2016.0454

Blinc, A., Francis, C. W., Trudnowski, J. L., & Carstensen, E. L. (1993). Characterization of ultrasound-potentiated fibrinolysis in vitro. *Blood*, *81*(10), 2636-2643. https://doi.org/10.1182/blood.v81.10.2636.2636

Bologna-Molina, R., Mosqueda-Taylor, A., Molina-Frechero, N., Mori-Estevez, A. D., & Sánchez-Acuña, G. (2013). Comparison of the value of PCNA and Ki-67 as markers of cell proliferation in ameloblastic tumors. *Medicina Oral, Patologia Oral y Cirugia Bucal*, *18*(2), 174–179. https://doi.org/10.4317/medoral.18573

Bols, N. C., Kawano, A., & Lee, L. E. J. (2011). *Cellular, molecular, genomics and biomedical approaches : culture of fish cell lines* (Vol. 1-3). https://doi.org/10.1016/B978-0-12-374553-8.00253-7

Bonewald, L. F. (2011). The amazing osteocyte. *Journal of Bone and Mineral Research*, *26*(2), 229-238. https://doi.org/10.1002/jbmr.320

Bosshardt, D. D., Chappuis, V., & Buser, D. (2017). Osseointegration of titanium, titanium alloy and zirconia dental implants: current knowledge and open questions. *Periodontology 2000*, *73*(1), 22-40. https://doi.org/10.1111/prd.12179

Boyle, W. J., Simonet Ws Fau - Lacey, D. L., & Lacey, D. L. (2003). Osteoclast differentiation and activation. *Nature*, *423*, 337–342. https://doi.org/10.1038/nature01658

Bozycki, L., Mroczek, J., Bessueille, L., Mebarek, S., Buchet, R., Pikula, S., & Strzelecka-Kiliszek, A. (2021). Annexins A2, A6 and Fetuin-A Affect the Process of Mineralization in Vesicles Derived from Human Osteoblastic hFOB 1.19 and Osteosarcoma Saos-2 Cells. *International Journal of Molecular Sciences*, *22*(8), 3993. https://doi.org/10.3390/ijms22083993

Branemark, P. I. (1983). Osseointegration and its experimental background. *The Journal of Prosthetic Dentistry*, *50*(3), 399-410. https://doi.org/10.1016/S0022-3913(83)80101-2

Brett, P. M., Harle, J., Salih, V., Mihoc, R., Olsen, I., Jones, F. H., & Tonetti, M. (2004). Roughness response genes in osteoblasts. *Bone*, *35*(1), 124-133. https://doi.org/10.1016/j.bone.2004.03.009

Burgess, S. E. P., Silverman, R. H., Coleman, D. J., Yablonski, M. E., Lizzi, F. L., Driller, J., Rosado, A., & Dennis, P. H. (1986). Treatment of Glaucoma with High-Intensity Focused Ultrasound. *Ophthalmology*, *93*(6), 831-838. https://doi.org/https://doi.org/10.1016/S0161-6420(86)33672-8

Burr, D. B., Milgrom, C., Fyhrie, D., Forwood, M., Nyska, M., Finestone, A., Hoshaw, S., Saiag, E., & Simkin, A. (1996). In vivo measurement of human tibial strains during vigorous activity. *Bone*, *18*(5), 405-410. https://doi.org/10.1016/8756-3282(96)00028-2

Busse, J. W., Bhandari, M., Einhorn, T. A., Schemitsch, E., Heckman, J. D., Tornetta, P., Leung, K. S., Heels-Ansdell, D., Makosso-Kallyth, S., Della Rocca, G. J., Jones, C. B., & Guyatt, G. H. (2016). Re-evaluation of low intensity pulsed ultrasound in treatment of tibial fractures (TRUST): Randomized clinical trial. *BMJ (Online)*, *355*. https://doi.org/10.1136/bmj.i5351

Buttitta, L. A., & Edgar, B. A. (2009). Mechanisms controlling cell cycle exit upon terminal differentiation. *Current Opinion in Cell Biology*, *19*(6), 697–704. https://doi.org/10.1016/j.ceb.2007.10.004

Buttitta, L. A., & Edgar, B. A. (2009). Mechanisms controlling cell cycle exit upon terminal differentiation. *Current Opinion in Cell Biology*, *19*(6), 697-704. https://doi.org/10.1016/j.ceb.2007.10.004.Mechanisms

Cabral-Pacheco, G. A., Garza-Veloz, I. A.-O., Castruita-De la Rosa, C., Ramirez-Acuña, J. A.-O., Perez-Romero, B. A., Guerrero-Rodriguez, J. F., Martinez-Avila, N., & Martinez-Fierro, M. A.-O. (2020). The Roles of Matrix Metalloproteinases and Their Inhibitors in Human Diseases. *International Journal of Molecular Sciences*, *21*(24), 9739. https://doi.org/10.3390/ijms21249739

Cadena-Herrera, D., Esparza-De Lara, J. E., Ramírez-Ibañez, N. D., López-Morales, C. A., Pérez, N. O., Flores-Ortiz, L. F., & Medina-Rivero, E. (2015). Validation of three viable-cell counting methods: Manual, semi-automated, and automated. *Biotechnology Reports*, *7*, 9-16. https://doi.org/10.1016/j.btre.2015.04.004

Cambier, D., D'Herde K Fau - Witvrouw, E., Witvrouw E Fau - Beck, M., Beck M Fau - Soenens, S., Soenens S Fau - Vanderstraeten, G., & Vanderstraeten, G. (2001). Therapeutic ultrasound: temperature increase at different depths by different modes in

a human cadaver. *Journal of Rehabilitation Medicine*, *33*(5), 212-215. https://doi.org/10.1080/165019701750419608

Campbell, S. (2013). A short history of sonography in obstetrics and gynaecology. *Facts, views & vision in ObGyn*, *5*(3), 213–229.

Cardoni, A., MacBeath, A., & Lucas, M. (2006). Methods for reducing cutting temperature in ultrasonic cutting of bone. *Ultrasonics*, *44*, e37-e42. https://doi.org/https://doi.org/10.1016/j.ultras.2006.06.046

Carina, V., Costa, V., Raimondi, L., Pagani, S., Sartori, M., Figallo, E., Setti, S., Alessandro, R., Fini, M., & Giavaresi, G. (2017). Effect of low-intensity pulsed ultrasound on osteogenic human mesenchymal stem cells commitment in a new bone scaffold. *Journal of Applied Biomaterials and Functional Materials*, *15*(3), 215-222. https://doi.org/10.5301/jabfm.5000342

Carovac, A., Smajlovic, F., & Junuzovic, D. (2011). Application of Ultrasound in Medicine. *Acta Informatica Medica*, *19*(3), 168–171. https://doi.org/10.5455/aim.2011.19.168-171

Casanova, M., Schindeler, A., Peacock, L., Lee, L., Schneider, P., Little, D. G., & Müller, R. (2021). Characterization of the Developing Lacunocanalicular Network During Fracture Repair. *JBMR Plus*, *5*(9). https://doi.org/10.1002/jbm4.10525

Castillo, A. B., Alam, I., Tanaka, S. M., Levenda, J., Li, J., Warden, S. J., & Turner, C. H. (2006). Low-amplitude, broad-frequency vibration effects on cortical bone formation in mice. *Bone*, *39*(5), 1087–1096. https://doi.org/10.1016/j.bone.2006.04.026

Catuna, M. C. (1953). Sonic surgery. *Annals of Dentistry*, *12*(100-129).

Chanen, A. M. (2010). The National Institute for Health and Clinical Excellence guideline for borderline personality disorder: More realistic than nihilistic. *Personality and Mental Health*, *4*(1), 41-44. https://doi.org/10.1002/pmh.116

Chauvel-Picard, J., Gourmet, R., Vercherin, P., Béra, J. C., & Gleizal, A. (2022). Stimulation of dental implant osseointegration by low-Intensity pulsed ultrasound: An in vivo preliminary study in a porcine model. *Journal of Prosthodontic Research*, *66*(4), 639–645. https://doi.org/10.2186/jpr.JPR_D_21_00115

Chen, B., Lin, T., Yang, X., Li, Y., Xie, D., Zheng, W., Cui, H., Deng, W., & Tan, X. (2016). Low-magnitude, high-frequency vibration promotes the adhesion and the osteogenic differentiation of bone marrow-derived mesenchymal stem cells cultured on a hydroxyapatite-coated surface: The direct role of Wnt/β-catenin signaling pathway activation. *International Journal of Molecular Medicine*, *38*, 1531–1540.

Chen, G., C., D., & Li, Y.-P. (2012). TGF-β and BMP signaling in osteoblast differentiation and bone formation. *International journal of biological sciences*, *8*(2), 272–288. https://doi.org/10.7150/ijbs.2929

Cheung, W. H., Chow, S. K. h., Sun, M. H., Qin, L., & Leung, K. S. (2011). Low-Intensity Pulsed Ultrasound Accelerated Callus Formation, Angiogenesis and Callus Remodeling in Osteoporotic Fracture Healing. *Ultrasound in Medicine and Biology*, *37*(2), 231–238. https://doi.org/10.1016/j.ultrasmedbio.2010.11.016

Cheung, W. H., Sun, M. H., Zheng, Y. P., Chu, W. C., Leung, A. H., Qin, L., Wei, F. Y., & Leung, K. S. (2012). Stimulated angiogenesis for fracture healing augmented by low-magnitude, high-frequency vibration in a rat model-evaluation of pulsed-wave doppler, 3-D power Doppler ultrasonography and micro-CT microangiography. *Ultrasound in Medicine & Biology*(1879-291X (Electronic)).

Chien, H. I., Chen, L. W., Liu, W. C., Lin, C. T., Ho, Y. Y., Tsai, W. H., & Yang, K. C. (2021). Bisphosphonate-Related Osteonecrosis of the Jaw. *Annals of plastic surgery*, *86*(2), 78–83. https://doi.org/10.1097/SAP.0000000000002650

Cho, M. I., Matsuda, N., Lin, W. L., Moshier, A., & Ramakrishnan, P. R. (1992). In vitro formation of mineralized nodules by periodontal ligament cells from the rat. *Calcified Tissue International*, *50*(5), 459-467. https://doi.org/10.1007/BF00296778

Cho, Y. D., Kim, W. J., Kim, S., Ku, Y., & Ryoo, H. M. (2021). Surface topography of titanium affects their osteogenic potential through DNA methylation. *International Journal of Molecular Sciences*, *22*(5), 2406. https://doi.org/10.3390/ijms22052406

Choi, J. U. A., Kijas, A. W., Lauko, J., & Rowan, A. E. (2022). The Mechanosensory Role of Osteocytes and Implications for Bone Health and Disease States. *Frontiers in cell and developmental biology*, *9*. https://doi.org/10.3389/fcell.2021.770143

Choy, M. V., Wong, R. M., Li, M. C., Wang, B. Y., Liu, X. D., Lee, W., Cheng, J. C., Chow, S. K., & Cheung, W. H. (2020). Can we enhance osteoporotic metaphyseal fracture healing through enhancing ultrastructural and functional changes of osteocytes in cortical bone with low-magnitude high-frequency vibration? *FASEB journal : official publication of the Federation of American Societies for Experimental Biology*, *34*, 4234–4252.

Chung, C. H., Golub Ee Fau - Forbes, E., Forbes E Fau - Tokuoka, T., Tokuoka T Fau - Shapiro, I. M., & Shapiro, I. M. (1992). Mechanism of action of beta-glycerophosphate on bone cell mineralization. *Calcified Tissue International*, *51*(4), 305–311. https://doi.org/10.1007/BF00334492

Church, C. C. (2002). Spontaneous homogeneous nucleation, inertial cavitation and the safety of diagnostic ultrasound. *Ultrasound in Medicine & Biology*, *28*(0301-5629 (Print)), 1349–1364.

Cmoch, A., Podszywalow-Bartnicka, P., Palczewska, M., Piwocka, K., Groves, P., & Pikula, S. (2014). Stimulators of mineralization limit the invasive phenotype of human osteosarcoma cells by a mechanism involving impaired invadopodia formation. *PLoS ONE*, *9*(10), e109938. https://doi.org/10.1371/journal.pone.0109938

Coelho, M. J., & Fernandes, M. H. (2000). Human bone cell cultures in biocompatibility testing. Part II: Effect of ascorbic acid, β-glycerophosphate and dexamethasone on osteoblastic differentiation. *Biomaterials*, *21*(11), 1095–1102. https://doi.org/10.1016/S0142-9612(99)00192-1

Coleman, A. J., & Saunders, J. E. (1993). A review of the physical properties and biological effects of the high amplitude acoustic field used in extracorporeal lithotripsy. *Ultrasonics*, *31*(0041-624X (Print)), 75–89.

Conner-Kerr, T., Malpass, G., Steele, A., & Howlett, A. (2015). Effects of 35 kHz, Low-frequency Ultrasound Application in Vitro on Human Fibroblast Morphology and Migration Patterns. *Ostomy Wound Management*, *61*(3), 34-41.

Conner-Kerr, T., & Oesterle, M. E. (2017). Current perspectives on therapeutic ultrasound in the management of chronic wounds: a review of evidence. *Chronic Wound Care Management and Research*, *4*, 89-98. https://doi.org/10.2147/cwcmr.s135982

Cooke, M. J., Phillips, S. R., Shah, D. S. H., Athey, D., Lakey, J. H., & Przyborski, S. A. (2008). Enhanced cell attachment using a novel cell culture surface presenting functional domains from extracellular matrix proteins. *Cytotechnology*, *56*(2), 71–79. https://doi.org/10.1007/s10616-007-9119-7

Coords, M., Breitbart, E., Paglia, D., Kappy, N., Gandhi, A., Cottrell, J., Cedeno, N., Pounder, N., O'Connor, J. P., & Lin, S. S. (2011). The effects of low-intensity pulsed ultrasound

upon diabetic fracture healing. *Journal of Orthopaedic Research*, *29*(2), 181–188. https://doi.org/10.1002/jor.21223

Copuroglu, C., Calori, G. M., & Giannoudis, P. V. (2013). Fracture non-union: Who is at risk? *Injury*, *44*(11), 1379–1382. https://doi.org/10.1016/j.injury.2013.08.003

Corradi, C., & Cozzolino, A. (1953). Gli ultrasuoni e l'evoluzione del callo osseo nei focolai di frattura. *Archivio di ortopedia*, *66*(1).

Cui, J., Dean, D., Hornicek, F. J., Chen, Z., & Duan, Z. (2020). The role of extracelluar matrix in osteosarcoma progression and metastasis. *Journal of Experimental & Clinical Cancer Research*, *39*(1), 178. https://doi.org/10.1186/s13046-020-01685-w

Curie, J., & Curie, P. (1880). Développement par compression de l'électricité polaire dans les cristaux hémièdres à faces inclinées. *Bulletin de la Société minéralogique de France*, *3*(4), 90-93. https://doi.org/10.3406/bulmi.1880.1564

Czekanska, E. M., Stoddart, M. J., Ralphs, J. R., Richards, R. G., & Hayes, J. S. (2014). A phenotypic comparison of osteoblast cell lines versus human primary osteoblasts for biomaterials testing. *Journal of Biomedical Materials Research - Part A*, *102*(8). https://doi.org/10.1002/jbm.a.34937

Czekanska, E. M., Stoddart, M. J., Richards, R. G., & Hayes, J. S. (2012). In search of an osteoblast cell model for in vitro research. *European Cells and Materials*, *24*, 1–17. https://doi.org/10.22203/eCM.v024a01

Datta, N., Pham, Q. P., Sharma, U., Sikavitsas, V. I., Jansen, J. A., & Mikos, A. G. (2006). In vitro generated extracellular matrix and fluid shear stress synergistically enhance 3D osteoblastic differentiation. *Proceedings of the National Academy of Sciences of the United States of America*, *103*(8), 2488–2493. https://doi.org/10.1073/pnas.0505661103

Daugaard, H., Elmengaard, B., Bechtold, J., Jensen, T., & Soballe, K. (2013). The effect on bone growth enhancement of implant coatings with hydroxyapatite and collagen deposited electrochemically and by plasma spray. *Journal of Biomedical Materials Research*, *92*(1552-4965 (Electronic)), 913–921. https://doi.org/10.1002/jbm.a.32303

de Viteri, V. S., & Fuentes, E. (2013). Titanium and Titanium Alloys as Biomaterials. In J. Gegner (Ed.), *Tribology - Fundamentals and Advancements*. InTech. https://doi.org/10.5772/55860

de-Freitas, N. R., Lima, L. B., de-Moura, M. B., Veloso-Guedes, C. d. C. F., Simamoto-Júnior, P. C., & de-Magalhães, D. (2016). Bisphosphonate treatment and dental implants: A systematic review. *Medicina Oral, Patologia Oral y Cirugia Bucal*, *21*(5), 644–651. https://doi.org/10.4317/medoral.20920

Deere, K., Whitehouse, M. R., Kunutsor, S. K., Sayers, A., Mason, J., & Blom, A. W. (2022). How long do revised and multiply revised hip replacements last? A retrospective observational study of the National Joint Registry. *The Lancet Rheumatology*, *4*(7), 468-479. https://doi.org/10.1016/S2665-9913(22)00097-2

Delacour, C., Lutz, C., & Kuhn, S. (2019). Pulsed ultrasound for temperature control and clogging prevention in micro-reactors. *Ultrasonics Sonochemistry*, *55*, 67-74. https://doi.org/https://doi.org/10.1016/j.ultsonch.2019.03.012

Della Rocca, G. J. (2009). The science of ultrasound therapy for fracture healing. *Indian Journal of Orthopaedics*, *43*(2), 121–126. https://doi.org/10.4103/0019-5413.50845

Dinno, M. A., Dyson, M., Young, S. R., Mortimer, A. J., Hart, J., & Crum, L. A. (1989). The significance of membrane changes in the safe and effective use of therapeutic and diagnostic ultrasound. *Physics in Medicine and Biology*, *34*(11), 1543-1552. https://doi.org/10.1088/0031-9155/34/11/003

Doan, N., Reher, P., Meghji, S., & Harris, M. (1999). In vitro effects of therapeutic ultrasound on cell proliferation, protein synthesis, and cytokine production by human fibroblasts, osteoblasts, and monocytes. *Journal of Oral and Maxillofacial Surgery*, *57*(4), 409-419. https://doi.org/10.1016/S0278-2391(99)90281-1

Dolan, E. B., Haugh, M. G., Tallon, D., Casey, C., & McNamara, L. M. (2012). Heat-shock-induced cellular responses to temperature elevations occurring during orthopaedic cutting. *Journal of the Royal Society Interface*, *9*, 3503–3513.

Donahue, H. J. (2000). Gap junctions and biophysical regulation of bone cell differentiation. *Bone*, *26*(5), 417-422. https://doi.org/https://doi.org/10.1016/S8756-3282(00)00245-3

Donald, I., Macvicar, J., & Brown, T. G. (1958). Investigation of abdominal masses by pulsed ultrasound. *The Lancet*, *271*(7032), 1188-1195. https://doi.org/10.1016/S0140-6736(58)91905-6

Duarte, L. R. (1983). The stimulation of bone growth by ultrasound. *Archives of Orthopaedic and Traumatic Surgery*, *101*(3), 153-159. https://doi.org/10.1007/BF00436764

Dussik, K. T. (1948). Ultrasound diagnostics, especially for brain diseases, using hyperphonography. *Zeitschrift fur physikalische Therapie, Bader und Klimaheilkunde*, *1*(9-10), 140-155.

Dvorakova, J., Wiesnerova, L., Chocholata, P., Kulda, V., Landsmann, L., Cedikova, M., Kripnerova, M., Eberlova, L., & Babuska, V. (2023). Human cells with osteogenic potential in bone tissue research. *Biomedical engineering online*, *22*(1475-925X (Electronic)), 33.

Dwivedi, R., Kumar, S., Pandey, R., Mahajan, A., Nandana, D., Katti, D. S., & Mehrotra, D. (2020). Polycaprolactone as biomaterial for bone scaffolds: Review of literature. *Journal of Oral Biology and Craniofacial Research*, *10*(1), 381-388. https://doi.org/10.1016/j.jobcr.2019.10.003

Dyson, M. (1982). Non-thermal cellular effects of ultrasound. *British Journal of Cancer*, *45*, 165–171.

Ekegren, C. L., Edwards, E. R., de Steiger, R., & Gabbe, B. J. (2018). Incidence, costs and predictors of non-union, delayed union and mal-union following long bone fracture. *International Journal of Environmental Research and Public Health*, *15*(12), 2845. https://doi.org/10.3390/ijerph15122845

Elias, C. N., Lima, J. H. C., Valiev, R., & Meyers, M. A. (2008). Biomedical applications of titanium and its alloys. *JOM*, *60*, 46–49. https://doi.org/10.1007/s11837-008-0031-1

Eliaz, N. (2019). Corrosion of Metallic Biomaterials: A Review. *Materials*, *12*, 407.

Emami, A., Petrén-Mallmin, M., & Larsson, S. (1999). No effect of low-intensity ultrasound on healing time of intramedullary fixed tibial fractures. *Journal of Orthopaedic Trauma*, *13*(4), 252–257. https://doi.org/10.1097/00005131-199905000-00005

Eriksson, A. R., & Albrektsson, T. (1983). Temperature threshold levels for heat-induced bone tissue injury: a vital-microscopic study in the rabbit. *The Journal of prosthetic dentistry*, *50*, 101-107.

Eriksson, R. E., Albrektsson, T., & Magnusson, B. (1984). Assessment of bone viability after heat trauma. A histological, histochemical and vital microscopic study in the rabbit. *Scandinavian journal of plastic and reconstructive surgery*, *18*, 261–268.

Everts, V., Delaissié, J. M., Korper, W., Jansen, D. C., Tigchelaar-Gutter, W., Saftig, P., & Beertsen, W. (2002). The bone lining cell: Its role in cleaning Howship's lacunae and initiating bone formation. *Journal of Bone and Mineral Research*, *17*(1), 77-90. https://doi.org/10.1359/jbmr.2002.17.1.77

Felsovalyi, F. (2012). *Mechanistic Study of the Adsorption and Desorption of Proteins on Silica* Columbia University].

Feng, X. (2009). Chemical and Biochemical Basis of Cell-Bone Matrix Interaction in Health and Disease. *Current Chemical Biology*, *3*(2), 189–196. https://doi.org/10.2174/187231309788166398

Fernandes, R. J., Harkey, M. A., Weis, M., Askew, J. W., & Eyre, D. R. (2007). The post-translational phenotype of collagen synthesized by SAOS-2 osteosarcoma cells. *Bone*, *40*(5), 1343-1351. https://doi.org/10.1016/j.bone.2007.01.011

Fernandez de Grado, G., Keller, L., Idoux-Gillet, Y., Wagner, Q., Musset, A. M., Benkirane-Jessel, N., Bornert, F., & Offner, D. (2018). Bone substitutes: a review of their characteristics, clinical use, and perspectives for large bone defects management. *Journal of Tissue Engineering*, *9*, 1-18. https://doi.org/10.1177/2041731418776819

Fielding, G. A., Sarkar, N., Vahabzadeh, S., & Bose, S. (2019). Regulation of osteogenic markers at late stage of osteoblast differentiation in silicon and zinc doped porous TCP. *Journal of Functional Biomaterials*, *10*(4). https://doi.org/10.3390/jfb10040048

Fini, M., Giavaresi, G., Aldini, N. N., Torricelli, P., Morrone, G., Guzzardella, G. A., Giardino, R., Krajewski, A., Ravaglioli, A., Belmonte, M. M., De Benedittis, A., & Biagini, G. (2000). The effect of osteopenia on the osteointegration of different biomaterials: Histomorphometric study in rats. *Journal of Materials Science: Materials in Medicine*, *11*(9), 579-585. https://doi.org/10.1023/A:1008932303913

Firoz, B. P., Polepalle, T., Loya, M., Mani Deepthi, C. H., & Nayyar, A. S. (2016). Piezosurgery: A Boon to Dentistry. *Journal of Dental Applications*, *3*(4), 365-369.

Florencio-Silva, R., Sasso, G. R. D. S., Sasso-Cerri, E., Simões, M. J., & Cerri, P. S. (2015). Biology of Bone Tissue: Structure, Function, and Factors That Influence Bone Cells. *BioMed research international*, *2015*. https://doi.org/10.1155/2015/421746

Fogh, J., & Trempe, G. (1975). New human tumor cell lines in human tumor cells in vitro. In J. Fogh (Ed.), *Human Tumor Cells in Vitro* (pp. 115–159). Springer Science+Business Media.

Fraldi, M., Cugno, A., Deseri, L., Dayal, K., & Pugno, N. M. (2015). A frequency-based hypothesis for mechanically targeting and selectively attacking cancer cells. *Journal of the Royal Society Interface*, *12*(111). https://doi.org/10.1098/rsif.2015.0656

Friedenberg, Z. B., Roberts, P. G., Didizian, N. H., & Brighton, C. T. (1971). Stimulation of fracture healing by direct current in the rabbit fibula. *The Journal of bone and joint surgery. American volume*, *53*(7), 1400–1408. https://doi.org/10.2106/00004623-197153070-00018

Fry, W. J., Fry, F. J., Barnard, J. W., Krumins, R. F., & Brennan, J. F. (1955). Ultrasonic Lesions in the Mammalian Central Nervous System. *Science*, *122*(3168), 517-518. https://doi.org/10.1126/science.122.3168.517

Fukada, E., & Yasuda, I. (1957). On the Piezoelectric Effect of Bone. *Journal of the Physical Society of Japan*, *12*(10), 1158-1162. https://doi.org/10.1143/JPSJ.12.1158

Fyfe, M. C., & Bullock, M. I. (1985). Therapeutic Ultrasound: Some Historical Background and Development in Knowledge of its Effect on Healing. *Australian Journal of Physiotherapy*, *31*(6), 220-224. https://doi.org/https://doi.org/10.1016/S0004-9514(14)60635-8

Fyfe, M. C., & Chahl, L. A. (1984). Mast cell degranulation and increased vascular permeability induced by 'therapeutic' ultrasound in the rat ankle joint. *British Journal of Experimental Pathology*, *65*(6), 671–676.

Gabbi, C., Borghetti, P., Antolotti, N., & Pitteri, S. (1992). Experimental Study on the Properties of Hydroxyapatite Coated Implants. In A. Ravaglioli & A. Krajewski (Eds.), *Bioceramics and the Human Body* (pp. 195-202). Springer Netherlands. https://doi.org/10.1007/978-94-011-2896-4_24

Gallagher, J. A. (2003). Human osteoblast culture. *Methods in molecular medicine*, *80*, 3-18. https://doi.org/10.1385/1-59259-366-6:3

Gao, H., Pei, K., Hu, G., Liu, W., Meng, A., Wang, H., Shao, H., & Li, W. (2022). The influence of pressure on the acoustic cavitation in saturated CO2-expanded N, N-dimethylformamide. *Ultrasonics Sonochemistry*, *83*, 105934. https://doi.org/https://doi.org/10.1016/j.ultsonch.2022.105934

Gardinier, J. D., Majumdar, S., Duncan, R. L., & Wang, L. (2009). Cyclic hydraulic pressure and fluid flow differentially modulate cytoskeleton re-organization in MC3T3 osteoblasts. *Cellular and Molecular Bioengineering*, *2*(1), 133-143. https://doi.org/10.1007/s12195-008-0038-2

Ghiasi, M. S., Chen, J., Vaziri, A., Rodriguez, E. K., & Nazarian, A. (2017). Bone fracture healing in mechanobiological modeling: A review of principles and methods. *Bone Reports*, *6*, 323-327. https://doi.org/10.1016/j.bonr.2017.03.002

Ghorayeb, S. R., Patel, U. S., Walmsley, A. D., & Scheven, B. A. (2013). Biophysical characterization of low-frequency ultrasound interaction with dental pulp stem cells. *Journal of Therapeutic Ultrasound*, *1*(12). https://doi.org/10.1186/2050-5736-1-12

Gibreel, S., Gassim Mohamed, H., Raj Suraj, A., & Anil, S. (2022). Osseointegration of Dental Implants and Osteoporosis. In. https://doi.org/10.5772/intechopen.100270

Gómez-de Diego, R., Mang-de la Rosa, M. d. R., Romero-Pérez, M. J., Cutando-Soriano, A., & López-Valverde-centeno, A. (2014). Indications and contraindications of dental implants in medically compromised patients: Update. *Medicina Oral, Patologia Oral y Cirugia Bucal*, *19*(5), 483-489. https://doi.org/10.4317/medoral.19565

Grediac, M., Sur, F., & Blaysat, B. (2016). The grid method for in-plane displacement and strain measurement: a review and analysis. *Strain*, *52*(3), 205-243. https://doi.org/10.1111/str.12182

Griffin, X. L., Parsons, N., Costa, M. L., & Metcalfe, D. (2014). Ultrasound and shockwave therapy for acute fractures in adults. *Cochrane Database of Systematic Reviews*, *2*. https://doi.org/10.1002/14651858.CD008579.pub3

Grishagin, I. V. (2015). Automatic cell counting with ImageJ. *Analytical Biochemistry*, *473*, 63-65. https://doi.org/10.1016/j.ab.2014.12.007

Gulfam, R. A.-O., & Chen, Y. A.-O. (2022). Recent Growth of Wettability Gradient Surfaces: A Review. *Research (Washington, D.C.)*, e9873075. https://doi.org/10.34133/2022/9873075

Gupta, D., Savva, J., Li, X., Chandler, J. H., Shelton, R. M., Scheven, B. A., Mulvana, H., Valdastri, P., Lucas, M., & Walmsley, A. D. (2022). Traditional Multiwell Plates and Petri Dishes Limit the Evaluation of the Effects of Ultrasound on Cells In Vitro. *Ultrasound in Medicine and Biology*, *48*(9), 1745-1761. https://doi.org/10.1016/j.ultrasmedbio.2022.05.001

Gupta, R., K., K., & Weber, D. D. S. (2023). Dental Implants. BTI - StatPearls. *StatPearls*.

Guzman, M. L., Rossi, R. M., Karnischky, L., Li, X., Peterson, D. R., Howard, D. S., & Jordan, C. T. (2005). The sesquiterpene lactone parthenolide induces apoptosis of human acute myelogenous leukemia stem and progenitor cells. *Blood*, *105*(11), 4163–4169. https://doi.org/10.1182/blood-2004-10-4135

Habib, A., Mehanna, A., & Medra, A. (2013). Cyanoacrylate: a handy tissue glue in maxillofacial surgery: our experience in alexandria, egypt. *Journal of maxillofacial and oral surgery*, *12*, 243–247.

Hampel, G. A., Yilmaz, E., Massrey, C., Clifton, W., Iwanaga, J., Loukas, M., & Tubbs, R. S. (2022). History of Bone Grafts in Spine Surgery. *Cureus*, *14*(5). https://doi.org/10.7759/cureus.24655

Hashish, I., Harvey, W., & Harris, M. (1986). Anti-inflammatory effects of ultrasound therapy: Evidence for a major placebo effect. *Rheumatology*, *25*(1), 77-81. https://doi.org/10.1093/rheumatology/25.1.77

Hauff, P., Reinhardt, M., & Foster, S. (2008). Ultrasound basics. In W. Semmler & M. Schwaiger (Eds.), *Handbook of Experimental Pharmacology* (Vol. 185, pp. 91–107). Springer. https://doi.org/10.1007/978-3-540-72718-7_5

Hausser, H. J., & Brenner, R. E. (2005). Phenotypic instability of Saos-2 cells in long-term culture. *Biochemical and Biophysical Research Communications*, *333*(1). https://doi.org/10.1016/j.bbrc.2005.05.097

Haut, J., Colliac, J. P., Falque, L., & Renard, Y. (1990). Indications and results of Sonocare (ultrasound) in the treatment of ocular hypertension. A preliminary study of 395 cases [Indications et résultats du Sonocare (ultrasons) dans le traitement des hypertonies oculaires. Etude préliminaire sur 395 cas.]. *Ophtalmologie : organe de la Societe francaise d'ophtalmologie*, *4*(0989-3105 (Print)), 138–141.

Hayflick, L., & Moorhead, P. S. (1961). The serial cultivation of human diploid cell strains. *Experimental cell research*, *25*, 585–621.

Heckman, J. D., Ryaby, J. P., McCabe, J., Frey, J. J., & Kilcoyne, R. F. (1994). Acceleration of tibial fracture-healing by non-invasive, low-intensity pulsed ultrasound. *Journal of Bone and Joint Surgery*, *76*(1), 26-34. https://doi.org/10.2106/00004623-199401000-00004

Heinemann, C., Adam, J., Kruppke, B., Hintze, V., Wiesmann, H. P., & Hanke, T. (2021). How to get them off?—assessment of innovative techniques for generation and detachment of mature osteoclasts for biomaterial resorption studies. *International Journal of Molecular Sciences*, *22*(3), 1329. https://doi.org/10.3390/ijms22031329

Henrich, D., Nau, C., Kraft, S. B., Zollfrank, M., Kontradowitz, K., Oppermann, E., Schultheiss, J., Meier, S., Frank, J., Marzi, I., & Seebach, C. (2016). Effect of the harvest procedure and tissue site on the osteogenic function of and gene expression in human mesenchymal stem cells. *International Journal of Molecular Medicine*, *37*(4), 976–988. https://doi.org/10.3892/ijmm.2016.2489

Hernandez-Segura, A., Brandenburg, S., & Demaria, M. (2018). Induction and validation of cellular senescence in primary human cells. *Journal of Visualized Experiments*, *2018*(136), 57782. https://doi.org/10.3791/57782

Heybeli, N., Yeşildağ, A., Oyar, O., Gülsoy, U. K., Tekinsoy, M. A., & Mumcu, E. F. (2002). Diagnostic ultrasound treatment increases the bone fracture-healing rate in an internally fixed rat femoral osteotomy model. *Journal of Ultrasound in Medicine*, *21*(12), 1357–1363. https://doi.org/10.7863/jum.2002.21.12.1357

Hoffman, A. S. (1982). Blood—Biomaterial Interactions: An Overview. In S. L. Cooper, N. A. Peppas, A. S. Hoffman, & B. D. Ratner (Eds.), *Biomaterials: Interfacial Phenomena and Applications* (Vol. 199, pp. 3-8). American chemical society. https://doi.org/doi:10.1021/ba-1982-0199.ch001

10.1021/ba-1982-0199.ch001

Hong, A. R., & Kim, S. W. (2018). Effects of resistance exercise on bone health. *Endocrinology and Metabolism*, *33*(4), 435–444. https://doi.org/10.3803/EnM.2018.33.4.435

Hou, C., An, J., Zhao, D., Ma, X., Zhang, W., Zhao, W., Wu, M., Zhang, Z., & Yuan, F. (2022). Surface Modification Techniques to Produce Micro/Nano-scale Topographies on Ti-Based Implant Surfaces for Improved Osseointegration. *Frontiers in Bioengineering and Biotechnology*, *10*, 835008. https://doi.org/10.3389/fbioe.2022.835008

Hsu, S.-K., Huang, W.-T., Liu, B.-S., Li, S.-M., Chen, H.-T., & Chang, C.-J. (2011). Effects of Near-Field Ultrasound Stimulation on New Bone Formation and Osseointegration of Dental Titanium Implants In Vitro and In Vivo. *Ultrasound in Medicine & Biology*, *37*(3), 403-416. https://doi.org/10.1016/j.ultrasmedbio.2010.12.004

Hu, C. Y., & Yoon, T. R. (2018). Recent updates for biomaterials used in total hip arthroplasty. *Biomaterials Research*, *22*(33). https://doi.org/10.1186/s40824-018-0144-8

Huang, H.-L., Hsing, H.-W., Lai, T.-C., Chen, Y.-W., Lee, T.-R., Chan, H.-T., Lyu, P.-C., Wu, C.-L., Lu, Y.-C., Lin, S.-T., Lin, C.-W., Lai, C.-H., Chang, H.-T., Chou, H.-C., & Chan, H.-L. (2010). Trypsin-induced proteome alteration during cell subculture in mammalian cells. *Journal of Biomedical Science*, *17*(1), 36. https://doi.org/10.1186/1423-0127-17-36

Huang, W., Yang, S., Shao, J., & Li, Y. P. (2007). Signaling and transcriptional regulation in osteoblast commitment and differentiation. *Frontiers in Bioscience*, *12*, 3068–3092. https://doi.org/10.2741/2296

Huiskes, R., Rulmerman, R., Van Lenthe, G. H., & Janssen, J. D. (2000). Effects of mechanical forces on maintenance and adaptation of form in trabecular bone. *Nature*, *405*(6787), 704–706. https://doi.org/10.1038/35015116

Huiskes, R., Weinans H Fau - van Rietbergen, B., & van Rietbergen, B. (1992). The relationship between stress shielding and bone resorption around total hip stems and the effects of flexible materials. *Clinical Orthopaedics and Related Research*, *274*, 124–134.

Jacobs, C. R., Temiyasathit, S., & Castillo, A. B. (2010). Osteocyte mechanobiology and pericellular mechanics. *Annual Review of Biomedical Engineering*, *12*, 369-400. https://doi.org/10.1146/annurev-bioeng-070909-105302

Jager, L. D., Canda, C. M., Hall, C. A., Heilingoetter, C. L., Huynh, J., Kwok, S. S., Kwon, J. H., Richie, J. R., & Jensen, M. B. (2016). Effect of enzymatic and mechanical methods of dissociation on neural progenitor cells derived from induced pluripotent stem cells. *Advances in Medical Sciences*, *61*(1898-4002 (Electronic)), 78-84. https://doi.org/10.1016/j.advms.2015.09.005

James, A. W. (2013). Review of Signaling Pathways Governing MSC Osteogenic and Adipogenic Differentiation. *Scientifica*, *2013*, 684736. https://doi.org/10.1155/2013/684736

Jara-Oseguera, A., Simon, S., & Rosenbaum, T. (2010). TRPV1: On the Road to Pain Relief. *Current Molecular Pharmacology*, *1*(3), 255–269. https://doi.org/10.2174/1874467210801030255

Jaros, J. (2019). From Biology to Bytes: Predicting the Path of Ultrasound Waves Through the Human Body. *Acoustics Today*, *15*(2), 36-44.

Jastrzebska, E., Zuchowska, A., Flis, S., Sokolowska, P., Bulka, M., Dybko, A., & Brzozka, Z. (2018). Biological characterization of the modified poly(dimethylsiloxane) surfaces based on cell attachment and toxicity assays. *Biomicrofluidics*, *12*, 1932-1058.

Jedrzejczak-Silicka, M. (2017). History of Cell Culture. In *New Insights into Cell Culture Technology*. https://doi.org/10.5772/66905

Jemat, A., Ghazali, M. J., Razali, M., & Otsuka, Y. (2015). Surface Modifications and Their Effects on Titanium Dental Implants. *BioMed research international*(2314-6141 (Electronic)). https://doi.org/10.1155/2015/791725

Jiang, L. (2010). Reassessment of Carrel's Immortal Tissue Culture Experiments. In *Embryo Project Encyclopedia*.

Jiao, H., Xiao, E., & Graves, D. T. (2015). Diabetes and Its Effect on Bone and Fracture Healing. *Current osteoporosis reports*, *13*(5), 327–335. https://doi.org/10.1007/s11914-015-0286-8

Johns, L. D. (2002). Nonthermal effects of therapeutic ultrasound: The frequency resonance hypothesis. *Journal of Athletic Training*, *37*(3), 293–299.

Ju, T. J., Zhao, Z. Y., Ma, L. Q., Li, W. L., Li, S., & Zhang, J. (2021). Cyclic Adenosine Monophosphate-Enhanced Calvarial Regeneration by Bone Marrow-Derived Mesenchymal Stem Cells on a Hydroxyapatite/Gelatin Scaffold. *ACS Omega*, *6*(21), 13684–13694. https://doi.org/10.1021/acsomega.1c00881

Judge, A., Carr, A., Price, A., Garriga, C., Cooper, C., Prieto-Alhambra, D., Old, F., Peat, G., Murphy, J., Leal, J., Barker, K., Underdown, L., Arden, N., Gooberman-Hill, R., Fitzpatrick, R., Drew, S., & Pritchard, M. G. (2020). Health economics of enhanced recovery and joint replacement. In *The impact of the enhanced recovery pathway and other factors on outcomes and costs following hip and knee replacement: routine data study* (Vol. 7). NIHR Journals Library CTI - Health Services and Delivery Research.

Kalajzic, I., Matthews, B. G., Torreggiani, E., Harris, M. A., Divieti Pajevic, P., & Harris, S. E. (2013). In vitro and in vivo approaches to study osteocyte biology. *Bone*, *54*(2), 296-306. https://doi.org/10.1016/j.bone.2012.09.040

Kanatani, M., Sugimoto, T., Kano, J., Kanzawa, M., & Chihara, K. (2003). Effect of high phosphate concentration on osteoclast differentiation as well as bone-resorbing activity. *Journal of Cellular Physiology*, *196*(1), 180–189. https://doi.org/10.1002/jcp.10270

Kang, D. A.-O., Kim, S. A.-O., Choi, Y. A.-O., & Kim, Y. A.-O. (2019). Repeated failure of implants at the same site: a retrospective clinical study. *Maxillofacial Plastic and Reconstructive Surgery*, *41*(1), 27. https://doi.org/10.1186/s40902-019-0209-1

Kang, T., Lanni, S., Nam, J., Emery, P., & Wakefield, R. J. (2012). The evolution of ultrasound in rheumatology. *Therapeutic Advances in Musculoskeletal Disease*, *4*(6), 399–411. https://doi.org/10.1177/1759720X12460116

Kaur, G., & Dufour, J. M. (2012). Cell lines: Valuable tools or useless artifacts. *Spermatogenesis*, *2*(1), 1-5. https://doi.org/10.4161/spmg.19885

Keller, J., Klamer A Fau - Bak, B., Bak B Fau - Suder, P., & Suder, P. (1993). Effect of local prostaglandin E2 on fracture callus in rabbits. *Acta orthopaedica Scandinavica*, *64*(1), 59–63. https://doi.org/10.3109/17453679308994530

Keller, J. C., Stewart, M., Roehm, M., & Schneider, G. B. (2004). Osteoporosis-like bone conditions affect osseointegration of implants. *The International Journal of Oral & Maxillofacial Implants*, *19*(5), 687-694.

Kim, J. M., Lin, C., Stavre, Z., Greenblatt, M. B., & Shim, J. H. (2020). Osteoblast-Osteoclast Communication and Bone Homeostasis. *Cells*, *9*(9). https://doi.org/10.3390/cells9092073

Kim, Y. S., Rhim, H., Min, J. C., Hyo, K. L., & Choi, D. (2008). High-intensity focused ultrasound therapy: An overview for radiologists. *Korean Journal of Radiology*, *9*(4), 291–302. https://doi.org/10.3348/kjr.2008.9.4.291

Kirkpatrick, C. J., & Mittermayer, C. (1990). Theoretical and practical aspects of testing potential biomaterials in vitro. *Journal of Materials Science: Materials in Medicine*, *1*(1), 9–13. https://doi.org/10.1007/BF00705347

Knapik, D. M., Perera, P., Nam, J., Blazek, A. D., Rath, B., Leblebicioglu, B., Das, H., Wu, L. C., Hewett, T. E., Agarwal, S. K., Jr, R., A. G.,, Flanigan, D. C., Lee, B. S., & Agarwal, S. (2014). Mechanosignaling in bone health, trauma and inflammation. *Antioxidants & Redox Signaling*, *20*(6), 970–985. https://doi.org/10.1089/ars.2013.5467

Kocaoğlu, B., Çabukoglu, C., Özeras, N., Seyhan, M., Karahan, M., & Yalcin, S. (2011). The effect of therapeutic ultrasound on metallic implants: A study in rats. *Archives of Physical Medicine and Rehabilitation*, *92*(11), 1858-1862. https://doi.org/10.1016/j.apmr.2011.06.002

Kochar, S. P., Reche, A., & Paul, P. (2022). The Etiology and Management of Dental Implant Failure: A Review. *Cureus*, *14*(20), e30455. https://doi.org/10.7759/cureus.30455

Kokubu, T., Matsui, N., Fujioka, H., Tsunoda, M., & Mizuno, K. (1999). Low intensity pulsed ultrasound exposure increases prostaglandin E2 production via the induction of cyclooxygenase-2 mRNA in mouse osteoblasts. *Biochemical and Biophysical Research Communications*, *256*(2), 284–287. https://doi.org/10.1006/bbrc.1999.0318

Komori, T. (2020). Functions of osteocalcin in bone, pancreas, testis, and muscle. *International Journal of Molecular Sciences*, *21*(20), 7513. https://doi.org/10.3390/ijms21207513

Krampe, B., & Al-Rubeai, M. (2010). Cell death in mammalian cell culture: Molecular mechanisms and cell line engineering strategies. *Cytotechnology*, *62*(3), 175–188. https://doi.org/10.1007/s10616-010-9274-0

Kriebitzsch, C., Verlinden, L., Eelen, G., Biauw, K. T., Van Camp, M., Bouillon, R., & Verstuyf, A. (2009). The impact of 1,25(OH)2D3 and its structural analogs on gene expression in cancer cells - A microarray approach. *Anticancer Research*, *29*(9), 3471–3483.

Krishna, B. V., Bose, S., & Bandyopadhyay, A. (2007). Low stiffness porous Ti structures for load-bearing implants. *Acta Biomaterialia*, *3*(6), 997-1006. https://doi.org/10.1016/j.actbio.2007.03.008

Kristiansen, T. K., Ryaby, J. P., McCabe, J., Frey, J. J., & Roe, L. R. (1997). Accelerated healing of distal radial fractures with the use of specific, low-intensity ultrasound: A multicenter, prospective, randomized, double- blind, placebo-controlled study. *Journal of Bone and Joint Surgery*, *79*(7), 961-973. https://doi.org/10.2106/00004623-199707000-00002

Kumar, P., Nagarajan, A., & Uchil, P. D. (2018). Analysis of Cell Viability by the Lactate Dehydrogenase Assay. LID - 10.1101/pdb.prot095497 [doi]. *Cold Spring Harbor Protocols*, *6*(2018), 465-468. https://doi.org/10.1101/pdb.prot095497

Kumar, P., Vinitha, B., & Fathima, G. (2013). Bone grafts in dentistry. *Journal of Pharmacy and Bioallied Sciences*, *5*, 125–127. https://doi.org/10.4103/0975-7406.113312

Kumari, R., & Jat, P. (2021). Mechanisms of Cellular Senescence: Cell Cycle Arrest and Senescence Associated Secretory Phenotype. *Frontiers in cell and developmental biology*, *9*, 645593. https://doi.org/10.3389/fcell.2021.645593

Lai, T. Y., Cao, J., Ou-Yang, P., Tsai, C. Y., Lin, C. W., Chen, C. C., Tsai, M. K., & Lee, C. Y. (2022). Different methods of detaching adherent cells and their effects on the cell surface expression of Fas receptor and Fas ligand. *Scientific Reports*, *12*(1), 5713. https://doi.org/10.1038/s41598-022-09605-y

Langenbach, F., & Handschel, J. (2013). Effects of dexamethasone, ascorbic acid and β-glycerophosphate on the osteogenic differentiation of stem cells in vitro. *Stem Cell Research and Therapy*, *4*(117). https://doi.org/10.1186/scrt328

Le Guéhennec, L., Soueidan, A., Layrolle, P., & Amouriq, Y. (2007). Surface treatments of titanium dental implants for rapid osseointegration. *Dental Materials*, *23*(7), 844-854. https://doi.org/https://doi.org/10.1016/j.dental.2006.06.025

Lehmann, J. F. (1953). The present status of ultrasonic therapy. *Archives of Physical Medicine and Rehabilitation*, *34*(12), 748-749.

Leighton, R., Watson, J. T., Giannoudis, P., Papakostidis, C., Harrison, A., & Steen, R. G. (2017). Healing of fracture nonunions treated with low-intensity pulsed ultrasound (LIPUS): A systematic review and meta-analysis. *Injury*, *48*(7), 1339-1347. https://doi.org/10.1016/j.injury.2017.05.016

Leskinen, J. (2015). *Ultrasound Stimulation of Bone and Cartilage — Interactions in Common In Vitro and Tissue Engineering Configurations* University of Eastern Finland]. Kuopio.

Leskinen, J. J., & Hynynen, K. (2012). Study of factors affecting the magnitude and nature of ultrasound exposure with in vitro set-ups. *Ultrasound in Medicine & Biology*, *38*, 777–794. https://doi.org/10.1016/j.ultrasmedbio.2012.01.019

Leung, K. S., Cheung, W. H., Zhang, C., Lee, K. M., & Lo, H. K. (2004). Low Intensity Pulsed Ultrasound Stimulates Osteogenic Activity of Human Periosteal Cells. *Clinical Orthopaedics and Related Research*, *418*, 253-259. https://doi.org/10.1097/00003086-200401000-00044

Levin, M., Spiro, R. C., Jain, H., & Falk, M. M. (2022). Effects of Titanium Implant Surface Topology on Bone Cell Attachment and Proliferation in vitro. *Medical Devices: Evidence and Research*, *15*, 103-119. https://doi.org/10.2147/MDER.S360297

Li, X., Stritch, T., Manley, K., & Lucas, M. (2021). Limits and Opportunities for Miniaturizing Ultrasonic Surgical Devices Based on a Langevin Transducer. *IEEE transactions on ultrasonics, ferroelectrics, and frequency control*, *68*, 2543–2553.

Li, Z. (2011). In Vitro Micro-Tissue and -Organ Models for Toxicity Testing. *Comprehensive Biotechnology, Second Edition*, *5*, 551-563. https://doi.org/10.1016/B978-0-08-088504-9.00503-1

Liang, C., Liu, X., Yan, Y., Sun, R., Li, J., & Geng, W. (2022). Effectiveness and Mechanisms of Low-Intensity Pulsed Ultrasound on Osseointegration of Dental Implants and Biological Functions of Bone Marrow Mesenchymal Stem Cells. *Stem Cells International*, *2022*, 7397335. https://doi.org/10.1155/2022/7397335

Lim, J. Y., Shaughnessy, M. C., Zhou, Z., Noh, H., Vogler, E. A., & Donahue, H. J. (2008). Surface energy effects on osteoblast spatial growth and mineralization. *Biomaterials*, *29*(12), 1776-1784. https://doi.org/https://doi.org/10.1016/j.biomaterials.2007.12.026

Lima de Andrade, C., Carvalho, M., Bordin, D., da Silva, W., Del Bel Cury, A., & Sotto-Maior, B. (2017). Biomechanical Behavior of the Dental Implant Macrodesign. *The International Journal of Oral & Maxillofacial Implants*, *32*(2), 264-270. https://doi.org/10.11607/jomi.4797

Lin, X., Patil, S., Gao, Y. G., & Qian, A. (2020). The Bone Extracellular Matrix in Bone Formation and Regeneration. *Frontiers in Pharmacology*, *11*, 757. https://doi.org/10.3389/fphar.2020.00757

Lin, X., Zhou, L., Li, S., Lu, H., & Ding, X. (2014). Behavior of acid etching on titanium: topography, hydrophility and hydrogen concentration. *Biomedical materials (Bristol, England)*, *9*(1748-605X (Electronic)), 015002.

Liu, C., Zhao, Y., Cheung, W. Y., Gandhi, R., Wang, L., & You, L. (2010). Effects of cyclic hydraulic pressure on osteocytes. *Bone*, *46* 1449–1456. https://doi.org/10.1016/j.bone.2010.02.006

Liu, J., Li, X., Zhang, D., Jiao, J., Wu, L., Hao, F., & Qin, Y. X. (2018). Acceleration of Bone Defect Healing and Regeneration by Low-Intensity Ultrasound Radiation Force in a Rat Tibial Model. *Ultrasound in Medicine and Biology*, *44*(12), 2646-2654. https://doi.org/10.1016/j.ultrasmedbio.2018.08.002

Liu, Q., Liu, X., Liu, B., Hu, K., Zhou, X., & Ding, Y. (2012). The effect of low-intensity pulsed ultrasound on the osseointegration of titanium dental implants. *British Journal of Oral and Maxillofacial Surgery*, *50*(3), 244-250. https://doi.org/10.1016/j.bjoms.2011.03.001

Liu, X., Chu, P. K., & Ding, C. (2004). Surface modification of titanium, titanium alloys, and related materials for biomedical applications. *Materials Science and Engineering: R: Reports*, *47*(3), 49-121. https://doi.org/https://doi.org/10.1016/j.mser.2004.11.001

Lu, H., Liu, F., Chen, H., Chen, C., Qu, J., Xu, D., Zhang, T., Zhou, J., & Hu, J. (2016). The effect of low-intensity pulsed ultrasound on bone-tendon junction healing: Initiating after inflammation stage. *Journal of Orthopaedic Research*, *34*(10), 1697-1706. https://doi.org/10.1002/jor.23180

Lu, Y., Zhao, Q., Liu, Y., Zhang, L., Li, D., Zhu, Z., Gan, X., & Yu, H. (2018). Vibration loading promotes osteogenic differentiation of bone marrow-derived mesenchymal stem cells via p38 MAPK signaling pathway. *Journal of biomechanics*, *71*, 67–75.

Lucas, M., & Mathieson, A. (2015). Ultrasonic cutting for surgical applications. In J. A. Gallego-Juárez & K. F. Graff (Eds.), *Power Ultrasonics* (pp. 695-721). Woodhead Publishing. https://doi.org/https://doi.org/10.1016/B978-1-78242-028-6.00023-5

Lundquist, P., Murer, H., & Biber, J. (2007). Type II Na+-Pi cotransporters in osteoblast mineral formation: regulation by inorganic phosphate. *Cellular Physiology and Biochemistry*, *19*, 43-56. https://doi.org/10.1159/000099191

Lynn, J. G., Zwemer, R. L., Chick, A. J., & Miller, A. E. (1942). A new method for the generation and use of focused ultrasound in experimental biology. *Journal of General Physiology*, *26*(2), 179-193. https://doi.org/10.1085/jgp.26.2.179

Madara, K. C., Marmon, A., Aljehani, M., Hunter-Giordano, A., Zeni, J., & Raisis, L. (2019). Progressive rehabilitation after total hip arthroplasty: a pilot and feasibility study. . *International Journal of Sports Physical Therapy*, *14*(4), 564–581. https://doi.org/10.26603/ijspt20190564

Mahonen, A., Pirskanen, A., Keinänen, R., & Mäenpää, P. H. (1990). Effect of 1,25(OH)2D3 on its receptor mRNA levels and osteocalcin synthesis in human osteosarcoma cells. *BBA - Gene Structure and Expression*, *1048*(1). https://doi.org/10.1016/0167-4781(90)90018-W

Maleki, M., & Esmaeilzadeh, M. (2012). The evolutionary development of echocardiography. *Iranian Journal of Medical Sciences*, *37*, 222-232.

Malone, A. M. D., Anderson, C. T., Tummala, P., Kwon, R. Y., Johnston, T. R., Stearns, T., & Jacobs, C. R. (2007). Primary cilia mediate mechanosensing in bone cells by a calcium-independent mechanism. *Proceedings of the National Academy of Sciences*, *104*(33), 13325-13330. https://doi.org/10.1073/pnas.0700636104

Man, J., Shelton, R. M., Cooper, P. R., & Scheven, B. A. (2012). Low-intensity low-frequency ultrasound promotes proliferation and differentiation of odontoblast-like cells. *Journal of endodontics*, *38*(5), 608-613. https://doi.org/10.1016/j.joen.2012.01.015

Manolagas, S. C. (2000). Birth and Death of Bone Cells: Basic Regulatory Mechanisms and Implications for the Pathogenesis and Treatment of Osteoporosis*. *Endocrine Reviews*, *21*(2), 115-137. https://doi.org/10.1210/edrv.21.2.0395

Manzoor, H., & Saikali, S. W. (2023). *Renal Extracorporeal Lithotripsy*. StatPearls.

Marin, C., Luyten, F. P., Van der Schueren, B., Kerckhofs, G., & Vandamme, K. (2018). The impact of Type 2 diabetes on bone fracture healing. *Frontiers in Endocrinology*, *9*, 6. https://doi.org/10.3389/fendo.2018.00006

Marsell, R., & Einhorn, T. A. (2011). The biology of fracture healing. *Injury*, *42*(6). https://doi.org/10.1016/j.injury.2011.03.031

Martin, J. Y., Schwartz, Z., Hummert, T. W., Schraub, D. M., Simpson, J., Lankford, J., Dean, D. D., Cochran, D. L., & Boyan, B. D. (1995). Effect of titanium surface roughness on proliferation, differentiation, and protein synthesis of human osteoblast-like cells (MG63). *Journal of Biomedical Materials Research*, *29*(3), 389-401. https://doi.org/10.1002/jbm.820290314

Martínez, M. E., Campo, M. T. d., Medina, S., Sánchez, M., Sánchez-Cabezudo, M. J., Esbrit, P., Martínez, P., Moreno, I., Rodrigo, A., Garcés, M. V., & Munuera, L. (1999). Influence of Skeletal Site of Origin and Donor Age on Osteoblastic Cell Growth and Differentiation. *Calcified Tissue International*, *64*(4), 280-286. https://doi.org/10.1007/s002239900619

Matos, G. R. M. (2021). Surface Roughness of Dental Implant and Osseointegration. *Journal of maxillofacial and oral surgery*, *20*(1), 1-4. https://doi.org/10.1007/s12663-020-01437-5

Matsuura, T., Tokutomi, K., Sasaki, M., Katafuchi, M., Mizumachi, E., & Sato, H. (2014). Distinct characteristics of mandibular bone collagen relative to long bone collagen: Relevance to clinical dentistry. *BioMed research international*, *2014*, 769414. https://doi.org/10.1155/2014/769414

Maxwell, L. (1992). Therapeutic Ultrasound: Its Effects on the Cellular and Molecular Mechanisms of Inflammation and Repair. *Physiotherapy*, *78*(6), 421-426. https://doi.org/10.1016/S0031-9406(10)61528-3

Mayor, R., & Carmona-Fontaine, C. (2010). Keeping in touch with contact inhibition of locomotion. *Trends in Cell Biology*, *20*(6-3), 319–328. https://doi.org/10.1016/j.tcb.2010.03.005

McKinnon, K. M. (2018). Flow cytometry: An overview. *Current Protocols in Immunology*, *120*, 5.1.1–5.1.11. https://doi.org/10.1002/cpim.40

McQuillan, D. J., Richardson, M. D., & Bateman, J. F. (1995). Matrix deposition by a calcifying human osteogenic sarcoma cell line (SAOS-2). *Bone*, *16*(4), 415-426. https://doi.org/10.1016/8756-3282(95)90186-8

Mechiche Alami, S., Gangloff, S. C., Laurent-Maquin, D., Wang, Y., & Kerdjoudj, H. (2016). Concise Review: In Vitro Formation of Bone - Like Nodules Sheds Light on the Application of Stem Cells for Bone Regeneration. *Stem Cells Translational Medicine*, *5*(11), 1587–1593. https://doi.org/10.5966/sctm.2015-0413

Meleti, Z., Shapiro, I. M., & Adams, C. S. (2000). Inorganic phosphate induces apoptosis of osteoblast-like cells in culture. *Bone*, *27*(3), 359-366. https://doi.org/10.1016/S8756-3282(00)00346-X

Metavarayuth, K., Villarreal, E., Wang, H., & Wang, Q. (2021). Surface topography and free energy regulate osteogenesis of stem cells: effects of shape-controlled gold nanoparticles. *Biomaterials Translational*, *2*(2), 165–173. https://doi.org/10.12336/biomatertransl.2021.02.006

Michalakis, K., Bakopoulou, A., Papachristou, E., Vasilaki, D., Tsouknidas, A., Michailidis, N., & Johnstone, E. (2021). Evaluation of the Response of HOS and Saos-2 Osteosarcoma Cell Lines When Exposed to Different Sizes and Concentrations of Silver Nanoparticles. *BioMed research international*, *2021*, 5013065. https://doi.org/10.1155/2021/5013065

Miller, D. L., Smith, N. B., Bailey, M. R., Czarnota, G. J., Hynynen, K., & Makin, I. R. S. (2012). Overview of therapeutic ultrasound applications and safety considerations. *Journal of Ultrasound in Medicine*, *31*(4), 623–634. https://doi.org/10.7863/jum.2012.31.4.623

Miller, M. W., Miller, D. L., & Brayman, A. A. (1996). A review of in vitro bioeffects of inertial ultrasonic cavitation from a mechanistic perspective. *Ultrasound in Medicine and Biology*, *22*(9), 1131-1154. https://doi.org/10.1016/S0301-5629(96)00089-0

Mirza, Y. H., Teoh, K. H., Golding, D., Wong, J. F., & Nathdwarawala, Y. (2019). Is there a role for low intensity pulsed ultrasound (LIPUS) in delayed or nonunion following arthrodesis in foot and ankle surgery? *Foot and ankle surgery : official journal of the European Society of Foot and Ankle Surgeons*, *26*(6), 842-848.

Misch, C. E., Qu, Z., & Bidez, M. W. (1999). Mechanical properties of trabecular bone in the human mandible: Implications for dental implant treatment planning and surgical placement. *Journal of Oral and Maxillofacial Surgery*, *57*(6), 700-706. https://doi.org/https://doi.org/10.1016/S0278-2391(99)90437-8

Mohamed, A. M. F. S. (2008). An overview of bone cells and their regulating factors of differentiation. *Malaysian Journal of Medical Sciences*, *15*(1), 4–12.

Mohseny, A. B., MacHado, I., Cai, Y., Schaefer, K. L., Serra, M., Hogendoorn, P. C. W., Llombart-Bosch, A., & Cleton-Jansen, A. M. (2011). Functional characterization of osteosarcoma cell lines provides representative models to study the human disease. *Laboratory Investigation*, *91*(8), 1195-1205. https://doi.org/10.1038/labinvest.2011.72

Moorthy, R. S. (2002). Dopppler ultrasound. *Medical Journal Armed Forces India*, *58*(1), 1-2. https://doi.org/10.1016/S0377-1237(02)80001-6

Morelli, R., Clissa, L., Amici, R., Cerri, M., Hitrec, T., Luppi, M., Rinaldi, L., Squarcio, F., & Zoccoli, A. (2021). Automating cell counting in fluorescent microscopy through deep learning with c-ResUnet. *Scientific Reports*, *11*(1), 22920. https://doi.org/10.1038/s41598-021-01929-5

Muff, R., Rath, P., Kumar, R. M. R., Husmann, K., Born, W., Baudis, M., & Fuchs, B. (2015). Genomic instability of osteosarcoma cell lines in culture: Impact on the prediction of metastasis relevant genes. *PLoS ONE*, *10*(5), e0125611. https://doi.org/10.1371/journal.pone.0125611

Mundi, R., Petis, S., Kaloty, R., Shetty, V., & Bhandari, M. (2009). Low-intensity pulsed ultrasound: Fracture healing. *Indian Journal of Orthopaedics*, *43*(2), 132–140. https://doi.org/10.4103/0019-5413.50847

Muz, B., de la Puente, P., Azab, F., & Azab, A. K. (2015). The role of hypoxia in cancer progression, angiogenesis, metastasis, and resistance to therapy. *Hypoxia (Auckland, N.Z.)*, *3*, 83–92. https://doi.org/10.2147/HP.S93413

Myeroff, C., & Archdeacon, M. (2011). Autogenous Bone Graft: Donor Sites and Techniques. *the journal of bone and joint surgery*, *93*(23), 2227-2236. https://journals.lww.com/jbjsjournal/Fulltext/2011/12070/Autogenous_Bone_Graft__Donor_Sites_and_Techniques.12.aspx

Nadler, S. F., Weingand, K., & Kruse, R. J. (2004). The physiologic basis and clinical applications of cryotherapy and thermotherapy for the pain practitioner. *Pain Physician*, *7*(3), 395-399. https://doi.org/10.36076/ppj.2004/7/395

Nasello, G., Alamán-Díez, P., Schiavi, J., Pérez, M. Á., McNamara, L., & García-Aznar, J. M. (2020). Primary Human Osteoblasts Cultured in a 3D Microenvironment Create a Unique Representative Model of Their Differentiation Into Osteocytes. *Frontiers in Bioengineering and Biotechnology*, *8*, 336. https://doi.org/10.3389/fbioe.2020.00336

Nelson, F. R. T., Brighton, C. T., Ryaby, J., Simon, B. J., Nielson, J. H., Lorich, D. G., Bolander, M., & Seelig, J. (2003). Use of physical forces in bone healing. *The Journal of the American Academy of Orthopaedic Surgeons*, *11*(5), 344-354. https://doi.org/10.5435/00124635-200309000-00007

Nguyen, T. T., Quan, X., Hwang, K. H., Xu, S., Das, R., Choi, S. K., Wiederkehr, A., Wollheim, C. B., Cha, S. K., & Park, K. S. (2015). Mitochondrial oxidative stress mediates high-phosphate-induced secretory defects and apoptosis in insulin-secreting cells. *American Journal of Physiology - Endocrinology and Metabolism*, *308*(11), 933–941. https://doi.org/10.1152/ajpendo.00009.2015

Nolte, P. A., Klein-Nulend, J., Albers, G. H. R., Marti, R. K., Semeins, C. M., Goei, S. W., & Burger, E. H. (2001). Low-intensity ultrasound stimulates endochondral ossification in vitro. *Journal of Orthopaedic Research*, *19*(2), 301–307. https://doi.org/10.1016/S0736-0266(00)00027-9

Nørgaard, R., Kassem, M., & Rattan, S. I. (2006). Heat shock-induced enhancement of osteoblastic differentiation of hTERT-immortalized mesenchymal stem cells. *Annals of the New York Academy of Sciences*, *1067*, 443–447.

Nussbaum, E. L. (1997). Ultrasound: to heat or not to heat—that is the question. *Physical Therapy Reviews*, *2*(2), 59-72. https://doi.org/10.1179/ptr.1997.2.2.59

Nykanen, M. (1995). Pulsed ultrasound treatment of the painful shoulder a randomized, double-blind, placebo-controlled study. *Scandinavian Journal of Rehabilitation Medicine*, *27*(2), 105-108.

Ogawa, R. (2016). Mechanobiology and Mechanotherapy in Tissue Engineering. In S. J. Lee, J. J. Yoo, & A. Atala (Eds.), *In Situ Tissue Regeneration* (pp. 165-181). Academic Press. https://doi.org/https://doi.org/10.1016/B978-0-12-802225-2.00009-X

Ogura, Y., Parsons, W. H., Kamat, S. S., & Cravatt, B. F. (2017). Lizard Tail Regeneration As An Instructive Model of Enhanced Healing Capabilities In An Adult Amniote. *Physiology & behavior*, *176*(10), 139-148. https://doi.org/10.1080/03008207.2016.1215444.Lizard

Olson, S., Clinton, J. M., Working, Z., Lynch, J. R., Warme, W. J., Womack, W., & Matsen, F. A. (2011). Thermal effects of glenoid reaming during shoulder arthroplasty in vivo. *The Journal of bone and joint surgery. American volume*, *93*, 11-19.

Ongena, K., Das, C., Smith, J. L., Gil, S., & Johnston, G. (2010). Determining cell number during cell culture using the scepter cell counter. *Journal of Visualized Experiments*(45), 2204. https://doi.org/10.3791/2204

Orimo, H., & Shimada, T. (2006). Effects of phosphates on the expression of tissue-nonspecific alkaline phosphatase gene and phosphate-regulating genes in short-term cultures of human osteosarcoma cell lines. *Molecular and Cellular Biochemistry*, *282*(1-2), 101-108. https://doi.org/10.1007/s11010-006-1520-6

Ouriel, K., Welch, E. L., Shortell, C. K., Geary, K., Fiore, W. M., & Cimino, C. (1995). Comparison of streptokinase, urokinase, and recombinant tissue plasminogen activator

in an in vitro model of venous thrombolysis. *Journal of Vascular Surgery*, *22*(5), 593-597. https://doi.org/10.1016/S0741-5214(95)70045-5

Owen, M. (1988). Marrow stromal stem cells. *Journal of cell science*, *10*(1), 63-76.

Ozer, H. L., Banga, S. S., Dasgupta, T., Houghton, J., Hubbard, K., Jha, K. K., Kim, S. H., Lenahan, M., Pang, Z., Pardinas, J. R., & Patsalis, P. C. (1996). SV40-mediated immortalization of human fibroblasts. *Experimental Gerontology*, *31*(1-2), 303-310. https://doi.org/10.1016/0531-5565(95)00024-0

Padilla, F., Puts, R., Vico, L., & Raum, K. (2014). Stimulation of bone repair with ultrasound: A review of the possible mechanic effects. *Ultrasonics*, *54*(5), 1125-1145. https://doi.org/10.1016/j.ultras.2014.01.004

Palanisamy, P., Alam, M., Li, S., Chow, S. K. H., & Zheng, Y. P. (2022). Low-Intensity Pulsed Ultrasound Stimulation for Bone Fractures Healing: A Review. *Journal of Ultrasound in Medicine*, *41*(3), 547-563. https://doi.org/10.1002/jum.15738

Palazzo, E., Fu, Y., Ji, G., Maione, S., & Neugebauer, V. (2008). Group III mGluR7 and mGluR8 in the amygdala differentially modulate nocifensive and affective pain behaviors. *Neuropharmacology*, *55*(4), 537-545. https://doi.org/10.1016/j.neuropharm.2008.05.007

Parithimarkalaignan, S., & Padmanabhan, T. V. (2013). Osseointegration: An update. *Journal of Indian Prosthodontist Society*, *13*(1), 2-6. https://doi.org/10.1007/s13191-013-0252-z

Parmar, D., Mann, M., Walmsley, A. D., & Lea, S. C. (2011). Cutting characteristics of ultrasonic surgical instruments. *Clinical Oral Implants Research*, *22*, 1385–1390.

Patel, U. S., Ghorayeb, S. R., Yamashita, Y., Atanda, F., Walmsley, A. D., & Scheven, B. A. (2015). Ultrasound field characterization and bioeffects in multiwell culture plates. *Journal of Therapeutic Ultrasound*, *3*(1). https://doi.org/10.1186/s40349-015-0028-5

Patey, S. J., & Corcoran, J. P. (2021). Physics of ultrasound. *Anaesthesia and Intensive Care Medicine*, *22*(1), 58-63. https://doi.org/10.1016/j.mpaic.2020.11.012

Pautke, C., Schieker, M., Tischer, T., Kolk, A., Neth, P., Mutschler, W., & Milz, S. (2004). Characterization of osteosarcoma cell lines MG-63, Saos-2 and U-2 OS in comparison to human osteoblasts. *Anticancer Research*, *24*(6), 3743-3748.

Pavel, M., Renna, M., Park, S. J., Menzies, F. M., Ricketts, T., Füllgrabe, J., Ashkenazi, A., Frake, R. A., Lombarte, A. C., Bento, C. F., Franze, K., & Rubinsztein, D. C. (2018). Contact inhibition controls cell survival and proliferation via YAP/TAZ-autophagy axis. *Nature Communications*, *9*(1), 2961. https://doi.org/10.1038/s41467-018-05388-x

Perin, M., Chinigò, G., Genova, T. A.-O., Mussano, F. A.-O., & Munaron, L. A.-O. (2023). The Impact of Plasma Membrane Ion Channels on Bone Remodeling in Response to Mechanical Stress, Oxidative Imbalance, and Acidosis. *Antioxidants & Redox Signaling*, *12*(3), 689. https://doi.org/10.3390/antiox12030689

Petrini, M., Pierfelice, T. V., D'amico, E., Di Pietro, N., Pandolfi, A., D'arcangelo, C., Angelis, F. D., Mandatori, D., Schiavone, V., Piattelli, A., & Iezzi, G. (2021). Influence of nano, micro and macro topography of dental implant surfaces on human gingival fibroblasts. *International Journal of Molecular Sciences*, *22*(18), 9871. https://doi.org/10.3390/ijms22189871

Pettersson, L. F., Kingham, P. J., Wiberg, M., & Kelk, P. (2017). In Vitro Osteogenic Differentiation of Human Mesenchymal Stem Cells from Jawbone Compared with Dental Tissue. *Tissue Engineering and Regenerative Medicine*, *14*(6), 763-774. https://doi.org/10.1007/s13770-017-0071-0

Pfaffl, M. W., A., T., C., P., & Neuvians, T. P. (2004). Determination of stable housekeeping genes, differentially regulated target genes and sample integrity: BestKeeper--Excel-based tool using pair-wise correlations. *26*, *6*, 509–515.

Phelan, M. C., & Lawler, G. (1997). Cell Counting. *Current Protocols in Cytometry*, *3*. https://doi.org/10.1002/0471142956.cya03as00

Pilla, A. A., Mont, M. A., Nasser, P. R., Khan, S. A., Figueiredo, M., Kaufman, J. J., & Siffert, R. S. (1990). Non-invasive low-intensity pulsed ultrasound accelerates bone healing in the rabbit. *Journal of Orthopaedic Trauma*, *4*(3), 246-253. https://doi.org/10.1097/00005131-199004030-00002

Pisciotta, A., Riccio, M., Carnevale, G., Beretti, F., Gibellini, L., Maraldi, T., Cavallini, G. M., Ferrari, A., Bruzzesi, G., & de Pol, A. (2012). Human Serum Promotes Osteogenic Differentiation of Human Dental Pulp Stem Cells In Vitro and In Vivo. *PLoS ONE*, *7*(11), e50542. https://doi.org/10.1371/journal.pone.0050542

Plecko, M., Sievert, C., Andermatt, D., Frigg, R., Kronen, P., Klein, K., Stübinger, S., Nuss, K., Bürki, A., Ferguson, S., Stoeckle, U., & Rechenberg, B. (2012). Osseointegration and biocompatibility of different metal implants--a comparative experimental investigation in sheep. *BMC musculoskeletal disorders*, *13*, 32.

Polat, B. E., Hart, D., Langer, R., & Blankschtein, D. (2011). Ultrasound-mediated transdermal drug delivery: Mechanisms, scope, and emerging trends. *Journal of Controlled Release*, *152*(3), 330-348. https://doi.org/10.1016/j.jconrel.2011.01.006

Pollock, N. K., Bernard, P. J., Gutin, B., Davis, C. L., Zhu, H., & Dong, Y. (2011). Adolescent obesity, bone mass, and cardiometabolic risk factors. *Journal of Pediatrics*, *158*(5), 727–734. https://doi.org/10.1016/j.jpeds.2010.11.052

Pomini, K. T., Andreo, J. C., De Rodrigues, A. C., De Gonçalves, J. B. O., Daré, L. R., German, I. J. S., Rosa, G. M., & Buchaim, R. L. (2014). Effect of low-intensity pulsed ultrasound on bone regeneration biochemical and radiologic analyses. *Journal of Ultrasound in Medicine*, *33*(4), 713–717. https://doi.org/10.7863/ultra.33.4.713

Ponzetti, M., & Rucci, N. (2021). Osteoblast differentiation and signaling: Established concepts and emerging topics. *International Journal of Molecular Sciences*, *22*(13), 6651. https://doi.org/10.3390/ijms22136651

Poolman, R. W., Agoritsas, T., Siemieniuk, R. A. C., Harris, I. A., Schipper, I. B., Mollon, B., Smith, M., Albin, A., Nador, S., Sasges, W., Schandelmaier, S., Lytvyn, L., Kuijpers, T., Van Beers, L. W. A. H., Verhofstad, M. H. J., & Vandvik, P. O. (2017). Low intensity pulsed ultrasound (LIPUS) for bone healing: A clinical practice guideline. *BMJ (Online)*, *356*. https://doi.org/10.1136/bmj.j576

Poundarik, A. A., Boskey, A., Gundberg, C., & Vashishth, D. (2018). Biomolecular regulation, composition and nanoarchitecture of bone mineral. *Scientific Reports*, *8*(1), 1191. https://doi.org/10.1038/s41598-018-19253-w

Pourgiv, S., Mosavar, A., Jamshidi, N., & Mohammadi, A. (2024). Ultrasonic-assisted drilling of cortical and cancellous bone in a comparative point of view. *Heliyon*, *10*(2405-8440 (Print)), e26248.

Pramojanee, S. N., Phimphilai, M., Chattipakorn, N., & Chattipakorn, S. C. (2014). Possible roles of insulin signaling in osteoblasts. *Endocrine Research*, *39*(4), 144–151. https://doi.org/10.3109/07435800.2013.879168

Pretorius, J., Mohamed, Y., Mustafa, A., Nemat, N., Ellanti, P., Hammad, Y., Shaju, T., & Nadeem, S. (2022). A Retrospective Study: Is Low-Intensity Pulsed Ultrasound (LIPUS) an Effective Alternate Treatment Option for Non-union? *Cureus*, *14*(9), e29230. https://doi.org/10.7759/cureus.29230

Prideaux, M., Wijenayaka, A. R., Kumarasinghe, D. D., Ormsby, R. T., Evdokiou, A., Findlay, D. M., & Atkins, G. J. (2014). SaOS2 osteosarcoma cells as an in vitro model for studying the transition of human osteoblasts to osteocytes. *Calcified Tissue International*, *95*(2), 183–193. https://doi.org/10.1007/s00223-014-9879-y

Qin, Y. X., & Hu, M. (2014). Mechanotransduction in musculoskeletal tissue regeneration: Effects of fluid flow, loading, and cellular-molecular pathways. *BioMed research international*, *2014*, 863421. https://doi.org/10.1155/2014/863421

Quarato, C. M. I., Lacedonia, D., Salvemini, M., Tuccari, G., Mastrodonato, G., Villani, R., Fiore, L. A., Scioscia, G., Mirijello, A., Saponara, A., & Sperandeo, M. (2023). A Review on Biological Effects of Ultrasounds: Key Messages for Clinicians. *Diagnostics (Basel, Switzerland)*, *13*(2075-4418 (Print)), 855.

Rabe, M., Verdes, D., & Seeger, S. (2011). Understanding protein adsorption phenomena at solid surfaces. *Advances in Colloid and Interface Science*, *162*(1), 87-106. https://doi.org/10.1016/j.cis.2010.12.007

Raggatt, L. J., Wullschleger, M. E., Alexander, K. A., Wu, A. C. K., Millard, S. M., Kaur, S., Maugham, M. L., Gregory, L. S., Steck, R., & Pettit, A. R. (2014). Fracture healing via periosteal callus formation requires macrophages for both initiation and progression of early endochondral ossification. *American Journal of Pathology*, *184*(12), 3192–3204. https://doi.org/10.1016/j.ajpath.2014.08.017

Ramaglia, L., Postiglione, L., Spigna, G., Capece, G., Salzano, S., & Rossi, G. (2011). Sandblasted-acid-etched titanium surface influences in vitro the biological behavior of SaOS-2 human osteoblast-like cells. *Dental materials journal*, *30*, 183-192. https://doi.org/10.4012/dmj.2010-107

Rathod, V. T. (2019). A Review of Electric Impedance Matching Techniques for Piezoelectric Sensors, Actuators and Transducers. *Electronics*, *20*(14), 4051. https://doi.org/10.3390/electronics8020169

Ray, P. D., Huang, B. W., & Tsuji, Y. (2012). Reactive oxygen species (ROS) homeostasis and redox regulation in cellular signaling. *Cellular Signalling*, *24*(5), 981–990. https://doi.org/10.1016/j.cellsig.2012.01.008

Reher, P., Harris, M., Whiteman, M., Hai, H. K., & Meghji, S. (2002). Ultrasound stimulates nitric oxide and prostaglandin E2 production by human osteoblasts. *Bone*, *31*(1), 236–241. https://doi.org/10.1016/S8756-3282(02)00789-5

Reich, K. M., Gay, C. V., & Frangos, J. A. (1990). Fluid shear stress as a mediator of osteoblast cyclic adenosine monophosphate production. *Journal of Cellular Physiology*, *143*(1), 100–104. https://doi.org/10.1002/jcp.1041430113

Reichard, A., & Asosingh, K. (2019). Best Practices for Preparing a Single Cell Suspension from Solid Tissues for Flow Cytometry. *Cytometry. Part A : the journal of the International Society for Analytical Cytology*, *95*(2), 219–226. https://doi.org/10.1002/cyto.a.23690

Reissis, Y., García-Gareta, E., Korda, M., Blunn, G. W., & Hua, J. (2013). The effect of temperature on the viability of human mesenchymal stem cells. *Stem Cell Research and Therapy*, *4*(6), 139. https://doi.org/10.1186/scrt350

Riesz, P., & Kondo, T. (1992). Free radical formation induced by ultrasound and its biological implications. *Free Radical Biology and Medicine*, *13*(3), 247–270. https://doi.org/10.1016/0891-5849(92)90021-8

Riss, T., Moravec, R., & Niles, A. (2013). Cell Viability Assays. In S. Markossian, A. Grossman, & K. Brimacombe (Eds.), *Assay Guidance Manual*. Eli Lilly & Company

and the National Center for Advancing Translational Sciences. https://www.ncbi.nlm.nih.gov/books/NBK144065/

Robert, A. W., Marcon, B. H., Dallagiovanna, B., & Shigunov, P. (2020). Adipogenesis, Osteogenesis, and Chondrogenesis of Human Mesenchymal Stem/Stromal Cells: A Comparative Transcriptome Approach. *Frontiers in cell and developmental biology*, *8*, 561. https://doi.org/10.3389/fcell.2020.00561

Robey, P. G., Boskey, A. L., & Leikin, S. (2020). The regulatory role of matrix proteins in mineralization of bone. In *Marcus and Feldman's Osteoporosis* (Vol. 1, pp. 165-187). Elsevier Inc. https://doi.org/10.1016/B978-0-12-813073-5.00008-3

Rodan, S. B., Imai, Y., Thiede, M. A., Wesolowski, G., Thompson, D., Bar-Shavit, Z., Shull, S., Mann, K., & Rodan, G. A. (1987). Characterization of a Human Osteosarcoma Cell Line (Saos-2) with Osteoblastic Properties. *Cancer Research*, *47*(18).

Rosales-Leal, J. I., Rodríguez-Valverde, M. A., Mazzaglia, G., Ramón-Torregrosa, P. J., Díaz-Rodríguez, L., García-Martínez, O., Vallecillo-Capilla, M., Ruiz, C., & Cabrerizo-Vílchez, M. A. (2010). Effect of roughness, wettability and morphology of engineered titanium surfaces on osteoblast-like cell adhesion. *Colloids and Surfaces A: Physicochemical and Engineering Aspects*, *365*(1), 222-229. https://doi.org/https://doi.org/10.1016/j.colsurfa.2009.12.017

Rosenberg, N., Rosenberg, O., & Soudry, M. (2012). Osteoblasts in Bone Physiology – Mini Review. *Rambam Maimonides Medical Journal*, *3*(2), e0013. https://doi.org/10.5041/rmmj.10080

Rubin, C., Bolander, M., Ryaby, J. P., & Hadjiargyrou, M. (2001). The use of low-intensity ultrasound to accelerate the healing of fractures. *Journal of Bone and Joint Surgery*, *83*(2), 259–270. https://doi.org/10.2106/00004623-200102000-00015

Rubin, C., Turner, A. S., Mallinckrodt, C., Jerome, C., McLeod, K., & Bain, S. (2002). Mechanical strain, induced noninvasively in the high-frequency domain, is anabolic to cancellous bone, but not cortical bone. *Bone*, *30*(3), 445–452. https://doi.org/10.1016/S8756-3282(01)00689-5

Rubin, C. T., & Lanyon, L. E. (1984). Regulation of bone formation by applied dynamic loads. *Journal of Bone and Joint Surgery - Series A*, *66*(3), 397-402. https://doi.org/10.2106/00004623-198466030-00012

Rue, J. P. H., Armstrong, D. W., Frassica, F. J., Deafenbaugh, M., & Wilckens, J. H. (2004). The effect of pulsed ultrasound in the treatment of tibial stress fractures. *Orthopedics*, *27*(11), 1192–1195. https://doi.org/10.3928/0147-7447-20041101-18

Rupp, M., Biehl, C., Budak, M., Thormann, U., Heiss, C., & Alt, V. (2018). Diaphyseal long bone nonunions — types, aetiology, economics, and treatment recommendations. *International Orthopaedics*, *42*(2), 247–258. https://doi.org/10.1007/s00264-017-3734-5

Ruppert, D. S., Harrysson, O. L. A., Marcellin-Little, D. J., Bollenbecker, S., & Weinhold, P. S. (2019). Osteogenic benefits of low-intensity pulsed ultrasound and vibration in a rodent osseointegration model. *Journal of Musculoskeletal Neuronal Interactions*, *19*(2), 150-158.

Saigusa, Y. (2010). Quartz-based piezoelectric materials. In K. Uchino (Ed.), *Advanced Piezoelectric Materials* (pp. 171-203). Woodhead Publishing. https://doi.org/https://doi.org/10.1533/9781845699758.1.171

Saldaña, L., Bensiamar, F., Boré, A., & Vilaboa, N. (2011). In search of representative models of human bone-forming cells for cytocompatibility studies. *Acta Biomaterialia*, *7*(12), 4210–4221. https://doi.org/10.1016/j.actbio.2011.07.019

Salzig, D., Schmiermund, A., P, P. G., Elseberg, C., Weber, C., & Czermak, P. (2013). Enzymatic detachment of therapeutic mesenchymal stromal cells grown on glass carriers in a bioreactor. *The open biomedical engineering journal*, *7*, 147–158. https://doi.org/10.2174/1874120701307010147

Sant'Anna, E. F., Leven, R. M., Virdi, A. S., & Sumner, D. R. (2005). Effect of low intensity pulsed ultrasound and BMP-2 on rat bone marrow stromal cell gene expression. *Journal of Orthopaedic Research*, *23*(3), 646-652. https://doi.org/10.1016/j.orthres.2004.09.007

Savva, J., Lucas, M., & Mulvana, H. (2019, 6-9 Oct. 2019). A controlled in vitro study of optimal low intensity pulsed ultrasound fields for stimulation of proliferation in murine osteoblasts. 2019 IEEE International Ultrasonics Symposium (IUS), Glasgow.

Sawai, Y., Murata, H., Koto, K., Matsui, T., Horie, N., Ashihara, E., Maekawa, T., Fushiki, S., & Kubo, T. (2012). Effects of low-intensity pulsed ultrasound on osteosarcoma and cancer cells. *Oncology Reports*, *28*(2), 481–486. https://doi.org/10.3892/or.2012.1816

Schabrun, S., Walker, H., & Chipchase, L. (2008). How Accurate are Therapeutic Ultrasound Machines? *Hong Kong Physiotherapy Journal*, *26*(1), 39-44. https://doi.org/https://doi.org/10.1016/S1013-7025(09)70006-5

Schandelmaier, S., Kaushal, A., Lytvyn, L., Heels-Ansdell, D., Siemieniuk, R. A. C., Agoritsas, T., Guyatt, G. H., Vandvik, P. O., Couban, R., Mollon, B., & Busse, J. W. (2017). Low intensity pulsed ultrasound for bone healing: systematic review of randomized controlled trials. *BMJ (Clinical research ed.)*, *356*, j656. https://doi.org/10.1136/bmj.j656

Scheven, B. A. A., Shelton, R. M., Cooper, P. R., Walmsley, A. D., & Smith, A. J. (2009). Therapeutic ultrasound for dental tissue repair. *Medical Hypotheses*, *73*(4), 591-593. https://doi.org/10.1016/j.mehy.2009.05.032

Schiller, I., Huat Lu, Z., Vaughan, L., Weilenmann, R., Koundrioukoff, S., & Pospischil, A. (2003). Establishment of proliferative cell nuclear antigen gene as an internal reference gene for polymerase chain reaction of a wide range of archival and fresh mammalian tissues. *Journal of Veterinary Diagnostic Investigation*, *15*(6), 585–588. https://doi.org/10.1177/104063870301500614

Schulte, P. M. (2015). The effects of temperature on aerobic metabolism: Towards a mechanistic understanding of the responses of ectotherms to a changing environment. *Journal of Experimental Biology*, *218*(12), 1856–1866. https://doi.org/10.1242/jeb.118851

Secomski, W., Bilmin, K., Kujawska, T., Nowicki, A., Grieb, P., & Lewin, P. A. (2017). In vitro ultrasound experiments: Standing wave and multiple reflections influence on the outcome. *Ultrasonics*, *77*. https://doi.org/10.1016/j.ultras.2017.02.008

Seghir, R., & Pierron, F. (2018). A Novel Image-based Ultrasonic Test to Map Material Mechanical Properties at High Strain-rates. *Experimental Mechanics*, *58*(2), 183-206. https://doi.org/10.1007/s11340-017-0329-4

Shapira, L., & Halabi, A. (2009). Behavior of two osteoblast-like cell lines cultured on machined or rough titanium surfaces. *Clinical Oral Implants Research*, *20*(1), 50–55. https://doi.org/10.1111/j.1600-0501.2008.01594.x

Sheen, J. R., & Garla, V. V. (2019). Fracture Healing Overview. In *StatPearls*.

Shi, H., Chen, Z., Chen, X., Liu, S., & Cao, W. (2021). Self-heating phenomenon of piezoelectric elements excited by a tone-burst electric field. *Ultrasonics*, *117*, 106562. https://doi.org/https://doi.org/10.1016/j.ultras.2021.106562

Shi, L., Shi, L., Wang, L., Duan, Y., Lei, W., Wang, Z., Li, J., Fan, X., Li, X., Li, S., & Guo, Z. (2013). The Improved Biological Performance of a Novel Low Elastic Modulus Implant. *PLoS ONE*, *8*(2), e55015. https://doi.org/10.1371/journal.pone.0055015

Shui, C., & Scutt, A. (2009). Mild Heat Shock Induces Proliferation, Alkaline Phosphatase Activity, and Mineralization in Human Bone Marrow Stromal Cells and Mg-63 Cells In Vitro. *Journal of Bone and Mineral Research*, *16*(4), 731-741. https://doi.org/10.1359/jbmr.2001.16.4.731

Sidambe, A. T. (2014). Biocompatibility of advanced manufactured titanium implants-A review. In *Materials* (Vol. 7).

Sikavitsas, V. I., Bancroft, G. N., Van Den Dolder, J., Sheffield, T. L., Jansen, J. A., Ambrose, C. G., & Mikos, A. G. (2002). Fluid flow increases mineralized matrix deposition in three-dimensional perfusion culture of marrow stromal osteoblasts in a dose-dependent manner. Annual International Conference of the IEEE Engineering in Medicine and Biology - Proceedings,

Singh, S., & Goyal, A. (2007). The origin of echocardiography: a tribute to Inge Edler. *Texas Heart Institute journal / from the Texas Heart Institute of St. Luke's Episcopal Hospital, Texas Children's Hospital*, *34*(4), 431-438.

Snehota, M., Vachutka, J., ter Haar, G., Dolezal, L., & Kolarova, H. (2020). Therapeutic ultrasound experiments in vitro: Review of factors influencing outcomes and reproducibility. *Ultrasonics*, *107*, 106167. https://doi.org/10.1016/j.ultras.2020.106167

Snow, C. J. (1982). Ultrasound therapy units in Manitoba and Northwestern Ontario: performance evaluation. *Physiotherapy Canada*, *34*(0300-0508 (Print)), 185–189.

Soice, E., & Johnston, J. (2021). Immortalizing cells for human consumption. *International Journal of Molecular Sciences*, *22*(21), 11660. https://doi.org/10.3390/ijms222111660

Song, L., & Tuan, R. S. (2004). Transdifferentiation potential of human mesenchymal stem cells derived from bone marrow. *FASEB journal: official publication of the Federation of American Societies for Experimental Biology*, *18*(1530-6860), 980–982.

Sordi, M. B., Curtarelli, R. B., da Silva, I. T., Fongaro, G., Benfatti, C. A. M., de Souza Magini, R., & Cabral da Cruz, A. C. (2021). Effect of dexamethasone as osteogenic supplementation in in vitro osteogenic differentiation of stem cells from human exfoliated deciduous teeth. *Journal of Materials Science: Materials in Medicine*, *32*(1), 1. https://doi.org/10.1007/s10856-020-06475-6

Speed, C. A. (2001). Therapeutic ultrasound in soft tissue lesions. *Revmatologiia*, *40*(12), 1331-1336. https://doi.org/10.1093/rheumatology/40.12.1331

Spiegelberg, B., Parratt, T., Dheerendra, S. K., Khan, W. S., Jennings, R., & Marsh, D. R. (2010). Ilizarov principles of deformity correction. *Annals of the Royal College of Surgeons of England*, *92*(2). https://doi.org/10.1308/003588410X12518836439326

Stavnichuk, M., Mikolajewicz, N., Corlett, T., Morris, M., & Komarova, S. V. (2020). A systematic review and meta-analysis of bone loss in space travelers. *npj Microgravity*, *6*(1). https://doi.org/10.1038/s41526-020-0103-2

Steele, S. L., Wu, Y., Kolb, R. J., Gooz, M., Haycraft, C. J., Keyser, K. T., Guay-Woodford, L., Yao, H., & Bell, P. D. (2010). Telomerase immortalization of principal cells from mouse collecting duct. *American Journal of Physiology - Renal Physiology*, *299*(6), 1507–1514. https://doi.org/10.1152/ajprenal.00183.2010

Steppe, L., Liedert, A., Ignatius, A., & Haffner-Luntzer, M. (2020). Influence of Low-Magnitude High-Frequency Vibration on Bone Cells and Bone Regeneration. *Frontiers in Bioengineering and Biotechnology*, *8*, 595139. https://doi.org/10.3389/fbioe.2020.595139

Stewart, S., Darwood, A., Masouros, S., Higgins, C., & Ramasamy, A. (2020). Mechanotransduction in osteogenesis. *Bone & Joint Research*, *9*(1), 1-14. https://doi.org/doi:10.1302/2046-3758.91.BJR-2019-0043.R2

Stremnitzer, C., Manzano-Szalai, K., Willensdorfer, A., Starkl, P., Pieper, M., König, P., Mildner, M., Tschachler, E., Reichart, U., & Jensen-Jarolim, E. (2015). Papain Degrades Tight Junction Proteins of Human Keratinocytes In Vitro and Sensitizes C57BL/6 Mice via the Skin Independent of its Enzymatic Activity or TLR4 Activation. *The Journal of investigative dermatology*, *135*(7), 1790–1800. https://doi.org/10.1038/jid.2015.58

Sun, J. S., Hong, R. C., Chang, W. H. S., Chen, L. T., Lin, F. H., & Liu, H. C. (2001). In vitro effects of low-intensity ultrasound stimulation on the bone cells. *Journal of Biomedical Materials Research*, *57*(3), 449-456. https://doi.org/10.1002/1097-4636(20011205)57:3<449::aid-jbm1188>3.0.co;2-0

Sun, W., Chi, S., Li, Y., Ling, S., Tan, Y., Xu, Y., Jiang, F., Li, J., Liu, C., Zhong, G., Cao, D., Jin, X., Zhao, D., Gao, X., Liu, Z., Xiao, B., & Li, Y. A.-O. (2019). The mechanosensitive Piezo1 channel is required for bone formation. *eLife*, *8*, 47454. https://doi.org/10.7554/eLife.47454

Sun, X., & Kaufman, P. D. (2018). Ki-67: more than a proliferation marker. *Chromosoma*, *127*(2), 175–186. https://doi.org/10.1007/s00412-018-0659-8

Tabassum, A. (2022). Effect of dexamethasone on the growth and differentiation of osteoblast-like cells derived from the human alveolar bone. *Journal of Taibah University Medical Sciences*, *17*(4), 707-714. https://doi.org/10.1016/j.jtumed.2021.12.008

Tachibana, K., & Tachibana, S. (1997). Prototype therapeutic ultrasound emitting catheter for accelerating thrombolysis. *Journal of Ultrasound in Medicine*, *16*(8), 529-535. https://doi.org/10.7863/jum.1997.16.8.529

Takayama, T., Suzuki, N., Ikeda, K., Shimada, T., Suzuki, A., Maeno, M., Otsuka, K., & Ito, K. (2007). Low-intensity pulsed ultrasound stimulates osteogenic differentiation in ROS 17/2.8 cells. *Life Sciences*, *80*(10), 965–971. https://doi.org/10.1016/j.lfs.2006.11.037

Talib, R. J., & Toff, M. R. (2004). Plasma-sprayed coating of hydroxyapatite on metal implants--a review. *The Medical journal of Malaysia*, *59*(B), 153–154.

Tang, N., Song, W. X., Luo, J., Haydon, R. C., & He, T. C. (2008). Osteosarcoma development and stem cell differentiation. *Clinical Orthopaedics and Related Research*, *466*(9), 2114–2130. https://doi.org/10.1007/s11999-008-0335-z

Tanzer, M., Harvey, E., Kay, A., Morton, P., & Bobyn, J. D. (1996). Effect of noninvasive low intensity ultrasound on bone growth into porous-coated implants. *Journal of Orthopaedic Research*, *14*(6), 901–906. https://doi.org/10.1002/jor.1100140609

Tapscott, D. C., & Wottowa, C. (2020). *Orthopedic Implant Materials*.

Teitelbaum, S. L. (2007). Osteoclasts: What do they do and how do they do it? *American Journal of Pathology*, *170*(2), 427–435. https://doi.org/10.2353/ajpath.2007.060834

Tenenbaum, H. C., & Heersche, J. N. M. (1982). Differentiation of osteoblasts and formation of mineralized bone in vitro. *Calcified Tissue International*, *34*(1), 3542-3550. https://doi.org/10.1007/BF02411212

ter Haar, G., Shaw, A., Pye, S., Ward, B., Bottomley, F., Nolan, R., & Coady, A.-M. (2011). Guidance on Reporting Ultrasound Exposure Conditions for Bio-Effects Studies. *Ultrasound in Medicine & Biology*, *37*(2), 177-183. https://doi.org/https://doi.org/10.1016/j.ultrasmedbio.2010.10.021

Tippett, V. L., Tattersall, L., Ab Latif, N. B., Shah, K. M., Lawson, M. A., & Gartland, A. (2023). The strategy and clinical relevance of in vitro models of MAP resistance in osteosarcoma: a systematic review. *Oncogene*, *42*(4), 259-277. https://doi.org/10.1038/s41388-022-02529-x

Tomšíčková, V., Frankova, J., Dolezel, P., & Ulrichova, J. (2013). The Response of Osteoblast-Like SaOS-2 Cells to Modified Titanium Surfaces. *The International Journal of Oral & Maxillofacial Implants*, *28*, 1386-1394. https://doi.org/10.11607/jomi.3039

Turner, C. H., & Pavalko, F. M. (1998). Mechanotransduction and functional response of the skeleton to physical stress: The mechanisms and mechanics of bone adaptation. *Journal of Orthopaedic Science*, *3*(6), 346–355. https://doi.org/10.1007/s007760050064

Uddin, S. M. Z., Komatsu, D. E., Motyka, T., & Petterson, S. (2021). Low-Intensity Continuous Ultrasound Therapies—A Systematic Review of Current State-of-the-Art and Future Perspectives. *Journal of Clinical Medicine*, *10*(12), 2698. https://doi.org/10.3390/jcm10122698

Uddin, S. M. Z., & Qin, Y. X. (2013). Enhancement of Osteogenic Differentiation and Proliferation in Human Mesenchymal Stem Cells by a Modified Low Intensity Ultrasound Stimulation under Simulated Microgravity. *PLoS ONE*, *8*(9), e73914. https://doi.org/10.1371/journal.pone.0073914

Uddin, S. M. Z., & Qin, Y. X. (2015). Dynamic acoustic radiation force retains bone structural and mechanical integrity in a functional disuse osteopenia model. *Bone*, *75*, 8–17. https://doi.org/10.1016/j.bone.2015.01.020

Uhthoff, H. K., & Jaworski, Z. F. G. (1978). Bone loss in response to long-term immobilisation. *Journal of Bone and Joint Surgery - Series B*, *60 B*(3), 420–429. https://doi.org/10.1302/0301-620x.60b3.681422

Uxa, S., Castillo-Binder, P., Kohler, R., Stangner, K., Müller, G. A., & Engeland, K. (2021). Ki-67 gene expression. *Cell Death & Differentiation*, *28*(12), 3357-3370. https://doi.org/10.1038/s41418-021-00823-x

Valenti, M. T., Zanatta, M., Donatelli, L., Viviano, G., Cavallini, C., Scupoli, M. T., & Carbonare, L. D. (2014). Ascorbic acid induces either differentiation or apoptosis in MG-63 osteosarcoma lineage. *Anticancer Research*, *34*(4), 1617-1627.

Vannucci, L., Fossi, C., Quattrini, S., Guasti, L., Pampaloni, B., Gronchi, G., Giusti, F., Romagnoli, C., Cianferotti, L., Marcucci, G., & Brandi, M. L. (2018). Calcium Intake in bone health: A focus on calcium-rich mineral waters. *Nutrients*, *10*(12), 1930. https://doi.org/10.3390/nu10121930

Vater, C., Kasten, P., & Stiehler, M. (2011). Culture media for the differentiation of mesenchymal stromal cells. *Acta Biomaterialia*, *7*(2), 463-477. https://doi.org/10.1016/j.actbio.2010.07.037

Vercaigne, S., Wolke Jg Fau - Naert, I., Naert I Fau - Jansen, J. A., & Jansen, J. A. (1998). Bone healing capacity of titanium plasma-sprayed and hydroxylapatite-coated oral implants. *Clinical Oral Implants Research*, *9*(4), 261–271. https://doi.org/10.1034/j.1600-0501.1998.090407.x

Vercellotti, T., De Paoli, S., & Nevins, M. (2001). The piezoelectric bony window osteotomy and sinus membrane elevation: introduction of a new technique for simplification of

the sinus augmentation procedure. *The International journal of periodontics & restorative dentistry*, *21*(6), 561–567.

Verma, A., Verma, M., & Singh, A. (2020). Animal tissue culture principles and applications. *Animal Biotechnology: Models in Discovery and Translation*, 269–293. https://doi.org/10.1016/B978-0-12-811710-1.00012-4

Villar, C. C., Huynh-Ba, G., Mills, M. P., & Cochran, D. L. (2011). Wound healing around dental implants. *Endodontic Topics*, *25*(1), 44-62. https://doi.org/10.1111/etp.12018

Volk, S. W., Shah, S. R., Cohen, A. J., Wang, Y., Brisson, B. K., Vogel, L. K., Hankenson, K. D., & Adams, S. L. (2014). Type III collagen regulates osteoblastogenesis and the quantity of trabecular bone. *Calcified Tissue International*, *94*(6), 621–631. https://doi.org/10.1007/s00223-014-9843-x

Volovitz, I., Shapira, N., Ezer, H., Gafni, A., Lustgarten, M., Alter, T., Ben-Horin, I., Barzilai, O., Shahar, T., Kanner, A., Fried, I., Veshchev, I., Grossman, R., & Ram, Z. (2016). A non-aggressive, highly efficient, enzymatic method for dissociation of human brain-tumors and brain-tissues to viable single-cells. *BMC Neuroscience*, *17*(1), 30. https://doi.org/10.1186/s12868-016-0262-y

Wang, J., Leung, K. S., Chow, S. K. H., & Cheung, W. H. (2017). The effect of whole body vibration on fracture healing – a systematic review. *European Cells and Materials*, *34*, 108–127. https://doi.org/10.22203/eCM.v034a08

Wang, L., Liu, Y., Wang, S., Li, J., Sun, Y., Wang, J., & Zou, Q. (2024). Research on ultrasonic bone cutting mechanism based on extended finite element method. *Biomechanics and modeling in mechanobiology*(1617-7940).

Wang, S. J. J., Lewallen, D. G., Bolander, M. E., Chao, E. Y. S., Ilstrup, D. M., & Greenleaf, J. F. (1994). Low intensity ultrasound treatment increases strength in a rat femoral fracture model. *Journal of Orthopaedic Research*, *12*(1), 40-47. https://doi.org/10.1002/jor.1100120106

Wang, W., & Khoon, C. (2013). Titanium Alloys in Orthopaedics. In J. Sieniawski (Ed.), *Titanium Alloys - Advances in Properties Control*. IntechOpen. https://doi.org/10.5772/55353

Warnez, M., Vlaisavljevich, E., Xu, Z., & Johnsen, E. (2017). Damage mechanisms for ultrasound-induced cavitation in tissue. *AIP Conference Proceedings*, *1821*(1), 080004. https://doi.org/10.1063/1.4977634

Watson, T. (2006). Electrotherapy and Tissue Repair Sport Ex. *School of Paramedic Sciences, Physiotherapy and Radiography University of Hertfordshire*.

Webber, M. B., Michida, S. M., Marson, F. C., de Oliveira, G. C., & Silva Cde, O. (2015). Analysis of bond strength by pull out test on fiber glass posts cemented in different lengths. *Journal of international oral health*, *7*, 7-12.

Webster, D. F., Harvey, W., Dyson, M., & Pond, J. B. (1980). The role of ultrasound-induced cavitation in the 'in vitro' stimulation of collagen synthesis in human fibroblasts. *Ultrasonics*, *18*(1), 33–37. https://doi.org/10.1016/0041-624X(80)90050-5

Wei, D., & Yixin, Y. (2014). Genomic Instability and Cancer. *Journal of Carcinogenesis & Mutagenesis*, *05*(02), 1000165. https://doi.org/10.4172/2157-2518.1000165

Wei, J., Igarashi, T., Okumori, N., Igarashi, T., Maetani, T., Liu, B., & Yoshinari, M. (2009). Influence of surface wettability on competitive protein adsorption and initial attachment of osteoblasts. *Biomedical Materials*, *4*(4), 045002. https://doi.org/10.1088/1748-6041/4/4/045002

Wellington, I. J., Hawthorne, B. C., Dorsey, C., Connors, J. P., Mazzocca, A. D., & Solovyova, O. (2022). Optimization of tissue adhesive curing time for surgical wound closure. *Bone & joint open*, *3*, 601-610.

Wells, P. N. (1977). Ultrasonics in medicine and biology. *Physics in Medicine & Biology*, *22*(4). https://doi.org/10.1088/0031-9155/22/4/001

Wilkesmann, S., Fellenberg, J., Nawaz, Q., Reible, B., Moghaddam, A., Boccaccini, A., & Westhauser, F. (2020). Primary osteoblasts, osteoblast precursor cells or osteoblast-like cell lines: Which human cell types are (most) suitable for characterizing 45S5-bioactive glass? *Journal of biomedical materials research. Part A*, *108*, 663–674. https://doi.org/10.1002/jbm.a.36846

Williams, A. R., & Miller, D. L. (1989). The role of non-acoustic factors in the induction and proliferation of cavitational activity in vitro (cell suspensions). *Physics in Medicine and Biology*, *34*(11), 1561. https://doi.org/10.1088/0031-9155/34/11/005

Wolff, J. (1892). Das Gesetz der Transformation der Knochen. *Deutsche Medizinische Wochenschrift*, *19*(47), 1222-1224.

Wu, Y., Zitelli, J. P., TenHuisen, K. S., Yu, X., & Libera, M. R. (2011). Differential response of Staphylococci and osteoblasts to varying titanium surface roughness. *Biomaterials*, *32*(4), 951-960. https://doi.org/10.1016/j.biomaterials.2010.10.001

Xiao, L., Zhou, Y. j., Jiang, Y. b., Tam, M. S., Cheang, L. H., Wang, H. j., Zha, Z. g., & Zheng, X. f. (2022). Effect of Diabetes Mellitus on Implant Osseointegration of Titanium Screws: An Animal Experimental Study. *Orthopaedic Surgery*, *14*(6), 1217–1228. https://doi.org/10.1111/os.13274

Xin, Z., Lin, G., Lei, H., Lue, T. F., & Guo, Y. (2016). Clinical applications of low-intensity pulsed ultrasound and its potential role in urology. *Translational Andrology and Urology*, *5*(2), 255–266. https://doi.org/10.21037/tau.2016.02.04

Xu, L. C., & Siedlecki, C. A. (2007). Effects of surface wettability and contact time on protein adhesion to biomaterial surfaces. *Biomaterials*, *28*(22), 3273–3283. https://doi.org/10.1016/j.biomaterials.2007.03.032

Xu, X., Liu, S., Liu, H., Ru, K., Jia, Y., Wu, Z., Liang, S., Khan, Z., Chen, Z., Qian, A., & Hu, L. (2021). Piezo Channels: Awesome Mechanosensitive Structures in Cellular Mechanotransduction and Their Role in Bone. *International Journal of Molecular Sciences*, *22*(12), 6429.

Yadav, Y. K., Salgotra, K. R., & Banerjee, A. (2008). Role of ultrasound therapy in the healing of tibial stress fractures. *Medical Journal Armed Forces India*, *64*(3), 234–236. https://doi.org/10.1016/S0377-1237(08)80101-3

Yang, D., Wijenayaka, A. R., & Atkins, G. J. (2018). A Fluorometric Method for the Quantification of Cell Number in Complex Differentiating Osteoblast-Osteocyte Cultures. LID - 14. *Methods Protoc.*, *1*(2), 14. https://doi.org/10.3390/mps1020014

Yang, L., Tsang, K. Y., Tang, H. C., Chan, D., & Cheah, K. S. E. (2014). Hypertrophic chondrocytes can become osteoblasts and osteocytes in endochondral bone formation. *Proceedings of the National Academy of Sciences of the United States of America*, *111*(33), 12097–12102. https://doi.org/10.1073/pnas.1302703111

Yang, R. S., Lin, W. L., Chen, Y. Z., Tang, C. H., Huang, T. H., Lu, B. Y., & Fu, W. M. (2005). Regulation by ultrasound treatment on the integrin expression and differentiation of osteoblasts. *Bone*, *36*(2), 276–283. https://doi.org/10.1016/j.bone.2004.10.009

Yavropoulou, M. P., & Yovos, J. G. (2016). The molecular basis of bone mechanotransduction. *Journal of Musculoskeletal Neuronal Interactions*, *16*(3), 221–236.

Yevlashevskaya, O. S., Scheven, B. A., Walmsley, A. D., & Shelton, R. M. (2023). Differing responses of osteogenic cell lines to β-glycerophosphate. *Scientific Reports*, *13*, 14472. https://doi.org/10.1038/s41598-023-40835-w

Yourek, G., McCormick, S. M., Mao, J. J., & Reilly, G. C. (2010). Shear stress induces osteogenic differentiation of human mesenchymal stem cells. *Regenerative Medicine*, *5*(5), 713–724. https://doi.org/10.2217/rme.10.60

Yu, H., de Vos, P., & Ren, Y. (2011). Overexpression of osteoprotegerin promotes preosteoblast differentiation to mature osteoblasts. *The Angle orthodontist*, *81*(1), 100–106. https://doi.org/10.2319/050210-238.1

Yu, Y. Y., Lieu, S., Lu, C., Miclau, T., Marcucio, R. S., & Colnot, C. (2010). Immunolocalization of BMPs, BMP antagonists, receptors, and effectors during fracture repair. *Bone*, *46*(3), 841–851. https://doi.org/10.1016/j.bone.2009.11.005

Zawiślak, T., Turmiński, P., Latosiewicz, R., Chapska, O., Estevez, D., & Majcher, P. (2016). The impact of ultrasound waves on changes in temperature around titanium orthopaedic implants – experimental studies. *European Journal of Medical Technologies*, *2*(11), 28-36.

Zhang, M., Gu, L., Zheng, P., Chen, Z., Dou, X., Qin, Q., & Cai, X. (2020). Improvement of cell counting method for Neubauer counting chamber. *Journal of Clinical Laboratory Analysis*, *34*(1), e23024. https://doi.org/https://doi.org/10.1002/jcla.23024

Zhou, H., Hou, Y., Zhu, Z., Xiao, W., Xu, Q., Li, L., Li, X., & Chen, W. (2016). Effects of low-intensity pulsed ultrasound on implant osseointegration in ovariectomized rats. *Journal of Ultrasound in Medicine*, *35*(4), 747–754. https://doi.org/10.7863/ultra.15.01083

Zhou, Q., Lam, K. H., Zheng, H., Qiu, W., & Shung, K. K. (2014). Piezoelectric single crystals for ultrasonic transducers in biomedical applications. *Progress in Materials Science*, *66*, 87-111. https://doi.org/10.1016/j.pmatsci.2014.06.001

zur Nieden, N. I., Kempka, G., & Ahr, H. J. (2003). In vitro differentiation of embryonic stem cells into mineralized osteoblasts. *Differentiation*, *71*(1), 18-27. https://doi.org/10.1046/j.1432-0436.2003.700602.x

7 Appendix

7.1 QPCR amplification specificity validation

The specificity of DNA amplification in qPCR reaction was assessed using melting curve analysis (Figure 7.1). Melting curves depict changes in fluorescence signal as double-stranded DNA denatures as a function of temperature. The melting temperature (Tm) indicates the temperature at which 50% of the double-stranded DNA in the reaction denatures into single-stranded DNA molecules. Additional peaks may signify the presence of multiple PCR products, typically arising from non-specific amplification or primer-dimer formation. These were not prominently observed in the presented results, indicating the specificity of DNA amplification (Figure 3.12, Figure 3.13).

A. YWHAZ

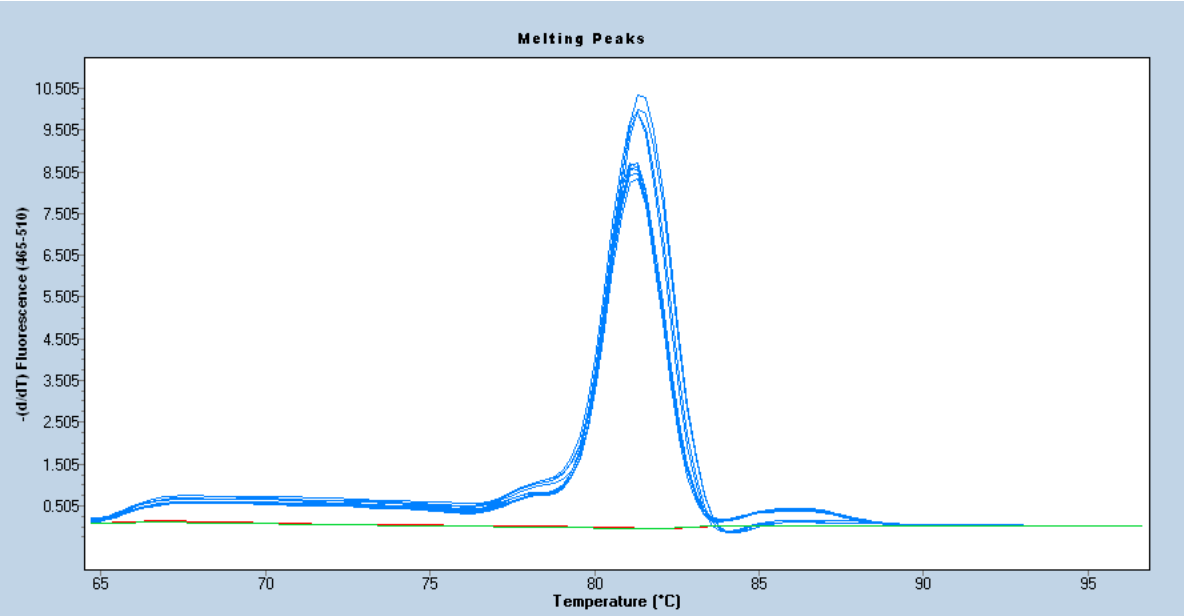

B. MKI67

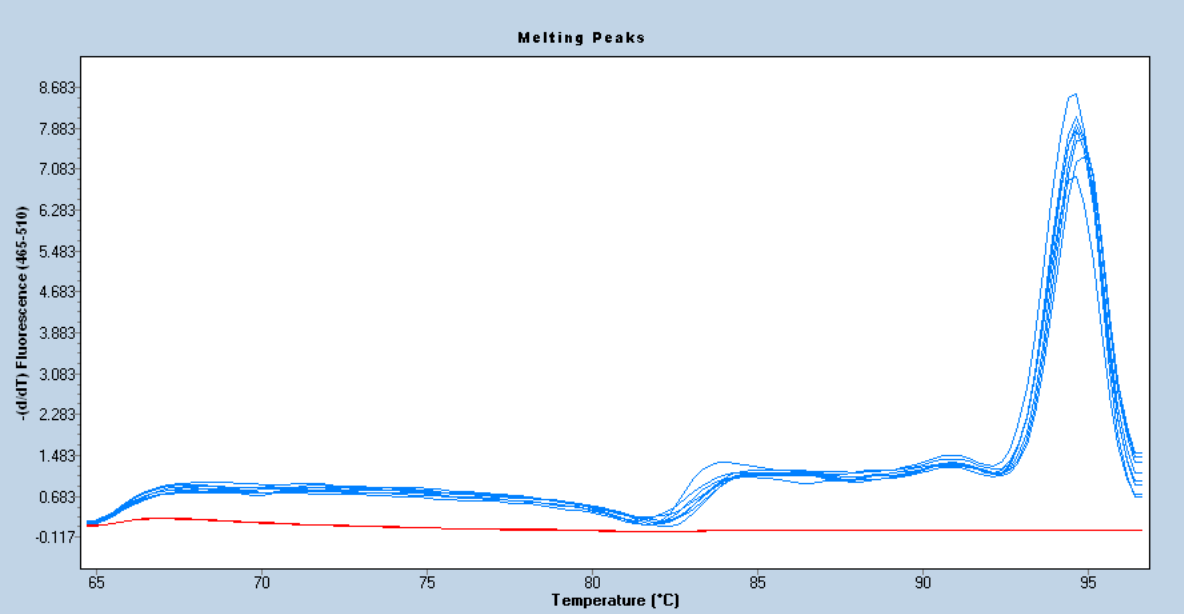

C. PCNA

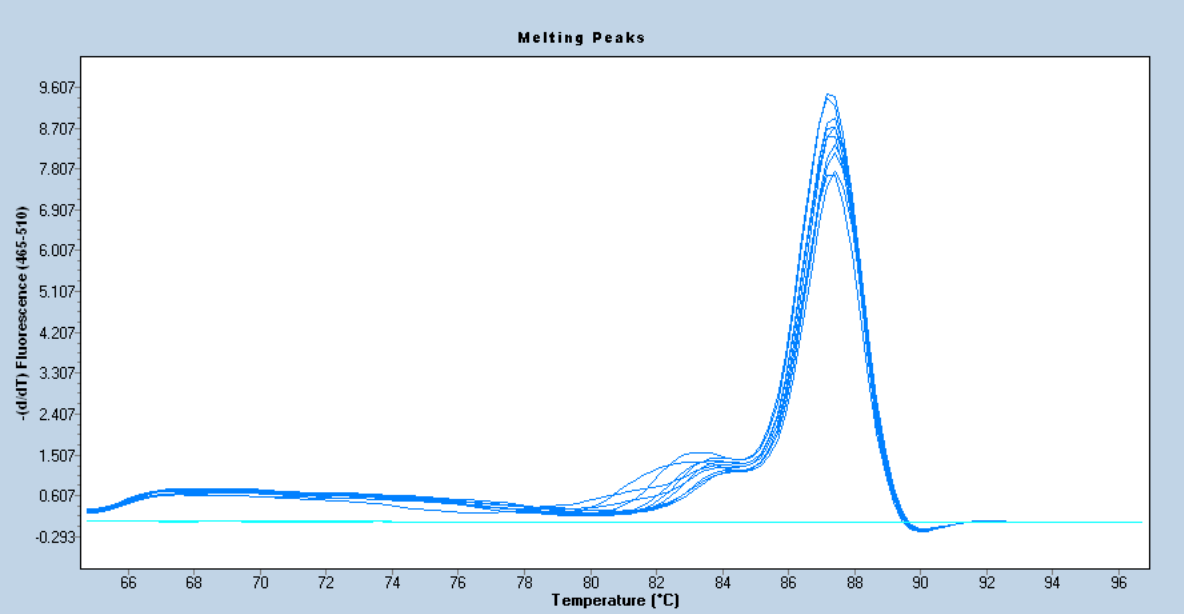

D. ALP

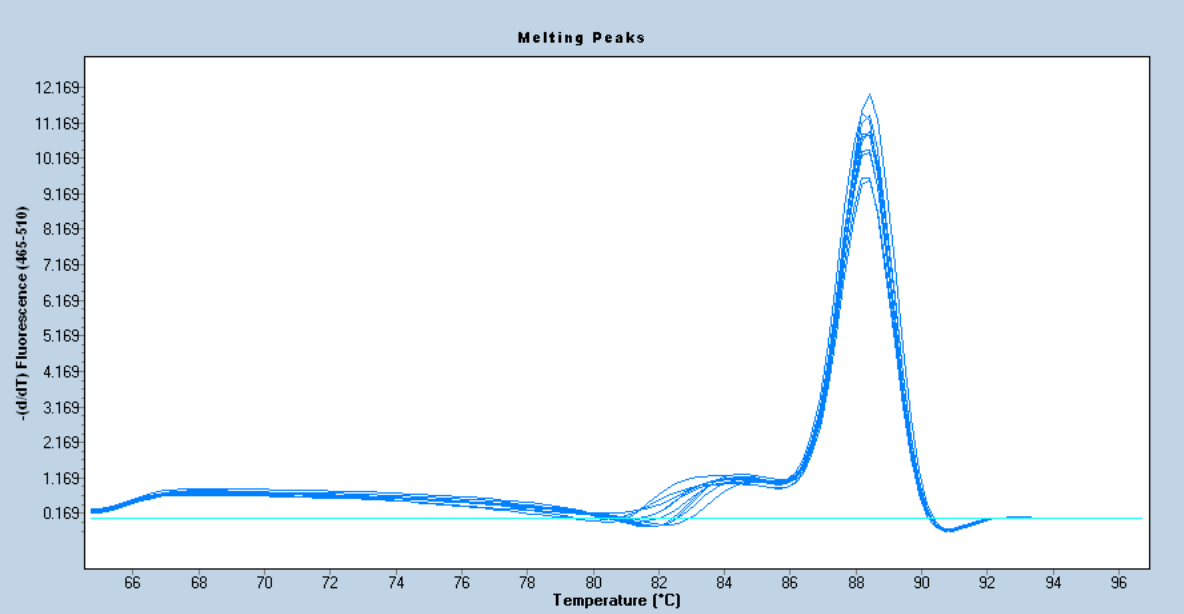
Melting Peaks
-(d/dT) Fluorescence (465-510)
12.169
11.169
10.169
9.169
8.169
7.169
6.169
5.169
4.169
3.169
2.169
1.169
0.169
66
68
70
72
74
76
78
80
82
84
86
88
90
92
94
96
Temperature (°C)

E. RUNX2

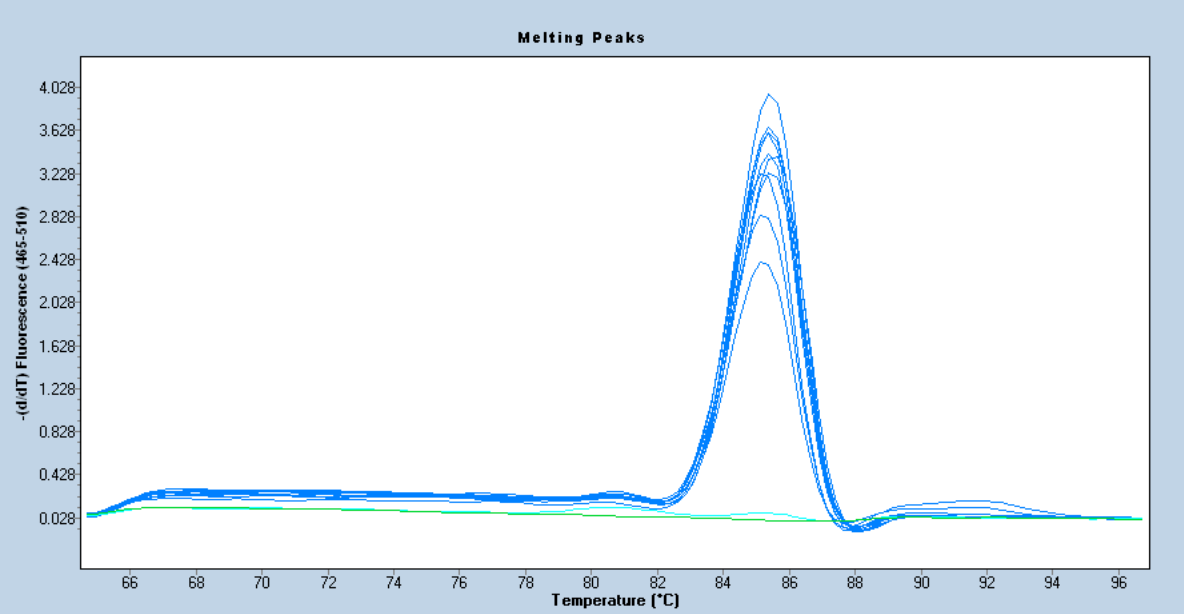
Melting Peaks
-(d/dT) Fluorescence (465-510)
4.028
3.628
3.228
2.828
2.428
2.028
1.628
1.228
0.828
0.428
0.028
66
68
70
72
74
76
78
80
82
84
86
88
90
92
94
96
Temperature (°C)

F. OCN

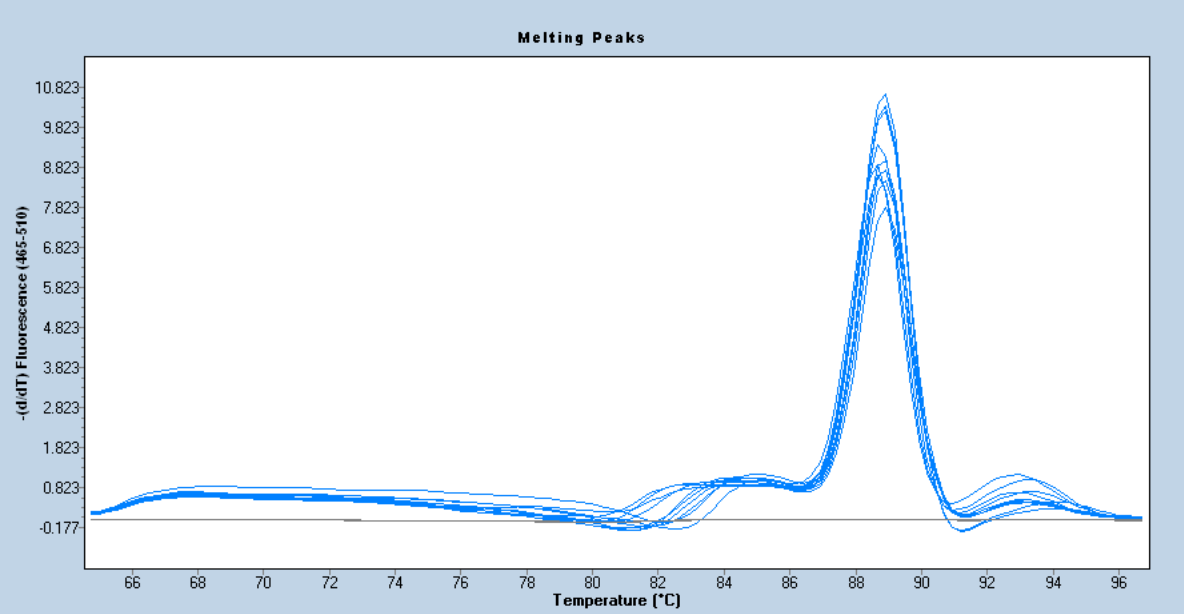

G. PHEX

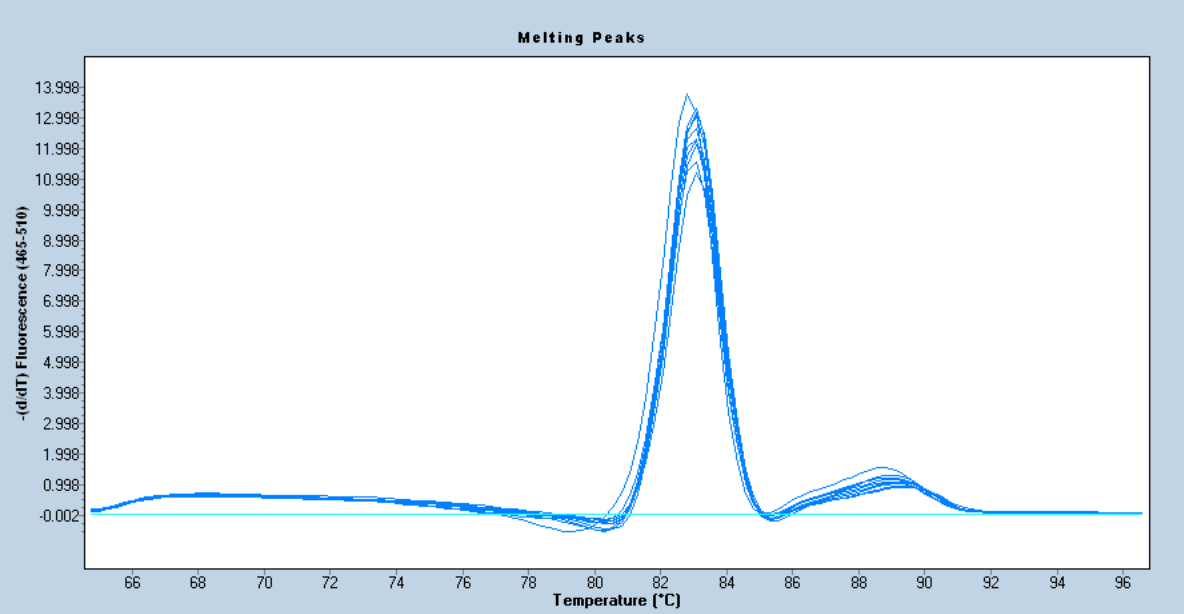

Figure 7.1: Melting curves generated from the qPCR analysis of the following genes: YWHAZ (A), MKI67 (B), PCNA (C), ALP (D), RUNX2 (E), OCN (F), and PHEX (G). No significant peaks, indicative of non-specific DNA amplification or primer-dimer formation, were observed. Therefore, the amplification reactions demonstrate high specificity and reliability.

7.2 Characterisation of Ti-based device for ultrasonic vibration of osteoblasts *in vitro*

The figures in this section were kindly provided by Dr Xuan Li and Dr Aleksander Marek, who created and characterised the ultrasonic vibration device used in this thesis.

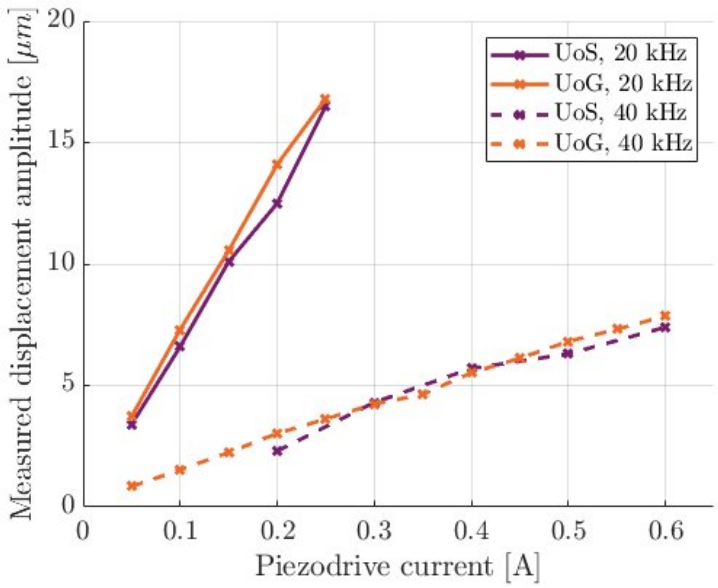

Figure 7.2: A graph depicting displacement amplitude of Ti-paddles oscillating at 20 and 40 kHz was measured by applying a speckle pattern by spray painting and using digital image correlation at varying currents. It was observed that the 20 kHz paddles exhibited a greater increase in vibration with increasing current compared to the 40 kHz paddles. Characterization was conducted twice by collaborators at the University of Glasgow (Dr Xuan Li) and the University of Southampton (Dr Aleksander Marek).

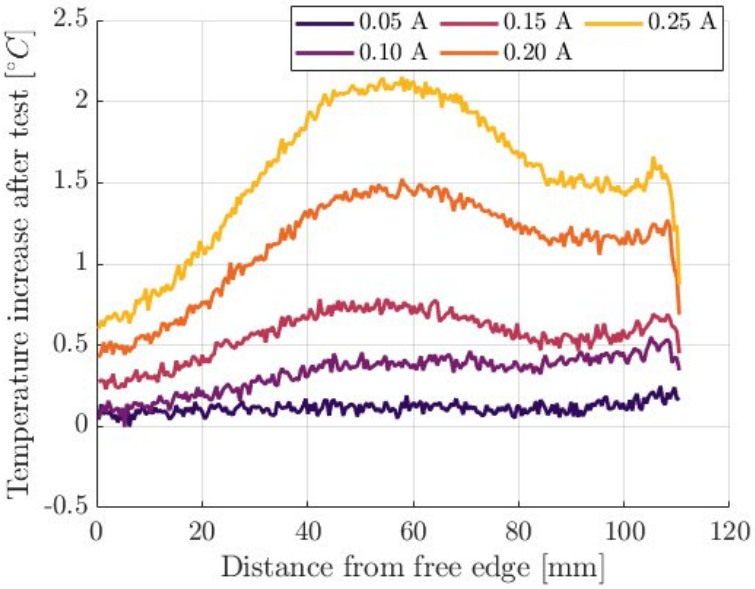

Figure 7.3: A graph illustrating the temperature increase across the Ti paddles oscillating at 20 and 40 kHz, as determined with the infrared camera, revealed that an increase in current amplitude led to a greater temperature rise. Notably, the greatest temperature increase was consistently observed at all current levels in the middle of the strips, corresponding to the node of the standing wave. This location experienced the maximum strain, resulting in the highest temperature increase. Conversely, the proximal and distal ends of the paddles, corresponding to the antinodes of the standing wave, exhibited a lower temperature increase, consistent with the minimal strain experienced in those regions.

7.3 Conference abstracts arising from the present work

- **Importance of dexamethasone in mineralised matrix production in Saos-2 cells.**
  - Olga Yevlashevskaya, Dr Ben A Scheven, Prof A. Damien Walmsley, Dr Richard M Shelton
  - British Society for Oral and Dental Research, Annual Scientific Meeting 2021, Birmingham, UK
  - Oral presentation

- **β-glycerophosphate demonstrates an anti-proliferative effect on mature osteoblast-like Saos-2 cells but not in immature mesenchymal stromal cells.**
    - Olga Yevlashevskaya, Dr Ben A Scheven, Prof A. Damien Walmsley, Dr Richard M Shelton
    - American Society for Bone and Mineral Research, Annual Meeting 2022, Austin, USA
    - Poster presentation
- **Comparison of cell detachment and counting procedures of osteoblasts cultured on titanium surfaces.**
    - Olga Yevlashevskaya, Dr Ben A Scheven, Prof A. Damien Walmsley, Dr Richard M Shelton
    - International Association for Dental Research, Oral Health Research Congress 2022, Marseille, France
    - Poster presentation
- **Novel ultrasonic device for studying cells on titanium surfaces *in vitro*.**
    - Olga Yevlashevskaya, Dr Aleksander Marek, Dr Xuan Li, Miranda Ballard, Dr Ben A Scheven, Prof A. Damien Walmsley, Dr Richard M Shelton
    - Ultrasonics Industry Association, Annual Symposium 2023, Utrecht, Netherlands
    - Oral presentation

7.4 Publications arising from the present work

- Yevlashevskaya, O. S., Scheven, B. A., Walmsley, A. D., & Shelton, R. M. (2023). Differing responses of osteogenic cell lines to β-glycerophosphate. *Scientific Reports*, *13*(2045-2322 (Electronic)). https://doi.org/10.1038/s41598-023-40835-w

7.5 Declaration of COVID-19 disruption to planned research

Due to the COVID-19 pandemic, certain aspects of the presented work were conducted under unique circumstances, resulting in adjustments to the originally planned experimental outline. The encountered disruptions included the closure of research facilities between March 2020 and August 2020, shortage of laboratory supplies, and travel restrictions. Particularly, the travel difficulties significantly impacted the ability to visit collaborating laboratories focusing on ultrasonics, causing a delay in testing the novel ultrasonic device for *in vitro* experiments. The disruptions had a cascading impact on the work timeline, leaving insufficient time for testing the osteogenic behaviour of osteoblasts on ultrasonically vibrating titanium surfaces. These experiments are described within sections dedicated to future research directions (4.5.7). Consequently, the efforts were redirected towards the characterisation of the ultrasonic behaviour of the Saos-2 cell line and the immortalised hMSCs (2.2), since all necessary facilities were available within the School of Dentistry at the University of Birmingham. Therefore, the focus of the work presented in this thesis shifted from the original intention of demonstrating the relevance of ultrasonic therapy in influencing the osteogenic behaviour of osteoblasts on titanium through experimental methods.

scientific reports

Check for updates

OPEN

Differing responses of osteogenic cell lines to β-glycerophosphate

Olga S. Yevlashevskaya, Ben A. Scheven, A. Damien Walmsley & Richard M. Shelton✉

Ascorbic acid (Asc), dexamethasone (Dex) and β-glycerophosphate (β-Gly) are commonly used to promote osteogenic behaviour by osteoblasts in vitro. According to the literature, several osteosarcoma cells lines appear to respond differently to the latter with regards to proliferation kinetics and osteogenic gene transcription. Unsurprisingly, these differences lead to contrasting data between publications that necessitate preliminary studies to confirm the phenotype of the chosen osteosarcoma cell line in the presence of Asc, Dex and β-Gly. The present study exposed Saos-2 cells to different combinations of Asc, Dex and β-Gly for 14 days and compared the response with immortalised human mesenchymal stromal/stem cells (MSCs). Cell numbers, cytotoxicity, mineralised matrix deposition and cell proliferation were analysed to assess osteoblast-like behaviour in the presence of Asc, Dex and β-Gly. Additionally, gene expression of runt-related transcription factor 2 (*RUNX2*); osteocalcin (*OCN*); alkaline phosphatase (*ALP*); phosphate regulating endopeptidase homolog X-linked (*PHEX*); marker of proliferation *MKI67* and proliferating cell nuclear antigen (*PCNA*) was performed every two days during the 14-day cultures. It was found that proliferation of Saos-2 cells was significantly decreased by the presence of β-Gly which contrasted with hMSCs where no change was observed. Furthermore, unlike hMSCs, Saos-2 cells demonstrated an upregulated expression of late osteoblastic markers, *OCN* and *PHEX* that suggested β-Gly could affect later stages of osteogenic differentiation. In summary, it is important to consider that β-Gly significantly affects key cell processes of Saos-2 when using it as an osteoblast-like cell model.

Osteogenic supplementation consisting of ascorbic acid (Asc), dexamethasone (Dex) and β-glycerophosphate (β-Gly) is routinely used to induce the osteogenic phenotype in osteoblast cultures[1,2] Asc serves as a cofactor for proline hydroxylation involved in collagen synthesis, which is required for mineral matrix deposition[3], whilst Dex promotes osteogenic differentiation by upregulating the transcription of *RUNX2*[1,4]. β-Gly provides a source of organic phosphate for extracellular matrix mineralisation in vitro[5].

However, with the variety of osteogenic models available including the range of osteosarcoma cell lines MG-63, U2OS and Saos-2, the reported effects of Asc, Dex and β-Gly in vitro are not consistent in the literature. Valenti et al.[6] showed Asc-induced osteogenic differentiation at up to 250 µM with no signs of apoptosis below 750 µM in relatively undifferentiated osteoblast-like MG-63 cells. Whereas Cmoch et al.[7] described activated matrix mineralisation accompanied by apoptosis in more fully differentiated Saos-2 cells exposed to 283 µM Asc and 7.5 mM β-Gly. The latter suggested a possible role of β-Gly in apoptosis which was not addressed by the authors. Orimo and Shimada[8] used 10 mM β-Gly in Saos-2 cells and reported reduced cell numbers which was suggested to be linked to apoptosis. Additionally, there was an upregulated expression of *PHEX* and *MEPE*[9] both associated with decreased mineral production and differentiation into osteocytes. In contrast, Cmoch et al.[7] observed increased mineralisation by Saos-2 cells at a similar β-Gly concentration. However, whilst many studies use β-Gly, some authors recommend avoiding the use of ~ 10 mM β-Gly as it causes non-physiological levels of extracellular phosphate that can alter normal osteogenic gene transcription[10]. Moreover, there have been conflicting reports on the influence of Dex in osteogenic induction in vitro. Coelho and Fernandes[11] reported significantly higher cell numbers in human mesenchymal stromal/stem cells (MSCs) exposed to 10^{-8} M Dex than in controls. This contrasted with Sordi et al.[12] using 10 mM Dex for osteogenic induction where a decrease in proliferation of human exfoliated deciduous teeth cells was observed. Some studies[7] omitted the use of Dex in osteogenic stimulation completely and still observed matrix mineralisation.

Osteosarcoma is an heterogenous cancer and the cell lines derived from such tumours show varying phenotypes[13]. Thus, the choice of osteosarcoma cell line as an osteoblast-like model can significantly affect the outcome of in vitro experiments. The role of Asc, Dex and β-Gly in key cell processes including proliferation, apoptosis and osteogenic gene expression must be defined specifically for particular osteosarcoma cell lines to

School of Dentistry, College of Medical and Dental Sciences, University of Birmingham, 5 Mill Pool Way, Edgbaston, Birmingham B5 7EG, UK. ✉email: r.m.shelton@bham.ac.uk

produce data which is comparable. The present study compared the response of the Saos-2 osteosarcoma cell line and a non-carcinogenic cell model with Asc, Dex and β-Gly. Saos-2 is a commonly used osteoblast-like cell line derived from an 11-year-old Caucasian female patient suffering from primary osteosarcoma[14]. Saos-2 presents features characteristic of relatively mature osteoblasts including mineralised matrix synthesis, expression of 1,25-dihydroxyvitamin D3 receptors and elevated production of collagen-1[3] Furthermore, the relative ease of maintenance of Saos-2 in tissue culture and the short doubling time make it an attractive cell model for in vitro research. However, the cancerous nature of the Saos-2 cells causes several biological variations including altered proliferation kinetics and the absence of contact inhibition in vitro[15]. The latter contrasts markedly with the in vivo environment and therefore limits the physiological relevance of data obtained using these cells so a non-tumour derived cell model was used to compare the effects of Asc, Dex and β-Gly with those from Saos-2. An immortalised human bone marrow cell line (hMSC) was selected due to its non-cancerous origin in contrast with Saos-2. The hMSC line was immortalised via serial passaging combined with viral-mediated transfection of SV40 large T antigen[16]. However, despite a shorter doubling time than observed in primary cells, the hMSC line retains contact inhibition properties and the potential for adipogenic, chondrogenic and osteogenic differentiation. As a result, the hMSC line offers a physiologically relevant osteoblast-like model system while still allowing for the convenience of working with a cell line.

Considering the conflicting data discussed, the aim of the present study was to compare the effect of Asc, Dex and β-Gly on the osteogenic behaviour of the Saos-2 cell line and a relatively undifferentiated non-cancer derived hMSC line. This investigation provides a unique set of data demonstrating the relevance of Saos-2 as an osteoblast-like model system in vitro.

Materials and methods

Cell culture and osteogenic differentiation. Saos-2 and non-differentiated hMSCs were obtained from laboratory stores and Abm (T0520, Abm, Canada) respectively. Saos-2 cells were maintained in Dulbecco's Modified Eagle's Medium (DMEM)/Ham's Nutrient Mixture F12 (Sigma, UK) supplemented with 1% penicillin/streptomycin, 1% L-glutamine and 10% foetal bovine serum (FBS). hMSCs were cultured in DMEM (low glucose, pyruvate) (Gibco, UK) with 0.5% penicillin/streptomycin and 10% FBS. Both cell lines were maintained at 37 °C in an atmosphere of 5% CO_2. Cells were seeded at a density of 8.4×10^3 cells cm^{-2} and expanded for 72 h until confluence which was day 0 of the experiment. Osteogenic supplements were introduced on day 0 using 283 μM Asc, 9.3 mM β-Gly and 10^{-8} M Dex. The following combinations of osteogenic supplements were established: control (no osteogenic supplementation); Asc Dex β-Gly; Asc Dex; Asc β-Gly; Dex β-Gly; Asc; Dex and β-Gly. Cells were incubated in variously supplemented culture media for up to 14 days with a change of media every 3 days. Cell growth in terms of numbers was examined every 2 days until day 14 of incubation. First, cell monolayers were detached from the polystyrene surface using 0.05% trypsin in 0.02% EDTA (Sigma, UK) for 10 min at 37 °C, centrifuged and resuspended in 1 ml 10% FBS in DMEM/Ham's F-12. Viable cell counts were performed using trypan blue staining and a Neubauer haemocytometer.

Cytotoxicity assay. The lactate dehydrogenase (LDH) cytotoxicity assay was performed to examine cell death in cultures by quantifying the release of LDH. The LDH-Glo™ kit was used (Promega, UK) according to the manufacturer's instructions. Briefly, a 2 μl aliquot of culture media was collected on day 7 of incubation in osteogenic media and diluted in 50 μl LDH storage buffer before 25 μl of this solution was transferred into an opaque walled, transparent bottom 96 well plate and mixed with an equal volume of LDH detection reagent. Luminescence was recorded using a plate reader (Tecan Spark, Switzerland) after 60 min of incubation at room temperature. Two negative controls were used in this experiment: a no cells control—to assess the background luminescence of the culture media and no treatment control—to assess cell death in cultures without the osteogenic supplementation. A positive control with LDH was prepared by permeabilising the no treatment control cells with 10% Triton-X100 for 10 min immediately before collecting the culture media samples.

Alizarin red S staining. To examine mineral deposition in cell cultures Alizarin red S staining (ARS) was performed on day 14 of incubation in osteogenic media as described by Gregory et al.[17]. The cells were fixed with 10% formalin and stained with 40 mM Alizarin red S stain (pH 4.2) for 20 min at room temperature. Stain quantification was performed by extracting the stain with 10% acetic acid for 30 min followed by neutralisation with 0.1% ammonium hydroxide. The optical density of samples was quantified using a plate reader at 450 nm and compared with a standard curve of serial dilutions.

Assessment of gene expression using qPCR. Total RNA was isolated every 2 days up to day 14 of osteogenic treatment using the RNeasy Mini kit (Qiagen, UK) according to the manufacturer's instructions. The samples were generated in 3 separate experiments to produce 3 biological replicates. Cell monolayers were dissociated using a lysis buffer followed by dilution with the 70% molecular grade ethanol. Then the suspensions were passed through the RNeasy spin column and centrifuged at 10,000 RPM for 30 s. Any non-specifically bound organic molecules and salts were removed using a wash buffer provided in the kit. Genomic DNA was digested using the On-Column DNAse kit (Sigma, UK) by adding the DNase solution directly to the samples and incubating for 15 min at room temperature. RNA was collected by adding 30 μl of RNAse-free water to the samples and centrifuging at 10,000 RPM for 1 min before storing the RNA samples at − 80 °C until later use. The quality of the resulting RNA was established using spectrophotometry (Genova Nano, Jenway™, UK).

Then, complementary DNA (cDNA) was produced from the isolated RNA via reverse transcription (RT) using the Tetro cDNA synthesis kit (Bioline, UK). The reaction master mix was prepared by combining 1 μl of 10 mM deoxynulceoside triphosphate (dNTP) mix, 4 μl of RT reaction buffer, 1 μl of RNase inhibitor and

1 µl of reverse transcriptase (200 U/µl). The reaction contained 8 µl of the master mix, 2 µg of RNA sample and DEPC-treated water to a final reaction volume of 20 µl. The mix was transferred to the thermocycler (Veriti, 96 well thermal cycler, Applied Biosystems, USA) and incubated at 45 °C for 1 h to allow RT followed by 85 °C for 5 min to terminate the reaction. The resulting cDNA samples were stored at − 20 °C before use.

Finally, real-time PCR (qPCR) was performed using LightCycler® 480 SYBR Green I Master and 480 LightCycler® system (Roche Diagnostics). The expression of the following osteogenic markers was analysed: runt-related transcription factor 2 (*RUNX2*); osteocalcin (*OCN*); alkaline phosphatase (*ALP*) and phosphate regulating endopeptidase homolog X-linked (*PHEX*). The expression of a marker of proliferation (*MKI67*) and proliferating cell nuclear antigen (*PCNA*) were used to provide a comparison of proliferative markers. Sequences of the primers used are provided in supplementary materials. The gene expression levels were normalised to the expression of *YWHAZ* (tyrosine 3-monooxygenase). Data quantification was performed using the second derivative maximum method. This involved an algorithm identifying crossing points (Cp)—the number of PCR cycles after which the exponential phase of the target sequence amplification began. The starting concentration of target gene samples were found by comparing the Cp values against those in the standard curve of serial dilutions of log primer concentrations.

Determination of cell proliferation. Cell proliferation was examined on day 4 of incubation with full osteogenic culture media (Asc, Dex and β-Gly) to avoid examining confluent cell layers where proliferation may be compromised by contact inhibition. Cultures were incubated in 6 well plates. BrdU (5-Bromo-2′-deoxy-uridine) uptake was measured to identify replicating cells according to the manufacturer's instructions (ab287841, Abcam, UK). Briefly, cells were exposed to the BrdU labelling solution for 6 h at 37 °C in 5% CO_2. Samples were fixed with ethanol (50 mM glycine, 70% ethanol) for 20 min at − 20 °C and washed three times with the washing buffer provided in the kit. Then, samples were incubated with anti-BrdU antibody for 30 min at 37 °C and washed again, followed by incubation with anti-mouse Ig-fluorescein antibody for 30 min at 37 °C. Mounting media containing DAPI was applied for 10 min at room temperature to stain cell nuclei. BrdU and DAPI incorporation were examined using fluorescence microscopy (Eclipse TE300, Nikon, Japan). The following negative controls were established to prevent non-specific staining: (1) no BrdU, (2) no anti-BrdU antibody, (3) no secondary antibody. Images were captures using digital camera (D5100, Nikon, Japan). Brightness and contrast were enhanced equally in all images using Image J without obscuring or eliminating any details. BrdU-stained and non-stained nuclei were counted manually.

Statistical analysis. All experiments were established with three technical replicates (i.e., 3 wells) and undertaken independently 3 times. The data was presented as the median of 3 biological replicates as well as the minimum, maximum, lower quartile, and upper quartile values. Differences in parametric data were compared using Brown-Forthyse and Welch ANOVA tests and $P < 0.05$ was considered statistically significant. Statistical analysis and figures were generated using GraphPad Prism, Version 9.5.0 (GraphPad Software, San Diego, California US).

Results

Cell growth. The effect of osteogenic supplements on cell growth was studied by quantifying viable cell numbers for 14 days. Saos-2 cultures exposed to β-Gly demonstrated a significantly lower number of viable cells compared with Dex and/or Asc supplemented cultures after day 4 of incubation (Fig. 1) and at all subsequent time points examined. In contrast, the number of viable hMSCs was not statistically significantly affected by any of the osteogenic supplements in comparison with controls (Fig. 2).

Cytotoxicity assay. To evaluate the cause of the reduced Saos-2 cell numbers in β-Gly-positive cultures an LDH assay was performed. No significant change in LDH release was observed between the osteogenically treated cells and controls (Fig. 3) in either Saos-2 (A) or hMCSs (B).

Proliferation assay. Saos-2 cells incubated in the presence of β-Gly showed significantly fewer (3.1%) BrdU-stained nuclei than cells not exposed to β-Gly (Figs. 4, 6) with 35.6% of all nuclei being stained with BrdU. Hence, the proliferative activity of Saos-2 was decreased in the presence of β-Gly. No statistically significant difference was identified in the number of BrdU-stained nuclei in hMSCs with 23.7% of BrdU stained nuclei in β-Gly exposed cells and 25% of BrdU-stained nuclei in negative controls (Figs. 5, 6). Therefore, cell proliferation was not affected by the presence of β-Gly in hMSCs relative to control cultures. Negative controls with either no BrdU, no anti-BrdU antibody or no secondary antibody did not generate any fluorescence.

Alizarin red staining. ARS was used to assess mineral matrix deposition in osteogenically-supplemented cultures on day 14 of incubation. ARS showed a 24 and four-fold increase in mineral matrix production in β-Gly supplemented Saos-2 and hMSC cultures respectively (Fig. 7). Asc and Dex did not appear to affect mineral deposition in either cell line. However, there was an increased ARS concentration in β-Gly-negative hMSCs compared with in β-Gly-negative Saos-2.

Gene expression analysis. The expression of proliferation markers and osteoblast-associated genes was normalised to the expression of *YWHAZ* and determined every two days of incubation with the different combinations of osteogenic supplements (Figs. 8, 9). Saos-2 cells demonstrated a gradual decrease in *MKI67* (Fig. 8a) and *PCNA* (Fig. 8b) expression during the 14 days, however a clear difference between cells exposed to different

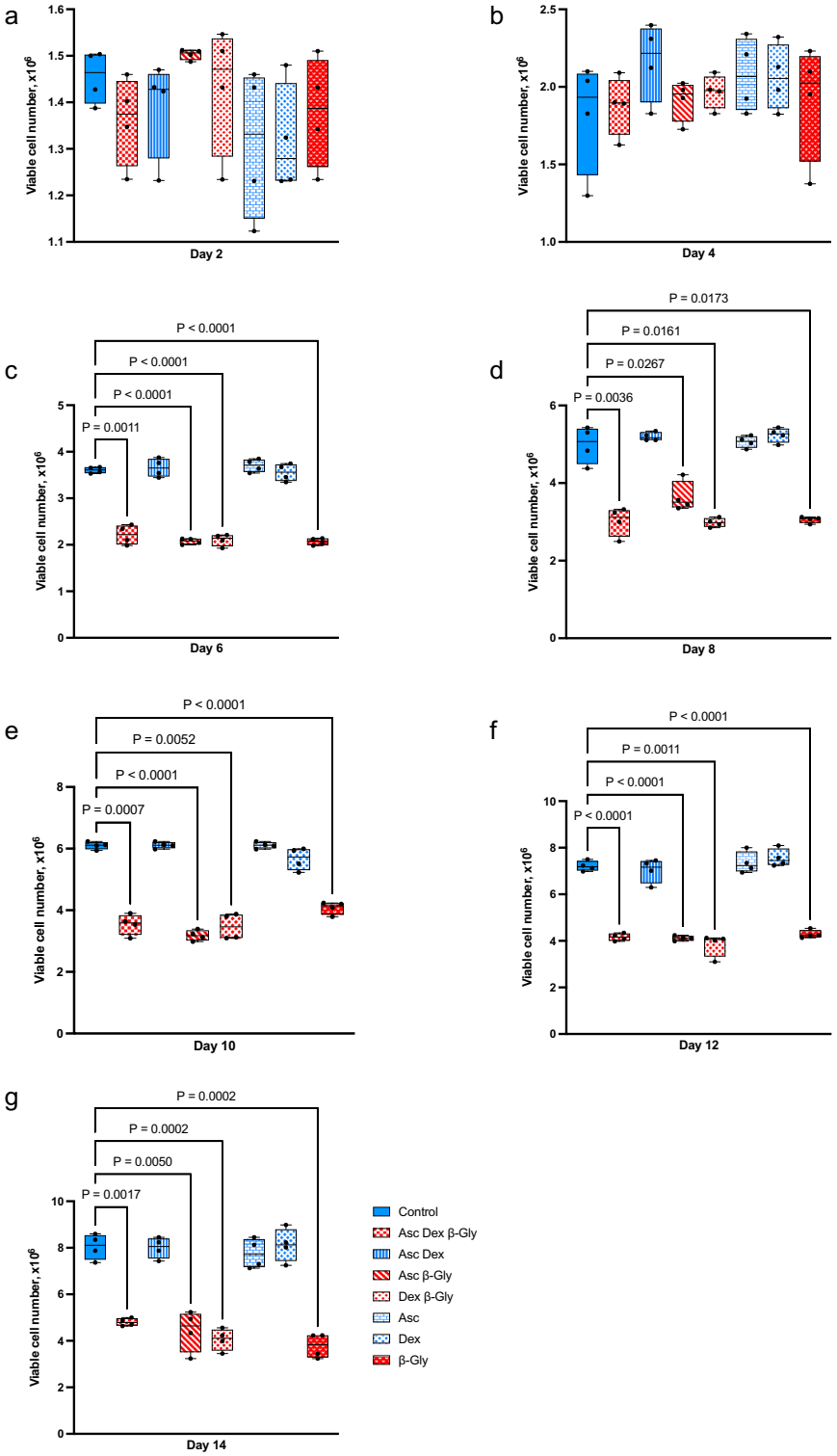

Figure 1. Mean viable cell numbers of Saos-2 after incubation with different combinations of osteogenic supplements for 14 days. Numbers of Saos-2 cells were significantly reduced in the presence of β-Gly after 4 days of supplementation relative to the control of the corresponding day (**c**–**g**). Asc and/or Dex did not affect Saos-2 numbers compared with the control (**a**–**g**). Blue and red bars represent cultures without and with β-Gly respectively. n = 3.

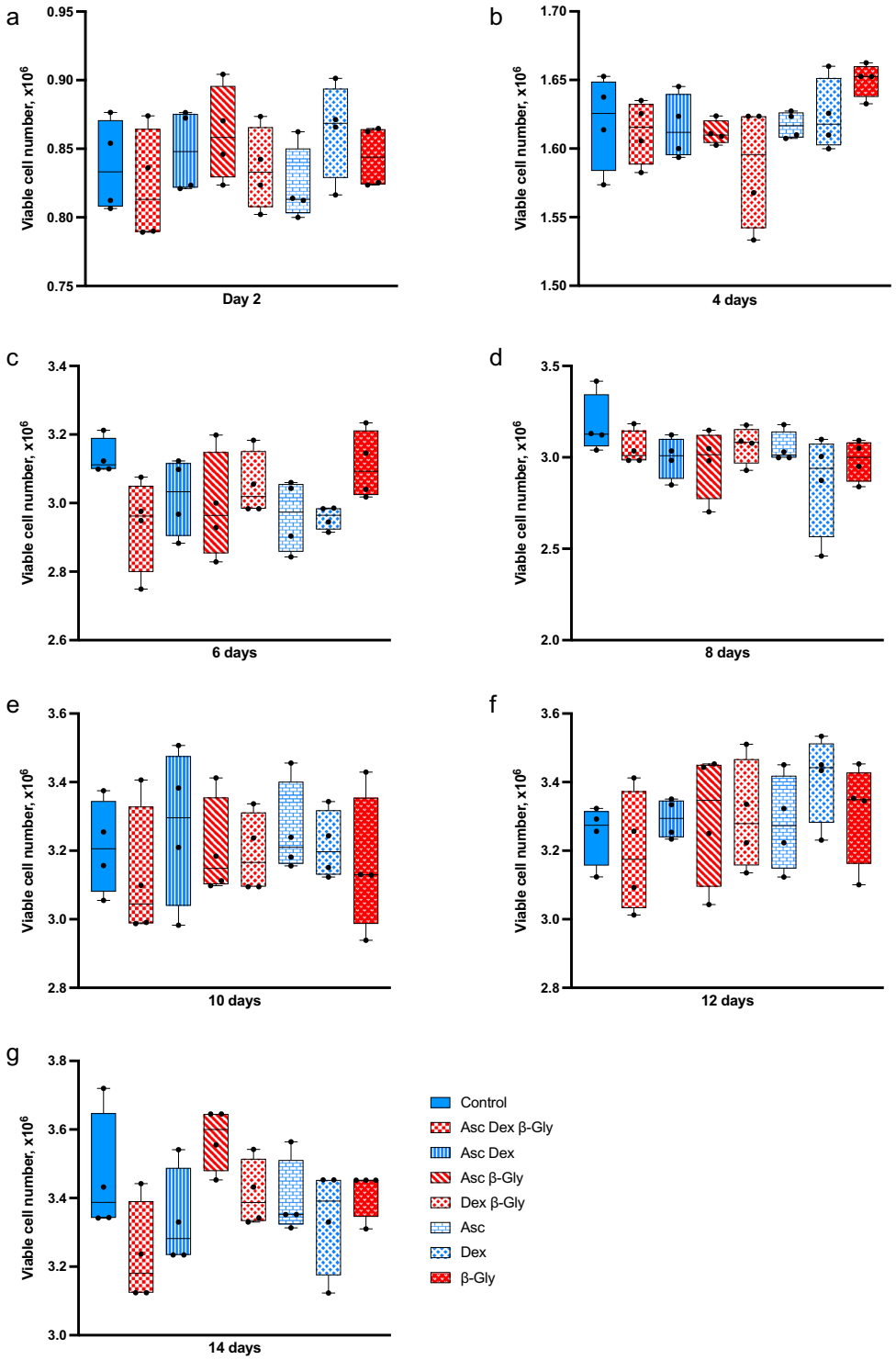

Figure 2. Mean viable cell numbers of hMSCs after incubation with different combinations of osteogenic supplements for 14 days. In contrast to the Saos-2 cells (Fig. 1), hMSCs did not show a significant change in numbers with the addition of β-Gly. Nor did Asc and/or Dex affect hMSCs numbers compared with the control. Blue and red bars represent cultures without and with β-Gly respectively. n = 3.

combinations of Asc, Dex and β-Gly was not identified. hMSCs showed a similar trend for *MKI67* expression (Fig. 9a) but a more marked decrease in the mRNA synthesis of *PCNA* (Fig. 9b) after 4 days of osteogenic supplementation than Saos-2 (Fig. 8b). *RUNX2* expression was significantly upregulated by the presence of osteogenic

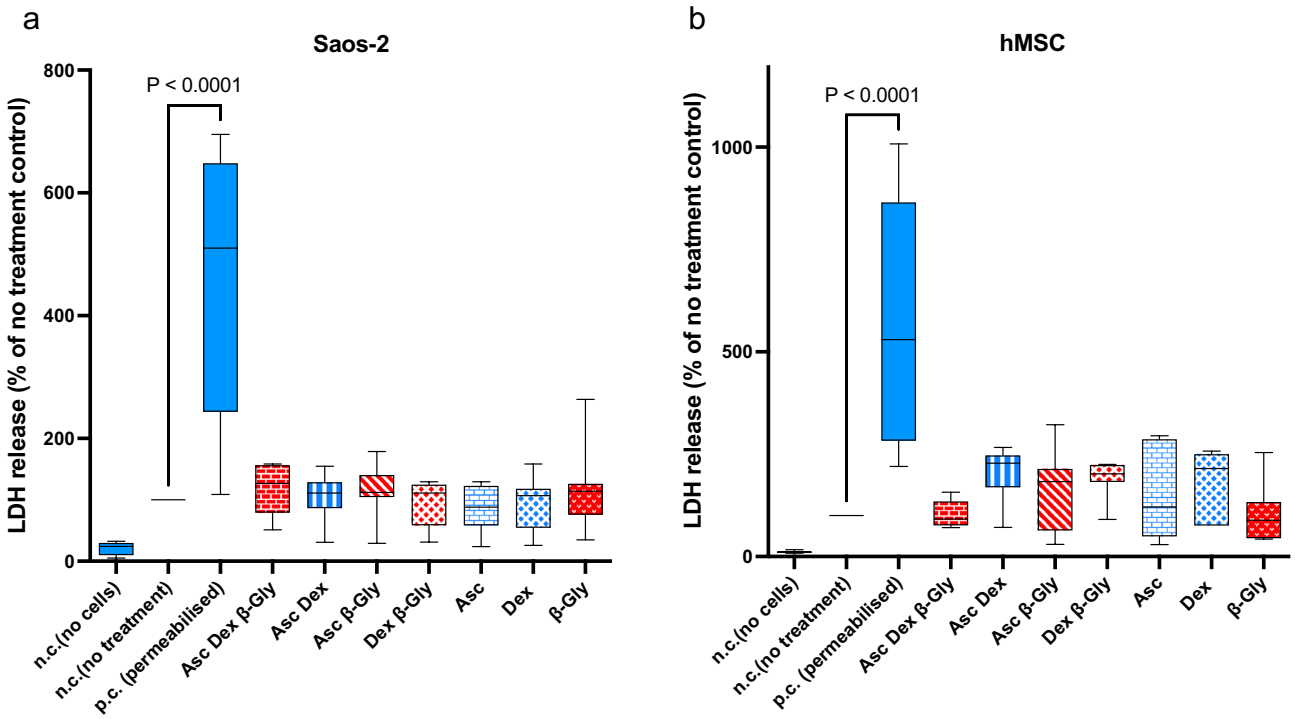

Figure 3. The LDH assay demonstrates LDH released from damaged/dead cells. A negligible amount of LDH was detected in the no-cells negative control (n.c.). A 4.5-fold increase in LDH was observed in the positive control (p.c.) containing Triton-permeabilised cells when compared with no treatment controls. No significant change in LDH release was seen between the different osteogenic supplemented cultures in either Saos-2 (**a**) or hMSCs (**b**). Red bars represent cultures with β-Gly and blue bars do not. n = 3.

supplements in Saos-2 cells and increased during the incubation period relative to negative controls (Fig. 8d). In contrast, the *RUNX2* activity increased only at day 8 of the experiment and thereafter in osteogenically supplemented hMSCs (Fig. 9d). *ALP* expression was upregulated in the Dex, Asc, β-Gly supplemented hMSCs (Fig. 9c) and peaked on day 8 of incubation. Saos-2 showed an upregulation of *OCN* in the presence of β-Gly (Fig. 8e) at day 8 of the experiment. *PHEX*, an osteocyte-associated gene was significantly activated in all Saos-2 cultures containing osteogenic supplements at day 8 of incubation (Fig. 8f). No significant trend in *PHEX* expression was observed in hMSCs (Fig. 9f) at any stage of the experiment.

Discussion

The diverse in vitro models used in osteoblast research create challenges with comparability of data between studies[14,15]. Osteosarcoma cell lines represent an affordable and straightforward option for researchers, however different cell origins can generate varying osteogenic gene expression profiles and phenotypes. The latter can produce variable data between studies and influence potential interpretation. The present study evaluated the response of an osteosarcoma cell line, Saos-2 to Asc, Dex and β-Gly used to induce osteogenic cell behaviour. An immortalised multipotent hMSC line was used for comparison of responses to osteogenic supplements by Saos-2 that may have been influenced by its tumour origin. It is crucial to emphasize that although the hMSCs did not originate from malignant tissue, they were immortalized through telomerase induction using transformation with SV40 Large T antigen[16]. This process resulted in a cellular phenotype that is more physiologically representative and "normal" when compared with Saos-2 cells. However, it is important to acknowledge that the cell line underwent certain modifications to achieve this state.

Previously it has been reported that[6,7] Asc and/or Dex supplementation did not affect cell numbers in osteosarcoma cell lines including MG63 and Saos-3 suggesting either an anti-proliferative or toxic effect of β-Gly. However, in the present study Saos-2 cells demonstrated a decrease in cell number in the presence of β-Gly (Fig. 1) which was not observed in hMSCs (Fig. 2). β-Gly is used to promote mineralisation of the ECM by providing organic phosphate ions[5]. Inorganic phosphate concentrations of 5–7 mM in culture medium have been reported to induce apoptosis in osteoblasts[18], possibly mediated by the mitochondrial damage via hyperpolarisation of the electrochemical gradient across the inner mitochondrial membrane and a consequent release of excess reactive oxygen species[19,20] However, it has also been indicated that organic phosphates, such as β-Gly were not harmful to cells at similar concentrations[21]. Furthermore, osteoblasts are suggested to be adapted to the elevated phosphate concentrations in comparison with other cell types arising from involvement in bone-remodelling[18]. In the present study, the LDH assay confirmed that β-Gly did not change cell viability and therefore was not cytotoxic to Saos-2 at 9.3 mM (Fig. 3).

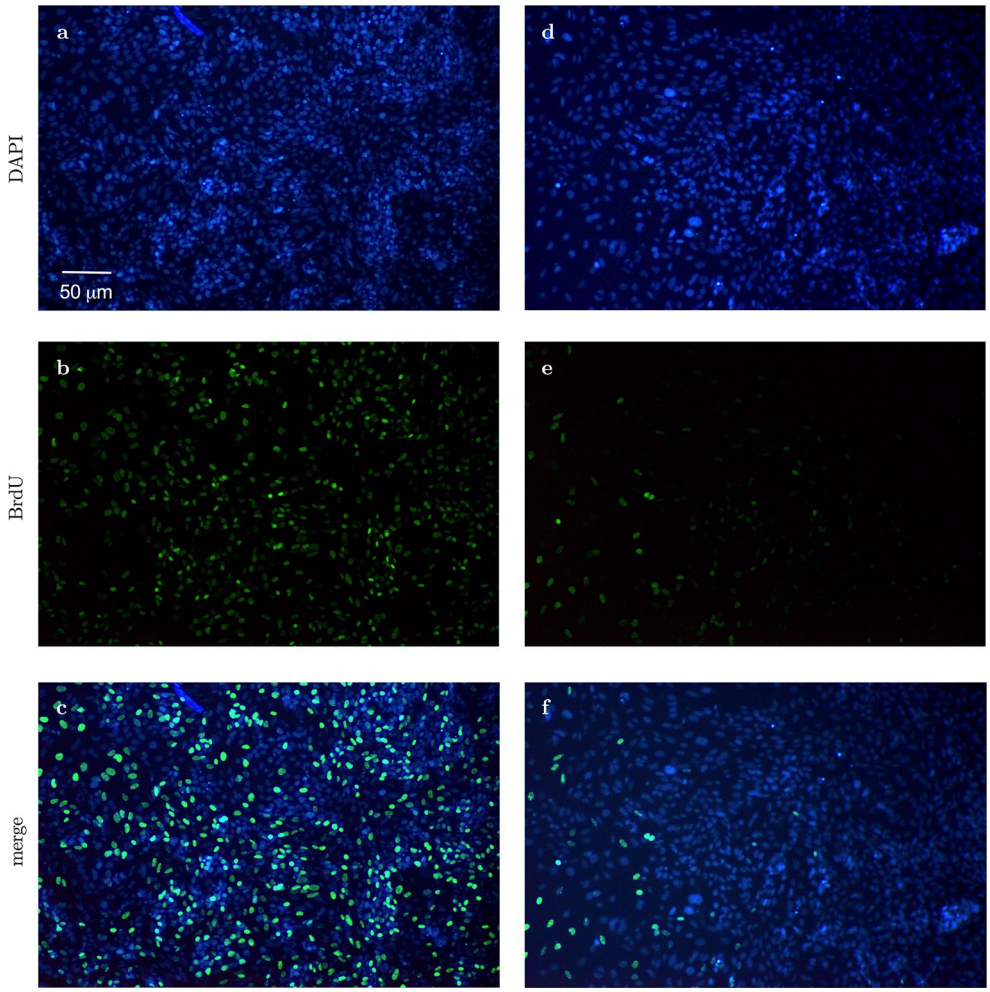

Figure 4. Representative fluorescence micrographs of BrdU staining of Saos-2 cells after 4 days supplementation with β-Gly. Saos-2 cells exposed to β-Gly (**d**–**f**) demonstrated a lower proportion of BrdU-stained nuclei than Saos-2 controls (**a**–**c**). n = 3.

Interestingly, β-Gly appeared to decrease proliferation of Saos-2 cells but not hMSCs as shown by the BrdU staining (Figs. 4, 5 and 6). A decrease in cell proliferation rate and arrest in the G_0 phase are expected events at the later stages of the cell cycle[22], which would explain the decrease in cell numbers in the later phases of incubation of Saos-2 cells. Mature cell phenotypes can enter a non-dividing, G_0 state via either terminal differentiation, senescence or quiescence[23], expressing low to non-detectable levels of *MKI67* and *PCNA* mRNA[24] *MKI67* gene codes for Ki-67, a protein involved in the formation of the perichromosomal layer necessary for chromosome condensation in mitosis[25]. It is expressed in G_1, S, G_2 and M phases of the cell cycle[26]. Whereas *PCNA*, typically transcribed in G_1 and S[27], codes for an accessory protein for DNA polymerase alpha[26]. Hence, the increased activity of *MKI67* and *PCNA* were used as indicators of cell proliferation in addition to BrdU staining. A significantly lower *MKI67* expression level characteristic of G_0 was observed in the later stages of the experiment in all osteogenic conditions both in the Saos-2 cells and hMSCs (Figs. 8A and 9A). Furthermore, the decrease in *PCNA* expression after 2 and 4 days in all Saos-2 and hMSCs cultures respectively suggested the cell cycle arrest in G_0 or exit from G_1 and S. The reduction in transcription of both genes in all osteogenic conditions including those not containing β-Gly was possibly caused by quiescence typically arising from nutrient and/or oxygen deprivation or the build-up of toxic metabolites with increased cell numbers in longer cell cultures[28] However, a marked decrease of BrdU-stained nuclei observed only in β-Gly-exposed Saos-2 (Fig. 4C, F) implied a unique role for β-Gly in the cell cycle arrest of Saos-2. Decreased BrdU uptake showed that fewer Saos-2 cells were in S phase after 4 days of incubation that corresponded with a reduction in proliferation. A possible cause of the latter is the cell cycle arrest triggered by terminal differentiation of Saos-2.

Terminal differentiation leads to a permanent cell cycle exit in most cell types. Terminally differentiated osteoblasts become either lining cells, osteocytes or undergo apoptosis[29]. It is necessary to highlight the mature osteoblastic phenotype of Saos-2 relative to the earlier phase of osteogenic differentiation of hMSCs as the latter affects proliferation kinetics in cells. Coelho and Fernandes[11] reported decreased proliferation of human bone marrow cells in the presence of β-Gly after 42 days and linked it with progression of osteogenic differentiation. Interestingly in the present study, *PHEX*, an osteocyte associated marker was upregulated in osteogenically

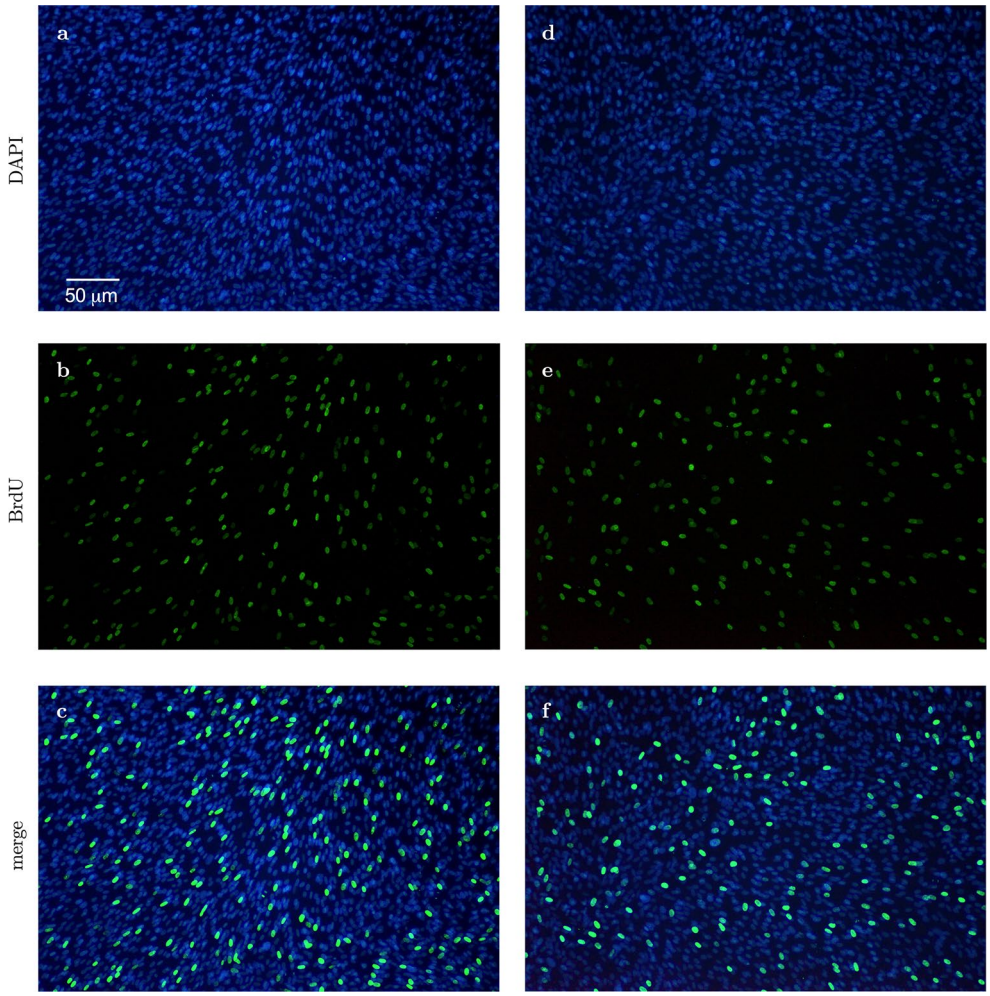

Figure 5. Representative fluorescence micrographs of BrdU staining of hMSCs after 4 days supplementation with β-Gly. The proportion of BrdU-labelled hMSCs nuclei did not differ significantly between β-Gly-positive (**d**–**f**) and β-Gly-negative (**a**–**c**) cultures. n = 3.

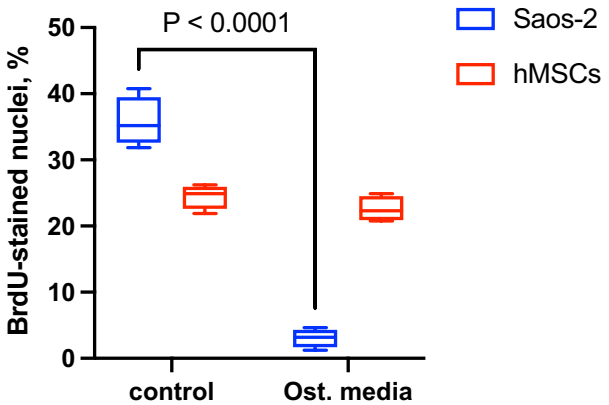

Figure 6. Saos-2 exposed to β-Gly demonstrated a lower proportion of BrdU-stained nuclei than Saos-2 controls, 3.1% and 35.6% respectively. β-Gly-positive and β-Gly-negative hMSCs cultures did not show a significant difference in the proportion of BrdU labelled nuclei—23.7% and 25% respectively. n = 3.

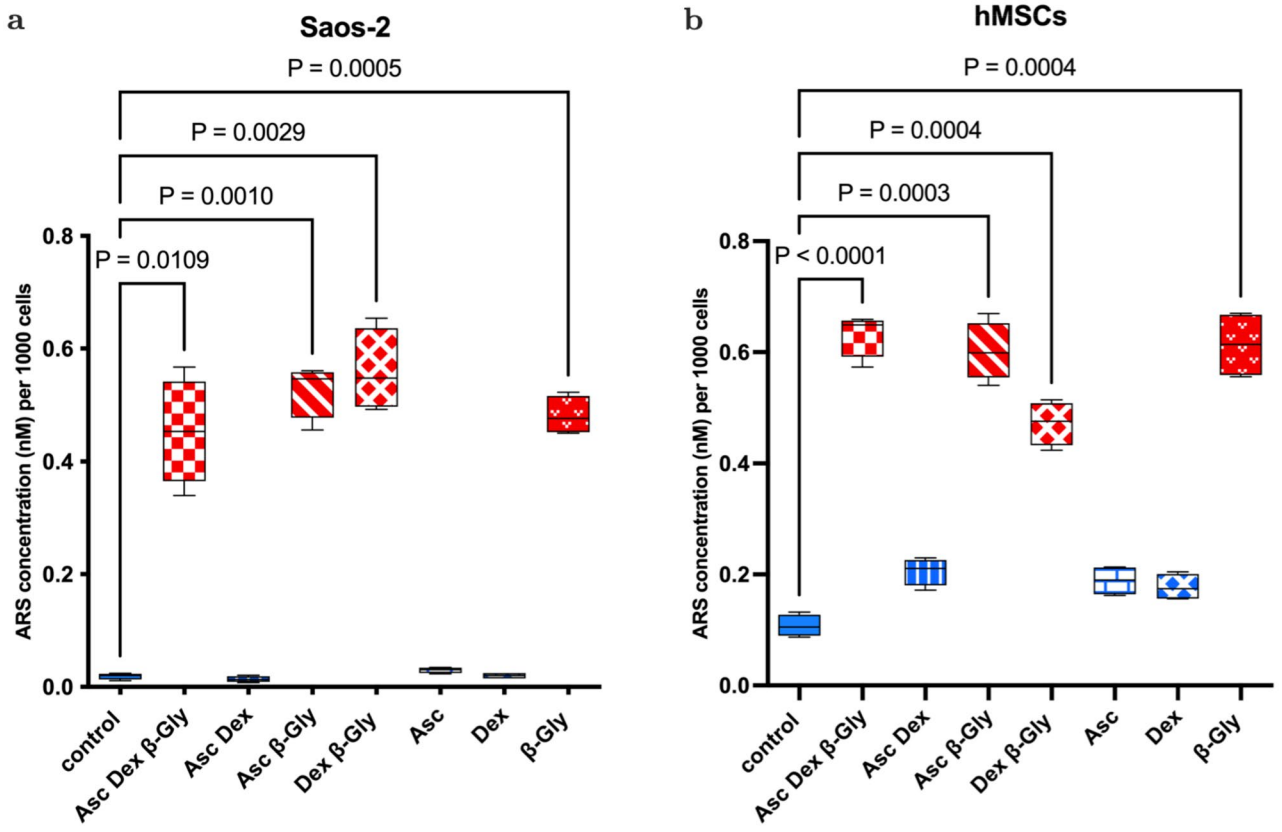

Figure 7. ARS showed a significant increase in calcified matrix synthesis in the presence of β-Gly in Saos-2 (**a**) and hMSCs (**b**) cultures. Asc and Dex did not increase mineral matrix production in either cell line. Red bars represent cultures with β-Gly and blue bars do not. n = 3.

induced Saos-2 cultures, unlike hMSCs further confirming the phenotypic difference of the two in the presence of β-Gly. However, Saos-2 cells continued to express *PCNA* and *MKI67* as well as synthesising mineralised matrix which are not typical of terminally differentiated cells. Although, it is worth noting that osteocytes are notoriously difficult to maintain in vitro[30], so terminal differentiation should not be excluded as the cause of the anti-proliferative effect of β-Gly on Saos-2.

RUNX2 is an important regulator of osteogenic differentiation[31] and *ALP* has often been described as an early osteogenic marker[32]. Although, since *ALP* proteins are not unique to bone, it may be argued that the *ALP* expression level is inadequate for addressing osteoblast differentiation. Saos-2 cells showed no particularly defined patterns of *RUNX2* or *ALP* expression depending on the osteogenic supplements provided and no significant difference was detected between treated and control cells. (Fig. 8C, D). This suggested that Asc, Dex and β-Gly did not affect early osteoblastic differentiation in Saos-2 cells as expected due to the relatively "mature" phenotype. This contrasted with the hMSCs where an upregulation of *RUNX2* and *ALP* expression was observed in cells subjected to Asc and/or Dex and/or β-Gly promoting early osteoblastic differentiation (Fig. 9C, D). Expression of *OCN* was increased in Saos-2 in the presence of β-Gly (Fig. 8E). Increased *OCN* transcription indicated β-Gly interaction with the later stages of osteogenesis, whilst the activity of *OCN* in hMSCs did not appear to be affected exclusively by β-Gly and was upregulated in all supplemented cultures after day 10 (Fig. 9E). This implied a transition of hMSCs into a later stage of osteogenic differentiation during the course of the experiment similarly to healthy osteoblasts described in the literature[29]. These findings suggested a potential distinct role of β-Gly in later osteogenic differentiation of Saos-2 cells not detected in hMSCs. Based on this data, it was likely β-Gly affected Saos-2 proliferation via interacting with molecular pathways in the late osteogenesis.

Conclusion

β-Gly was shown to have a unique anti-proliferative effect on Saos-2 cells, which was not observed in a less differentiated hMSC line. Such a response may be mediated via interaction with late osteogenic differentiation of Saos-2. The derivation of Saos-2 from an osteosarcoma may have affected the response to osteogenic supplementation resulting in altered proliferation kinetics. It is important these findings are considered during selection of a model for osteogenesis in vitro.

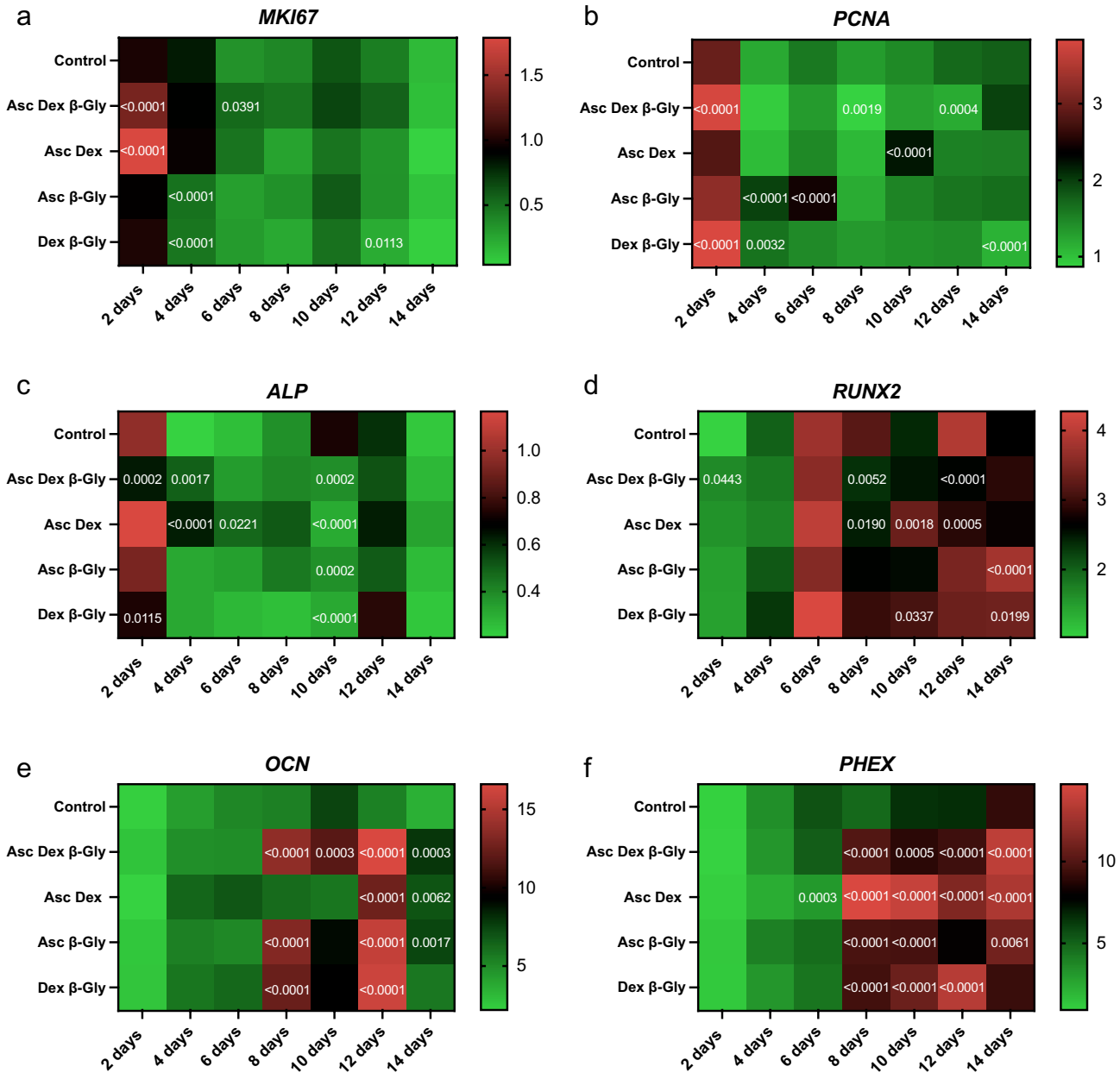

Figure 8. Heatmaps for the relative gene expression levels by Saos-2 cells incubated in osteogenic media over 14 days compared with the expression of *YWHAZ*. The data from each osteogenic condition were statistically compared with the control cultures at the corresponding time point. Where significant statistical differences existed, these are indicated as P values. The expression of proliferation markers *MKI67* (**a**) and *PCNA* (**b**) decreased over 14 days in all conditions. The activity concentration of *ALP* mRNA decreased (**c**) followed by significantly upregulated *RUNX2* expression (**d**) as of day 4 in the presence of β-Gly. A later osteoblast marker, *OCN* and the osteocyte-characteristic marker, *PHEX* increased expression after 8 days in β-Gly supplemented Saos-2 (**e**, **f**). n = 3. The heatmaps were created using GraphPad Prism, Version 9.5.0 (https://www.graphpad.com/updates/prism-950-release-notes).

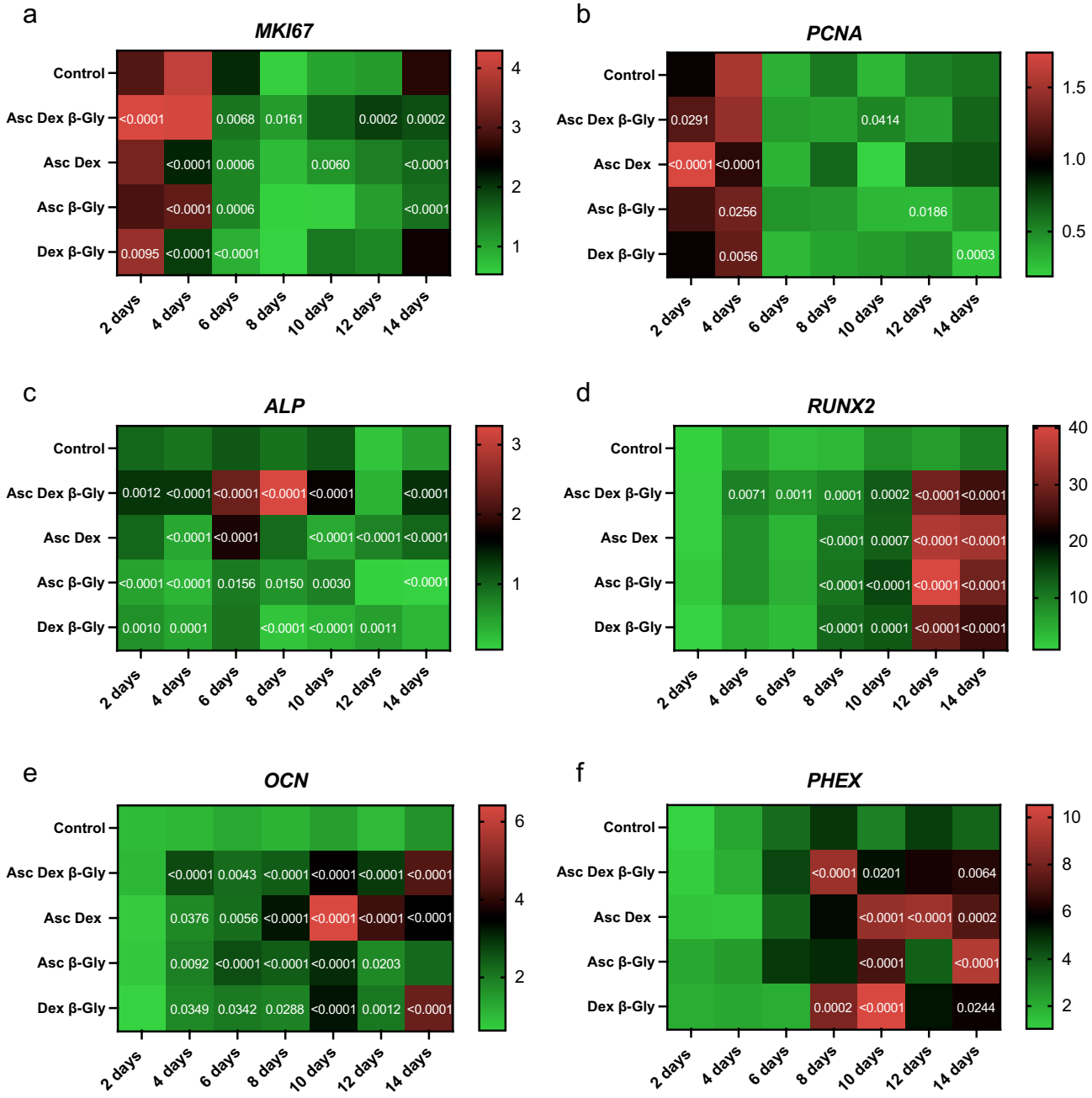

Figure 9. Heatmaps for the gene expression levels by hMSCs incubated in osteogenic media over 14 days relative to the expression of *YWHAZ*. The data from each osteogenic condition were statistically analysed in comparison with control cultures at the corresponding time point. Where significant statistical differences existed, these are indicated as P values. Like Saos-2 cells, hMSCs showed downregulation in the expression of *MKI67* (**a**) and *PCNA* (**b**) for all culture conditions. *ALP* (**c**) expression was upregulated in all osteogenic conditions, with the highest increase observed with Dex, Asc, and β-Gly. The upregulation peaked on day 8 of incubation. *RUNX2* expression increased only in hMSCs after 8 days of incubation (**d**). A less marked increase in transcription of *OCN* and *PHEX* was detected in β-Gly supplemented hMSCs after 8 days (**e**, **f**) than in Saos-2. n = 3. The heatmaps were created using GraphPad Prism, Version 9.5.0 (https://www.graphpad.com/updates/prism-950-release-notes).

Data availability

The data created during this research are openly available from the Open Scientific Framework repository at https://osf.io/t6skh/.

Received: 1 June 2023; Accepted: 17 August 2023
Published online: 02 September 2023

References

1. Bellows, C. G., Aubin, J. E. & Heersche, J. N. M. Physiological concentrations of glucocorticoids stimulate formation of bone nodules from isolated rat calvaria cells in vitro. *Endocrinology* **121**, 6 (1987).
2. Maniatopoulos, C., Sodek, J. & Melcher, A. H. Bone formation in vitro by stromal cells obtained from bone marrow of young adult rats. *Cell Tissue Res.* **254**, 2 (1988).
3. Rodan, S. B. *et al.* Characterization of a human osteosarcoma cell line (Saos-2) with osteoblastic properties. *Cancer Res.* **47**, 18 (1987).
4. Vater, C., Kasten, P. & Stiehler, M. Culture media for the differentiation of mesenchymal stromal cells. *Acta Biomater.* **2011**, 7 (2011).
5. Tenenbaum, H. C. & Heersche, J. N. M. Differentiation of osteoblasts and formation of mineralized bone in vitro. *Calcif Tissue Int.* **34**(1), 76 (1982).
6. Valenti, M. T. *et al.* Ascorbic acid induces either differentiation or apoptosis in MG-63 osteosarcoma lineage. *Anticancer Res.* **34**(4), 79 (2014).
7. Cmoch, A. *et al.* Stimulators of mineralization limit the invasive phenotype of human osteosarcoma cells by a mechanism involving impaired invadopodia formation. *PLoS ONE* **9**, 10 (2014).
8. Orimo, H. & Shimada, T. Effects of phosphates on the expression of tissue-nonspecific alkaline phosphatase gene and phosphate-regulating genes in short-term cultures of human osteosarcoma cell lines. *Mol. Cell Biochem.* **282**, 1–2 (2006).
9. Atkins, G. J. *et al.* Sclerostin is a locally acting regulator of late-osteoblast/preosteocyte differentiation and regulates mineralization through a MEPE-ASARM-dependent mechanism. *J. Bone Miner. Res.* **26**(7), 1425 (2011).
10. Schäck, L. M. *et al.* The phosphate source influences gene expression and quality of mineralization during In vitro osteogenic differentiation of human mesenchymal stem cells. *PLoS ONE* **8**(6), 5693 (2013).
11. Coelho, M. J. & Fernandes, M. H. Human bone cell cultures in biocompatibility testing. Part II: Effect of ascorbic acid, β-glycerophosphate and dexamethasone on osteoblastic differentiation. *Biomaterials* **21**(11), 1095 (2000).
12. Sordi, M. B. *et al.* Effect of dexamethasone as osteogenic supplementation in in vitro osteogenic differentiation of stem cells from human exfoliated deciduous teeth. *J Mater. Sci. Mater. Med.* **32**(1), 85 (2021).
13. Mohseny, A. B. *et al.* Functional characterization of osteosarcoma cell lines provides representative models to study the human disease. *Lab. Investig.* **91**(8), 1195 (2011).
14. Fogh, J. & Trempe, G. New human tumor cell lines in human tumor cells in vitro. *Hum. Tumor Cells In Vitro* **91**, 1195 (1975).
15. Pautke, C. *et al.* Characterization of osteosarcoma cell lines MG-63, Saos-2 and U-2 OS in comparison to human osteoblasts. *Anticancer Res.* **24**(6), 85 (2004).
16. Applied Biological Materials Inc. (abm): Immortalized human bone marrow mesenchymal stem cells SV40. (2023). Available from: https://www.abmgood.com/immortalized-bone-marrow-mesenchymal-stem-cells-sv40-t0520.html.
17. Gregory, C. A., Gunn, W. G., Peister, A. & Prockop, D. J. An Alizarin red-based assay of mineralization by adherent cells in culture: Comparison with cetylpyridinium chloride extraction. *Anal. Biochem.* **329**(1), 77–84 (2004).
18. Meleti, Z., Shapiro, I. M. & Adams, C. S. Inorganic phosphate induces apoptosis of osteoblast-like cells in culture. *Bone* **27**(3), 359 (2000).
19. Nguyen, T. T. *et al.* Mitochondrial oxidative stress mediates high-phosphate-induced secretory defects and apoptosis in insulin-secreting cells. *Am. J. Physiol. Endocrinol. Metab.* **308**(11), 933 (2015).
20. Kanatani, M., Sugimoto, T., Kano, J., Kanzawa, M. & Chihara, K. Effect of high phosphate concentration on osteoclast differentiation as well as bone-resorbing activity. *J. Cell Physiol.* **196**, 1 (2003).
21. Pisciotta, A. *et al.* Human serum promotes osteogenic differentiation of human dental pulp stem vells in vitro and in vivo. *PLoS ONE* **7**, 11 (2012).
22. Tang, N., Song, W. X., Luo, J., Haydon, R. C. & He, T. C. Osteosarcoma development and stem cell differentiation. *Clin. Orthopaed. Relat. Res.* **466**, 2114 (2008).
23. Kumari, R. & Jat, P. Mechanisms of cellular senescence: Cell cycle arrest and senescence associated secretory phenotype. *Front. Cell Dev. Biol.* **2021**, 9 (2021).
24. Uxa, S. *et al.* Ki-67 gene expression. *Cell Death Differ.* **28**(12), 3357–3370 (2021).
25. Sun, X. & Kaufman, P. D. Ki-67: More than a proliferation marker. *Chromosoma* **127**, 2 (2018).
26. Bologna-Molina, R., Mosqueda-Taylor, A., Molina-Frechero, N., Mori-Estevez, A. D. & Sánchez-Acuña, G. Comparison of the value of PCNA and Ki-67 as markers of cell proliferation in ameloblastic tumors. *Med. Oral Patol. Oral Cir. Bucal.* **18**(2), 174 (2013).
27. Schiller, I. *et al.* Establishment of proliferative cell nuclear antigen gene as an internal reference gene for polymerase chain reaction of a wide range of archival and fresh mammalian tissues. *J. Vet. Diagn. Investig.* **15**(6), 585 (2003).
28. Krampe, B. & Al-Rubeai, M. Cell death in mammalian cell culture: Molecular mechanisms and cell line engineering strategies. *Cytotechnology* **2010**, 62 (2010).
29. Aubin, J. E. Advances in the osteoblast lineage. *Biochem. Cell Biol.* **76**, 899 (1998).
30. Kalajzic, I. *et al.* In vitro and in vivo approaches to study osteocyte biology. *Bone* **54**(2), 296–306 (2013).
31. James, A. W. Review of signalling pathways governing msc osteogenic and adipogenic differentiation. *Sci. (Cairo)* **2013**, 74 (2013).
32. Zur Nieden, N. I., Kempka, G. & Ahr, H. J. In vitro differentiation of embryonic stem cells into mineralized osteoblasts. *Differentiation* **71**(1), 18–27 (2003).

Acknowledgements

The present research was funded by the Engineering and Physical Sciences Research Council, UK (grant number EP/R045291/1). The authors thank the technician team in the Birmingham Dental Hospital research laboratories (Birmingham, UK) for providing technical assistance for this study and are grateful to Dr D. Gupta for identifying that the hMSC line could be maintained in low glucose DMEM.

Author contributions

O.S.Y.: conceptualisation; data curation; formal analysis; investigation; methodology; visualisation; writing (original draft preparation). B.A.S.: conceptualisation; funding acquisition; methodology; supervision; writing (review

and editing). A.D.W.: conceptualisation; funding acquisition; methodology; supervision; writing (review and editing). R.M.S.: conceptualisation; funding acquisition; methodology; supervision; writing (review and editing).

Competing interests
The authors declare no competing interests.

Additional information
Supplementary Information The online version contains supplementary material available at https://doi.org/10.1038/s41598-023-40835-w.

Correspondence and requests for materials should be addressed to R.M.S.

Reprints and permissions information is available at www.nature.com/reprints.

Publisher's note Springer Nature remains neutral with regard to jurisdictional claims in published maps and institutional affiliations.